The age of Tasmanian Cenozoic basalts, determined by the $^{40}Ar/^{39}Ar$ method

Geological Survey Technical Report 42

Tasmanian Government

Geological Survey Technical Report 42:

The age of Tasmanian Cenozoic basalts, determined by the ^{40}Ar/^{39}Ar method

by

J. L. Everard, Ching-Hua Lo and M. Zhang

Cover: Small hill at Blessington, NE Tasmania, the topographic expression of a 36.8 Ma plug of basanite, bearing spinel lherzolite xenoliths, which has erupted through Triassic quartz sandstone.

Tasmanian Government

Mineral Resources Tasmania   www.mrt.tas.gov.au   Department of State Growth

The age of Tasmanian Cenozoic basalts, determined by the ^{40}Ar/^{39}Ar method

by J. L. Everard, Ching-Hua Lo[1] & M. Zhang[2]

[1]Department of Geosciences, National University of Taiwan, Taipei 106, Republic of China

[2]GEMOC ARC National Key Centre, Department of Earth and Planetary Sciences, Macquarie University, Sydney 2109, Australia

CONTENTS

TABLES

FIGURES

APPENDICES

Abstract

Twenty-five samples of Cenozoic basalts, collected from widely dispersed localities throughout Tasmania and ranging in composition from quartz tholeiite to olivine melilitite, were dated by the $^{40}Ar/^{39}Ar$ incremental heating method on whole rocks. Twenty-four samples yielded valid plateau ages, ranging from 16.3 ± 0.2 Ma to 45.5 ±1.0 Ma (at 1σ), whereas an olivine tholeiite from southeast Tasmania yielded only an integrated age of 64.2 ± 0.6 Ma. For 23 samples, the intercept and plateau ages are statistically indistinguishable. The integrated (total fusion ages) are either similar to the plateau ages (15 samples) or significantly older (9 samples) due to anomalously old apparent ages in the lower and/or higher temperature heating steps.

The new $^{40}Ar/^{39}Ar$ ages have a median age of 29.4 Ma and are broadly congruent with previous K/Ar geochronology on Tasmanian Cenozoic basalts. The overall pattern is of gradually increasing activity from the Paleocene, peaking in the Oligocene at 25 – 30 Ma when the compositionally most diverse basalts were erupted, and thereafter declining rapidly until the last eruptions at about 10 Ma. Few trends between age and either location or composition can be identified, except possibly that tholeiitic activity mostly coincides with the peak of volcanism, whereas the youngest basalts are alkalic and possibly restricted to northern Tasmania. The quasi-random pattern of volcanism does not support, (nor necessarily invalidate) plume-based models which would be expected to generate age-progressive volcanic tracks due to plate motion. Refinements of local geology are possible from the new dates, particularly when used in conjunction with magnetostratigraphy and palynology; for instance the sedimentary fill of the Scottsdale Sub-basin is older than previously thought.

1.0 INTRODUCTION

Almost all previous geochronology of Tasmanian Cenozoic basalts has utilised the $^{40}K/^{39}Ar$ method (e.g. compilation of Gibson, 2007). The $^{40}Ar/^{39}Ar$ method (e.g. McDougall & Harrison, 1988) is also based on the decay of ^{40}K, but involves irradiation of the sample, together with a standard (flux monitor) of known age, with fast neutrons in a nuclear reactor to convert some of the ^{40}K to ^{39}Ar. The $^{40}Ar/^{39}Ar$ of the sample can then be measured very accurately in a mass spectrometer and, after corrections for other nuclear reactions and for atmospheric argon, can yield its age. Typically $^{40}Ar/^{39}Ar$ ages can be more precise than $^{40}K/^{40}Ar$ ages, which require separate determinations of K and ^{40}Ar. The major advantage of the $^{40}Ar/^{39}Ar$ method, however, is that incremental step heating can be used to degas the sample at successively higher temperatures, yielding additional information about the distribution of Ar and K in the sample. This can enable the identification of any parts of the sample that have lost or gained Ar since crystallisation, for example due to alteration, which would result in an erroneous K/Ar ages. With the $^{40}Ar/^{39}Ar$ step-heating technique, however, the true crystallisation age can be inferred in many instances.

The 25 samples dated by the $^{40}Ar/^{39}Ar$ method are a subset of a larger set of 109 samples of Tasmanian Cenozoic basalts, representative of their geochemical variety and geographical range, which were selected for detailed petrological study, including major, trace element and isotopic (Sr, Nd, Pb) analysis, at Macquarie University. A summary of both the petrological and geochronological results has been presented in conference abstracts (Everard et al., 2004; Zhang et al., 2004) and in Chapter 9 of "The Geological Evolution of Tasmania (Everard et al. in Corbett, Quilty and Calver, 2014). The purpose of this report is to fully document the geochronological data and supporting information for these 25 dated samples (Figure 1; Table 1).

2.0 GEOLOGICAL BACKGROUND

Tasmanian Cenozoic volcanics, dominantly basaltic lavas, represent the southern extremity of the Cenozoic volcanic provinces of eastern Australia. They crop out over about 4,000 km², or about 6%, of the Tasmanian landmass. Although widespread, they are most extensive and voluminous in the northwest, and absent from central west and southwest (Figure 1). They also occur on many Bass Strait islands and form part of the Cenozoic fill of Bass Basin (Baillie and Everard, 2014). Intraplate basalts have been dredged from seamounts on the East Tasman Plateau, South Tasman Rise and elsewhere on thin continental crust, south of Tasmania (Crawford et al., 1997).

The basalts have been reviewed in numerous publications (Edwards, 1950; Spry, 1962; Sutherland, 1969; 1989a, b) and most recently by Sutherland et al. (2004) and Everard et al. (2014). Thus only a brief summary is presented here.

Over 120 eruptive centres have been identified or inferred (Sutherland, 1989b) ranging from large eroded necks and probable crater fills up to 1 km across, to small plugs and dykes a few metres wide. Associated flows may be up to 50 km long, whilst in parts of the northwest lavas have formed a lava pile up to 370 m thick, largely burying the pre-volcanic topography (Seymour, 1989).

The basalts are usually coherent subaerial lavas but, particularly in the far northwest, marine sequences with pillow lavas and hyaloclastites of phreatomagmatic origin are also present (e.g. Sutherland and Corbett, 1967; Fox et al., 2023). Subaqueous pyroclastics have also developed where large flows have entered large highland lakes or dammed major streams (e.g. Sutherland and Hale, 1970; Sutherland, 1980).

Pyroclastic deposits derived from explosions of magmatic origin are also common (e.g. von Lichtan, 2000), but much less well preserved than those of the much younger volcanic provinces of western Victoria and north Queensland.

The basalts have a wide compositional range (e.g. SiO_2 36-53%). Quartz- and olivine tholeiites and mildly alkalic basalts (alkali olivine basalts and hawaiites, with many transitional olivine basalts), are most voluminous, but strongly undersaturated types (basanites, olivine nephelinites and a few melilitites) are more common than in mainland Australia (e.g. Everard et al., 2014). Many strongly evolved undersaturated alkaline types (sodic hawaiites, mugearites, sodic nepheline hawaiites and mugearites) are present, particularly as plugs and small flows in southeastern Tasmania. These commonly contain mantle xenoliths, indicating that fractionation occurred at mantle depths (e.g. Everard, 2001; Beyer et al., 2014).

3.0 PREVIOUS GEOCHRONOLOGY

The first Tasmanian basalts to be radiometrically dated were five tholeiites from near Great Lake, central Tasmania, for which a syn-glacial Pleistocene age had been suggested on physiographic grounds (Sutherland and Hale, 1970). They, however, yielded K/Ar ages ranging from 22.3 to 24.3 Ma (Sutherland et al., 1973; recalculated for new decay constants).

Sutherland and Wellman (1986) published 16 new dates, and compiled other data available at that time, including a further 7 dates published between 1973 and 1986. Since then, about a further 30 basalts have been dated, including

Table 1. Sample locations. Coordinates UTM, Zone 55G, Datum GDA94.

Field No	Reg No	Analysis No	Rock Type	IUGS classification	Age (Ma) ±1σ	Location	mE (GDA94)	mN(GDA94)	longitude	latitude	MRT map
TJ3602	R005376	930733	hawaiite	basalt	27.0 ± 0.3 Ma	Wedge Plains Link Road	356140	5454640	145.2883	41.0467	Tayatea 25k
TJ3591	R005365	930647	transitional olivine basalt	basalt	34.3 ± 0.3 Ma	Rabalga Track	363250	5451230	145.3721	41.0787	Milabena 25k
KJ634	R005410	930659	basanite	basanite	25.4 ± 0.2 Ma	Eastons Ck, lower flow	362460	5440160	145.3602	41.1483	Folly 25k
TJ3228	R005353	930630	nepheline hawaiite	basanite	21.4 ± 0.2 Ma	Knoll, Neasey Plains	357220	5441980	145.2982	41.1609	Holder 25k
CVH	R010192	970039	nepheline hawaiite	basanite	21.5 ± 0.2 Ma	Coastview Hill, via Hampshire	398910	5432780	145.7935	41.2500	Tewkesbury 25k
SRN	R010187	970032	basanite	basanite	22.0 ± 0.3 Ma	South Riana plug	415690	5431180	145.9935	41.2664	Riana 25k
LLC	R010186	970031	alkali olivine basalt	basalt	37.5 ± 0.2 Ma	Lillicos Beach, via Devonport; lower flow	441710	5443380	146.3053	41.1588	Devonport 25k
AJ99	R004332	910742	olivine nephelinite	foidite (nephelinite)	17.5 ± 0.2 Ma	Olivers Hill, via Ringarooma	562632	5427613	147.7481	41.3005	Victoria 25k
AJ1424	R004366	940240	basanite	basanite	17.5 ± 0.2 Ma	northern hill, via Sweets Creek, Upper Esk	559530	5418160	147.7120	41.3858	Ben Nevis 25k
AJ1425	R004367	940241	hawaiite	basalt	16.3 ± 0.2 Ma	southern hill, via Sweets Creek, Upper Esk	559590	5417370	147.7128	41.3930	Ben Nevis 25k
AJ1426	R004368	940242	olivine nephelinite	basanite (melanephelinite)	16.8 ± 0.4 Ma	Upper Esk	560920	5413380	147.7291	41.4288	Saddleback 25k
PP20.5	R027027	920718	olivine nephelinite	basanite (melanephelinite)	41.0 ± 0.2 Ma	Pebble Plain DDH/20.5m, via Beauty Flat	582760	5403860	147.9918	41.5126	Dublin Town 25k
WSc	R010201	970056	olivine nephelinite	foidite (nephelinite)	34.2 ± 0.4 Ma	Sledge Track,W Scottsdale	540710	5440980	147.4854	41.1815	Scottsdale 25k
SDL	R010202	980652	olivine nephelinite	foidite (nephelinite)	29.4 ± 0.5 Ma	The Sideling (Knockup), via Weelaty	533810	5430980	147.4037	41.2719	Lisle 25k
BLS	R010204	980656	basanite	basanite	36.8 ± 0.2 Ma	Blessington plug	538810	5403470	147.4652	41.5194	Blessington 25k
SB9	R005506	910719	olivine tholeiite	basalt	29.6 ± 0.6 Ma	"Eastbourne", via Avoca	554940	5371110	147.6615	41.8099	Hanleth 25k
SB11	R005508	910721	nepheline hawaiite	basanite	30.3 ± 0.2 Ma	Llewellyn, via Conara	548000	5370920	147.5779	41.8121	Hanleth 25k
LSB24	R004501	910352	nepheline hawaiite	basanite	27.3 ± 0.1 Ma	Burburys Sugarloaf, via Ross	532610	5350680	147.3938	41.9952	Lake River 50k
LCr	R010295	970028	olivine nephelinite	basanite (melanephelinite)	29.4 ± 0.2 Ma	W side of Lake Crescent	511380	5330210	147.1378	42.1801	Interlaken 50k
ATr	R010218	970040	olivine melilitite	foidite (melanephelinite)	36.5 ± 0.2 Ma	Alma Tier, via Interlaken	504140	5332900	147.0501	42.1560	Interlaken 50k
BRJ1	R010055	970027	quartz tholeiite	basaltic andesite	26.7 ± 0.3 Ma	Crooked Billet Creek, Brighton	519550	5270510	147.2388	42.7176	Broadmarsh 25k
HBJ23	R010093	970024	quartz tholeiite	basaltic andesite	25.1 ± 0.3 Ma	Dragon Point, Claremont	521480	5262940	147.2627	42.7857	Richmond 25k
GFN	G402497	970026	basanite	basanite	45.5 ± 1.0 Ma	Glenfern	498310	5257180	146.9793	42.8379	SE Tasmania 250k
HBJ6	R010076	961031	hawaiite	potassic trachybasalt	29.4 ± 0.2 Ma	Pickett Hill, via Kingston	520620	5243300	147.2529	42.9626	Taroona 25k
SBA21	R010159	980456	olivine tholeiite	basalt	64.2 ± 0.6 Ma#	quarry, Marion Bay	569710	5257480	147.8530	42.8320	Sorell 50k

Integrated age; others are plateau ages (see Table 3)
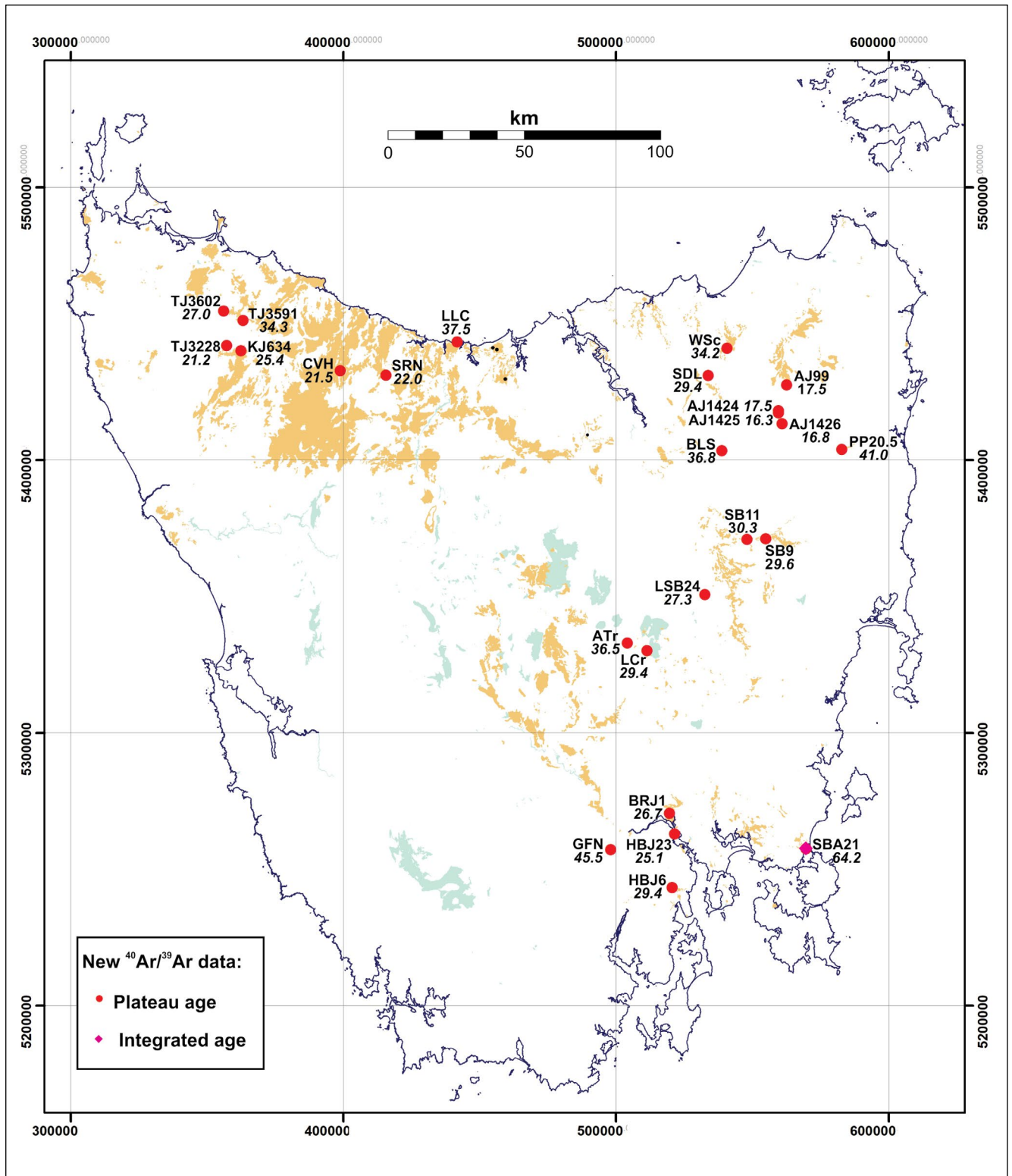
Figure 1. Locations and ages of samples newly dated by the $^{40}Ar/^{39}Ar$ method, with distribution of Cenozoic basalt also shown from MRT 1:250 000 digital data.

the oldest (61.7 ± 1.3 Ma) and youngest (8.5 ± 0.1 Ma) so far determined (Sutherland et al., 2002; Baillie, 1986b). Most of these ages were determined by the K/Ar method on whole rocks, and many are mentioned in the following discussion. Sutherland et al. (1996) also published two fission track ages from zircon megacrysts in basalt from near Boat Harbour, northwest Tasmania. Locations and ages are shown in Figure 2.

Dates available up to 2013 are summarised by Everard et al., (2014, p.470 - 471) and K/Ar data were also compiled by Gibson (2007).

4.0 METHODS

4.1 Sampling

Samples were collected between 1991 and 1998 during Geological Survey regional mapping projects, or specifically for petrological study. Selection criteria included freshness and low abundance of secondary minerals such as zeolite, carbonate or clay minerals in amygdales. Patina, weathering rinds and any patches of alteration were removed using a rock saw before further processing.

The subset of 25 samples chosen for age dating were selected mainly on the basis that their ages could not

reasonably be inferred from previous geochronology, palynology of associated sediments or other field relations. Tewnty four of the selected samples were collected from surface outcrop and one from a drill hole.

Sampling preceded the easy availability of accurate global positioning systems (GPS), but locations were recorded on detailed 1:25,000 topographic maps, or enlargements thereof. Location accuracy is estimated at better than ± 50 m and commonly ± 25 m (Table 1).

4.2 Petrography

Thin sections were prepared of all samples, and petrographic descriptions are given in Appendix 1. Photomicrographs are presented in Appendix 2 (Figures 13-40). X-ray diffraction (XRD) of a subset of 12 powdered samples, mainly nephelinites with a very fine-grained groundmass, was undertaken in order to better document their mineralogy. The results (Table 2, Appendix 3) show that analcime, plagioclase and zeolite minerals are commonly present in the groundmass, as well as nepheline. As expected, olivine, clinopyroxene, magnetite and minor apatite are ubiquitous.
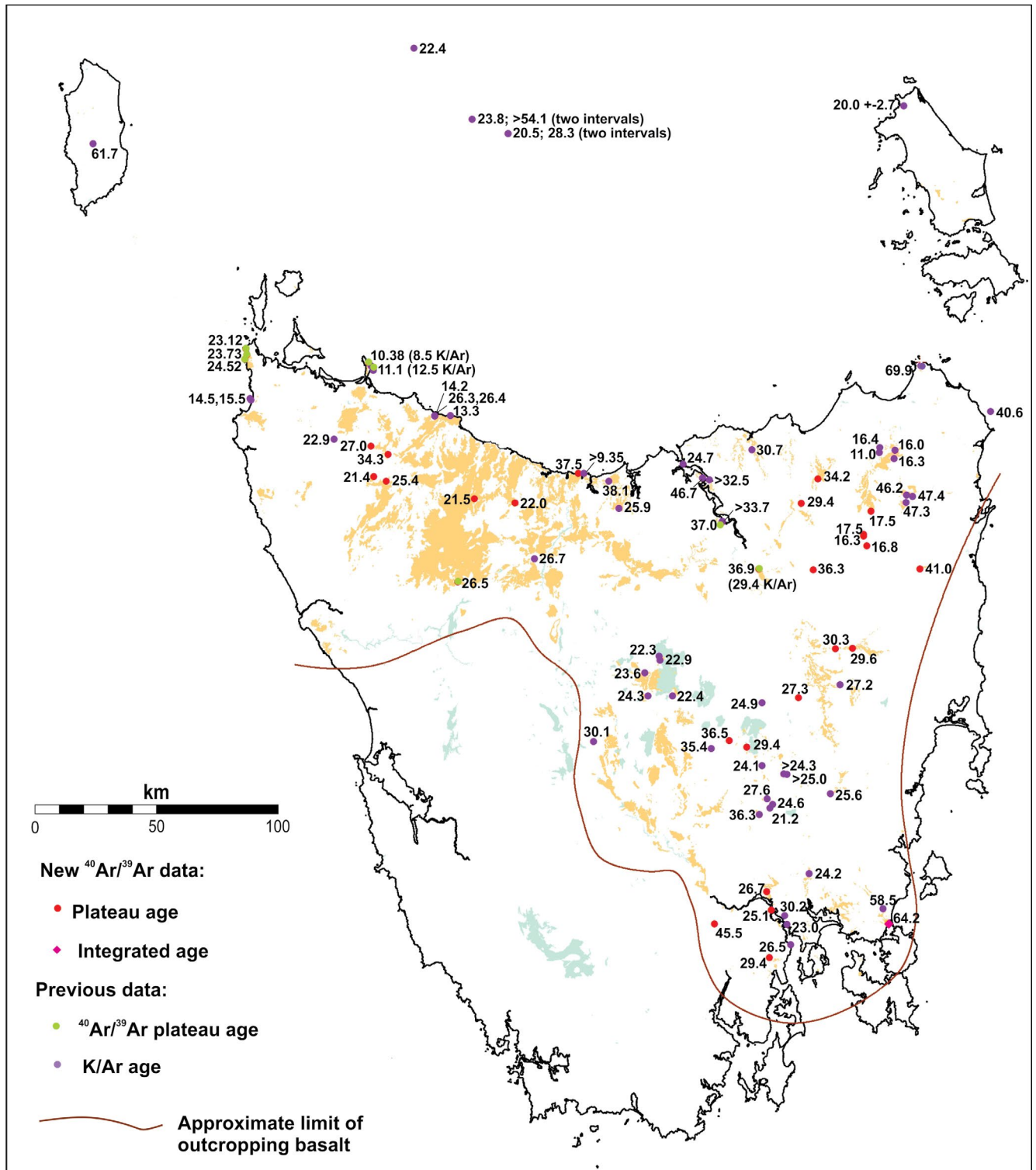
Figure 2. Locations and ages of samples newly dated by the $^{40}Ar/^{39}Ar$ method, compared with previous K/Ar and $^{40}Ar/^{39}Ar$ ages (see Gibson, 2007 and Everard et al., 2014 for sources).

Table 2. Qualitative mineralogy of selected samples, determined by x-ray diffraction.

Field No	Reg No	Rock Type	Location	Olivine	Clinopyroxene	Plagioclase	Anorthoclase	Nepheline	Melilite	Analcime	Chabazite	Mesolite	Phillipsite	Stilbite	Zeolite (undiff)	Magnetite	Spinel	Fluorapatite	Amphibole	Mica (undiff)	Chlorite	Smectite	Serpentine
TJ3228	R005353	nepheline hawaiite	Knoll, Neasey Plains	X	X			X						X		X		X				X	
CVH	R010192	nepheline hawaiite	Coastview Hill, via Hampshire	X	X	X		X		X						X		X			X		
SRN	R010187	basanite	South Riana plug	X	X	X	X	X		X						X	X	X			X	X	X
AJ99	R004332	olivine nephelinite	Olivers Hill, via Ringarooma	X	X			X		X						X		X					
AJ1424	R004366	basanite	northern hill, via Sweets Creek, Upper Esk	X	X	X	X	X		X	X					X		X		X	X	X	
AJ1426	R004368	olivine nephelinite	Upper Esk	X	X	X		X		X			X			X		X			X		
PP20.5	R027027	olivine nephelinite	Pebble Plain DDH/20.5m, via Beauty Flat	X	X	X	X	X			X				X	X		X		X	X	X	
WSc	R010201	olivine nephelinite	Sledge Track, W Scottsdale	X	X	X	X	X				X				X		X			X	X	
SDL	R010202	olivine nephelinite	The Sideling (Knockup), via Weelaty	X	X	X		X								X		X					
LCr	R010205	olivine nephelinite	W side of Lake Crescent	X	X	X		X		X						X		X	X	X			
ATr	R010218	olivine melilitite	Alma Tier, via Interlaken	X	X	?		X	X			X				X		X			X		
GFN	G402497	basanite	Glenfern	X	X	X	X	X							X	X		X					

4.3 Geochemistry

All samples were analysed for major and trace element analyses at Mineral Resources Tasmania (MRT) laboratories by x-ray fluorescence (XRF) using standard techniques. Fe_2O_3/FeO was determined by digestion with HF/H_2SO_4 followed by titration with $KMnO_4$, CO_2 was determined by loss in a Leco induction furnace, and H_2O+ calculated from loss on ignition, with correction for CO_2, FeO and S as required. Eleven samples were also analysed at Macquarie University by XRF, and one in duplicate at MRT. In each case, results are in good to excellent agreement (Table 3).

Trace elements of all samples were also determined by inductively coupled plasma mass spectroscopy (ICPMS) at Macquarie University. Results are in good to excellent agreement with XRF results (Table 3).

Basalt nomenclature follows the CIPW-norm based scheme of Johnson (1989); the total alkali-silica IUGS classification (Le Maitre, 2002) is also presented (Figure 3).

4.4 Analytical method

Chips of 20-50 mesh size, derived from a coarse jaw crush, were hand-picked for freshness, leached in cold 1N HCl for 8 hours and ultrasonically cleaned in distilled water. The chip samples, each weighing ~600 mg, were wrapped in aluminium foil packets and stacked in a 9 cm long aluminium canister. Three aliquots of LP-6 biotite standards (Odin et al., 1982) with a calibrated $^{40}Ar/^{39}Ar$ age of 128.4 ± 0.2 Ma (Baksi et al., 1996; Renne et al., 1998) were positioned in the top, bottom and centre of the canister. The samples and standards were then irradiated in the VT-C position of the Tsing-Hwa THOR research reactor for 30 hours. After irradiation, standards and samples were incrementally heated in a double-vacuum Mo resistance furnace. The released gas was purified by a Ti-sponge and two SASE Zr-Al getters (one was kept at 450°C and the other at room temperature), and then measured by a Varian-MAT GD150 mass spectrometer operated in static mode, at the National Taiwan University. The detailed analytical procedure is similar to that outlined by Lo et al. (1994, 2002).

Measured isotopic ratios were corrected for mass discrimination, system blanks, radioactive decays and interfering isotopes produced during irradiation using factors reported by Lo et al. (2002). The neutron flux gradient across the top and bottom of the irradiation canister was less than 0.9%, as indicated by the variation of J values from the flux monitors (LP-6 biotite standard. An average J value of 0.00318766 ± 0.00000317 is adopted in the age calculations. The Ca/K and Cl/K ratios were derived from the measured $^{37}Ar_{Ca}/^{39}Ar_K$ and $^{38}Ar_{Cl}/^{39}Ar_K$ ratios according to the relationships: Ca/K = 3.32 x $^{37}Ar_{Ca}/^{39}Ar_K$ and Cl/K = 0.52 x $^{38}Ar_{Cl}/^{39}Ar_K$.
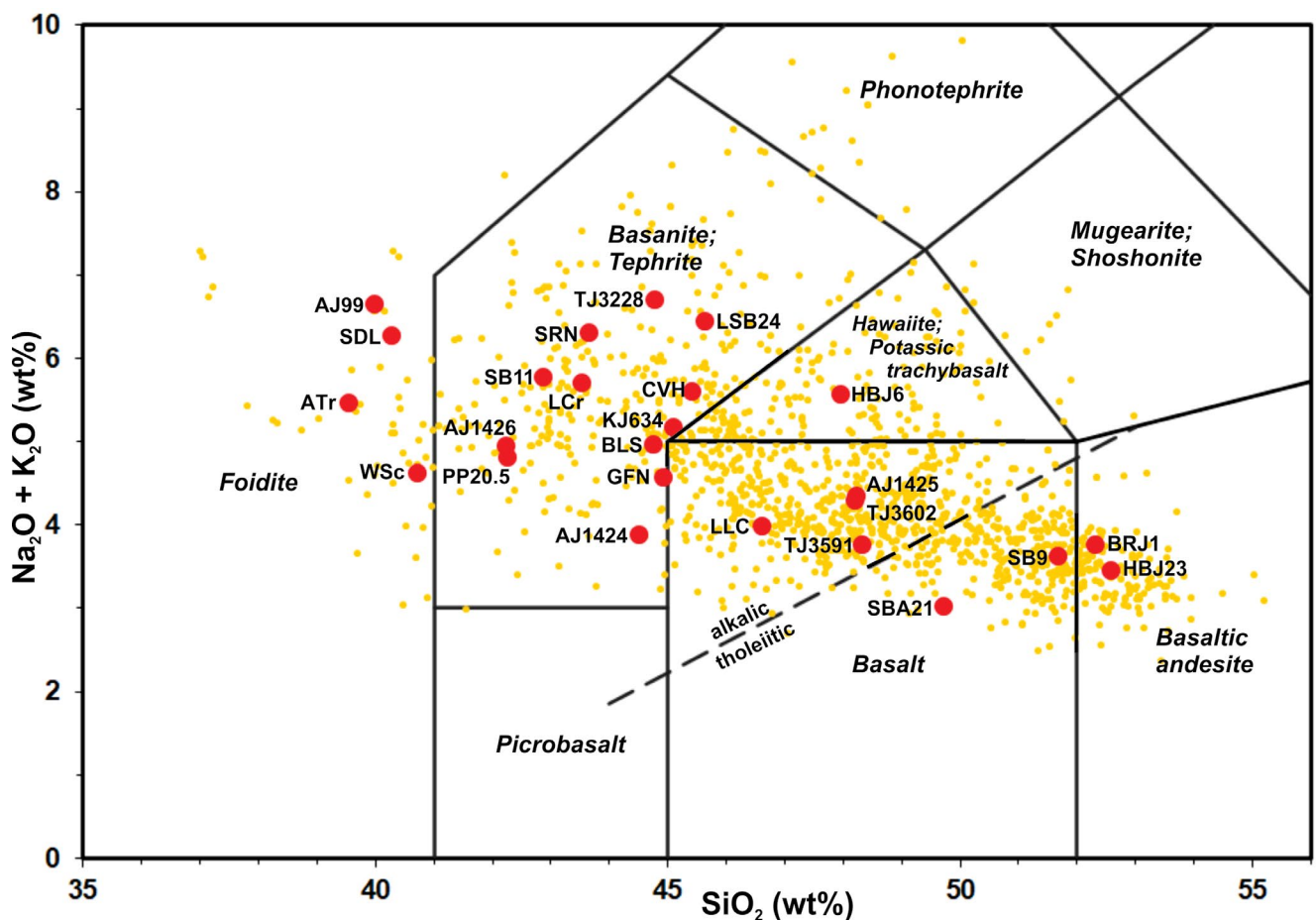

Figure 3. Total alkalis versus silica (TAS) plot for samples newly dated by the $^{40}Ar/^{39}Ar$ method (red symbols) and other Tasmanian Cainozoic basalts (orange symbols). Major element analyses normalised to 100% anhydrous. IUGS classification (Le Maitre 2002) and empirical tholeiitic-alkalic boundary (Macdonald & Katsura 1964) also shown.

Table 3. Whole rock analyses and CIPW norms of dated samples.

MRT Reg No	R005379	R005368	R005410	R005353	R010192	R010192	R010187	R010187	R010186	R010186	R004332	R004366	R004366	R004367	R004368	R027027	R010201	R010201	R010202	R010202	R010204
Field No	TJ3602	TJ3591	KJ634	TJ3228	CVH	CVH	SRN	SRN	LLC	LLC#	AJ99	AJ1424	AJ1424	AJ1425	AJ1426	PP20.5m	WSc	WSc	SDL	SDL	BLS
Lab	MRT	MRT	MRT	MRT	MRT	MU	MRT	MU	MRT	MU	MRT	MRT	MU	MRT	MRT	MRT	MRT	MU	MRT	MU	MRT
Analysis No.	930733	930647	930659	930630	970039		970032		970031		910742	940240		940241	940242	920718	970056		980652		980656
SiO2 (wt%)	46.81	46.82	44.46	43.50	44.53	44.00	41.85	40.96	45.41	45.44	39.65	42.98	42.93	47.44	40.80	41.11	38.67	38.32	39.68	39.97	43.70
TiO2	1.68	2.17	2.63	2.43	2.55	2.60	2.44	2.53	2.24	2.28	3.21	2.75	2.58	2.44	3.05	2.93	3.28	3.47	2.82	2.92	2.39
Al2O3	14.11	13.18	13.94	13.59	13.97	14.00	12.03	11.97	13.61	13.69	10.61	10.94	10.95	13.14	10.81	13.48	9.19	9.05	9.99	9.88	14.19
Fe2O3	1.66	2.53	3.11	4.09	2.70	3.09	5.08	5.72	2.63	3.01	5.47	4.65	4.38	3.22	5.01	1.97	4.92	5.66	4.27	5.11	2.79
FeO	9.58	9.05	9.98	8.85	9.23	8.66	8.59	8.44	8.85	8.44	8.52	7.47	7.49	8.52	8.39	11.83	10.53	10.04	8.98	8.16	8.72
MnO	0.17	0.17	0.18	0.19	0.19	0.18	0.21	0.21	0.17	0.17	0.21	0.18	0.18	0.17	0.21	0.18	0.22	0.22	0.21	0.20	0.20
MgO	10.67	10.11	9.58	8.98	9.85	9.82	10.89	10.23	11.05	10.99	13.03	13.25	13.12	10.10	12.17	10.61	12.73	11.81	14.49	14.36	10.77
CaO	8.09	8.97	9.28	8.50	8.96	8.90	8.17	8.17	9.34	9.21	4.87	10.22	10.24	8.80	10.83	10.00	10.67	11.04	11.21	11.24	9.66
Na2O	2.92	2.43	3.00	4.80	4.15	4.18	4.25	4.23	2.56	2.61	2.82	2.58	2.73	2.98	3.57	3.16	3.55	3.81	4.45	4.78	3.09
K2O	0.31	0.47	2.10	1.70	0.82	0.85	1.07	1.16	0.50	0.48	1.31	0.81	0.84	0.56	1.07	0.69	0.84	0.90	1.08	1.19	0.66
P2O5	nd	—	0.62	0.92	1.82	0.57	3.62	3.79	1.81	1.97	1.97	2.82	2.82	1.74	3.13	1.32	3.47	3.60	0.74	0.79	1.80
H2O+	2.44	2.31	1.53	1.68	nd	nd	nd	nd	nd	nd	nd	nd	nd	nd	nd	nd	3.47	nd	0.00	0.25	0.66
H2O-	nd	nd	nd	nd	nd	nd	nd	nd	nd	nd	0.54	nd	nd	nd	nd	nd	0.25	0.10	0.00	nd	1.80
SO3	0.08	0.02	0.10	0.11	0.09	0.03	0.10	0.07	0.09	0.04	nd	0.10	0.10	0.09	0.09	0.09	0.18	0.10	0.08	0.10	0.00
CO2	nd	0.04	0.09	0.14	0.10	nd	0.11	nd	0.10	0.09	nd	0.03	nd	0.03	nd	nd	nd	nd	0.08	nd	0.08
FeS2	nd	nd	nd	nd	nd	nd	nd	nd	nd	nd	nd	nd	nd	nd	nd	nd	nd	nd	nd	nd	nd
TOTAL	99.85	99.48	100.60	99.48	100.31	100.22	100.20	99.88	99.67	100.18	100.18	99.95	100.20	100.52	100.38	98.97	99.35	100.06	99.72	100.69	99.81
LOI*	1.45	1.33	0.52	12.53	0.89	—	2.76	—	0.91	—	0.04	2.09	—	0.88	2.29	—	2.55	—	−0.25	—	0.83
FeOtot	11.07	11.33	12.78	—	11.66	11.44	13.16	13.26	11.22	11.15	13.67	11.65	11.43	11.42	12.90	13.60	14.95	15.13	12.82	12.76	11.23
Mg#(0.20)	66.96	65.25	61.19	60.12	63.99	64.36	63.51	61.88	67.44	67.46	66.72	70.51	70.71	65.04	66.50	62.13	64.16	62.14	70.38	70.30	66.96

CIPW norms calculated at Fe2O3/FeO = 0.20

	R005379	R005368	R005410	R005353	R010192	R010192	R010187	R010187	R010186	R010186	R004332	R004366	R004366	R004367	R004368	R027027	R010201	R010201	R010202	R010202	R010204
Q	—	—	—	—	—	—	—	—	7.98	7.94	—	7.15	7.17	7.74	7.32	9.21	2.08	—	—	—	10.60
or	7.53	7.37	12.56	10.32	8.05	8.12	11.06	11.34	17.90	18.41	—	10.18	9.91	25.21	2.03	2.97	7.01	5.23	20.67	22.06	8.73
ab	24.11	21.18	10.32	11.06	15.09	14.50	7.76	7.33	22.31	22.32	—	15.31	14.70	18.94	10.25	18.56	2.45	4.34	25.43	26.83	20.08
an	22.34	22.13	18.59	10.80	15.81	15.87	8.77	8.75	—	—	—	—	—	—	—	—	17.07	18.40	—	—	—
lc	—	—	—	—	—	—	—	—	—	—	2.02	—	—	—	—	—	—	—	—	—	—
ne	0.70	—	8.33	16.60	11.20	11.79	16.06	16.48	2.31	2.29	8.02	6.71	7.61	0.20	15.79	13.24	34.58	18.40	20.67	22.06	9.76
di	13.63	16.64	19.45	21.46	19.41	19.19	21.20	21.15	17.65	17.20	22.45	25.40	25.96	17.52	30.67	22.48	—	—	—	—	19.75
hy	—	7.00	—	—	—	—	—	—	—	—	—	—	—	—	—	—	—	—	—	—	—
ol	24.86	17.42	21.05	19.64	20.62	20.53	24.35	23.55	23.48	23.43	27.49	24.93	24.59	21.50	22.08	22.74	24.28	21.83	27.67	26.54	22.03
cs	—	—	—	—	—	—	—	—	—	—	—	—	—	—	—	—	0.28	0.28	4.75	4.51	—
mt	2.80	2.87	3.18	3.16	2.92	2.88	3.36	3.44	2.82	2.81	2.82	2.96	2.91	2.85	3.27	3.43	3.86	3.92	3.19	3.16	2.82
il	3.28	4.25	5.06	4.74	4.92	5.06	4.82	5.07	4.36	4.44	6.13	5.40	5.08	4.70	5.98	5.71	6.55	6.94	5.42	5.58	4.64
ap	0.75	1.14	1.48	2.23	1.98	2.06	2.62	2.89	1.20	1.16	3.18	1.97	2.06	1.34	2.61	1.67	2.12	2.24	2.59	2.83	1.60
total	100.00	100.00	100.00	100.00	100.31	100.00	100.00	100.00	100.00	100.00	100.00	100.00	100.00	100.00	100.00	100.00	100.00	100.00	100.00	100.00	100.00
An%plag	46.62	49.61	62.94	47.91	49.68	50.77	51.59	52.96	54.02	53.33	100.00	58.64	58.30	41.45	82.65	85.47	64.16	62.14	70.38	70.30	68.44
Type	HW-A	TOB	BSN-1	NH-2A	NH-2A	BSN-2	BSN-2	BSN-2	AOB	AOB	ON-3	BSN-1	BSN-1	HW-A	ON-1	ON-1	ON-2	ON-3	ON-3	ON-3	BSN-1

Trace elements (XRF at MRT, ICPMS at MU)

Element	R005379 (ICPMS)	R010192 (ICPMS)	R010187 (ICPMS)	R010186 (ICPMS)	R004366 (ICPMS)	R010201 (ICPMS)	R010202 (ICPMS)
Li (ppm)	6.71	8.12	11.34	7.94	10.18	9.58	3.62
Be	1.44	14.50	7.33	18.41	9.91	5.44	18.63
Sc	20.35	15.87	8.75	22.32	14.70	14.22	16492
Ti	10633	14445	14253	13247	15759	18037	17334
V	185.28	191.43	310.94	204.44	175.43	179.05	238.31
Cr	355.81	48.05	243.44	347.89	202.34	60.09	286.66
Co	55.13	186.77	151.23	53.72	59.09	237.82	56.48
Ni	256.43	55.84	41.56	69.99	125.88	54.57	218.38
Cu	57.19	103.82	24.31	96.31	106.85	166.02	72.72
Zn	99.74	24.31	21.50	18.32	19.69	124.38	117.64
Ga	16.35	14.87	11.90	20.79	17.27	19.53	21.71
Rb	26.83	24.61	23.76	21.39	21.02	10.54	26.02
Sr	359.96	777.57	1272.34	588.24	670.51	1312.84	859.88
Y	21.11	24.61	189.25	21.39	23.96	27.03	22.85
Zr	138.32	250.27	363.66	172.05	277.15	399.95	236.33
Nb	26.11	65.49	94.59	42.50	91.83	127.00	68.74
Mo	2.36	5.80	6.02	2.28	6.54	0.03	3.95
Cd	0.05	0.07	0.08	0.04	0.02	2.84	0.08
Sn	1.73	3.60	3.03	1.88	3.23	3.99	2.52
Sb	0.09	0.20	0.09	0.09	0.04	0.13	0.07
Cs	0.66	0.34	0.32	0.44	0.06	0.27	0.26
Ba	190.59	253.01	211.15	255.50	227.37	279.34	338.96
La	17.92	40.91	64.82	26.43	49.82	277.43	43.96
Ce	37.35	103.09	123.25	53.21	48.45	111.23	86.30
Pr	4.55	9.64	15.14	6.51	11.53	13.39	10.79
Nd	18.32	37.28	58.99	25.98	45.80	52.87	41.86
Sm	4.36	7.81	11.69	5.66	9.56	8.28	8.28
Eu	1.49	2.49	3.52	1.85	3.00	4.21	2.69
Gd	4.39	7.27	9.85	5.44	8.47	12.04	7.52
Tb	0.7	1.03	1.31	0.81	1.14	3.23	1.04
Dy	3.7	5.01	5.47	4.12	5.16	9.41	4.85
Ho	0.75	0.90	1.08	0.77	0.84	1.26	0.83
Er	2.01	2.15	1.78	1.94	1.87	5.97	1.86
Yb	1.61	1.59	1.08	1.37	1.14	0.98	1.31
Lu	0.22	0.21	0.13	0.22	0.14	2.22	0.17
Hf	3.91	5.32	7.30	4.68	5.67	2.38	5.09
Ta	2.15	3.66	5.97	3.75	5.46	0.18	3.96
W	0.41	0.13	0.57	0.27	0.72	8.55	0.59
Pb	3.41	2.49	3.72	2.54	0.44	8.10	2.59
Bi			6				
Th	3.51	4.36	6.61	3.48	6.15	1.04	4.88
U	1.01	1.63	2.85	1.05	2.18	3.06	1.54

Element (XRF)	R005379	R005368	R005410	R005353	R010192	R010187	R010186	R004332	R004366	R004367	R004368	R027027	R010201	R010204
Li (ppm)	18	21	16	16	18	10	18	15	18	18	17	21	12	24
Sc	197	225	196	203	195	140	210	196	190	188	205	220	185	210
V	346	291	161	242	210	350	330	285	459	330	332	320	320	340
Cr	54	52	49	44	49	56	56	72	69	72	70	54	66	52
Co	257	223	171	201	210	330	260	239	372	226	278	290	330	290
Ni	45	63	50	39	41	23	59	61	45	49	37	130	31	64
Cu	92	98	116	116	115	23	110	125	103	97	120	101	175	92
Zn	<20	20	23	22	25	28	16	25	19	20	20	<20	21	20
Ga	360	580	750	1020	830	1350	610	1243	1192	762	1160	850	1350	340
As	66	23	<20	25	24	68	19	26	27	23	26	77	27	34
Rb	140	165	225	300	200	280	140	320	203	182	287	200	300	92
Sr	27	35	53	72	61	84	39	81	62	41	96	53	110	56
Y	<5	<5	<9	<9	5	7	<5	5	<5	<5	5	10	<5	<5
Nb	35	31	45	61	40	61	30	59	38	35	57	75	79	33
Ba	175	190	216	215	220	190	240	280	245	239	267	530	280	340
La	<20	<20	<20	45	29	68	<20	45	27	<20	33	77	58	34
Ce	41	54	77	123	88	155	73	125	102	70	134	145	180	92
Pb	35	<10	13	<10	13	13	15	<10	<10	12	<10	<10	13	<10
Th	11	<10	<10	<10	<10	<10	6	<10	19	12	22	<10	13	13
U	<10	<10	<10	<10	<10	<10	<10	<10	<10	<10	<10	<10	<10	<10

12

Table 3. continued...

	R005506	R005508	R004501	R010205	R010205	R010218	R010218	R010044	R010044	R010093	R010093	G402497	G402497	R010076	R010076	R010159	R010159
MRT Reg No	R005506	R005508	R004501	R010205	R010205	R010218	R010218	R010044	R010044	R010093	R010093	G402497	G402497	R010076	R010076	R010159	R010159
Field No	SB9	SB11	LSB24	LCr	LCr	ATR	ATR	BRJ1	BRJ1#	HBJ23	HBJ23	GFN	GFN	HBJ6	HBJ6/2	SBA21	SBA21#
Lab	MRT	MRT	MRT	MRT	MU	MRT	MU	MRT	MU	MRT	MU	MRT	MU	MRT	MRT	MRT	MU
Analysis No.	910719	910721	910352	970028		970040		970027		970024		970026		961031	961032	980456	
SiO2 (wt%)	51.17	42.17	43.77	42.33	42.20	38.75	38.63	51.87	52.17	52.04	51.74	44.37	43.90	46.64	47.12	48.78	48.65
TiO2	1.66	2.38	2.39	2.72	2.83	2.88	2.91	1.68	1.71	1.57	1.60	2.39	2.53	2.39	2.23	2.23	1.30
Al2O3	13.78	9.90	11.92	10.56	11.51	11.12	11.02	13.58	13.58	14.16	13.98	12.78	12.97	12.88	12.69	14.59	14.47
Fe2O3	1.06	3.12	5.96	5.80	5.84	3.83	3.90	0.78	1.24	1.71	1.78	3.83	3.91	3.98	3.90	1.32	1.77
FeO	10.59	10.65	7.30	6.78	6.40	9.49	9.13	9.88	9.40	9.10	8.69	9.43	9.21	8.27	8.27	9.81	9.46
MnO	0.16	0.22	0.22	0.20	0.19	0.23	0.22	0.15	0.16	0.16	0.15	0.22	0.22	0.16	0.16	0.17	0.17
MgO	7.62	14.56	8.57	12.98	12.69	11.44	11.46	8.55	8.55	7.58	8.69	11.25	10.83	10.18	10.46	9.51	9.35
CaO	9.19	8.17	8.46	9.64	9.72	14.24	14.23	8.66	8.55	9.15	9.03	9.57	9.62	6.92	6.79	9.56	9.59
Na2O	2.91	3.68	3.36	3.68	3.67	3.79	3.83	2.81	2.76	2.78	2.74	3.05	3.37	3.41	3.68	2.67	2.84
K2O	0.68	1.99	2.81	1.87	1.87	1.56	1.57	0.92	0.92	0.63	0.62	1.46	1.49	2.00	1.95	0.29	0.29
P2O5	0.27	1.84	1.72	1.23	1.33	1.04	1.10	0.31	0.25	0.26	0.21	0.76	0.81	0.94	0.94	0.28	0.27
H2O+	1.07	1.69	2.89	1.75	0.86	1.65	0.31	0.78	0.85	0.89	0.63	1.03	1.20	1.51	1.21	1.07	1.42
H2O-	nd	nd	nd	nd	0.03	nd	0.22	nd	0.07	nd	0.23	nd	0.10	nd	nd	nd	nd
CO2	0.09	0.17	0.11	0.10	–	0.22	–	0.08	–	0.21	–	0.09	–	0.13	0.09	0.15	0.54
SO3	0.09	0.04	0.03	0.10	–	0.24	–	0.14	–	0.17	–	0.11	–	0.07	0.07	0.08	0.16
FeS2	0.03	0.06	nd	nd	nd	nd	nd	nd	nd	nd	nd	nd	nd	nd	nd	nd	nd
TOTAL	100.37	100.64	99.51	99.73	101.12	100.47	100.19	100.20	100.47	100.41	99.94	100.34	100.47	99.35	99.56	99.53	100.28
LOI*	–	0.71	–	1.10	–	0.82	–	-0.24	–	0.09	–	0.07	–	–	0.13	0.13	–
FeOtot	11.54	13.46	12.66	12.00	11.65	12.93	12.64	10.58	10.52	10.64	10.29	12.88	12.73	11.85	11.78	11.00	11.05
Mg#(0.20)	58.13	69.47	58.74	69.46	69.61	65.03	65.60	62.95	63.68	59.99	60.03	64.76	64.15	64.37	65.13	64.51	64.02

CIPW norms calculated at Fe2O3/FeO = 0.20

	R005506	R005508	R004501	R010205	R010205	R010218	R010218	R010044	R010044	R010093	R010093	G402497	G402497	R010076	R010076	R010159	R010159
Q	–	–	–	–	–	–	–	0.05	0.63	1.68	2.40	–	–	–	–	–	–
or	4.05	11.92	17.27	11.33	11.29	–	–	5.49	5.47	3.75	3.74	8.71	8.92	12.12	11.75	1.74	1.75
ab	24.82	7.28	13.37	4.04	4.17	–	–	23.91	23.50	23.70	23.68	12.21	10.80	24.87	25.46	22.95	24.48
an	22.71	4.68	9.51	6.96	9.61	8.89	8.42	21.89	22.08	24.51	24.53	17.06	16.07	14.29	12.59	27.46	26.36
lc	–	–	–	–	–	7.35	7.43	–	–	–	–	–	–	–	–	–	–
ne	–	–	8.77	15.12	14.92	17.68	17.94	–	–	–	–	7.50	9.80	2.56	3.41	–	–
di	17.58	13.15	18.34	27.28	24.74	22.87	23.19	15.72	15.41	15.98	16.19	21.01	21.83	11.86	12.56	15.39	16.52
hy	23.10	19.52	–	–	–	–	–	26.36	26.45	24.11	23.26	–	–	–	–	15.81	12.21
ol	1.05	31.12	20.57	23.97	23.66	23.30	22.98	–	–	–	–	23.92	22.62	24.63	24.68	10.80	12.76
cs	–	–	–	–	–	8.62	8.57	–	–	–	–	–	–	–	–	–	–
mt	2.86	3.35	3.24	3.03	2.93	3.24	3.17	2.62	2.60	2.64	2.58	3.20	3.17	2.99	2.95	2.75	2.77
il	3.18	4.58	4.72	5.30	5.49	5.56	5.65	3.22	3.27	3.00	3.10	4.58	4.87	4.40	4.32	2.43	2.51
ap	0.64	4.40	4.22	2.97	3.20	2.50	2.65	0.74	0.59	0.62	0.51	1.81	1.94	2.27	2.26	0.67	0.65
total	100.00	100.00	100.00	100.00	100.00	100.00	100.00	100.00	100.00	100.00	100.00	100.00	100.00	100.00	100.00	100.00	100.00
An%plag	46.30	37.71	40.13	61.88	68.48	100.00	100.00	46.31	46.97	49.36	49.40	56.84	58.38	35.13	31.79	52.99	50.37
Type	OT	NH-2B	NH-1A	ON-1	ON-1	OML	OML	Q	Q	Q	Q	BSN-1	BSN-1	HW-B	HW-B	OT	OT

Trace elements (XRF at MRT, ICPMS at MU)

	SB9 (ICPMS)	SB9 (RPT)	SB11 (XRF)	LSB24 (ICPMS)	LCr (XRF)	LCr (ICPMS)	ATR (XRF)	ATR (ICPMS)	BRJ1 (XRF)	BRJ1 (ICPMS)	HBJ23 (XRF)	HBJ23 (ICPMS)	GFN (XRF)	GFN (ICPMS)	HBJ6 (XRF)	HBJ6/2 (ICPMS)	SBA21 (XRF)	SBA21 (ICPMS)
Li (ppm)	6.5	6.74	–	7.80	–	11.57	–	9.04	–	7.28	–	5.27	–	8.27	–	5.59	–	7.46
Be	2.3	2.77	–	4.90	–	6.16	–	3.10	–	1.70	–	1.20	–	2.60	–	0.80	–	3.62
Sc	23.4	25.00	11	12.85	14	11.17	17	20.18	19	23.77	24	23.89	20	19.26	13	12	29	15.1
Ti	16633.6	14253	11056	14239	15719	14751	16013	16703	11155	11155	10187	10187	13907	13907	15231	15231	8814	8814
V	195.81	207.08	123	107.73	150	154.45	250	246.11	165	179.13	180	172.86	175	168.92	120	120	180	192.49
Cr	432.69	391.41	623	600.92	510	512.81	220	225.95	250	313.67	230	231.59	320	297.97	390	410	370	397.01
Co	49.94	52.98	64	45.07	55	51.41	63	55.48	47	51.74	47	49.11	56	52.41	47	55	49	52.71
Ni	262.54	191.67	594	405.57	480	380.20	230	172.73	150	157.80	120	124.42	320	262.14	520	540	250	480.44
Cu	66.66	59.54	77	40.27	35	52.81	71	74.98	110	42.62	33	47.13	46	60.33	80	83	100	104.6
Zn	86.06	84.91	186	161.30	165	150.52	140	115.58	110	103.14	115	101.54	115	101.77	150	155	100	147.84
Ga	15.46	16.10	21	22.58	26	21.74	21	18.89	20	18.56	21	19.29	20	17.92	24	27	20	22.56
As	28.01	<20	<20	<20	<20	<20	<20	<20	<20	<20	<20	<20	<20	<20	<20	<20	<20	<20
Rb	34.13	27	48	45.09	62	63.48	46	44.37	28	27.41	20	16.71	45	41.03	42	34	11	39.2
Sr	733.03	767.60	42	1330.90	1450	1675.03	1150	1083.12	290	291.19	260	258.97	830	801.60	1050	1050	360	946.24
Y	27.95	28.98	42	105.98	94	122.97	70	71.61	22	22.29	22	23.37	27	56.81	56	34	21	36.74
Zr	233.46	248.67	572	199.12	400	234.63	185	134.02	110	126.90	96	109.66	230	286.26	400	400	105	407.87
Nb	91.92	64.07	97	25.92	125	31.28	115	15.91	17	17.80	11	12.31	73	13.67	74	73	15	105.63
Mo	3.83	2.58	13	3.97	<5	3.15	5	1.39	<5	1.59	<5	1.53	<5	3.49	6	6	<5	6.58
Cd	0.06	2.01	1.27	0.12		0.12		0.03		0.06		0.05		0.07				0.06
Sn	2.87	2.35	<9	5.41	<9	6.92		2.69		1.86		1.49		3.45	<9			5.32
Sb	0.12	0.10	0.03	0.21		0.19		0.12		0.04		0.02		0.14				0.18
Cs	0.29	0.22	0.94	1.11		0.88		0.56		1.15		0.54		0.60				0.4
Ba	335.74	363.69	708	681.11	620	846.92	560	603.80	125	142.79	110	110.21	410	421.30	520	520	180	559.87
La	38.14	39.99	105	105.98	94	122.97	70	71.61	13.99	13.99	10.46	10.46	56.81	56.81	57	57	14.42	64.72
Ce	75.36	76.71	238	199.12	210	234.63	170	134.59	32	30.53	28	23.24	135	109.87	150	150	31	131.03
Pr	8.96	9.44	–	25.92	–	31.28	–	15.91	–	3.89	–	3.15	–	13.67	–	–	–	17.65
Nd	35.13	35.99	123	101.37	88	122.35	68	59.76	<20	16.82	<20	13.98	47	51.53	73	67	<20	66.83
Sm	7	7.18	–	19.73	–	24.04	–	11.39	–	4.33	–	3.92	–	9.57	–	13.95	–	13.95
Eu	2.3	2.30	–	5.91	–	7.29	–	3.52	–	1.44	–	1.40	–	2.95	–	4.32	–	4.32
Gd	6.43	6.70	–	17.01	–	21.12	–	9.65	–	4.68	–	4.33	–	8.42	–	12.44	–	12.44
Tb	0.97	0.97	–	2.30	–	2.83	–	1.34	–	0.74	–	0.70	–	1.21	–	1.72	–	1.72
Dy	5.21	5.30	–	10.48	–	12.59	–	6.05	–	4.15	–	4.03	–	5.97	–	7.79	–	7.79
Ho	1.03	1.00	–	1.74	–	2.09	–	1.06	–	0.77	–	0.81	–	1.12	–	1.36	–	1.36
Er	2.69	2.73	–	3.77	–	4.62	–	2.46	–	2.03	–	2.16	–	2.82	–	3.15	–	3.15
Yb	2.15	2.24	–	2.46	–	2.87	–	1.65	–	1.71	–	1.70	–	2.07	–	2.21	–	2.21
Lu	0.31	0.32	–	0.30	–	0.35	–	0.22	–	0.24	–	0.24	–	0.29	–	0.26	–	0.26
Hf	4.91	5.01	–	13.31	–	17.67	–	5.43	–	3.22	–	2.68	–	6.04	–	9.62	–	6.85
Ta	6.7	3.75	–	7.98	–	9.46	–	6.91	–	1.13	–	0.73	–	4.76	–	–	–	2.85
W	0.75	0.43	<10	4.41	<10	1.84	<10	0.11	<10	0.88	<10	0.48	<10	1.11	<10	<10	<10	0.43
Pb	2.62	4.19	<10	6.73	16	7.72	6	3.65	18	3.33	17	2.39	13	5.79	5	<5	10	4.71
Bi	–	–	<5	–	6	–	6	–	<5	–	<5	–	5	–	<5	<5	<5	–
Th	5.06	5.30	<10	16.22	19	13.30	13	10.21	<10	2.44	<10	1.63	10	7.08	<10	<10	13	8.28
U	1.45	1.53	<10	4.49	<10	3.80	<10	2.74	<10	1.28	<10	0.89	<10	2.14	<10	<10	<10	2.36

4.5 Data reduction

Apparent $^{40}Ar/^{39}Ar$ ages were calculated from the corrected isotopic ratios using decay constants given by Steiger and Jäger (1977). One standard deviation, intra-laboratory uncertainties in each apparent age is reported. The full numerical analytical data are presented in Appendix 4, and the apparent age, Ca/K and Cl/K spectra and the $^{36}Ar/^{40}Ar-^{39}Ar/^{40}Ar$ correlation diagrams are plotted for each sample (Figures 4a - 4y). Integrated ages were computed from the sum total of the peak heights, and their errors from the square root of the sum square of the peak-height errors, for all of the temperature steps. Plateau ages were calculated by the same approach, but utilized only those contiguous steps that yielded dates, which do not differ at the 2σ level. In the $^{36}Ar/^{40}Ar-^{39}Ar/^{40}Ar$ correlation diagrams, the cubic least-squares fitting scheme outlined by York (1968) was employed to regress the data. The regression line yields two intercepts; the inverse of the $^{39}Ar/^{40}Ar$ intercept produces a so-called intercept date, whereas the inverse of the $^{36}Ar/^{40}Ar$ intercept indicates the composition of a non-radiogenic argon component.

5.0 GEOCHRONOLOGICAL RESULTS

Results, together with plateau, intercept and integrated $^{39}Ar/^{40}Ar$ ages are summarised in Table 4 and discussed below. Ages are quoted with uncertainties at 1σ unless indicated otherwise, and referred to the 2022/02 revision of the International Chronostratigraphic Chart (Cohen et al., 2013, updated 2022) and the geomagnetic polarity time scale of Ogg (2020) (Figures 5, 6).

Twenty-four samples yielded acceptable plateau ages, ranging from 16.3 ± 0.2 Ma (1σ) to 45.5 ± 1.0 Ma (1σ). The proportion of total degassed $^{39}Ar_K$ of the steps used for the plateau ages ranges from 72.4% to 98.2%, and is greater than 90% for 15 samples (Table 4; Appendix 4). For the remaining sample SBA21 (R010159), a tholeiite from Marion Bay in southeast Tasmania, the Ar release spectrum is irregular (Figure 4y) and no plateau or intercept age can be determined. However, the integrated age (64.2 ± 0.6 Ma) is consistent with local field evidence and may date this flow.

For 22 samples, the intercept and plateau ages are within 1 Myr of each other and are statistically indistinguishable at the 1σ level (Table 4; Figure 7). For sample GFN (G402497), a basanite from southern Tasmania, the difference between the plateau age (45.5 ± 1.0 Ma) and intercept age (43.4 ± 2.4 Ma) is greater but is also not statistically significant due to the relatively large uncertainties. For sample SDL (R010202), an olivine nephelinite from northeast Tasmania, the plateau age (29.4 ± 0.5 Ma) is preferred as it is similar to the integrated age (29.7 ± 0. 6 Ma), although both are significantly older than the intercept age (26.7 ± 1.2 Ma).

For 23 samples, the integrated (total fusion) ages are older than the plateau ages (Table 4; Figure 8), and for 9 samples significantly so (by 9.2 Myr in the case of sample BRJ1). Two samples (ATr and PP20.5) have integrated ages slightly less than the plateau ages.

The older integrated ages, relative to plateau ages, are perhaps unexpected, as the loss of ^{40}Ar from any low temperature secondary minerals or glass would decrease the apparent age. Inspection of the age spectra for these samples (Figures 4a, f, I, m, q, u, w, x) and the numerical data (Appendix 4) shows that the older integrated ages are attributable to anomalously old apparent ages in the lower temperature and/or the higher temperature heating steps. The apparently older ages could be due to either excess ^{40}Ar or loss of ^{39}Ar during or after irradiation.

For three samples (BRJ1, SB11 and GFN), the higher temperature steps make the principal contribution to the apparently older integrated ages. The latter two samples contain abundant xenocrysts derived from disaggregation of spinel lherzolite xenoliths, which are likely to be much older than the host rock. This could conceivably account for the older apparent ages of the high temperature steps. For SB11, the last four steps, at 1100° to 1600°C, account for 3.5% of the argon degassed, at apparent ages of 135 to 464 Ma. For GFN, the last step at 1600°C accounts for 7.4% of the argon degassed, at an apparent age of 122 Ma (Appendix 4). However, spinel lherzolite will contain very little K, and several other samples with abundant lherzolite debris (e.g. TJ3228, WSc, SDL and BLS) do not show anomalously old ages in the final degassing steps. Furthermore, sample BRJ1, for which the final four heating steps at temperatures of 1200 - 1600°C degassed 1.6% of its argon with apparent ages of 109 to 826 Ma, is a tholeiite lacking mantle (or other) xenoliths.

For six samples (AJ1424, SRN, TJ3591, HBJ6, TJ3602 and WSc) the main contribution to the older integrated ages is from lower temperature steps, in each case accounting for only a few per cent of degassing, but with apparent ages of >100 Ma. As ^{40}K in these samples is likely to be contained in fine- to very fine-grained groundmass phases, the old apparent old ages could conceivably be attributed to redistribution or loss of neutron-generated ^{39}Ar due to recoil (e.g. McDougall and Harrison, 1988, p. 118). However, several other samples with a very fine-grained groundmass do not show old ages of low temperature steps. Another possible explanation is incorporation of excess radiogenic ^{40}Ar of uncertain origin into low temperature phases.

Recalculation of the integrated ages using the remaining heating steps (>70% and commonly >90% of degassed argon) brings them into close agreement with the plateau ages, as expected.

Table 4. Summary of geochronological results.

Uncertainties quoted at 1σ

Field No	Reg No	Rock Type	Location	Plateau age	°C	gas fraction	Intercept age	$(^{40}Ar/^{36}Ar)_0$	MSWD	Integrated age	Polarity
TJ3602	R005376	hawaiite	Wedge Plains Link Road	**27.0 ± 0.3 Ma**	900-1400	0.955	26.3 ± 1.8 Ma	329.9 ± 50.1	1.967	29.1 ± 0.4 Ma	+
TJ3591	R005365	trans. olivine basalt	Rabalga Track	**34.3 ± 0.3 Ma**	900-1120	0.860	33.9 ± 0.9 Ma	306.1 ± 25.6	2.292	39.0 ± 0.4 Ma	**+?**
KJ634	R005410	basanite	Eastons Ck, lower flow	**25.4 ± 0.2 Ma**	680-1600	0.947	25.0 ± 0.5 Ma	319.2 ± 13.3	3.417	25.8 ± 0.1 Ma	-
TJ3228	R005353	nepheline hawaiite	Knoll, Neasey Plains	**21.4 ± 0.2 Ma**	600-1600	0.972	21.4 ± 0.6 Ma	313.7 ± 26.0	2.474	21.5 ± 0.2 Ma	+
CVH	R010192	nepheline hawaiite	Coastview Hill, via Hampshire	**21.5 ± 0.2 Ma**	600-1600	0.982	21.4 ± 0.4 Ma	321.5 ± 21.8	1.875	22.0 ± 0.2 Ma	**-?**
SRN	R010187	basanite	South Riana plug	**22.0 ± 0.3 Ma**	840-1200	0.779	22.8 ± 0.5 Ma	285.9 ± 6.9	0.912	28.2 ± 0.3 Ma	**+??**
LLC	R010186	alkali olivine basalt	Lillicos Beach, via Devonport; lower flow	**37.5 ± 0.2 Ma**	680-1400	0.909	37.7 ± 0.4 Ma	293.9 ± 14.6	3.218	38.1 ± 0.2 Ma	**+??**
AJ99	R004332	olivine nephelinite	Olivers Hill, via Ringarooma	**17.5 ± 0.2 Ma**	600-1400	0.965	17.1 ± 0.3 Ma	307.6 ± 14.4	1.819	18.5 ± 0.2 Ma	+
AJ1424	R004366	basanite	northern hill, via Sweets Creek, Upper Esk	**17.5 ± 0.2 Ma**	500-1020	0.790	17.5 ± 0.2 Ma	292.3 ± 1.7	1.356	25.4 ± 0.2 Ma	-
AJ1425	R004367	hawaiite	southern hill, via Sweets Creek, Upper Esk	**16.3 ± 0.2 Ma**	750-1300	0.793	16.2 ± 0.3 Ma	317.2 ± 26.9	1.860	17.7 ± 0.2 Ma	-
AJ1426	R004368	olivine nephelinite	Upper Esk	**16.8 ± 0.4 Ma**	500-1100	0.834	16.0 ± 0.6 Ma	299.1 ± 3.0	1.392	17.1 ± 0.3 Ma	**-?**
PP20.5	R027027	olivine nephelinite	Pebble Plain DDH/20.5m, via Beauty Flat	**41.0 ± 0.2 Ma**	680-1200	0.796	40.8 ± 0.6 Ma	298.9 ± 26.4	2.160	39.7 ± 0.2 Ma	-
WSc	R010201	olivine nephelinite	Sledge Track, W Scottsdale	**34.2 ± 0.4 Ma**	1020-1300	0.724	33.6 ± 1.3 Ma	308.3 ± 43.0	1.983	37.6 ± 0.6 Ma	**+?**
SDL	R010202	olivine nephelinite	The Sideling (Knockup), via Weelaty	**29.4 ± 0.5 Ma**	900-1600	0.905	26.7 ± 1.2 Ma	317.2 ± 13.8	2.266	29.7 ± 0.6 Ma	+
BLS	R010204	basanite	Blessington plug	**36.8 ± 0.2 Ma**	850-1600	0.935	36.5 ± 0.4 Ma	344.1 ± 37.6	0.906	38.5 ± 0.2 Ma	+
SB9	R005506	olivine tholeiite	"Eastbourne", via Avoca	**29.6 ± 0.6 Ma**	500-1300	0.968	29.3 ± 0.8 Ma	302.2 ± 5.8	2.701	29.8 ± 0.5 Ma	**-?**
SB11	R005508	nepheline hawaiite	Llewellyn, via Conara	**30.3 ± 0.2 Ma**	450-960	0.930	29.6 ± 0.5 Ma	336.2 ± 35.0	3.095	38.5 ± 0.1 Ma	**-?**
LSB24	R004501	nepheline hawaiite	Burburys Sugarloaf, via Ross	**27.3 ± 0.1 Ma**	700-1400	0.938	27.3 ± 0.2 Ma	292.1 ± 14.1	1.888	27.8 ± 0.1 Ma	**-?**
LCr	R010295	olivine nephelinite	W side of Lake Crescent	**29.4 ± 0.2 Ma**	600-1400	0.946	29.4 ± 0.4 Ma	312.1 ± 39.6	2.619	29.7 ± 0.2 Ma	**+??**
ATr	R010218	olivine melilitite	Alma Tier, via Interlaken	**36.5 ± 0.2 Ma**	650-1300	0.908	36.7 ± 0.7 Ma	292.7 ± 13.6	1.858	35.9 ± 0.2 Ma	**?**
BRJ1	R010055	quartz tholeiite	Crooked Billet Creek, Brighton	**26.7 ± 0.3 Ma**	450-840	0.904	26.7 ± 0.4 Ma	293.1 ± 10.2	1.072	35.9 ± 0.3 Ma	**-?**
HBJ23	R010093	quartz tholeiite	Dragon Point, Claremont	**25.1 ± 0.3 Ma**	500-1400	0.934	24.9 ± 0.8 Ma	295.9 ± 3.5	2.087	26.1 ± 0.3 Ma	-
GFN	G402497	basanite	Glenfern	**45.5 ± 1.0 Ma**	760-1400	0.862	43.4 ± 2.4 Ma	301.9 ± 7.5	1.458	52.3 ± 0.9 Ma	**?**
HBJ6	R010076	hawaiite	Pickett Hill, via Kingston	**29.4 ± 0.2 Ma**	950-1400	0.831	28.6 ± 0.8 Ma	317.1 ± 75.6	5.447	33.8 ± 0.1 Ma	+
SBA21	R010159	olivine tholeiite	quarry, Marion Bay							**64.2 ± 0.6 Ma**	**-?**

Figure 4 (a-y). Results of step heating experiments for each sample: apparent age, Ca/K and Cl/K versus fraction of $^{39}Ar_K$ released, and $^{36}Ar/^{40}Ar$ versus $^{39}Ar/^{40}Ar$ correlation diagram.

Figure 4 cont.

17

(j) Sweets Creek, southern hill AJ1425 whole rock

750-1300 °C
Intercept age = 16.2 ± 0.3 Ma
$(^{40}Ar/^{36}Ar)_0$ = 317.2 ± 26.9
MSWD = 1.860

Integrated age = 17.7 ± 0.2 Ma
16.3 ± 0.2 Ma

(i) Sweets Creek, northern hill AJ1424 whole rock

500-1020 °C
Intercept age = 17.5 ± 0.2 Ma
$(^{40}Ar/^{36}Ar)_0$ = 292.3 ± 1.7
MSWD = 1.356

Integrated age = 25.4 ± 0.2 Ma
17.5 ± 0.2 Ma

(l) Pebble Plain (Beauty Flat) PP20.5 whole rock

680-1200 °C
Intercept age = 40.8 ± 0.6 Ma
$(^{40}Ar/^{36}Ar)_0$ = 298.9 ± 26.4
MSWD = 2.160

Integrated age = 39.7 ± 0.2 Ma
41.0 ± 0.2 Ma

(k) Upper Esk AJ1426 whole rock

500-1100 °C
Intercept age = 16.0 ± 0.6 Ma
$(^{40}Ar/^{36}Ar)_0$ = 299.1 ± 3.0
MSWD = 1.392

Integrated age = 17.1 ± 0.3 Ma
16.8 ± 0.4 Ma

Figure 4 cont.

18

Figure 4 cont.

Figure 4 cont.

20

Figure 4 cont.

Figure 4 concluded.

Figure 5. New ^{40}Ar/^{39}Ar ages (2σ error bars) plotted on the chronostratigraphic time scale (Cohen et al. 2013, updated 2022) and geomagnetic polarity time scale (black, normal; white, reversed)(Ogg, 2020) for the Cenozoic era. Time scale ages in brackets are from Ogg (2020) where they differ from Cohen et al. (2022).

Figure 6. Detail of Figure 8 for 15 – 38 Ma.
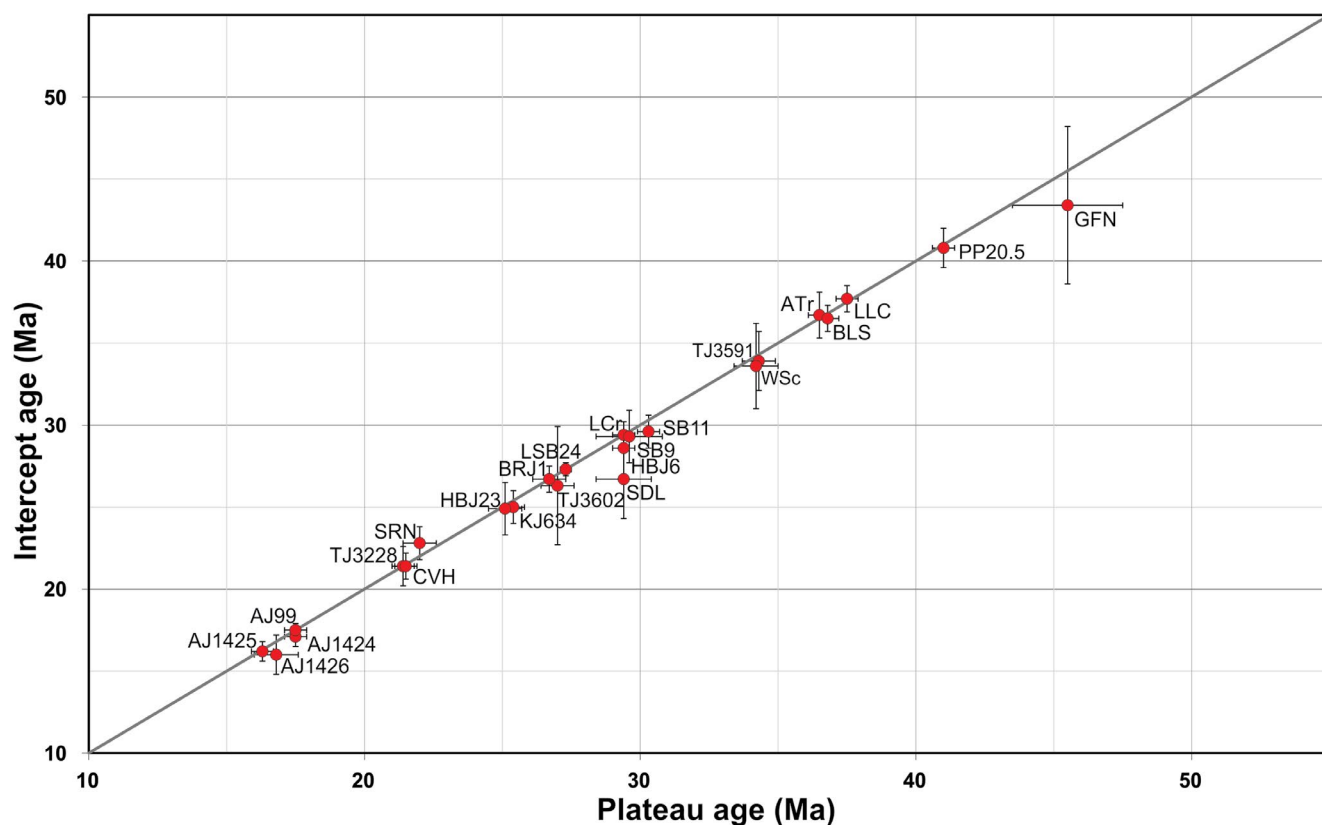
Figure 7. Plot of intercept ages versus plateau ages, with 2σ error bars shown.
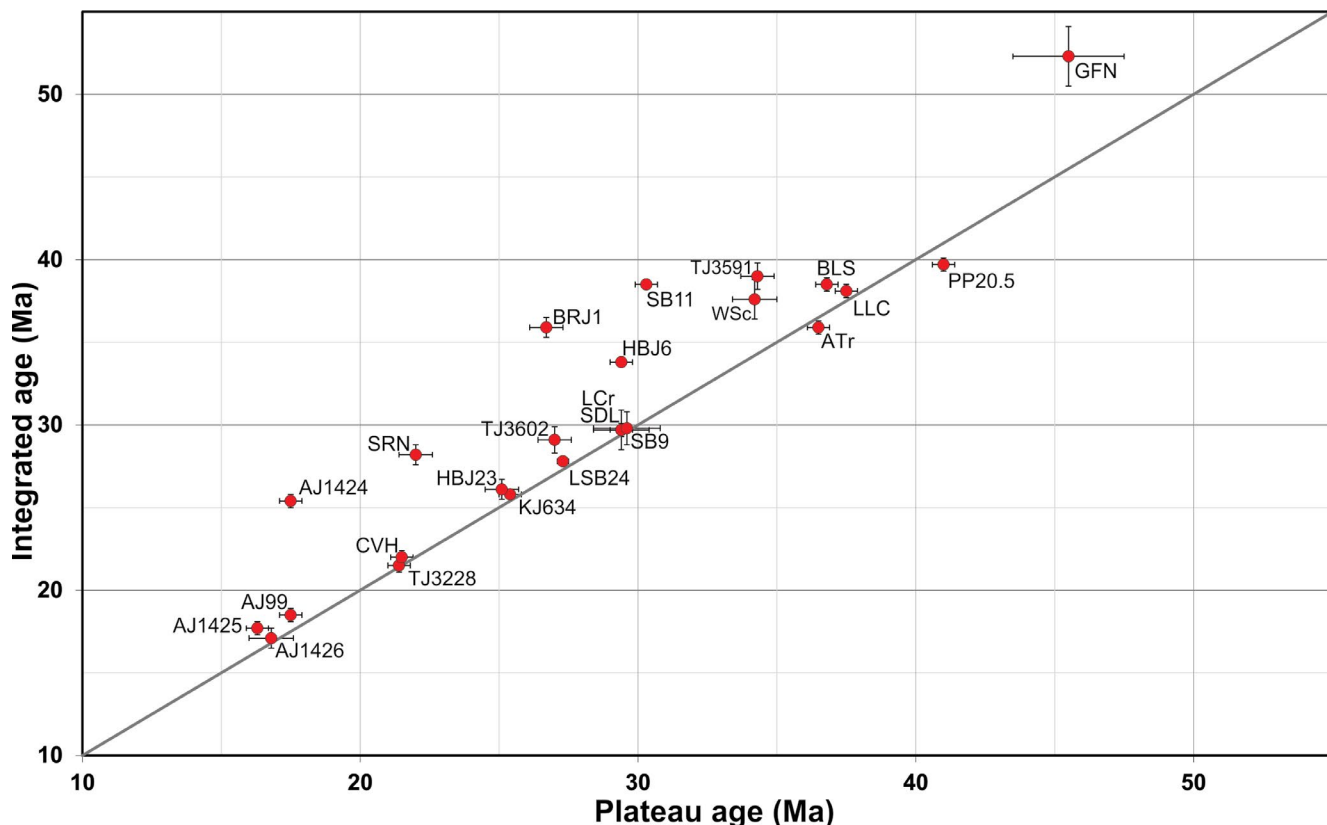
Figure 8. Plot of integrated ages versus plateau ages, with 2σ error bars shown.

As the integrated ages are analogous to K/Ar ages, the older integrated ages may have implications for the interpretation of K/Ar ages in altered rocks, which are commonly regarded as minimum ages due to the possibility of loss of ^{40}Ar. It may be that excess (inherited) ^{40}Ar is a more common source of error.

6.0 DISCUSSION

The 24 new plateau ages (16.3 – 45.5 Ma), together with the integrated age of 64.2 Ma, define a median of 29.4 Ma. Four ages are identical or very close to this median. This compares to a range of 8.5 – 61.7 Ma, with a median of 24.8 Ma, from 56 previously published K/Ar dates. However, several of the latter were regarded as minimum ages (e.g. Gibson, 2007; Everard et al., 2014).

The early Paleocene integrated age of 64.2 ± 0.6 Ma of a tholeiite from Marion Bay is the oldest in this dataset, and exceeds a 58.5 Ma K/Ar age from a nearby basanite (Baillie, 1987). However, a poorly documented older age of 69.9 Ma (late Cretaceous, Maastrichtian) was reported from a "well-crystallised medium-grained feldspar-pyroxene rock", probably an alkali basalt, collected from Cape Portland (F. L. Sutherland, pers. comm.). The age, apparently the oldest in the province, was presented in a conference poster but is not mentioned in the accompanying abstract (Zwingmann et al., 2004).

Few large scale spatial trends with age of the basalts can be identified, either in our new ^{40}Ar/^{39}Ar data or previous, mainly K/Ar, data (Figure 2). A plot of northing against age (Figure 9) shows that all young (<20 Ma) basalt dates

are from northern Tasmania. A plot of age against easting (Figure 10) shows, together with Figure 2, that these young ages occur in two areas: along the northwest coast, ranging down to 8.5 Ma, and in the Ringarooma-Upper Esk area of northeast Tasmania at ~16-18 Ma. There are no very young ages (<15 Ma) in our new dataset. Except for a 61.7 Ma basanite from King Island (Sutherland et al., 2002), the older basalts (>40 Ma) all appear to be from the eastern half of Tasmania.

Basalt chemistry also correlates poorly with age. On a plot of SiO_2 against age (Figure 11), our new ^{40}Ar/^{39}Ar data are broadly congruent with previous data, but no clear trends are apparent.

A better measure of alkalic versus tholeiitic character is provided by the quantity ($Na_2O + K_2O - 0.37SiO_2 - 14.43$), which corresponds to the vertical distance above or below the empirical boundary defined by Macdonald and Katsura (1964) on a total alkali-silica plot (Figure 3). When plotted against age (Figure 12), our new ^{40}Ar/^{39}Ar dates also show a scattered distribution, together with previous data. However, tholeiitic basalts (with negative values), including three of our new ages, were mostly erupted in a relatively restricted time interval between ~22 Ma (Great Lake, Sutherland et al., 1973) and 30.6 Ma (Pipers River, Sutherland and Wellman, 1986). All the younger (<22 Ma) and most of the older (>31 Ma) basalts are alkalic in character. The exceptions are the Thirlstane Basalt near Port Sorell (38.1 Ma, Cromer, 1980) and our 64.2 ± 0.6 Ma sample from Marion Bay.
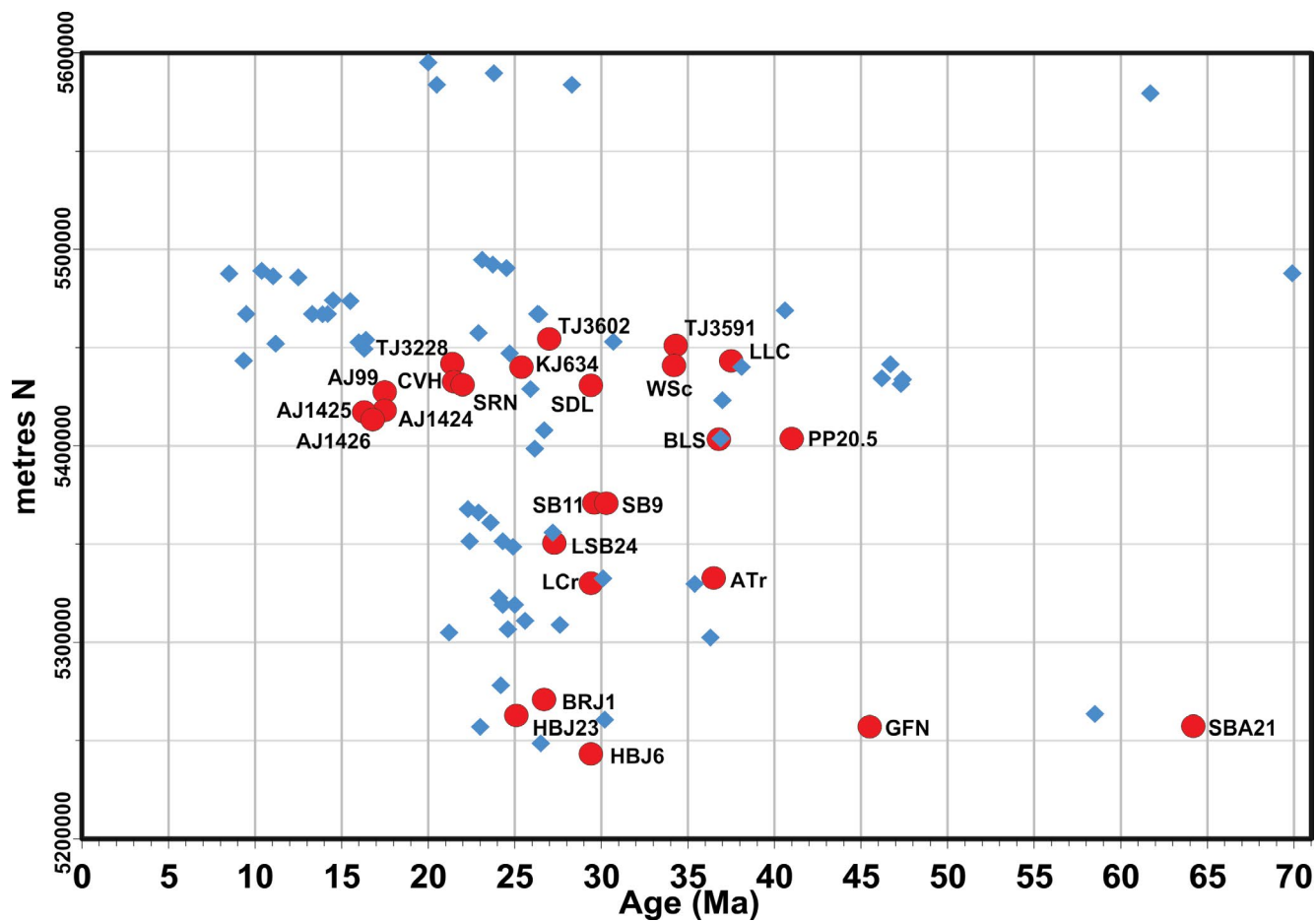
Figure 9. Plot of northing (metres north, GDA94) versus age. Red symbols, new ^{40}Ar/^{39}Ar data; blue symbols, K/Ar data (see Gibson 2007 and Everard et al. 2014 for sources).
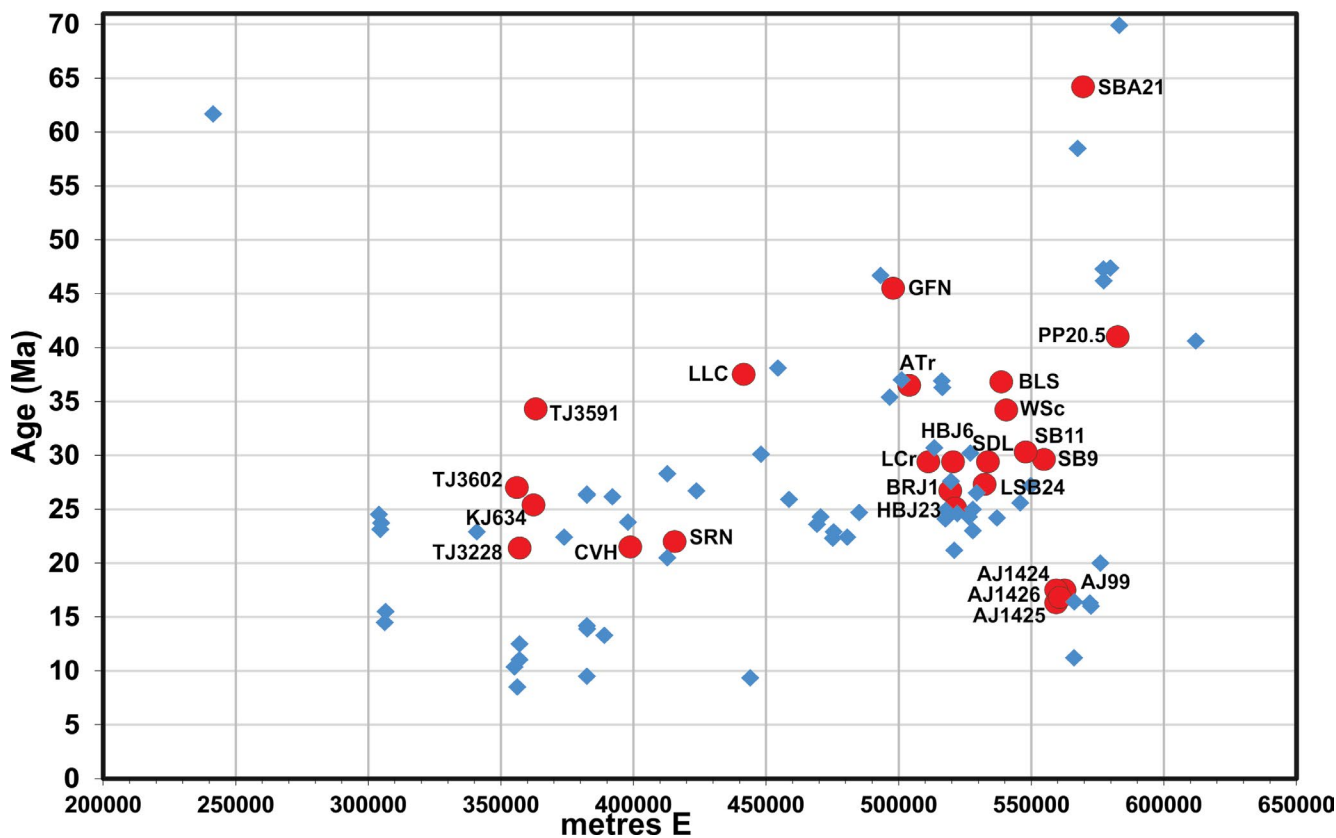
Figure 10. Plot of age versus easting (metres east, GDA94). Red symbols, new ^{40}Ar/^{39}Ar data; blue symbols, K/Ar data.
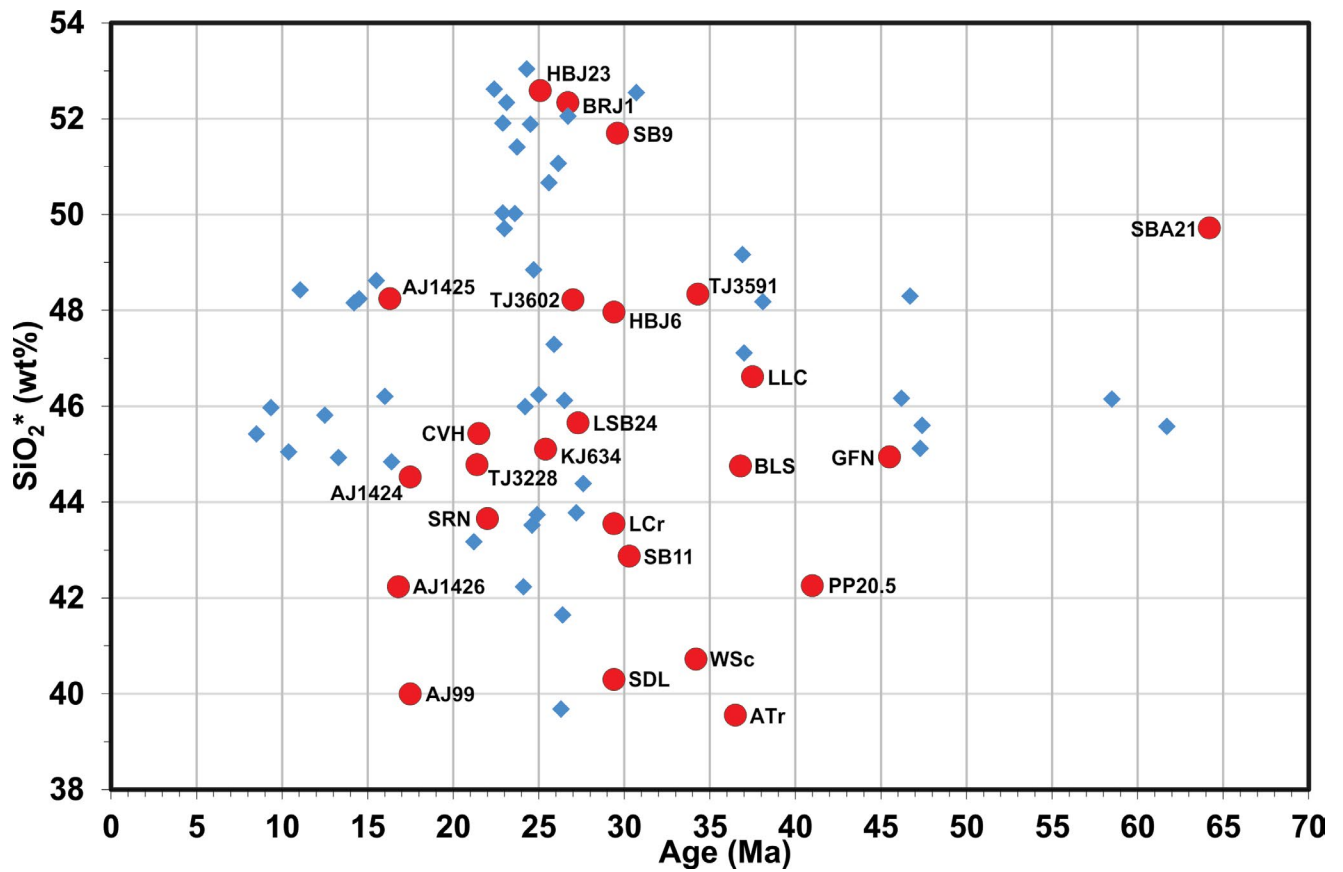
Figure 11. Plot of SiO_2 versus age. Red symbols, new $^{40}Ar/^{39}Ar$ data; blue symbols, available K/Ar data. Major element analyses normalised to 100% anhydrous. Note that corresponding whole rock analyses are not available for all previously published K/Ar dates.
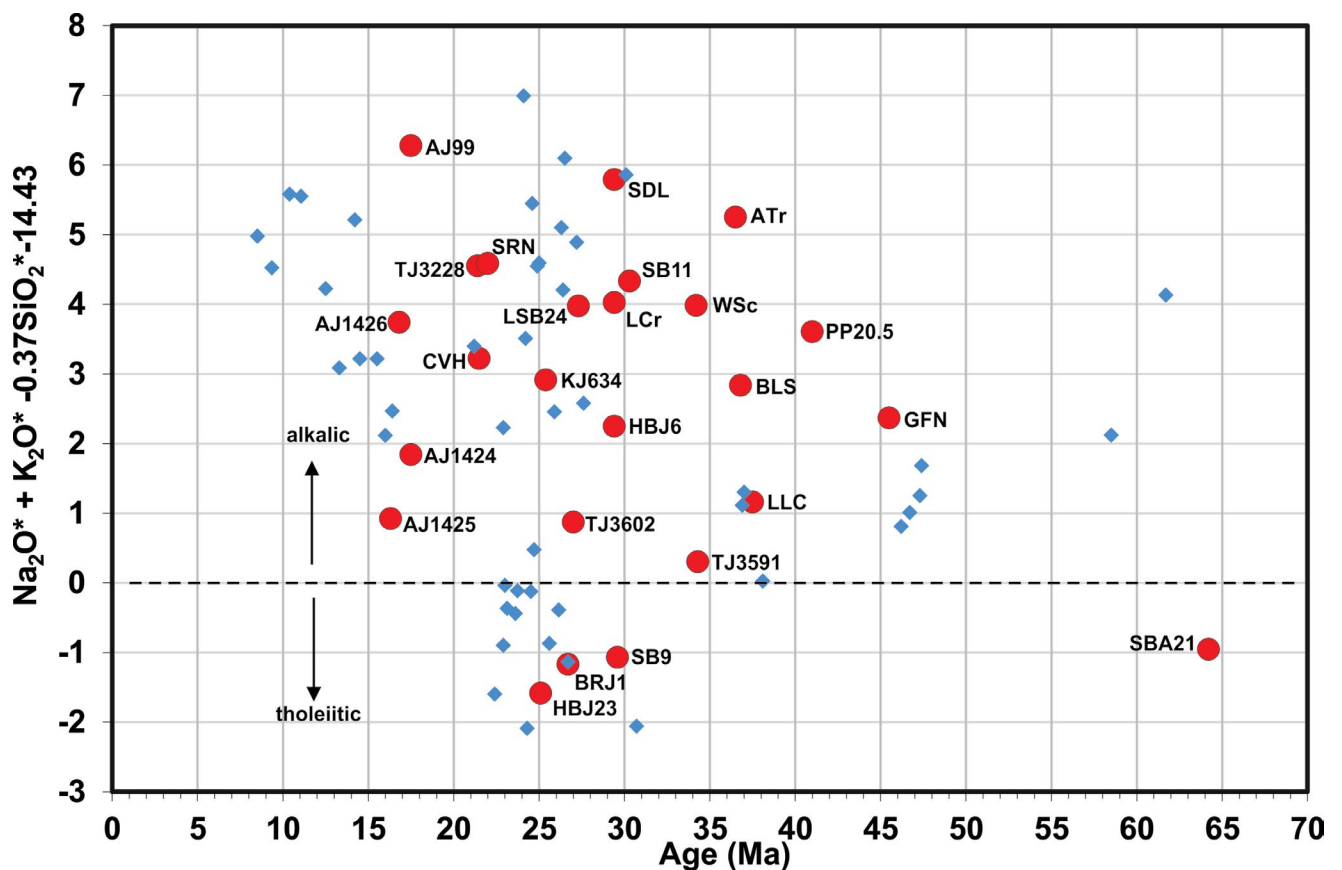
Figure 12. Plot of $(Na_2O + K_2O - 0.37SiO_2 -14.43)$ versus age. Red symbols, new $^{40}Ar/^{39}Ar$ data; blue symbols, available K/Ar data. The ordinate is graphically the vertical distance above the alkalic-tholeiitic boundary line in Figure 3.

Each of our new ^{40}Ar/^{39}Ar dates is discussed in more detail below, in a regional and local context. The regions are arbitrary and do not correspond to volcanic provinces of restricted age or characteristics, as have been defined in eastern Australia by some authors (e.g. Johnson, 1989).

6.1 Far northwest

This region is that part of Tasmania lying northwest of the Arthur Metamorphic Complex, a NE-SW trending belt up to 12 km wide and at least 100 km long of more intense deformation and metamorphism, locally up to blueschist facies. Rocks of Ordovician to Mesozoic age, apart from a few Devonian granites, are absent, and Cenozoic basalts in this region have erupted through and directly on to exposed Proterozoic, mainly Mesoproterozoic, rocks.

Some of the youngest known volcanism in Tasmania formed prominent coastal features in this region. Thus The Nut, a possible crater fill at Stanley, gave a K/Ar age of 12.5 ± 0.2 Ma and a nearby basanite at Green Hills (8.5 ± 0.1 Ma) (Baillie, 1986b). Recently these have been re-dated by the ^{40}Ar/^{39}Ar method at 11.1 ± 0.3 Ma and 10.38 ± 0.03 Ma, respectively (Fox, 2019; Fox et al., 2023). Further east, the Table Cape body is physiographically and geochemically similar to The Nut, but slightly older (13.3 ± 0.2 Ma; Sutherland & Wellman, 1986). Just west of Table Cape, Sutherland et al. (1996) dated a nepheline mugearite at 14.2 ± 0.1 Ma, but an olivine nephelinite and an olivine melilitite (Sutherland and Wellman, 1986) gave similar ages of 26.4 ± 0.2 and 26.3 ± 0.2 Ma respectively.

Further west near Marrawah, there are two dates (14.5 ± 0.2 and 15.5 ± 0.2 Ma) from the large Mt Cameron West (Preminghana) nepheline hawaiite neck (Seymour and Baillie, 1992). The volcanism at Cape Grim, however, is significantly older at ~23.1 – 25.5 Ma (Fox, 2019; Fox et al., 2023, ^{40}Ar/^{39}Ar).

Inland, extensive areas of Cenozoic basalt represent remnants of flows that probably covered much of the region. The present entrenched meanders of much of the Arthur River and its tributaries probably originally developed on flat basalt plains, and were later superimposed on to the Proterozoic basement after erosion of much of the basalt. However, away from the coast the only previously dated basalt is from a small outcrop of nepheline hawaiite near Trowutta, which gave an Early Miocene age of 22.9 ± 0.2 Ma (A. V. Brown, unpubl). A small deposit of fluvial sands near the Little Rapid River has yielded an important and diverse plant fossil assemblage of Late Oligocene age (Macphail et al., 1994; Jordan and Hill, 2002 and references therein). The sands overlie Mesoproterozoic Cowrie Siltstone and may have once been overlain by basalt, although none has been mapped in the immediate vicinity.

The four newly dated basalts are all from the middle Arthur River area, roughly between 26 and 42 km SE of Smithton, and were erupted on to Mesoproterozoic Rocky Cape Group sedimentary sequences or their metamorphosed equivalents.

6.1.1 Wedge Plains Road (TJ3602/R005376)

This hawaiite is from the western end of a flow remnant, north of the middle Arthur River and close to the watershed with Melin Rivulet, a tributary of the Dip River. The basalt rests on Mesoproterozoic Cowrie Siltstone. Its present thickness is about 20 m at the sample location, but 3 km to the east is about 50 m. The flow is associated with positive magnetic anomalies on airborne data, indicating normal polarity of magnetization.

The plateau age (27.0 ± 0.3 Ma, 1σ, Figure 4a) is Late Oligocene (Chattian) and, together with the normal polarity, is consistent with Chron C9n (26.420 – 27.439 Ma; Figure 6). The flow is therefore younger than Early Oligocene sub-basalt sediments at Little Rapid River, 12 km to the SSE (MacPhail et al., 1994b, Jordan and Hill, 2002 and references therein).

6.1.2 Rabalga Track (TJ3591/R005365)

At this locality, about 8 km ESE of the Wedge Plains sample, basalt flows 30 - 40 m thick also rest on Mesoproterozoic Cowrie Siltstone and are associated with dominantly positive magnetic anomalies. However this sample is a transitional olivine basalt with an older age of 34.3 ± 0.3 Ma (1σ, Figure 4b; latest Eocene, Priabonian). This time interval lies mainly within Chron C13r (33.726 - 35.102), but the apparent normal polarity is just compatible with the geochronological data (at 2σ) if the basalt was extruded at ~33.7 Ma, at the start of Chron C13n (Figure 6) .

There is some evidence from mapping that to the north the flow overlies an older reversely magnetized flow which may have cooled during Chron C13r. At Dip Falls, 5 km to the north, samples of the inferred older flow are compositionally hawaiite to nepheline hawaiite.

The most likely interpretation in this area is that an older hawaiite/nepheline hawaiite, erupted sometime during Chron C13r (33.726-35.102 Ma), was overlain by a transitional olivine basalt at about 33.7 Ma.

6.1.3 Eastons Creek (KJ634/R005410)

This basanite is from a flow that has partly filled the valley of Eastons Creek, a tributary of the Lyons River. The flow, at 270 m above sea level, forms a small waterfall (~5 m) in the creek and small (~10 m) cliffs of irregularly jointed basalt on the right bank. It rests on basement of Precambrian phyllite, derived from a Rocky Cape Group protolith and marginal to the Arthur Metamorphic Complex.

Aeromagnetic imagery shows that it is associated with dominantly negative anomalies and is therefore probably of reversed polarity.

Regional mapping and sampling (Everard et al., 1996) suggests that the basanite lies at the base of the volcanic sequence and has filled a palaeovalley cut into the basement of Precambrian phyllite, marginal to the Arthur Metamorphic Complex. To the south, the basanite is overlain by a sequence of dominantly hawaiitic flows, up to 100 m thick, that have locally infilled the topography to form a basalt plateau at 450 - 500 m above sea-level.

Similar basanite has been sampled, also from the base of the sequence, to the south in Pinner Creek and tributaries. A thin flow remnant at Winter Road, 7 km to the southeast, is a chemical correlate of the basal basanite.

The $^{40}Ar/^{39}Ar$ plateau age at Eastons Creek, 25.4 ± 0.2 Ma (1σ; Figure 4c) is Late Oligocene (Chattian). This time interval at 2σ (25.0 – 25.8 Ma) is of dominantly normal geomagnetic polarity (Figure 6) but overlaps with two reversed episodes, the start of C7Ar (24.766 – 25.099 Ma) and C8n.1r (25.264 – 25.304 Ma). The date also provides a maximum age for the overlying flows, which therefore could have once overlain the Early Oligocene sediments near Little Rapid River, about 10 km ENE (MacPhail et al., 1994a; Jordan and Hill, 2002).

The major flows south of the middle Arthur River are thus somewhat younger (≤ 25.3 Ma) than those to the north (27.0 to ≥ 34.3 Ma, see above).

6.1.4 Neasey Plains (TJ3228/R005353)

The dated sample is from a small, densely vegetated hill immediately west of the Savage River Pipeline Road, about 10 km south of the Arthur River and 5.5 km WNW of the Eastons Creek sample (KJ634). The rock is a nepheline hawaiite with common small lherzolite xenoliths (Figure 14). A positive aeromagnetic anomaly suggests a small plug. The extensive flows to the south are reversely magnetized and less undersaturated. The local country rock, Cowrie Siltstone, is strongly cleaved and phyllitic due to the proximity of the Arthur Lineament.

The plateau age of 21.4 ± 0.2 (1σ; Figure 4d) Ma is Early Miocene (Aquitanian). It falls, at the 95% (2σ) confidence level, within an interval of at least six field reversals and three Chrons of normal polarity (C6AAn, C6AAr.1n and C6AAr.2n; Figure 6). These cannot be resolved, but together enable the age to be slightly further refined to 21.130 – 21.722 Ma)

It is somewhat younger than 25.5 Ma basanite (sample KJ634, see above) at the base of the flows to the south, so this plug may be approximately coeval, or perhaps a little younger, than the overlying hawaiite. The date is also slightly younger than a 22.9 ± 0.2 Ma K/Ar age from a small flow remnant of hawaiite at Trowutta, 22 km to the northwest (A. V. Brown, unpublished data).

6.2 North and northwest

The voluminous basalt in this region was erupted on to a complex basement, principally of Proterozoic sedimentary sequences, Cambrian felsic volcanics, early to mid-Palaeozoic siliciclastics and limestone, and Devonian granite. Although this region contains the thickest and most extensive development of basalt in Tasmania, there are few previous constraints on its age. These include two K/Ar dates from east of Devonport, discussed below, and K/Ar date from a tholeiite near Wilmot Dam of 26.7 ± 0.6 (Macphail and Hill, 1994). There are also some palynological data on intercalated sediments, as discussed below.

The long history of volcanism in the Tamar Graben, which this report does not address, is reviewed by Sutherland et al. (2006), who provide 7 dates ranging from 24.7- 46.7 Ma.

6.2.1 Coastview Hill, Hampshire (CVH/R010192)

This small but prominent hill about 1.5 km north of Hampshire rises about 45 m above the surrounding basalt plains, and probably represents a small plug. It was mentioned as a likely eruptive centre by Edwards (1950). Rare small lherzolite xenoliths are present.

The MRT analysis (Table 3) is a nepheline hawaiite (normative plagioclase $An_{49.7}$) in the Johnson (1989) classification, whereas the slightly different analysis from Macquarie University is a basanite ($An_{50.7}$); both are basanites in IUGS nomenclature.

The surrounding mainly tholeiitic flows are probably quite thin, as Devonian granite protrudes through them a short distance to the south and east. They have not been dated, but are laterally continuous to the southwest with the thick basalt pile which has largely buried the basement topography east of Waratah. Drilling has demonstrated that there the basalt is up to 360 m thick and is intercalated with sediments in several holes. The nearest hole, WY1 located 18 km WSW of Coastview Hill, yielded an Early Oligocene microflora at depths of 79 - 114 m (Brown and Forsyth, 1984).

Aeromagnetic imagery suggests that the plug is probably reversely magnetized, but the local field is complex due to the effects of the surrounding flows.

The plateau age of the basanite, 21.5 ± 0.2 Ma (1σ, Figure 4e; early Miocene, Aquitanian) is therefore perhaps younger than expected. It suggests that the plug is a younger edifice constructed on the surrounding basalt plains, rather than an older structure surrounded by younger flows. Alternatively, the tholeiitic flows around Hampshire could be younger than those of the thicker pile to the southwest.

Magnetic polarity is of little use in refining the age of this sample, as the 95% confidence limits (21.1-21.9 Ma) encompass seven field reversals and four reversed Chrons (Figure 6).

6.2.2 South Riana (SRN/R010187)

This small hill of strongly undersaturated basalt contains abundant lherzolite xenoliths and is a probable plug (Seymour, 1989, p. 29). Although the dated sample is a basanite, another analysed sample has slightly lower SiO_2 and classifies as olivine nephelinite. The hill is flanked to the west and north by thin flows of transitional to mildly alkalic basalt, resting on outcropping Devonian Housetop granite and Middle to Late Cambrian sedimentary rocks.

The plateau age of 22.0 ± 0.3 Ma (1σ, Figure 4f; early Miocene, Aquitanian) is similar to that from Coastview Hill, 17 km to the west, and may represent a common age for strongly undersaturated volcanism in the region.

Aeromagnetic imagery suggests that normal polarity is likely, but this does not assist in refining the age due to its relatively large uncertainty and numerous changes of polarity in this interval (Figure 6).

6.2.3 Lillicos Beach (LLC/R010186)

Alkali olivine basalt crops out along the foreshore at Lillicos Beach, west of Devonport. Near the eastern end of the beach, it is overlain by a younger tholeiite, which extends along the coast for 2.5 km to Don Heads. In cliffs at the western headland of Don Heads, the tholeiite is in turn overlain by a flow of nepheline hawaiite, containing abundant lherzolite xenoliths, which yielded a K/Ar minimum age of 9.35 ± 0.5 Ma (H. Zwingmann, data). The geomagnetic polarity of these overlapping flows is difficult to determine from aeromagnetic data.

The alkali olivine basalt at Lillicos Beach yielded a $^{40}Ar/^{39}Ar$ plateau age of 37.5 ± 0.2 Ma (1σ, Figure 4g; Late Eocene) which is close to the Bartonian/Priabonian boundary at 37.71 Ma. This time interval encompasses several geomagnetic reversals (Figure 6).

Basalt 7 km west at Turners Beach, although formally an hawaiite, is geochemically similar and may be the same, or a closely related, flow. Our new date also constrains the age of the tholeiite flow or flows, cropping out on the between Don Heads and Lillicos Beach, as between ~37.5 and 9.35 Ma.

Hawaiites have also been sampled at Devonport just east of Mersey Bluff and at Moreland Bluff, ~7 km further east. At East Devonport, Sutherland (1973a) reports subaerial alkali basalts intercalated with thin intrabasaltic sediments containing a likely Upper Eocene to Lower Oligocene microflora, compatible with our ~37.5 Ma date at Lillicos Beach. However, analyses from these areas differ from the Lillicos Beach-Turners Beach alkali olivine basalt/hawaiite, which has significantly higher K_2O and lower Na_2O, and cannot represent the same eruption.

Correlation of basalts in the Devonport-Lillicos Beach area with those in the Port Sorell Sub-basin to the east and southeast is also problematic. Cromer (1993) describes the stratigraphy in the latter area as:

1. (Moriarty Basalt (≤ 50 m); usually deeply weathered but includes a nepheline hawaiite dated at Late Oligocene (25.9 ± 0.2 Ma, K/Ar) at Sassafras (Baillie, 1986a).

2. Wesley Vale Sand (≤ 75 m); Early to Late Oligocene

3. Thirlstane Basalt (≤ 175 m); tholeiitic basalt, dated at Wesley Vale as Late Eocene (38.1 ± 0.6 Ma; K/Ar, Cromer, 1980)

4. Harford Beds (> 250 m); known only from drillholes; Paleocene- Early Miocene.

Burns (1964, Figure 76) proposed a number of "deep leads" in the Devonport district, but these require re-evaluation using subsequent geochronological, geochemical, geophysical and drilling data. Sutherland (1973a) suggested that flows may have spilled to or from the "Devonport Lead" into the Port Sorell Sub-basin ("Northdown and Wesley Vale Leads"). However, although approximately contemporaneous, the Thirlstane Basalt and Lillicos Beach basalt are too dissimilar and spatially separated to be direct correlates, nor can the Moriarty Basalt be correlated with the tholeiites at Don Heads on geochemical grounds. Furthermore, it is likely that the Thirlstane Basalt and possibly the Moriarty Basalt include multiple flows which may have different compositions. Further work, including more detailed sampling, is required to refine the volcanic history of this area.

6.3 Northeast

In northeast Tasmania, basement consists of an Ordovician to Early Devonian quartzwacke turbidite flysch sequence, the Mathinna Supergroup, which was folded in the Middle Devonian and subsequently intruded by mostly post-orogenic granites. It is a fairly direct extension of the Lachlan Fold Belt of southeast Australia, with particular similarities to the Melbourne Zone (e.g. Calver et al., 2014 and references therein).

In this region many eruptive centres can be identified, some of which are the sources for long flows occupying ancestral drainages of major streams. Previous K/Ar data falls mainly into two age groups: ~16 Ma in the Ringarooma valley (Brown, 1982) and ~47 Ma around Weldborough Pass, with also a 30.7 Ma date for a tholeiite from Pipers Brook (Sutherland and Wellman, 1986).

6.3.1 Olivers Hill (AJ99/R004332)

This prominent hill 7 km south of Ringarooma consists of fine-grained olivine nephelinite with locally abundant lherzolite xenoliths (Figure 18), and corresponds to a series of magnetic anomalies with a large positive central zone. It is a major feeder for the large nephelinitic to basanitic flows that extend for 38 km NNE-ward down the Ringarooma valley. The 17.5 Ma ± 0.2 Ma (1σ) plateau age (Figure 4h) is early Miocene (Burdigalian) (Cohen et al., 2020) and, assuming normal polarity, most likely corresponds to Chron C5Dn (17.235-17.717 Ma), although the very short Chron C5Dr.1n (17.717-17.740 Ma) is also possible (Figure 6).

It is close to three K/Ar ages (16.0 ± 0.3, 16.3 ± 0.6, 16.4 ± 0.3 Ma) from similar basalts near Winnaleah, 24-27 km to the northeast (Brown, 1982). Although these may emanate from separate volcanic centres, the new date provides further evidence that the Ringarooma valley flows, although erupted from several major feeders, are coeval and represent the same volcanic episode.

6.3.2 Sweets Creek North (AJ1424/R004366)

Sweets Creek South (AJ1425/R004367)

Upper Esk (AJ1426/R004368)

The first two samples are from a small basalt-capped ridge, 4-5 km north of Upper Esk, between Sweets Creek and the South Esk River headwaters. It is associated with a distinct negative magnetic anomaly which is attributed to remanence and indicates eruption during a period of reversed polarity. The basalt rests on the Devonian Tombstone Creek Granite, a component of the Scottsdale Batholith. It appears to be only ~20 m thick at the northern end of the ridge, but up to 50 m at the southern end.

Sample AJ1424, from the highest point at the northern end of the ridge, is a basanite with common small lherzolite xenoliths. The plateau age of 17.5 ± 0.2 Ma (1σ, Figure 4i) is identical with that at Olivers Hill (AJ99), ~10 km to the NNE, but the reversed polarity suggests that it is either slightly younger (<17.235 Ma, Chron C5Cr) or slightly older (>17.533 Ma, Chron C5Dr-1r or C5Dr.2r) (Figure 6).

Sample AJ1425, from a subsidiary peak about 1 km to the south, is a hawaiite with sparse lherzolite xenoliths. The plateau age of 16.3 ± 0.2 Ma (1σ, Figure 4j) respectively is significantly different from AJ1424 at the 95% confidence level. This time interval is one of mainly normal polarity (C5Cn), but eruption may have occurred during the short reversed Chrons 5Cn.2r and 5Cn.1r, or possibly the beginning of Chron C5Br (Figure 6). Together with the different composition of the samples (e.g. 42.93% vs. 47.44% SiO_2), this suggests that the southern sample represents a slightly younger eruption from a related vent.

Sample AJ1426 is from a small area of olivine nephelinite, possibly a small flow about 40 - 50 m thick, which caps a small hill immediately east of Upper Esk, about 4 km south of the AJ1425 and close to the eastern contact of the Scottsdale Batholith. The associated magnetic anomaly is weak but predominantly negative, suggesting that this basalt also has reverse remanence. Adjacent NNW-trending positive anomalies are parallel to structural trends in the Mathinna Supergroup basement and are thus probably unrelated to the basalt. The plateau age of AJ1426, 16.8 ± 0.4 Ma (1σ, Figure 4k), lies between and overlaps those of AJ1424 and AJ1425, and cannot be confidently distinguished from either. However, geochemical differences (e.g. 40.80 % SiO_2) again suggest a related but separate eruption. Given the reversed polarity, the most likely Chron is C5Cr (16.721- 17.235 Ma) but the age, with its relatively large uncertainty, is also consistent with younger and older Chrons.

Overall, the most likely interpretation is a series of small eruptions of alkalic but varying composition at ~16 – 18 Ma from one or more feeders located below the ridge west of Sweets Creek (i.e. AJ1424, AJ1425), and that the Upper Esk locality (AJ1426) represents a related flow remnant. However, the possibility of a separate feeder at the latter locality cannot be excluded.

These three ages range, at the 95% confidence (± 2σ) level, between 15.9 and 17.9 Ma, spanning the interval between geomagnetic Chrons C5Br and C5Dr.2r, which includes ten changes of polarity and six reversed Chrons (Figure 6). It is not possible, within the precision of the data, to unequivocally assign any of the ages to a specific Chron.

All three dates are closely comparable to those obtained from feeders for the Ringarooma valley flows, including from Olivers Hill 10 - 15 km further north.

6.3.3 Beauty Flat (PP20.5m/R027027)

The dated sample is an olivine nephelinite, probably a small flow, from a drill hole (Everard, 1994) just east of the South Esk River, 14 km north of Fingal. In the hole the basalt, which is associated with a weak negative magnetic anomaly, is 25 m thick and overlies 1 m of sandy brown clay which in turn rests on Mathinna Supergroup lutite. Similar basalt crops out on the river bank near the Beauty Flat bridge site, 160 m to the west, whereas olivine tholeiite, also reversely magnetized, occurs about 1 km to the northeast. The age relationship between the two basalts cannot be established by field relations due to poor exposure and flat terrain.

The nephelinite gave a Middle Eocene (Bartonian) plateau age of 41.0 ± 0.2 Ma (1σ, Figure 4l), which corresponds to a period of mostly reversed geomagnetic polarity corresponding to either Chron C18r (40.073-41.030

Ma) or C19r (41.180- 42.19 Ma), separated by a short episode of normal polarity, Chron 19n (Figure 5). This is a relatively old date, although alkali basalts from the Weldborough area have been dated as Early Eocene (47.4 ± 0.5 to 46.2 ± 0.6 Ma; Sutherland and Wellman, 1986).

At Inside Plain, 11 km to the south down the South Esk River valley, drilling of a more intense negative magnetic anomaly intersected 20 m of similar olivine nephelinite to basanite, concealed beneath 55 m of Cenozoic sediments. This may represent the source of the nephelinite, and suggests northward drainage at 41 Ma, possibly ultimately into the ancestral Avenue and Scamander Rivers. The present surface elevation at Beauty Flat is 265 m compared to 235 m at Inside Plain, whilst the base of the basalt is about 85 m higher at Beauty Flat. Southward tilting of the land surface of less than half a degree since 41 Ma could account for the apparent reversal of drainage. There is some support for this in the northward increase in the elevation of the Permo-Carboniferous unconformity at the base of the Parmeener Supergroup in the region, from 230-300 m at Fingal to about 800 m at Mt Victoria, about 35 km to the north.

6.3.4 West Scottsdale (WSc/R010201)

This olivine nephelinite from a disused quarry adjacent to the Sledge Track, 3 km SW of Scottsdale, has previously been described by Frey et al. (1978). It contains abundant lherzolite xenoliths and is one of the most undersaturated basalts, other than a few melilitites, known from Tasmania. Petrographically similar olivine nephelinite is widespread in the Scottsdale area, although outcrop is poor due to deep weathering. The nephelinite overlies Cenozoic sediments, which in turn rest on the Diddleum Granodiorite, a component of the Devonian Scottsdale Batholith. Moore (1989) showed that two flows are present at North Scottsdale; the more extensive upper flow is 47 m thick and separated by 20 - 30 m of sediment from a lower 11 m thick flow. Subsequent sampling suggests that both flows are nephelinite.

The plateau age of 34.2 ± 0.4 Ma (1σ, Figure 4m) is apparently latest Eocene (Priabonian). However, aeromagnetic imagery suggests that these flows are predominantly normally magnetized. Together with the relatively large uncertainty, this suggests that they probably were erupted during Chron C13n (33.214 – 33.726 Ma; Figure 6) and are more likely earliest Oligocene (Rupelian). It provides a minimum age, at least locally, for the underlying Cenozoic sediments of the Scottsdale Sub-basin.

This is much older than the Early to Middle Miocene age suggested by Moore (1989), which was partly based on an assumption that these nephelinites were coeval with those of the Ringarooma valley further east (see above).

Harris (1968) reported a "mid-Tertiary" microflora from Scottsdale Sub-basin sediments at "Mt Stronach, Great Forester River", a locality about 8 km east of our dated sample but at a significantly lower elevation (~100 m vs. ~180 m). The age was interpreted as early Miocene by Moore (1989), but Forsyth et al. (2014) note that the report of *Nothofagidites asperus* indicates an age no older than middle Eocene (~48 Ma) or younger than earliest Oligocene (~33 Ma). The latter interpretation is more compatible with our 34.2 ± 0.4 Ma basalt age, and together imply that the remaining fill of the Scottsdale Sub-basin is much older than thought by Moore (1989). However, as he noted, much of younger sediments from the Scottsdale Sub-basin may have been eroded and re-deposited in Bass Strait.

6.3.5 The Sideling (SDL/R010202)

This olivine nephelinite overlies Mathinna Supergroup on the Sideling Range 15 km southwest of Scottsdale at an elevation of about 700 m. It is a very undersaturated rock and contains abundant lherzolite xenoliths (Figure 24).

Although it has the form of a basalt cap, an intense positive magnetic anomaly on aeromagnetic data suggests an underlying feeder. Jennings (1969) noted compass needle deviations of more than 80° over the basalt, and magnetic anomalies of ± 10,000nT, and locally up to 50,000nT, in the vertical component of the field, obtained with a fluxgate magnetometer.

The plateau age of 29.4 ± 0.5 Ma (1σ, Figure 4n) is Early Oligocene (Rupelian). The normal polarity allows the age to be further refined to Chron C11n.1n or C11n.2n (29.183 – 29.970 Ma), which are separated by a short reversed interval (Chron C11n.1r at 29.477-29.527 Ma) (Figure 6).

The nearest previously dated basalt is a slightly older quartz tholeiite (30.7 ± 0.4 Ma) from the extensive but dissected, mainly tholeiitic flows that occupy the Pipers Brook drainage system in lowlands to the northwest between Lebrina and the coast at Weymouth (Sutherland and Wellman, 1986). These authors and Barton (1969) showed that, near Lebrina, tholeiite is overlain by sediments, "alkaline lava" and olivine nephelinite. Although on present evidence it is chronologically possible to correlate the Lebrina nephelinites with those of The Sideling, they are more likely to be a separate flow from a local vent.

6.3.6 Blessington (BLS/R010204)

This small basanite plug penetrates early Triassic quartz sandstone at Blessington and is a well-documented mantle xenolith locality (Varne, 1977; Beyer et al., 2014). No related flows are known. Topographically, the plug is expressed as a small conical hill near the saddle between

Coxs Hill and Castle Hill, both of which are composed of Jurassic dolerite capping the sandstone. The northwesterly trending Castle Cary fault system, which here has an overall SW-side down throw of the order of ~240 m (approximately the total thickness of the Permian Lower Parmeener Supergroup), separates it from outcropping Mathinna Supergroup basement ~3 km to the east.

The plug coincides with a small positive magnetic anomaly on images derived from aeromagnetic data, which is inferred to be due to remanence with normal polarity.

The $^{40}Ar/^{39}Ar$ plateau age of 36.8 ± 0.2 Ma (1σ, Figure 4o) is late Eocene (Priabonian) on the ICS time scale of Cohen et al. (2013, updated 2022). The 95% (± 2σ) confidence limits (~36.4 – 37.2 Ma) coincide with polarity Chrons C16r (36.351-36.573 Ma) and C17n.1n (36.575-37.385 Ma) on the geomagnetic polarity time scale of Ogg (2022), with the latter being consistent with the observed normal polarity.

6.4 Midlands and Central Plateau

Basalts in this region range from extensive tholeiitic flows around Great Lake and in the northern Midlands, to numerous mostly small alkalic plugs and flows in the southern Midlands. They rest on essentially flat-lying Late Carboniferous to Middle Triassic sedimentary rocks (Parmeener Supergroup) of the Tasmania Basin, which was extensively intruded by Jurassic dolerite. The region straddles the inferred boundary between the Eastern and Western Tasmanian Terranes, and the pre-Carboniferous basement is at a depth of about 1 km over much of the region. However, a few inliers and some deep stratigraphic drilling suggests that basement may be similar to that of eastern Tasmania (i.e. Mathinna Supergroup) for the first two samples discussed, and may comprise Precambrian sedimentary sequences akin to western Tasmania for the other two.

Basalts of this region are relatively well-dated, with 17 previously published K/Ar ages ranging from 21.3 Ma to 36.3 Ma.

6.4.1 Eastbourne (SB9/R005506)

This olivine tholeiite was collected from a low cutting on the south side of the Esk Main Road, about 600 m east of the turnoff to the "Eastbourne" homestead. It is fairly typical of the lavas that have flowed westward down the valley of the South Esk River from the Henbury area, about 8 km northeast of Avoca and 14 km from the dated sample. Similar tholeiites also occupy the valley of the St Pauls River between Royal George and Avoca. Aeromagnetic imagery indicates that these flows have dominantly reversed polarity.

In the Henbury area, a line of drill holes within 1 km of outcropping basalt intersected up to 70 m of Cenozoic sediments. Two samples, from depths of 40 m and 70 m, yielded *Protoacidites pachypolus*-bearing *N. asperus* Zone palymorphs implying a mid-Eocene age (Threader, 1987; Forsyth et al., 2014, p. 444). Similar lower-middle *N. asperus* Zone spores also underlie basalt in a bore (IH59) 3 km E of Conara and 15 km W of the dated sample (Matthews et al., 1996, p. 40). A middle-late Eocene microflora is also widespread in the Longford Basin (Matthews, 1983).

The Early Oligocene plateau age of 29.6 ± 0.6 Ma (1σ, Figure 4p; Oligocene, Rupelian) is consistent with but a little younger than the maximum age permitted by the palynological evidence. It probably corresponds to Chron C10r or C11r (Figure 6), but the uncertainty in the age is too great to permit refining by magnetic polarity. It is older than the Early Miocene (22.4-24.3 Ma) tholeiites around Great Lake, on the central plateau some 40 km to the east (Sutherland et al., 1973; Sutherland and Wellman, 1986).

Extensive flows of petrologically similar tholeiite extend for ~40 km southward of Epping Forest to and beyond Ross, in the southern Longford Sub-basin (Everard in Matthews et al., 1996). At "Quorn Hall" near Campbell Town, however, tholeiitic basalt overlie a nepheline hawaiite dated at 27.2 ± 0.2 Ma (Everard et al., 2007). Therefore, at least some of the basalts in the Campbell Town area are younger than those near Avoca. They may have been erupted from a separate feeder near "Truelands", ~10 km ENE of Campbell Town (Gulline et al., 1991).

6.4.2 Llewellyn (SB11/R005508)

This nepheline hawaiite was sampled from near the southern bank of the South Esk River at the Llewellyn locality, between Avoca and Conara. The rock, previously described as limburgite by Edwards (1950), is heavily contaminated by lherzolite debris (Figures 27, 28) and the analysis (Table 3) does not represent a liquid composition. It is one of a series of remnants of a flow that erupted from a likely centre within Jurassic dolerite 4 km to the south, and flowed northward down the ancestral valley of Salisbury Rivulet to reach the South Esk River at Llewellyn. Aeromagnetic imagery suggests that the flow probably has reversed polarity, although this is uncertain due to anomalies from the underlying Jurassic dolerite.

In this region, the valley of the South Esk is occupied by more extensive flow remnants of tholeiite, which appear to have flowed westward from above Avoca, through "Eastbourne" toward "Glen Esk". At Llewellyn, the nepheline hawaiite and tholeiite flows intersect, but a rel-

ative age relationship is difficult to establish from field evidence. Basalt on the southern side of the river appears to be entirely nepheline hawaiite, whereas both types are present, but poorly exposed, on the northern side.

The nepheline hawaiite at Llewellyn yielded a plateau age of 30.3 ± 0.2 Ma (1σ, Figure 4q; Oligocene, Rupelian). If the inference of reversed polarity is correct, this probably corresponds to Chron C11r (29.970 – 30.571 Ma; Figure 6). The age is slightly older, but within error, of that of the tholeiite dated 7 km to the west at "Eastbourne" (29.6 ± 1.2 Ma, see above).

6.4.3 Burburys Sugarloaf (LSB24/R004501)

This small plug has penetrated Triassic sandstone on Macquarie Tier, 9 km WNW of Ross and on the western flank of the Midlands graben. Associated small flows are present, including a small remnant at "Fosterville", 4 km to the northeast.

The rock has previously been described by Everard (in Matthews et al., 1996). It is a potassic nepheline hawaiite bearing lherzolite xenoliths, despite its low Mg# (58.7), identifying it as a mantle-fractionated rock. The otherwise fine-grained groundmass contains large anorthoclase platelets which poikilitically enclose other phases, including minor biotite (Figure 29).

The relatively precise plateau age of 27.3 ± 0.1 Ma (1σ, Figure 4r; Miocene, Chattian) is close to the Chattian-Rupelian boundary at 27.62 Ma and probably corresponds to Chron C9n or 9Cr (Figure 6). The polarity of the plug, however, is difficult to deduce from aeromagnetic imagery due to anomalies related to nearby Jurassic dolerite, which has discordantly intruded the sandstone.

The plug lies at the northern end of a region in the southern Midlands of numerous similar small plugs and flows, mainly of alkalic composition and frequently containing mantle xenoliths. The date is within the range of available K/Ar dates from this region, which include four between 24.1 and 25.0 Ma, a basanite at Rose Hill Farm (27.6 ± 0.4 Ma) and an alkali olivine basalt at Big White Hill (36.3 ± 0.5 Ma) (Sutherland and Wellman, 1986).

6.4.4 West Lake Crescent (LCr/R010295)

This small plug has penetrated a small area of outcropping Triassic sandstone surrounded by Jurassic dolerite, 5 km SW of Interlaken. The rock, previously described by Sutherland (1989c), contains very abundant lherzolite xenoliths and megacrysts including Al-augite, pleonaste and rare kaersutite in a fine-grained groundmass (Figure 32). Although the whole rock analysis (Table 3) appears to be of a near-primitive olivine nephelinite, the sample is contaminated by lherzolite debris and the liquid composition may have had a lower Mg#, implying that it is also a mantle-fractionated type.

The geomagnetic polarity of the plug is uncertain due to anomalies related to nearby dolerite.

The plateau age of 29.4 ± 0.2 Ma (1σ, Figure 4s; Oligocene, Rupelian) is near the middle of the 21.2 - 36.3 Ma age range of previously dated alkalic basalts in the region (see above).

6.4.5 Alma Tier (ATr/R010218)

The dated sample is from a tiny flow remnant of olivine melilitite resting on Jurassic dolerite country rock, 11 km west of Interlaken on the Central Plateau. Its petrology has also been described by Sutherland (1989c).

The $^{40}Ar/^{39}Ar$ plateau age, 36.5 ± 0.2 Ma (1σ, Figure 4t; late Eocene, Priabonian), is comparable to a K/Ar age of 35.4 ± 0.4 Ma from a small melilitite plug known as The Haystack, 8.2 km to the WSW on Shannon Tier (Sutherland and Wellman, 1986). Due to the distance and slight differences in chemistry, it is unclear if the Alma Tier flow emanated from the Haystack. It is likely, however, to be part of the same volcanic episode, together with several other small undated melilitite plugs on Shannon Tier known as The Beehive, and The Anthill (Twelvetrees & Petterd 1899; Paul 1906; Erdmannsdorfer & Nieland 1928; Tilley 1928; Sutherland 1973b).

6.5 South and southeast

As in the Midlands, basalts in this region rest on thick Parmeener Supergroup rocks and Jurassic dolerite. The basalts were erupted after widespread faulting produced a horst-and-graben topography. Basalts include extensive flows of tholeiitic to transitional basalt particularly in major grabens, with small near-primitive alkalic plugs in the intervening horsts. South and east of Hobart, strongly evolved, mantle-fractionated hawaiitic to mugearitic lavas and their feldspathoidal analogues ("alkaline association" or Southern Hobart Group of Sutherland, 1976) are widespread.

Previous geochronological data are limited to five K/Ar data ages. A tholeiite from Kellevie yielded a Paleocene (58.5 ± 0.7 Ma) age (Baillie, 1987) and an alkali basalt from Campania is 24.2 ± 1.0 Ma (Sutherland et al., 1973, Green, 1976). Three dates within from the Derwent graben in the Hobart area range from 23 – 30 Ma, as discussed below.

6.5.1 Crooked Billet Creek, Brighton (BRJ1/R010055)

Dragon Point, Claremont (HBJ23/R010093)

North of Hobart, tholeiites extend for 15 km from Mangalore to Claremont. McDougall (1959) described in detail the variable petrography of the basalt in the Brighton area, where he considered that a single flow, locally at least 50 m thick, had partly filled the ancestral Jordan

River valley. He suggested a Late Tertiary age, mainly on the basis of its relatively undissected form. Sutherland (1976, 1977) reported flow foot breccia and pillow basalt at Bridgewater, indicating locally subaqueous extrusion into the Derwent estuary. He suggested that these flows at Bridgewater were older than extensions of the Brighton Basalt at Herdsmans Cove, where it was thought possible that two flows were present. Sutherland (1976) described in detail the field relations of at least partly subaqueous lava and tachylitic breccia near Claremont, which were thought to have erupted from an older separate feeder northwest of Claremont. Several analyses from Pontville to Claremont indicate, however, a very similar tholeiitic composition for all these basalts (Table 3 and authors' unpublished data). Silicified wood, including *Eucalyptus* and therefore relatively young, occurs in sediments between Elwick and Bridgewater, but these overlie basalt (Sutherland, 1976; Gill, 1962).

The two new $^{40}Ar/^{39}Ar$ plateau ages, 25.1 ± 0.3 Ma (Figure 4v) at Claremont and 26.7 ± 0.3 Ma at Brighton (Figure 4u) (both ± 1σ) are Late Oligocene (Chattian) and older than previous estimates. Although the Claremont date is significantly younger than that at Brighton (contra Sutherland, 1976), both probably belong to the same episode of volcanism, which may have lasted at least 1-2 Myr.

Aeromagnetic imagery suggests that the basalts at the Claremont locality, and probably at Brighton, are reversely magnetized, which would enable refinement of the ages. The local magnetic field is, however, complicated by dolerite-related anomalies, particularly near Brighton, and the polarity of the basalts needs to be determined by direct observations.

Further down the Derwent estuary, an olivine tholeiite at Geilston Bay gave a K/Ar age of 23.0 ± 0.5 Ma (Tedford et al., 1975), but this is from a flow extending from Elwick to below Lindisfarne with slightly alkalic affinities, subtly dissimilar to the Brighton-Claremont basalts. At East Risdon, a 30.2 ± 1.0 Ma date was obtained from hornblende megacrysts within a tuff that underlies hawaiite and overlies olivine nephelinite (Sutherland, 1976). Basalt at Lower Sandy Bay gave a K/Ar age of 26.5 ± 0.3 Ma (Sutherland and Wellman, 1986), similar to the Brighton Basalt, despite a very different composition (see below).

6.5.2 Glenfern (GFN/G402497)

This small probable plug of basanite has penetrated Jurassic dolerite 9 km SW of New Norfolk. The rock contains common spinel lherzolite xenoliths and associated megacrysts (Piestrzeniewicz, 1972). Available aeromagnetic data (best 500 m line spacing) is inadequate to determine the polarity.

The relatively imprecise plateau age of 45.5 ± 1.0 Ma (1σ, Figure 4w; Eocene, Lutetian) spans Chrons C20r and C21n (Figure 5) and could be refined if the polarity of the basanite were known. It is one of the oldest ages obtained from Tasmanian Cenozoic basalts. Voluminous volcanism of similar alkalic composition occurred in the Weldborough area, northeast Tasmania, at 46.2 ± 0.6 to 47.4 ± 0.6 Ma (Sutherland and Wellman, 1986).

6.5.3 Pickett Hill, Kingston (HBJ6/R010076)

This prominent plug of hawaiite at Leslie Vale, about 5 km WNW of Kingston, has previously been described by Sutherland (1976). It is associated with a positive magnetic anomaly on aeromagnetic data, suggesting normal remanence, and appears to be the source for flows descending eastward towards Kingston.

The rock contains contains abundant lherzolite xenoliths and associated debris, and the whole rock analysis (Table 3) probably overstates the Mg#. Petrologically, it is fairly representative of evolved hawaiitic to mugearitic lavas (Southern Hobart Group of Sutherland, 1976).

The plateau age of 29.4 ± 0.2 Ma (1σ, Figure 4x; early Oligocene, Rupelian) is very similar to those from West Lake Crescent, The Sideling and Lillicos Beach, presented here. It probably corresponds to either Chron C11n.1n or C11n.2n (29.183 – 29.970 Ma), which are separated by a short reversed interval (Chron C11n.1r at 29.477-29.527)(Figure 6).

The age may be representative of the mantle-fractionated hawaiites and mugearites widespread in southeastern Tasmania, although a nepheline mugearite to nepheline benmoreite at Lower Sandy Bay gave a slightly younger K/Ar age of 26.5 ± 0.3 Ma (Sutherland and Wellman, 1986).

6.5.4 Marion Bay (SBA21/R010159)

The petrography and geochemistry of basalts in this area were described by Everard (in Gulline, 1984), who distinguished two main types: coarse-grained tholeiites with mainly ophitic textures, and at least locally younger alkali basalts.

The dated sample is from a small quarry near the end of a flow of olivine tholeiite, which was probably erupted through Triassic sandstone from a centre about 2 km east of Copping and descended eastward toward Blackman Bay. At Tunbridges Hill, the basalt is overlain by basanite, which further north at Benders Hill has been dated at 58.7 ± 0.7 Ma (Paleocene) (Baillie, 1987). The polarity of these basalts is difficult to ambiguously determine from aeromagnetic data due to dolerite-related anomalies.

This sample exhibits some unusual geochemical features, such as a weakly concave REE patterns, compared to other Tasmanian Cenozoic tholeiites (Everard et al., 2014).

Although no well-defined plateau age date was obtained, the integrated age of 64.2 ± 0.6 Ma (1σ, Figure 4y; Paleocene, Danian) is consistent with field relations. It spans (at 2σ) Chrons C27r to C29n (Figure 5) and could be further refined if the polarity of the sample were known.

7.0 CONCLUSION

Our twenty-five new dates further refine rather than substantially modify the apparent temporal patterns of Tasmanian Cenozoic volcanism evident in previously published K/Ar ages and inferred palynological constraints.

The oldest volcanism was sporadic, dispersed, limited in volume and mainly alkalic in character. It includes possibly basanite at Cape Portland in northeast Tasmania (~70 Ma, Zwingmann et al., 2004), together with olivine tholeiite at Marion Bay (~64 Ma, this study) and basanite nearby at Kellevie (58.5 ± 0.7 Ma, Baillie, 1987), both in the southeast, and basanite on King Island (61.7 ± 1.3 Ma, Sutherland et al., 2002).

More voluminous but also alkalic activity occurred in the Weldborough area at ~46 – 47 Ma (Sutherland and Wellman, 1986). Other relatively old dates of alkalic rocks are from Rowella on the Tamar River (46.7 ± 1.0 Ma, Sutherland et al., 2006), Glenfern (45.5 ± 1.0 Ma, this study) and in the northeast at Beauty Flat (41.0 ± 0.2 Ma, this study) and George Rocks (40.6 ± 0.8 Ma, Zwingmann et al., 2004).

Increasing activity in the Late Eocene included the tholeiitic Thirlstane Basalt near Devonport (38.1 ± 0.6 Ma; Cromer, 1980) but otherwise was still mainly alkalic. Our new dates from Lillicos Beach, Blessington, Alma Tier, Rabalga Track and West Scottsdale fall into this interval.

The Oligocene encompasses almost half of the available dates, including 10 of our 25 new $^{39}Ar/^{40}Ar$ dates. In this epoch, basaltic volcanism was widespread throughout Tasmania and compositionally diverse, and ranged from olivine melilitites to quartz tholeiites. The volumetric peak of volcanism was probably in the Early Oligocene, when the bulk of the thick dominantly tholeiitic pile east of Waratah was erupted (Seymour, 1989). Voluminous tholeiitic lavas were also erupted at Pipers Brook (30.7 ± 0.4 Ma, Sutherland and Wellman, 1986), the northern midlands (e.g. Eastbourne, 29.6 ± 0.6 Ma, this study) and the Brighton-Claremont area (~26.7- 25.1 Ma, this study). Near the end of the Oligocene, further tholeiitic activity occurred at Cape Grim (~23.1 – 24.7 Ma, Fox et al., 2023) and Great Lake (22.3 – 24.3 Ma, Sutherland et al., 1973).

After the earliest Miocene, volcanism appears to have been exclusively alkalic and, apart from a nephelinitic plug at Spring Hill in the southern midlands (21.2 ± 0.5 Ma,

Zwingmann et al., 2004), possibly restricted to northern Tasmania. Our four new $^{39}Ar/^{40}Ar$ dates (16.3 – 17.5 Ma) from the Ringarooma-Upper Esk area in northeast Tasmania are clearly related to the long nephelinitic to basanitic flows in the Ringarooma valley, previously dated by the K/Ar method at ~16 Ma (Brown et al., 1977, p. 178). Other Miocene dates are mostly from the northwest and include our new $^{39}Ar/^{40}Ar$ dates from South Riana (22.0 ± 0.3 Ma), Coastview Hill (21.5 ± 0.2 Ma) and Neasey Plains (21.4 ± 0.2 Ma).

The youngest published dates are from the Green Hills Volcanics near Stanley (8.5 ± 0.1 Ma K/Ar, Baillie, 1986b; ~10.4 Ma, $^{39}Ar/^{40}Ar$, Fox, 2019), although a nepheline hawaiite at West Don Heads yielded a K/Ar minimum age of 9.35 ± 0.5 Ma (H. Zwingmann, data).

No overall, Tasmania-wide correlation is apparent between age and either geographic location or geochemistry. However, the oldest and youngest eruptions are largely alkalic, whilst tholeiites have a more restricted age range (all but one 25.1-29.6 Ma by $^{39}Ar/^{40}Ar$, 22.3-38.1 Ma by K/Ar), roughly corresponding to the circa-Oligocene peak when the most diverse variety of basalts was erupted.

As previously noted (Sutherland and Wellman, 1986), this is consistent with petrological models in which alkali basalts are generated by smaller degrees of partial melting of mantle than tholeiites (e.g. Frey et al., 1978). The major exception to this generalisation is the Early Paleocene (~64 Ma) tholeiite at Marion Bay, which however has a geochemical and isotopic signature distinct from the younger tholeiites (Everard et al., 2014).

Thus the overall picture is of a long-lived thermal anomaly, which commenced in the late Cretaceous or early Cenozoic, initially causing low degree partial melting of lithospheric mantle underlying Tasmania. The anomaly peaked in the late Oligocene, when more voluminous tholeiitic lavas were also erupted, and declined in the mid-Miocene, generating exclusively alkalic lavas.

The origin of the inferred thermal anomaly is unclear. Although a detailed discussion is beyond the scope of this report, it needs to be assessed in the broader context of eastern Australian volcanism and the ~65 mm/yr northward migration of the Australian plate during the Cenozoic (e.g. Duncan and McDougall, 1989).

Models proposed include plate migration over multiple plumes ("hot spots") that were initiated during opening of the Tasman and Coral Seas (e.g. Sutherland, 1991; 2003). In this model a younging of volcanism of 4-5 Myr from northern to southern Tasmania would be expected over any particular "hot-spot". This is not evident in the available geochronological data, but it is doubtful that it would be resolvable from scatter due to the small size of Tasmania.

A "plume-swathe" model of passive upwelling of hot mantle beneath eastern Australia, possibly as a delayed effect from opening of the Tasman Sea or Southern Ocean, resulting in small "plume heads" has also been proposed. Magma ascent may have been structurally controlled by local stress field in the lithosphere, resulting in a quasi-random time and space distribution of volcanism (e.g. Lister and Etheridge, 1989; O'Reilly and Zhang, 1995).

More recently, a mechanism of edge-driven convection has been proposed, whereby variations ("steps") in lithospheric thickness at the edge of a continent or craton cause passive asthenospheric upwelling, mantle decompression and partial melting beneath the thinner part of the lithosphere (e.g. King and Anderson, 1998; King, 2007; Davies and Rawlinson, 2014). This model is perhaps more compatible with the quasi-random spatio-temporal distribution of Tasmanian Cenozoic volcanism.

9.0 REFERENCES

Baillie, P. W. 1986a. A radiometric age for the Moriarty basalt, northern Tasmania. *Tasmania Department of Mines Report,* 1986/38.

Baillie, P. W. 1986b. Radiometric age for the Circular Head and Green Hill basalts, northwestern Tasmania. *Tasmania Department of Mines Report,* 1986/39.

Baillie, P. W. 1987. A Paleocene radiometric age for basalt at Bream Creek, south-eastern Tasmania. *Tasmania Department of Mines Report,* 1987/21.

Baillie, P. W. and Everard, J. L. 2014. Igneous influences in Bass Basin. In: Corbett K. D., Quilty P. G. and Calver C. R. (eds.). The Geological Evolution of Tasmania. *Geological Society of Australia Special Publication,* 24, 435-437.

Baksi, A. K., Arcibald, D. A. and Farrar, E. 1996. Intercalibration of $^{40}Ar/^{39}Ar$ dating standards. *Chemical Geology,* 129, 307-324.

Barton, C. M. 1969. Petrographical descriptions of Tertiary volcanic rocks from Pipers River area. In: Marshall, B. 1969. Geological Survey Explanatory Report. Geological Atlas 1 Mile Series. Zone 7 Sheet No 31 (8315N). *Pipers River*, p. 121-122. Tasmania Department of Mines.

Beyer, E. E., O'Reilly, S. Y., Zhang, M. and Everard, J. L. 2014. Mantle xenoliths, Cenozoic geotherms and the Tasmanian lithosphere. In: Corbett, K. D., Quilty, P. G. and Calver, C. R. (eds.). The Geological Evolution of Tasmania. *Geological Society of Australia Special Publication,* 24, 487 – 492.

Brown, A. V. 1982. Whole rock K/Ar ages of basalts. In: McClenaghan, M. P., Turner, N. J., Baillie, P. W., Brown, A. V., Williams, P. R. and Moore, W. R. 1982. Geology of the Ringarooma-Boobyalla area. *Geological Survey of Tasmania Bulletin,* 61.

Brown, A. V. and Forsyth, S. M. 1984. Chemistry of Tertiary basalt and palynology of sediments from BHP drill holes, EL33/79. *Tasmania Department of Mines Report,* 1984/39.

Brown, A. V., McClenaghan, M. P., Moore, W. R., Turner, N. J., McClenaghan, J., Williams, P. R., Baillie, P. W., Corbett, K. D., Corbett, E. B., Cox, S. F., Groves, D. I. and Pike, G. P. 1977. Geological Atlas 1:50000 series. Sheet 32 (8415N). *Ringarooma*. Tasmania Department of Mines.

Burns, K. L. 1964. Geological Survey Explanatory Report. Geological Atlas 1 Mile Series. Sheet 29 (8115N). *Devonport*. Tasmania Department of Mines.

Calver, C. R., Baillie, P. W., Banks, M. R. and Seymour D. B. 2014. Ordovician- Lower Devonian successions. In: Corbett, K. D., Quilty, P. G. and Calver, C. R. (eds.). The Geological Evolution of Tasmania. *Geological Society of Australia Special Publication,* 24, 241-271.

Cohen, K. M., Finney, S. C., Gibbard, P. L. and Fan, J.-X. 2013, updated 2022. The ICS International Chronostratigraphic Chart. *Episodes,* 36, 159-204.

Corbett, K. D., Quilty, P. G. and Calver, C. R. (eds.). 2014. The Geological Evolution of Tasmania. *Geological Society of Australia Special Publication,* 24.

Crawford, A. J., Lanyon, R., Elmes, M. and Eggins, S. 1997. Geochemistry and significance of basaltic rocks dredged from the South Tasman Rise and adjacent seamounts. *Australian Journal of Earth Sciences,* 44, 621-632.

Cromer, W. C. 1980. A Late Eocene basalt date from northern Tasmania. *Search,* 11, 294-295.

Davies, D. R. and Rawlinson, N. 2014. On the origin of recent intraplate volcanism in Australia. *Geology,* 42 (12), 1031-1034.

Duncan, R. A. and McDougall, I. 1989. Volcanic time-space relationships. In: Johnson, R. W. (ed.). *Intraplate Volcanism in Eastern Australia and New Zealand*, p. 43-54. Cambridge University Press.

Edwards, A. B. 1950. The petrology of the Cenozoic basaltic rocks of Tasmania. *Proceedings of the Royal Society of Victoria,* 62, 97-120.

Erdsmannsdorfer, O. H. and Nieland, H. 1928. Über melilithfuhrende fasinite von Tasmanien. *Fennia* 50(4).

Everard, J. L. 1994. Drilling Investigations of Geophysical Anomalies and Cenozoic Deposits, Fingal-Mathinna Area: Preliminary Report. *Tasmania Department of Mines Report,* 1994/13.

Everard, J. L. 2001. Inclusions of high pressure origin in Tasmanian Tertiary basalts: a catalogue of localities. *Tasmanian Geological Survey Record,* 2001/9

Everard J. L., Seymour D. B., Brown A. V. and Calver C. R. 1996. Geological Atlas 1:50,000 Series, Sheet 27 (7915N). *Trowutta*. Mineral Resources Tasmania.

Everard, J. L. Zhang, M., Lo, C.-H., O'Reilly, S. Y., Everard, J. L. and Forsyth, S. M. 2004. Overview of Tasmanian Tertiary basalts. *Geological Society of Australia Abstracts,* 73, p. 74.

Everard, J. L., Sutherland, F. L. and Forsyth, S. M. 2007. A Late Oligocene basalt from Keach Hill, near Campbell Town, and its stratigraphic significance. *Tasmanian Geological Survey Record,* 2007/03.

Everard, J. L., Baillie, P. W., Beyer, E. E., Doyle, R. B., O'Reilly, S. Y. and Zhang, M. 2014. Palaeogene-Neogene basaltic volcanism. In: Corbett, K. D., Quilty, P. G. and Calver, C. R. (eds.). The Geological Evolution of Tasmania. *Geological Society of Australia Special Publication,* 24, 463 – 494.

Forsyth, S. M., Quilty, P. G. and Calver, C. R. 2014. Cenozoic onshore basins and landscape evolution. In: Corbett, K. D., Quilty, P. G. and Calver, C. R. (eds.). The Geological Evolution of Tasmania. *Geological Society of Australia Special Publication,* 24, 437 – 450.

Fox, J. M. 2019. *Complex volcanic architecture produced by basaltic submarine and emergent volcanism in intraplate settings.* Ph.D. thesis, University of Tasmania.

Fox, J. M., Mcphie, J., Carey, R. J. and Jourdan, F. 2023. Revised stratigraphy and first geochronology of the Miocene submarine volcanic succession at Kennaook/Cape Grim, northwestern Tasmania. *Australian Journal of Earth Sciences,* 70, 510-534.

Frey, F. A., Green, D. H. and Roy, S. D. 1978. Integrated models of basalt petrogenesis: a study of quartz tholeiites to olivine melilitites from south eastern Australia utilizing geochemical and experimental petrological data. *Journal of Petrology,* 19, 463-513.

Gibson, D. L. 2007. Potassium-argon ages of Late Mesozoic and Cenozoic igneous rocks of eastern Australia. *CRC LEME Open file report series,* 193, 53 pp.

Gill, E. D. 1962. Non-marine succession. In: Spry A. and Banks M. R. The Geology of Tasmania. *Journal of the Geological Society of Australia,* 9 (2), 239-239.

Green, D. C. 1976. Cenozoic volcanic rocks: isotopic dating and implications. In: Leaman, D. E., Geological Survey Explanatory Report. Sheet 82 (8312S). *Hobart.* Tasmania Department of Mines.

Gulline, A. B. 1984. Geological Survey Explanatory Report. Geological Atlas 1:50 000 Series. Sheet 83 (8412S). *Sorell.* Tasmania Department of Mines.

Gulline, A. B., Forsyth, S. M., Everard, J. L., Calver, C. R. and Matthews, W. L. 1991. Geological Atlas 1:50,000 series. Sheet 55 (8414S). *Snow Hill.* Division of Mines and Mineral Resources, Tasmania Department of Resources and Energy.

Harris, W. K. 1968. Tasmanian Tertiary and Quaternary microfloras. Summary report. *Geological Survey of South Australia Palaeontological Reports,* 5/68.

Jennings, D. J. 1969. Anomalous magnetic field, Sideling basalt cap. *Tasmania Department of Mines Technical Reports,* 14, 25-27.

Johnson, R. W. (ed.) 1989. *Intraplate Volcanism in Eastern Australia and New Zealand.* Cambridge University Press.

Jordan, G. J. and Hill, R. S. 2002. Cenozoic plant macrofossil sites of Tasmania. *Papers and Proceedings of the Royal Society of Tasmania,* 136, 127-139.

King, S. D. 2007. Hotspots and edge-driven convection. *Geology,* 35 (3), 223-226.

King, S. D. and Anderson, D. L. 1998. Edge-driven convection. *Earth and Planetary Science Letters,* 160, 289-296.

Le Maitre, R. W. (ed.) 2002. *A Classification of Igneous Rocks and Glossary of Terms,* 2nd Edition. Cambridge University Press (236 pp.)

Lister, G. G. and Etheridge, M. A. 1989. Detachment models for uplift and volcanism in the Eastern Highlands, and their application to the origin of passive margin mountains. In: Johnson R. W. (ed.). *Intraplate Volcanism in Eastern Australia and New Zealand,* p. 297-313. Cambridge University Press.

Lo, C.-H., Onstott, T. C., Chen, C. H. and Lee, T. 1994. An assessment of $^{40}Ar/^{39}Ar$ dating for the whole-rock volcanic samples from the Luzon Arc near Taiwan. *Chemical Geology* (Isotope Geoscience Section), 114, 157-178.

Lo, C.-H., Chung, S.-L., Lee, T.-Y. and Wu, G.-Y. (2002) Age of the Emeishan flood magmatism and relations to Permian-Triassic boundary events. *Earth and Planetary Science Letters,* 198, 449-458.

McClenaghan, M. P., Turner, N. J., Baillie, P. W., Brown, A. V., Williams, P. R. and Moore, W. R. 1982. Geology of the Ringarooma-Boobyalla area. *Geological Survey of Tasmania Bulletin,* 59.

Macdonald, G. A. and Katsura, T. 1964. Chemical composition of Hawaiian lavas. *Journal of Petrology,* 5, 82-133.

McDougall I. 1959. The Brighton basalts, Tasmania. Papers and *Proceedings of the Royal Society of Tasmania,* 93, 17-38.

McDougall, I. and Harrison, T. M. 1988. *Geochronology and Thermochronology by the $^{40}Ar/^{39}Ar$ Method.* Oxford University Press.

Macphail, M. K. and Hill, R. S. 1994a. K-Ar dated palynofloras in Tasmania 1: Early Oligocene, Proteacidites tuberculatus Zone sediments, Wilmot Dam, northwestern Tasmania. *Papers and Proceedings of the Royal Society of Tasmania,* 128, 1-15.

Macphail, M. K., Alley, N., Truswell, E. M. and Sluiter, I. R. 1994b. Early Tertiary vegetation: evidence from pollens and spores. In: Hill R. S. (ed.). *History of the Australian vegetation: Cretaceous to Recent,* p. 189-261. Cambridge University Press.

Matthews, W. L. 1983. Geology and groundwater of the Longford Tertiary Basin. *Geological Survey of Tasmania Bulletin,* 61.

Matthews, W. L. 1989. In: Burrett, C. F. and Martin, E. L. (eds.) Geology and Mineral Resources of Tasmania. *Geological Society of Australia Special Publication,* 15, p. 370-372.

Matthews, W. L., Everard, J. L. and Clarke, M. J. 1996. Geological Survey Explanatory Report. Geological Atlas 1:50, 000 series. Sheet 54 (8314S). *Lake River.* Mineral Resources Tasmania.

Moore, W.R. 1989. Scottsdale Sub-basin. In: Burrett, C. F. and Martin, E. L. (eds.). Geology and Mineral Resources of Tasmania. *Geological Society of Australia Special Publication,* 15, p. 369-370.

Odin, G. S., Curry, D., Hale, N. H. and Kennedy, W. J. 1982. The Phanerozoic time scale in 1981. In: Odin, G.S. (ed.). *Numerical Methods in Stratigraphy*, p. 957-960. Wiley, Chichester.

Ogg, J. 2020. Geomagnetic polarity time scale. In: *Geological Time Scale 2020*, Chapter 5, p. 159-189. Elsevier.

O'Reilly, S. Y. and Zhang, M. 1995. Geochemical characteristics of lava-field basalts from eastern Australia and inferred sources: connections with the subcontinental lithospheric mantle?, *Contributions to Mineralogy and Petrology,* 121, 148-170.

Paul, F. P. 1906. Foyaitisch-theralitische gesteine aus Tasmanien. *Mineralogische und Petrographische Mitteilungen,* 25, n.f. 269-318.

Piestrzeniewicz, R. 1972. *Ultramafic inclusions in some Tasmanian basic volcanic rocks.* B.Sc. Hons. thesis, University of Tasmania.

Renne, P. R., Swisher, C. C., Deina, A. L., Karner, D. B., Owens, T. L. and De Paola, D. J. 1998. Intercalibration of standards, absolute ages and uncertainties in $^{40}Ar/^{39}Ar$ dating. *Chemical Geology,* 145, 117-152.

Seymour, D. B. 1989 (compiler.). Geological Survey Explanatory Report, Geological Atlas 1:50 000 series sheet 36 (8015N) *St Valentines.*

Seymour, D. B. and Baillie, P. W. 1992. Geological atlas 1:50000 series. Sheet 7816S (20). Woolnorth. Tasmania Department of Mines.

Spry, A. H. 1962. Igneous Activity. In: Spry, A. and Banks, M. R. (eds.). The Geology of Tasmania. *Journal of the Geological Society of Australia,* 9, 255-284.

Steiger, R. H. and Jäger, E. 1977. Subcommission on Geochronology: convention on the use of decay constants in geo- and cosmochronology. *Earth and Planetary Science Letters,* 36, 359-362.

Sutherland, F. L. 1969. A review of the Tasmanian Cenozoic volcanic province. *Geological Society of Australia Special Publication,* 2, 133-144.

Sutherland, F. L. 1973a. The geological development of the southern shores and islands of Bass Strait. *Proceedings of the Royal Society of Victoria,* 85, 133-144.

Sutherland, F. L. 1973b. Igneous rocks, Central Plateau. In: Banks, M.R. (ed.). *The lake country of Tasmania : a symposium conducted by the Royal Society of Tasmania at Poatina*, p. 43-54. Royal Society of Tasmania, Hobart.

Sutherland, F. L. 1976. Cenozoic volcanic rocks. In: Leaman, D. E. Geological Survey Explanatory Report. Sheet 82 (8312S). *Hobart.* Tasmania Department of Mines.

Sutherland, F. L. 1977. Cenozoic volcanic rocks. In: Leaman, D. E. Geological Survey Explanatory Report. Sheet 75 (8312N). *Brighton.* Tasmania Department of Mines.

Sutherland, F.L. 1980. Aquagene volcanism in the Tasmanian Tertiary, in relation to coastal seas and river systems. *Papers and Proceedings of the Royal Society of Tasmania,* 114, 177-199.

Sutherland, F. L. 1989a. Tasmania and Bass Strait. In: Johnson, R. W. (ed.). *Intraplate Volcanism in Eastern Australia and New Zealand*, p. 143-149. Cambridge University Press.

Sutherland, F. L. 1989b. Tertiary basaltic magmas and the Tasmanian lithosphere. In: Burrett, C. F. and Martin, E. L. (eds.). Geology and Mineral Resources of Tasmania., p. 386-398. *Geological Society of Australia Special Publication,* 15.

Sutherland, F. L. 1989c. Cenozoic volcanic rocks. In: Forsyth, S. M. Geological Survey Explanatory Report. Sheet 61 (8313N). *Interlaken.* Tasmania Department of Mines.

Sutherland, F. L. 1991. Cenozoic volcanism, eastern Australia: a predictive model based on migration over multiple 'hotspot' magma sources. In: Williams, M. A. J., De Decker, P. and Kershaw, A. P. (eds.). The Cenozoic in Australia: A reappraisal of the evidence. *Geological Society of Australia Special Publication,* 18, 15-43.

Sutherland, F. L. 2003. 'Boomerang' migratory intraplate Cenozoic volcanism, eastern Australian rift margins and the Indian-Pacific mantle boundary. In: Hillis, R. R. and Müller, R. D. (eds.). Evolution and Dynamics of the Australian Plate, p.203-221. *Geological Society of Australia Special Publication,* 22 and *Geological Society of America Special Paper,* 372.

Sutherland, F. L. and Corbett, K. D. 1967. The Tertiary volcanic rocks of far northwestern Tasmania. *Papers and Proceedings of the Royal Society of Tasmania,* 101, 71-90.

Sutherland, F. L. and Hale, G. E. A. 1970. Cenozoic volcanism in and around Great Lake, central Tasmania. *Papers and Proceedings of the Royal Society of Tasmania,* 104, 17-32.

Sutherland, F. L. and Wellman, P. 1986. Potassium-argon ages of Tertiary volcanic rocks, Tasmania. *Papers and Proceedings of the Royal Society of Tasmania,* 120, 77-86.

Sutherland, F. L., Green, D. C. and Wyatt, B. W. 1973. Age of the Great Lake basalts, Tasmania, in relation to Australian Cenozoic volcanism. *Journal of the Geological Society of Australia,* 20, 85-94.

Sutherland, F. L., Hendry, D. F., Barron, B. J., Matthews, W. L. and Hollis, J. D. 1996. An unusual Tasmanian Tertiary basalt sequence near Boat Harbour, Northwest Tasmania. *Records of the Australian Museum,* 48, 131-161.

Sutherland, F. L., Forsyth, S. M. and Zwingmann, H. 2002. Bassian basalts: Dating, Cenozoic biogeohistory and a new model for Tasmanian volcanism. *Geological Society of Australia Abstracts Series,* 67, 251.

Sutherland, F. L., Graham, I. T., Everard, J. L., Forsyth, S. M. and Zwingmann, H. 2004. Cenozoic basalts, Tasmania: landscapes, exposures, ages, petrography, geochemistry, entrainments and petrogenesis. *Geological Society of Australia Field Guide A5*, 17th Australian Geological Convention, Hobart, February 2004.

Sutherland, F. L., Graham, I. T., Forsyth, S. M., Zwingmann, H. and Everard, J. L. 2006. The Tamar Trough revisited: correlations between sedimentary beds, basalts, their ages and valley evolution, north Tasmania. *Papers and Proceedings of the Royal Society of Tasmania,* 140, 49-72.

Tedford, R. H., Banks, M. R., Kemp, N. R., McDougall, I. and Sutherland, F. L. 1975. Recognition of the oldest known fossil marsupials from Australia. *Nature,* 255, 141-142.

Threader, V. M. 1987. Prospecting for heavy minerals in the Fingal Valley. *Tasmania Department of Mines Report,* 1987/08.

Tilley, C.E. 1928. Monticellite-nepheline-basalt from Tasmania. *Geological Magazine,* 65, 218.

Twelvetrees, W. H. and Petterd, W. F. 1899. Nepheline and melilite rocks from Shannon Tier. *Report of the Secretary of Mines (Tasmania) for 1898-9*, 45-46. Government Printer, Hobart.

Varne, R. 1977. The origin of the spinel lherzolite inclusions in the basaltic rocks from Tasmania and elsewhere. *Journal of Petrology,* 18, 1-23.

von Lichtan, I. J. 2000. *Characteristics and origin of proximal volcanic breccias in hydrothermal Tertiary basalt centres, in south-east Tasmania.* B.Sc. Hons. thesis, University of Tasmania, Hobart.

York, D. 1968. Least-squares fitting of a straight line with correlated errors. *Earth and Planetary Science Letters,* 5, 320-324.

Zhang, M., O'Reilly, S. Y., Everard, J. L. and Griffin, W. L. 2004. Petrogenesis of Tasmanian Tertiary basalts. *Geological Society of Australia Abstracts,* 73, 300.

Zwingmann, H., Sutherland, F. L., Graham, I., Forsyth, S. M., Everard, J. L. and Wartho, J.-A. 2004. New K-Ar and Ar-Ar ages for NE Tasmanian basalts: implications for volcanic evolution following Tasman rifting. *Geological Society of Australia Abstracts,* 73, 141.

APPENDIX 1

Petrographic descriptions of dated samples

TJ3602 (R005376)   hawaiite   Wedge Plains Link Road

Euhedral to subhedral, ± equant olivine microphenocrysts, typically 400-500 μm but up to 1 mm long, grade down to the groundmass. Some are clumped into glomerocrysts. The phenocrysts are unaltered or with incipient to slight alteration along internal fractures.

The groundmass is fresh, intergranular and consists of unaligned plagioclase laths (~100-200 μm), faintly pinkish titaniferous augite granules (mostly ≤100 μm), olivine granules, elongate angular opaque grains (≤150 μm long) and minor amounts of a low birefringence mesostasis. Rare subspherical amygdales, ~ 750 μm across, are filled with low birefringence zeolites.

TJ3591 (R005365)   transitional olivine basalt   Rabalga Track

Numerous small (mostly ≤ 500 μm) ± equant olivine microphenocrysts are partially (~20%) altered around rims and along fractures to pale to dark brown "iddingsite." There are also rare glomerocrysts, each of 3-4 augite crystals (~100 μm across).

 The fine-grained intergranular, slightly turbid groundmass consists of randomly oriented plagioclase laths (mostly ≤ 300 μm) , almost colourless clinopyroxene, and equant and angular to ± acicular opaque grains. A subspherical amygdale ~500 μm across contains core of very fine-grained pale brown clay minerals, surrounded by a mantle of zeolite.

KJ634 (R005410)   basanite   Eastons Creek, lower flow

Microphenocrysts of olivine and minor titaniferous augite lie in a poorly crystalline, fine-grained, intersertal groundmass.

Olivine microphenocrysts (typically 400 μm-1 mm) are euhedral to subhedral, but commonly strongly embayed, and partly (~15-20%) replaced by fibrous khaki-brown to red-brown alteration products ("iddingsite"). Sparse small (≤ 400 μm) equant euhedra of pinkish titaniferous augite may be zoned and grade into the groundmass.

The groundmass consists of narrow, randomly oriented plagioclase laths (typically 100-200 μm long) in a dark turbid mesostasis ("black glass"). Under high magnification and strong illumination, the latter is seen to largely consist of titaniferous augite crystallites and densely disseminated equant angular opaque grains (~15-30 μm across).

Irregular clear patches within the groundmass, into which plagioclase laths protrude, appear to be filled with a fine-grained, low birefringence mineral, possibly a zeolite. They may represent tears in a crustal mush, formed in the final stages of crystallisation.

TJ3228 (R005353)   nepheline hawaiite   knoll, Neasey Plains

Olivine phenocrysts and lherzolite debris lie in a very fine grained groundmass. The olivine phenocrysts (≤ 1mm x 200 μm) are typically euhedral or embayed, are crudely aligned to define a weak foliation, and grade down in size to granules (~100 μm). There are also sparse microphenocrysts of Ti-augite. Olivine is partly (~10%) replaced by pale brown fibrous alteration, probably an amphibole.

Small lherzolite xenoliths are present and xenocrysts derived by their disaggregation are abundant. These include anhedral olivine and clinopyroxene, brown spinel with opaque reaction rims, and orthopyroxene with reaction rims of finely granular clinopyroxene.

In the groundmass, abundant, randomly oriented, weakly coloured titaniferous augite prisms (~40-150 μm long x 10-20 μm) and equant ± rounded magnetite blebs (~5 – 20 μm across) are resolvable. XRD analysis also indicates that nepheline, stilbite and apatite are also present (Table 2; Appendix 3). A few small (few hundred μm), very irregular amygdales are filled with pale brown, very fine-grained low birefringence clay minerals (probably smectite).

CVH (R010192)   basanite   Coastview Hill, Hampshire

Abundant olivine microphenocrysts and rare glomerocrysts of pink titaniferous augite prisms lie in a dark turbid, very fine-grained groundmass.

The olivine microphenocrysts (mostly ≤ 500 μm) are generally equant and show some replacement by khaki brown-green alteration products. Under high magnification and strong illumination, crystallites of titaniferous augite and possible plagioclase, and very abundant equant magnetite grains (10-20 μm across) can be resolved in the groundmass. XRD analysis (Table 2; Appendix 3) confirms the presence of plagioclase and magnetite, and indicates that nepheline, analcime and apatite are also present; the alteration product of olivine is chlorite possibly chamosite).

SRN (R010187) basanite South Riana

Abundant, partly reacted anhedral xenocrysts (~400 μm to 2 mm) lie in a very fine-grained groundmass.

The xenocrysts comprise olivine, brown spinel with opaque reaction rims, and finely granular clinopyroxene, probably formed by reaction of orthopyroxene with the magma. Most xenocrysts are probably derived from disaggregation of lherzolite xenoliths. A few small (~250 μm), weakly embayed olivine euhedra and subhedra may be cognate phenocrysts.

The groundmass can be partly resolved into narrow clinopyroxene prisms (≤ 40 μm long) and abundant equant magnetite grains (10 – 30 μm across), together with indeterminate low birefringence material in which nepheline, analcime, plagioclase, anorthoclase and apatite were detected by XRD analysis (Table 2; Appendix 3).

Much of the olivine is replaced by pale brown finely fibrous alteration products, which XRD suggests consists of smectite, chlorite and a serpentine group mineral. Numerous small (100-500 μm diameter), subspherical amygdales are filled with isotropic or low birefringence material, probably analcime.

LLC (R010186) alkali olivine basalt Lillicos Beach

This porphyritic basalt consists of olivine phenocrysts in a fine-grained fluidal intergranular groundmass.

Olivine phenocrysts (typically 0.5 – 2.5 mm) are euhedral, rarely weakly embayed and show slight to moderate (5-15%) replacement by pale brown fibrous material, possibly amphibole.

The groundmass consists of abundant plagioclase laths (100-200 μm long), locally aligned, intergranular weakly coloured augite granules and prisms (10-30 μm) and small equant opaque grains (~10-20 μm across).

AJ99 (R004332) olivine nephelinite Olivers Hill, via Ringarooma

Abundant olivine anhedra and subhedra (≤ 1.5 mm) grade down to a very fine-grained groundmass. Anhedral olivine is probably xenocrystal; some grains show signs of resorption and/or re-equilibration (zoning) near their rims. Subhedral to euhedral olivine is less abundant and generally smaller (≤ 500 μm).

The groundmass contains aligned narrow prisms of augite (~50 – 100 μm long), with small equant magnetite grains (~5-15 μm) and larger irregular aggregates (≤ 150 μm). The low birefringence mesostasis consists largely of nepheline and analcime, together with some apatite (XRD analysis, Table 2). Plagioclase was not detected. Rare inhomogeneities are suggestive of digested xenoliths.

A crude streaky foliation is defined by alignment of long axes of olivine phenocrysts, small augite prisms, and variations in the grain size and mineral proportions of the groundmass. Rare small elongate to cuspate amygdales (≤ 500 μm long) are aligned parallel to the foliation and filled with a pale brown isotropic mineral, possibly smectite. Otherwise, the rock is fresh.

AJ1424 (R004366) basanite N end of hill near Sweets Creek

This porphyritic basalt contains abundant olivine phenocrysts (≤ 3 mm, commonly 0.5-1.5 mm, grading down to groundmass), which are typically ±equant, subhedral, commonly embayed, or less often anhedral, rarely euhedral.

The groundmass consists mainly of pinkish prisms of titaniferous augite (≤ 200 μm), and equant magnetite grains (≤ 40 μm) in a low birefringence mesostasis in which some plagioclase and accessory finely acicular apatite are resolvable. XRD analysis (Table 2) also detected nepheline, analcime and anorthoclase. There is some development of plagioclase platelets (≤ several mm long). Sparse amygdales (1-2 mm across) are filled with zeolite, probably chabazite, and some secondary chlorite and smectite are also present.

AJ1425 (R004367) hawaiite S end of hill near Sweets Creek

This markedly porphyritic basalt consists of subhedral to euhedral, olivine phenocrysts (0.5 – 2 mm), some deeply embayed, and glomerocrysts. The intergranular groundmass consists of plagioclase laths (≤ 200 μm), weakly titaniferous augite, opaque grains (mostly ≤100 μm, polygonal to rarely skeletal) and a low birefringence mesostasis that may include some alkali feldspar.

A few olivine phenocrysts are slightly to partly (5 - 50%) altered to fine-grained orange-brown "iddingsite", whereas the groundmass is fresh.

AJ1426 (R004368)   olivine nephelinite   Upper Esk

Sparse, embayed olivine anhedra (≤4 mm) and numerous smaller, anhedral to euhedral olivine microphenocrysts lie in a fine-grained groundmass of titaniferous augite platelets, magnetite grains (mostly 10 – 50 μm) and a clear colourless mesostasis largely comprising nepheline, analcime, plagioclase and minor apatite (Table 2). Amygdales are filled with a zeolite, probably phillipsite, and minor chlorite is also present.

PP20.5m (R027027)   olivine nephelinite   "Pebble Plain", Beauty Flat

Euhedral phenocrysts of olivine (up to 3mm, but mostly ≤ 0.5 mm) and rare titaniferous augite (≤1 mm) grade down to a groundmass of olivine, titaniferous augite, sparse narrow plagioclase laths (typically 300 – 500 μm long x 30 – 50 μm wide) and rounded magnetite grains (~30-150 μm across) with interstitial nepheline, anorthoclase and finely acicular apatite. There is some incipient to partial alteration of olivine to yellow-green "bowlingite", which may consist of chlorite and smectite. An amygdale (~3 x 1 mm) is filled with zeolite, possibly chabazite (see Table 2), with a central core of colourless chlorite.

WSc (R010201)   olivine nephelinite   Sledge Track, West Scottsdale

Scattered xenocrysts comprise anhedral olivine (≤ 2 mm) and rare anhedral spinel (≤ 400 μm) with opaque rims, together with finely granular aggregates of olivine and/or augite, possibly reacted orthopyroxene xenocrysts. These are presumably derived from spinel lherzolite xenoliths, which are common at this locality. Smaller olivine grains, some of which display rounded but possibly subhedral form, may be partly resorbed cognate microphenocrysts.

The fine- to medium-grained, well crystallised groundmass consists of narrow augite prisms (≤200 μm), olivine granules, equant magnetite grains (~20 – 40 μm) and larger aggregates, together with a low birefringence mesostasis. XRD analysis (Table 2) suggests that the mesostasis largely consists of nepheline, plagioclase, anorthoclase and a zeolite, possibly mesolite, together with apatite. Patches of brown alteration, probably chlorite and smectite, are present in the groundmass.

SDL (R010202)   olivine nephelinite   The Sideling

Abundant xenocrysts are of all sizes from about 2.5 mm, grading down to a very fine-grained groundmass. Most are anhedral olivine, but there are also small rounded anhedral of yellow-brown spinel with narrow opaque rims, and aggregates of finely granular clinopyroxene, probably derived from reaction of orthopyroxene or recrystallisation of clinopyroxene xenocrysts. All are presumably derived from disaggregation of spinel lherzolite xenoliths which are abundant at this locality.

There is also some subordinate euhedral to subhedral olivine (≤ 1 mm), probably cognate phenocrysts.

The groundmass consists of minute elongate prisms of augite (≤ 50 μm long), olivine granules, abundant equant magnetite grains (~5 -20 μm across) and larger (~50 – 200 μm) aggregates thereof, and an indeterminate low birefringence mesostasis. XRD analysis (Table 2) indicates that the mesostasis is largely nepheline with minor apatite and plagioclase.

The only alteration is a slight pale brown discoloration along internal fractures within a few olivine xenocrysts.

BLS (R010204)   basanite   Blessington

The rock contains spinel lherzolite xenoliths and derived debris, including olivine, clinopyroxene and opaque (reacted) spinel xenocrysts to mm. Some colourless clinopyroxene xenocrysts have a narrow reaction rim of pink titaniferous augite.

Euhedral to subhedral phenocrysts (≤ 2 mm but mostly ~500 μm or smaller) of olivine, and less commonly pink titaniferous augite, are also present.

The groundmass consists of relatively sparse and small but strongly aligned plagioclase laths (~100 – 200 μm) . olivine granules (mostly > 50 μm), titaniferous augite granules (mostly <50 μm), together with equant opaque grains (~10-20 μm) and their larger aggregates.

A few small (~500 μm) irregular amygdales are filled with zeolite. Alteration is largely restricted to fractures within a few olivine phenocrysts.

SB9 (R005506)   olivine tholeiite "Eastbourne", via Avoca

Olivine phenocrysts lie in a fine-grained intersertal groundmass of randomly oriented plagioclase laths (~100 – 200 μm), augite and olivine granules (mostly ≤ 100 μm) and an interstitial dark turbid mesostasis of "black glass."

The olivine phenocrysts (≤ 1 mm) are euhedral to deeply embayed or skeletal, but largely unaltered. The mesostasis consists of trichites of plagioclase and augite, and densely disseminated, very fine-grained "opaque dust." A few irregular amygdales are filled with a pale yellow-brown ± isotropic clay mineral (smectite?).

SB11 (R005508)   nepheline hawaiite   Llewellyn, via Avoca

The rock contains very abundant xenocrysts derived from disaggregation of spinel lherzolite xenoliths, together with smaller more euhedral phenocrysts of olivine and titaniferous augite, in a very fine-grained but well crystallised, fresh groundmass.

Olivine anhedra (≤ 3 mm) are the most common xenocryst. Smaller, less abundant rounded anhedra of spinel (≤500 μm) have mostly reacted with the groundmass to an opaque phase, but a few preserve dark brown relict cores. A large corroded orthopyroxene xenocryst (biaxial positive, so En > 88) is surrounded by a reaction corona of finely granular (~50 μm) olivine, and xenocrysts of similar granular olivine may represent completely reacted former orthopyroxene. Rare colourless clinopyroxene xenocrysts also show signs of resorption and reaction with the groundmass, including embayment and rims of faintly yellow-pink (more titaniferous?) clinopyroxene.

Euhedral to subhedral phenocrysts and microphenocrysts of olivine (~0.5 – 1.5 mm) and subordinate titaniferous augite are smaller and grade down into the groundmass.

The groundmass consists of strongly aligned narrow prisms of augite (~50 – 150 μm long), equant opaque grains and aggregates (5 – 50 μm across), olivine granules and a low birefringence mesostasis. Sparse small irregular amygdales are filled with a pale yellow-brown isotropic material, possibly a smectite.

LSB24 (R004501)   nepheline hawaiite   Burburys Sugarloaf, via Ross

The rock consists of scattered olivine and augite anhedra in a fine-grained groundmass of augite, olivine, opaque minerals, minor biotite and nepheline (confirmed by X-ray diffraction), with a low birefringence mesostasis. The latter may largely consist of sodic plagioclase and anorthoclase, as large elongate lath-like plates (≤ 5 mm long) have in places crystallised, poikilitically enclosing the other groundmass phases.

The olivine anhedra are typically equant and range in size from 2 mm to a few hundred μm. Undoubtedly most, if not all, are derived from disaggregation of lherzolite nodules, or are related mantle-derived xenocrysts. Rare anhedral xenocrysts of finely granular (?)oIivine and/or clinopyroxene may result from the reaction of lherzolite-derived orthopyroxene with the liquid. Very rare spinel xenocrysts are also present.

The sparsely distributed, subhedral to euhedral clinopyroxene microphenocrysts range in grain size from a few hundred micrometres down to the groundmass. The mineral is very pale yellow-grey, biaxial positive with moderate 2V, and is probably slightly titaniferous augite. A few crystals are apparently zoned with a deeper yellowish, probably more titaniferous rim.

The groundmass consists mainly of equant granules (typically 50- I5O μm across) of both augite and olivine, as well as very abundant tiny augite laths (typically 30- 60 x 5- 10 μm) and abundant equidimensional, polygonal opaque minerals (typically 10-30 μm), probably titanomagnetite, together with an indeterminable low birefringence mesostasis. The groundmass olivine is optically negative and, in contrast to the phenocrysts, is therefore a relatively iron-rich variety, probably in equilibrium with the magma. Scattered rounded opaque patches up to 200 μm across appear to be aggregates of smaller grains. The groundmass also contains occasional small (50- 100 μm) ragged grains of biotite, pleochroic from deep red-brown to pale yellow-brown. Accessory apatite is also present.

In some thin sections, 40-50% of this groundmass has been poikilitically enclosed, with olivine, augite and opaque granules riddling elongate feldspar laths up to 5 mm long. Although the coarse nature of their twinning makes the Michel-Levy method difficult to apply, the low extinction angles and positive optic sign suggest that the majority are sodic plagioclase (albite or sodic oligoclase). However a few sections exhibit finely cross-hatched twinning and give an optically negative figure with moderate 2V, indicating anorthoclase.

Equidimensional patches, mostly 100- 150 ~m across, containing usually polycrystalline aggregates of colourless mineral grains with low relief and birefringence, are scattered throughout the slides. The majority are probably small amygdales, but a few have a crudely polygonal outline suggesting crystal faces. Most are filled with an undetermined, biaxial negative zeolite, but a few give uniaxial negative figures and may be small grains of primary nepheline.

In most thin sections alteration is confined to incipient orange-brown iddingsitisation of olivine.

LCr (R010205)   **olivine nephelinite**   **western side of Lake Crescent**

The rock consists of very abundant xenocrysts (spinel lherzolite debris), together with phenocrysts of olivine and titaniferous augite in a very fine-grained groundmass.

The xenocrysts comprise olivine (≤ 3 mm), anhedral brown spinel (≤ 500 μm) usually with opaque reaction rims, orthopyroxene surrounded by reaction coronas of granular clinopyroxene, and partly recrystallised colourless clinopyroxene with narrow pale yellow zoned rims (possibly titaniferous augite).

Euhedral to subhedral phenocrysts (typically 500 μm – 1 mm) of olivine and pinkish- yellow titaniferous augite grade down to the groundmass. The latter commonly consist of a core mottled with numerous minute opaque inclusions, surrounded by a narrow clear zoned rim.

The groundmass is composed of narrow titaniferous augite prisms (~100 μm long), equant magnetite grains (~5 – 50 μm across), olivine granules, a few minute grains of red-brown biotite, and a low birefringence mesostasis, mainly nepheline, analcime, plagioclase and apatite (see XRD results, Table 2). The augite prisms are locally strongly aligned, but there is no consistent foliation on thin section scale. Sparse small irregular amygdales are filled with a pale yellow-brown isotropic secondary mineral, possibly smectite.

Alteration is mainly limited to minor development of pale yellow-brown fibrous length-slow amphibole, probably anthophyllite, along internal fractures in olivine xenocrysts. XRD analysis confirms that amphibole and mica are present.

ATr (R010218)   **olivine melilitite**   **Alma Tier**

Euhedral microphenocrysts of olivine (≤ 500 μm) and sparser but larger (≤ 1.5 mm) euhedra of titaniferous augite lie in a very fine-grained groundmass of narrow melilite laths (≤ 80 μm long), clinopyroxene crystallites, abundant equant magnetite grains and aggregates (mostly 5 – 40 μm), together with veinlets and coarser patches of nepheline, alkali feldspar (?), twinned zeolite, and amygdales of fibrous zeolite. XRD analysis indicates that the zeolites include mesolite, and that apatite and possibly chlorite are present (Table 2). The diffractogram also contains weak peaks that were attributed to plagioclase (Appendix 3), but this is considered unlikely due to the presence of melilite and the strongly silica-undersaturated bulk composition (Table 3).

Another sample from this locality was described by Sutherland (in Forsyth, 1989, p. 49).

BRJ1 (R010044)   **quartz tholeiite**   **Crooked Billet Creek, via Brighton**

Typically subhedral and slightly to moderately embayed olivine phenocrysts (~1 – 2.5 mm) are little altered. The dominantly intergranular to intersertal groundmass consists of randomly unoriented plagioclase laths (~140 – 400 μm long), interstitial to less commonly subophitic colourless augite granules (~ 100 – 200 μm across) and abundant patches of a dark fine-grained poorly crystalline mesostasis ("black glass"). This consists largely of finely acicular opaque grains (≤ 500 μm long) and a dense dissemination of opaque blebs. Some yellow-brown isotropic palagonite is associated with the mesostasis. Rare small vesicles are present.

HBJ23 (R010093)   **quartz tholeiite**   **Dragon Point, Claremont**

The rock has an intersertal texture and consists of randomly oriented plagioclase laths (≤ 1.5 mm, but typically ~500 μm long), interstitial ± equant colourless augite granules (≤ 600 μm but typically ~100 μm) in a dark fine-grained turbid mesostasis. Olivine is absent.

Trichites of plagioclase and augite, and densely disseminated extremely fine-grained opaque dust, are resolvable in the mesostasis. Irregular amygdales are filled with a pale yellow-brown fine-grained very clay mineral (smectite?). Similar material, together with some fine-grained carbonate, fills a few ± spherical amygdales up to 1mm across.

GFN (G402497)   **basanite**   **Glenfern, via New Norfolk**

Abundant xenocrysts (spinel lherzolite debris) and phenocrysts of olivine and titaniferous augite lie in a fine-grained intergranular groundmass.

Embayed olivine xenocrysts (≤ 3 mm) and glomerocrysts are abundant. Less common orthopyroxene xenocrysts are surrounded by reaction coronas of fine-grained olivine. Sparse, rounded to lobate spinel (≤ 0.5 mm) may retain unaltered brown cores, but are mostly opaque. Aggregates of finely granular clinopyroxene and/or olivine may be completely recrystallised clinopyroxene or reacted orthopyroxene xenocrysts.

Euhedral phenocrysts (mostly 0.5 – 1.5 mm) of olivine and titaniferous augite grade down to the groundmass. Olivine may be strongly embayed to rarely skeletal, and titaniferous augite commonly contains mottled inclusion-rich cores and narrow clear zoned rims.

The intergranular groundmass consists of aligned narrow plagioclase laths (~ 40 – 100 μm long), with interstitial pinkish titaniferous granules and prisms, olivine granules, equant magnetite grains (~10-40 μm) and a low birefringence mesostasis in which x-ray diffraction detected nepheline, anorthoclase, apatite and an unidentified zeolite (Table 2). A few irregular, clear mesostasis-rich patches probably formed in the final stages of crystallisation.

There is minor partial alteration of olivine by fibrous yellow-brown secondary minerals, possibly including anthophyllite.

HBJ6 (R010076)   hawaiite   Pickett Hill, via Kingston

Anhedral xenocrysts of olivine, some several mm across, and reacted spinel are probably disaggregated lherzolite xenoliths. Smaller (~100 μm) olivine euhedra and subhedra, and a few euhedra of weakly coloured titaniferous augite, are probably cognate.

These lie in a fine-grained fluidal groundmass of aligned plagioclase laths (~100 μm), tiny clinopyroxene prisms (~50 μm long), abundant equant opaque grains (~5-20 μm) and a few per cent flakes of red-brown biotite. A streaky foliation is defined by alignment of plagioclase and clinopyroxene, and variations in grain size and possibly relative mineral abundance.

There are several coarser-grained ovoid, probably late magmatic segregations, up to 4 mm across, consisting of nepheline(?), narrow pale blue clinopyroxene or amphibole prisms, and biotite.

Alteration is largely confined to the margins and internal fractures of xenocrysts.

SBA21 (R010159)   olivine tholeiite   Quarry, Marion Bay

This slightly vesicular basalt consists of euhedral to embayed phenocrysts of olivine (typically 1 – 3mm long), lying in an intergranular groundmass of randomly oriented plagioclase laths (typically 200 – 500 μm long), granules of augite, elongate to acicular opaque grains and small interstitial patches of poorly crystalline mesostasis.

Olivine is partly altered to a bright orange-brown fibrous amphibole (? possibly anthophyllite). Minor patches of pale yellow-brown alteration (smectite?) occur in the groundmass. Irregular voids at least 2 mm long are present.

APPENDIX 2

Photomicrographs
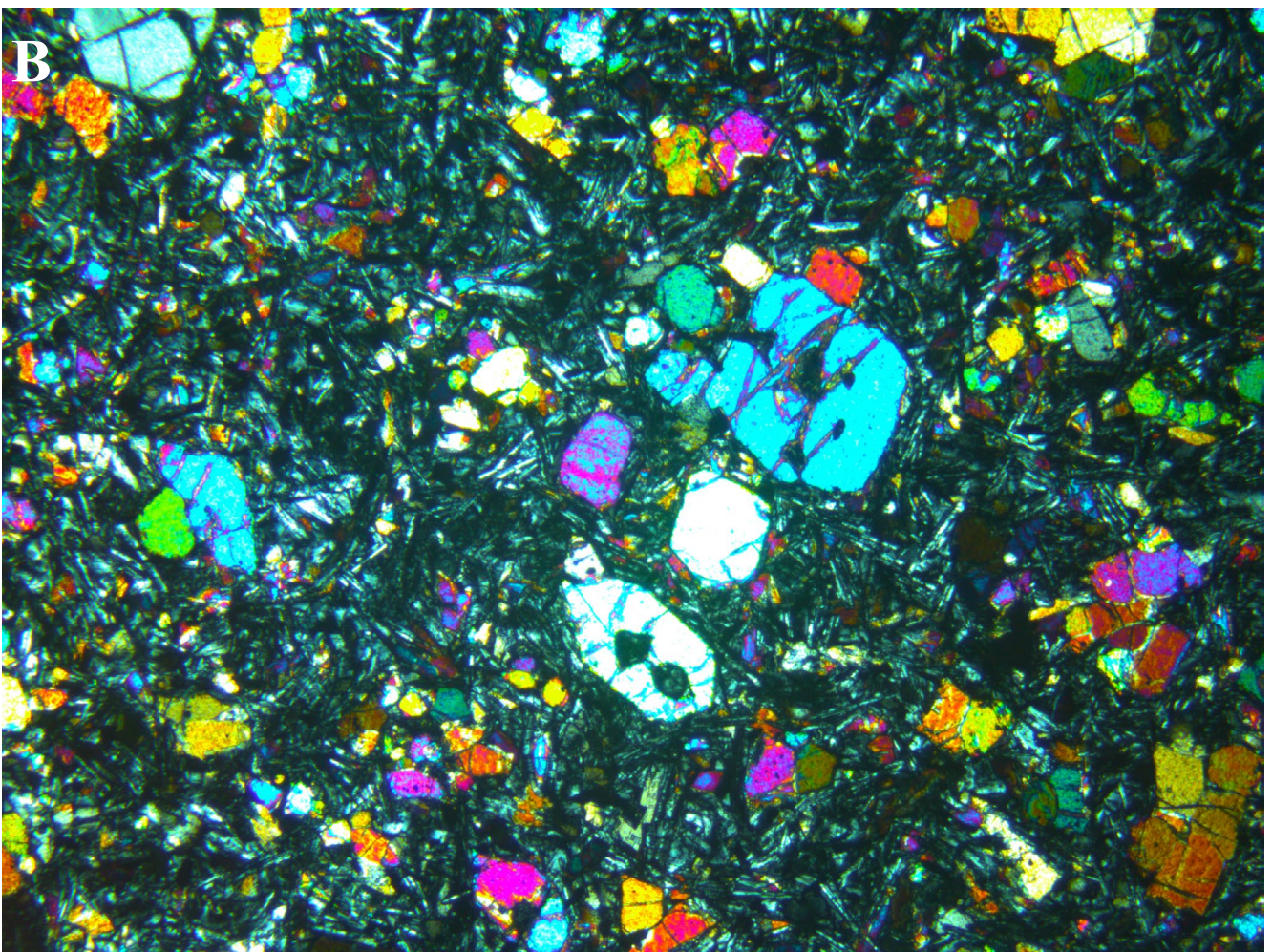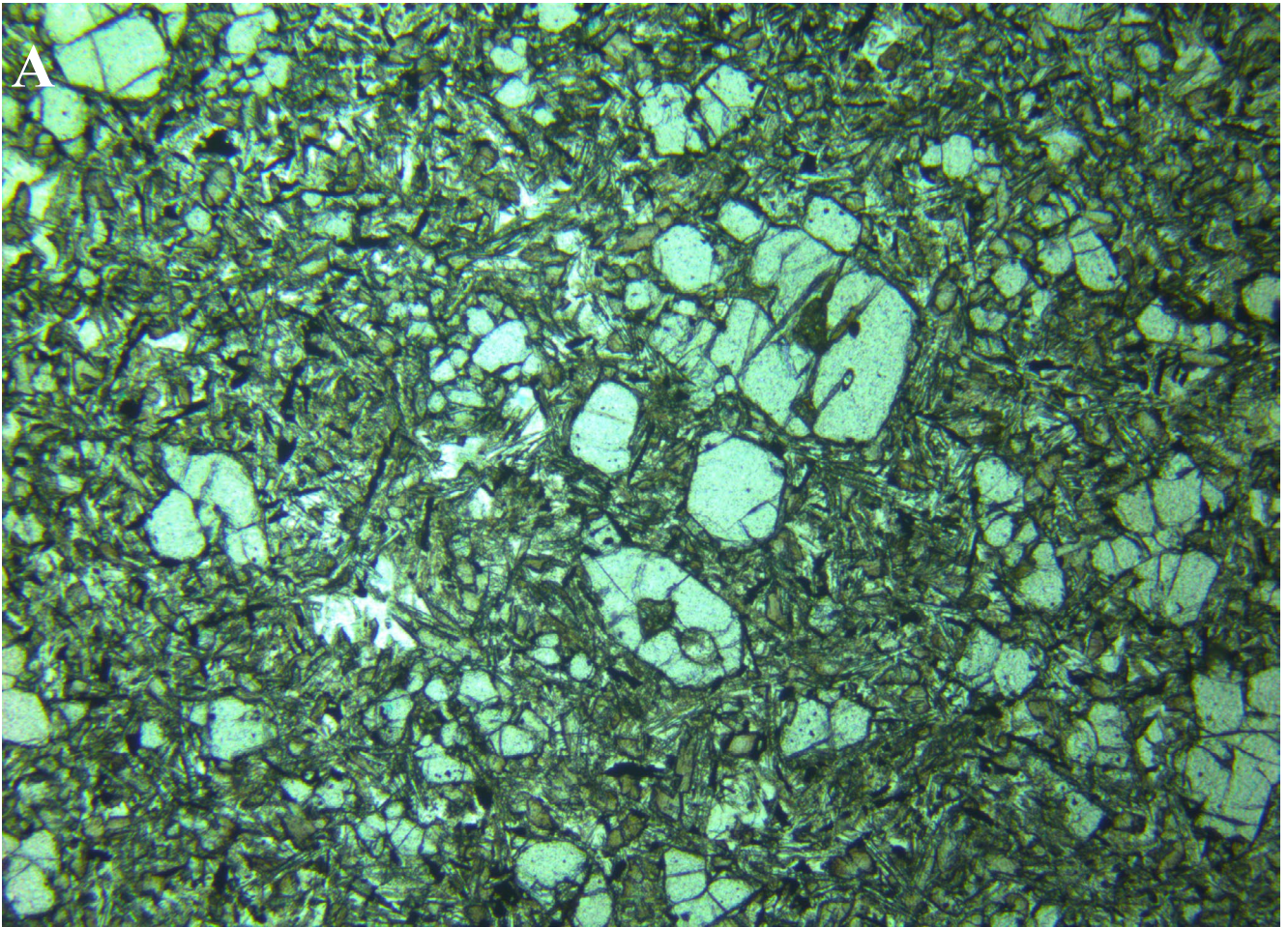
Figure 13. Photomicrograph of sample TJ3602, hawaiite, Wedge Plains Link Road, far NW Tasmania. Olivine microphenocrysts in an intergranular groundmass. Field of view~4.6 x 3.4 mm. (a) plane polarised light (b) crossed nicols.
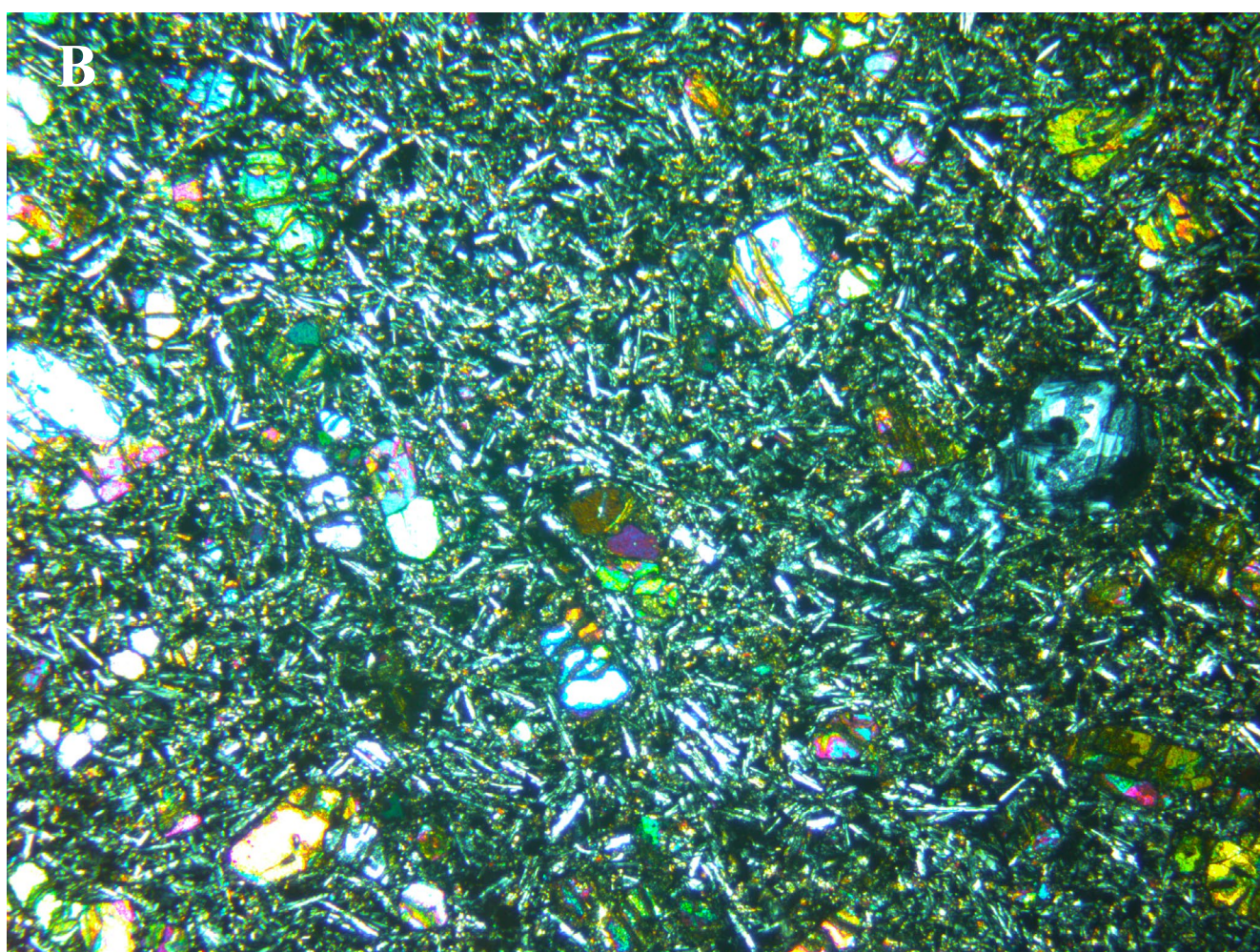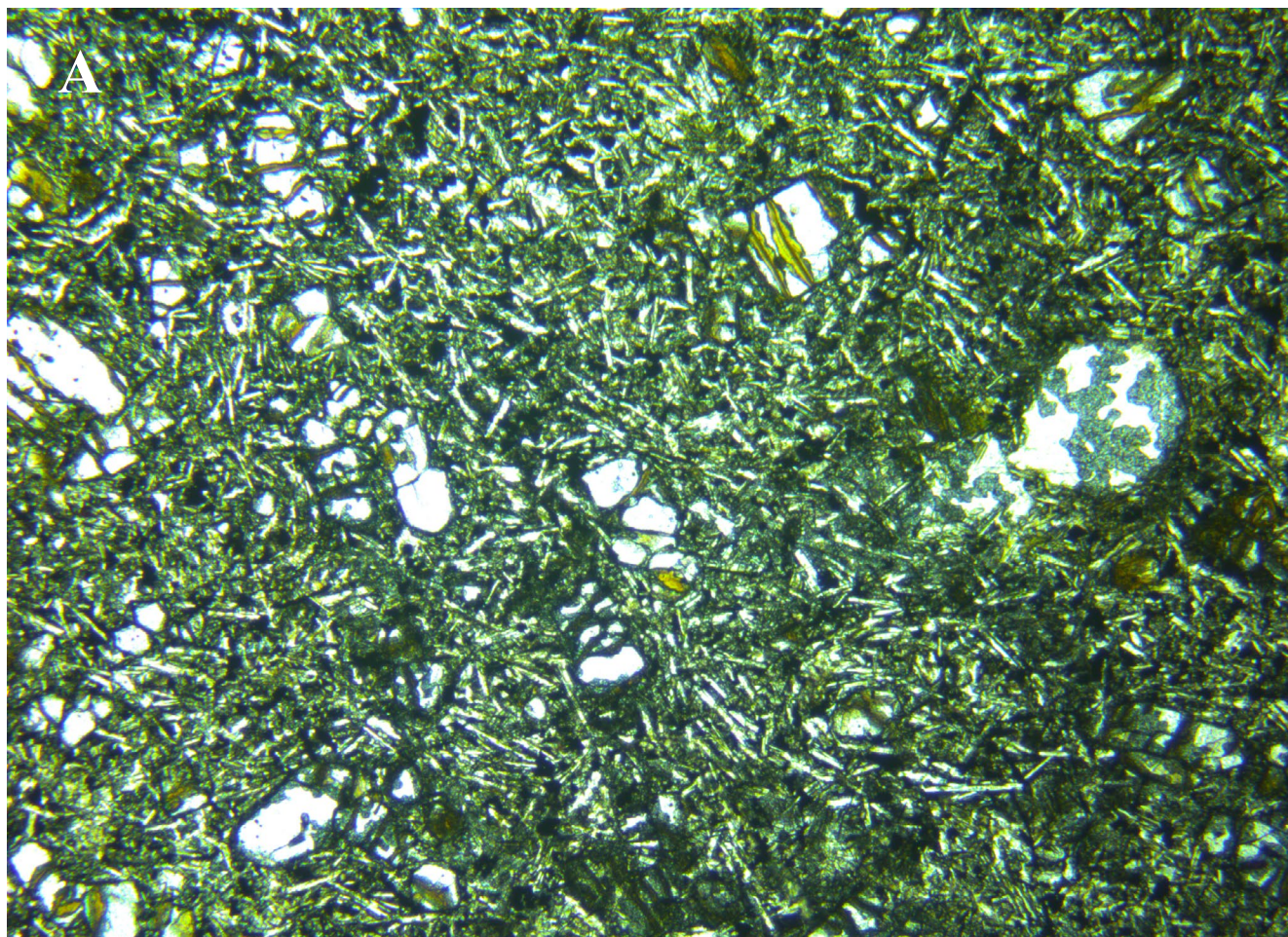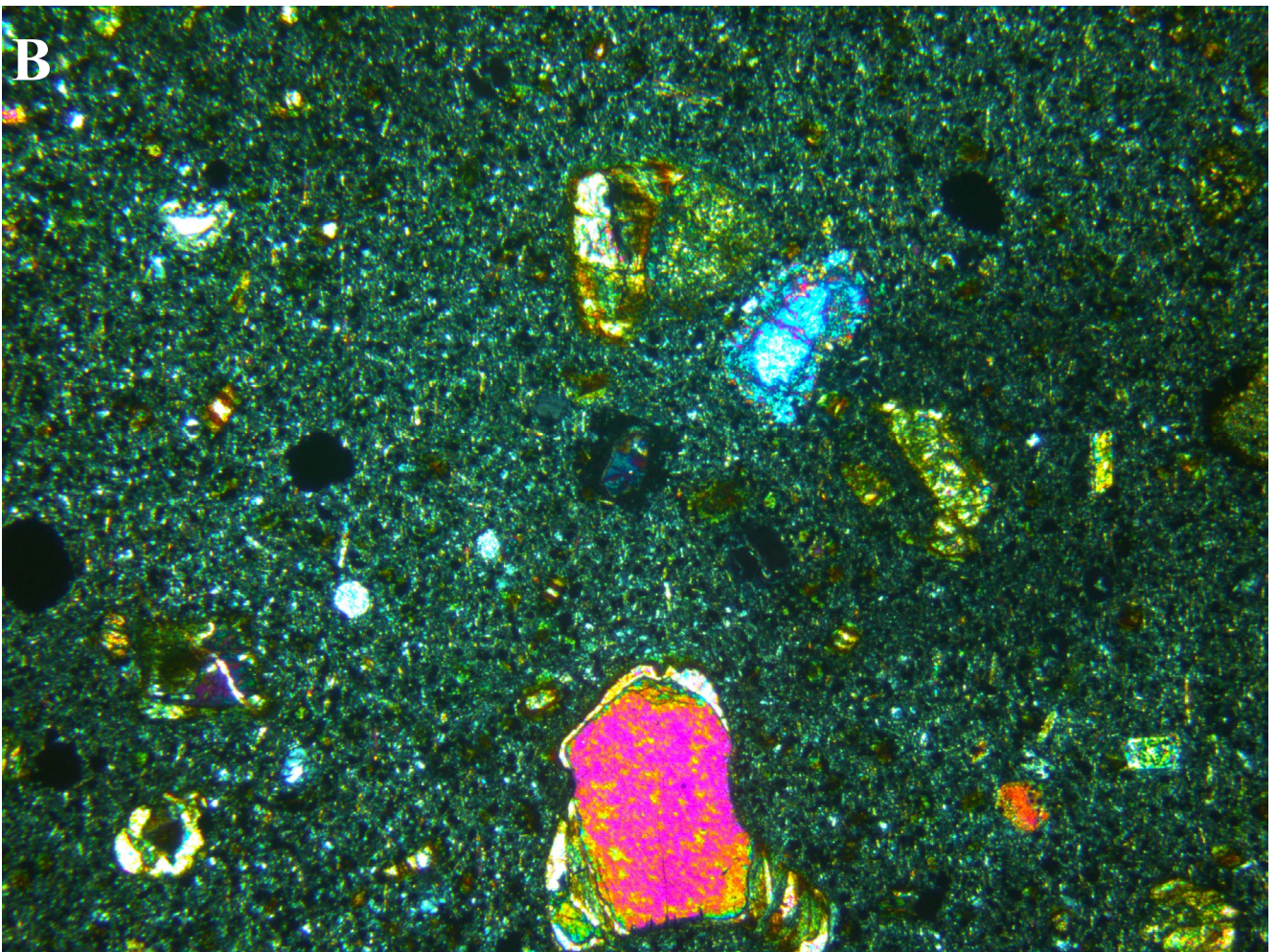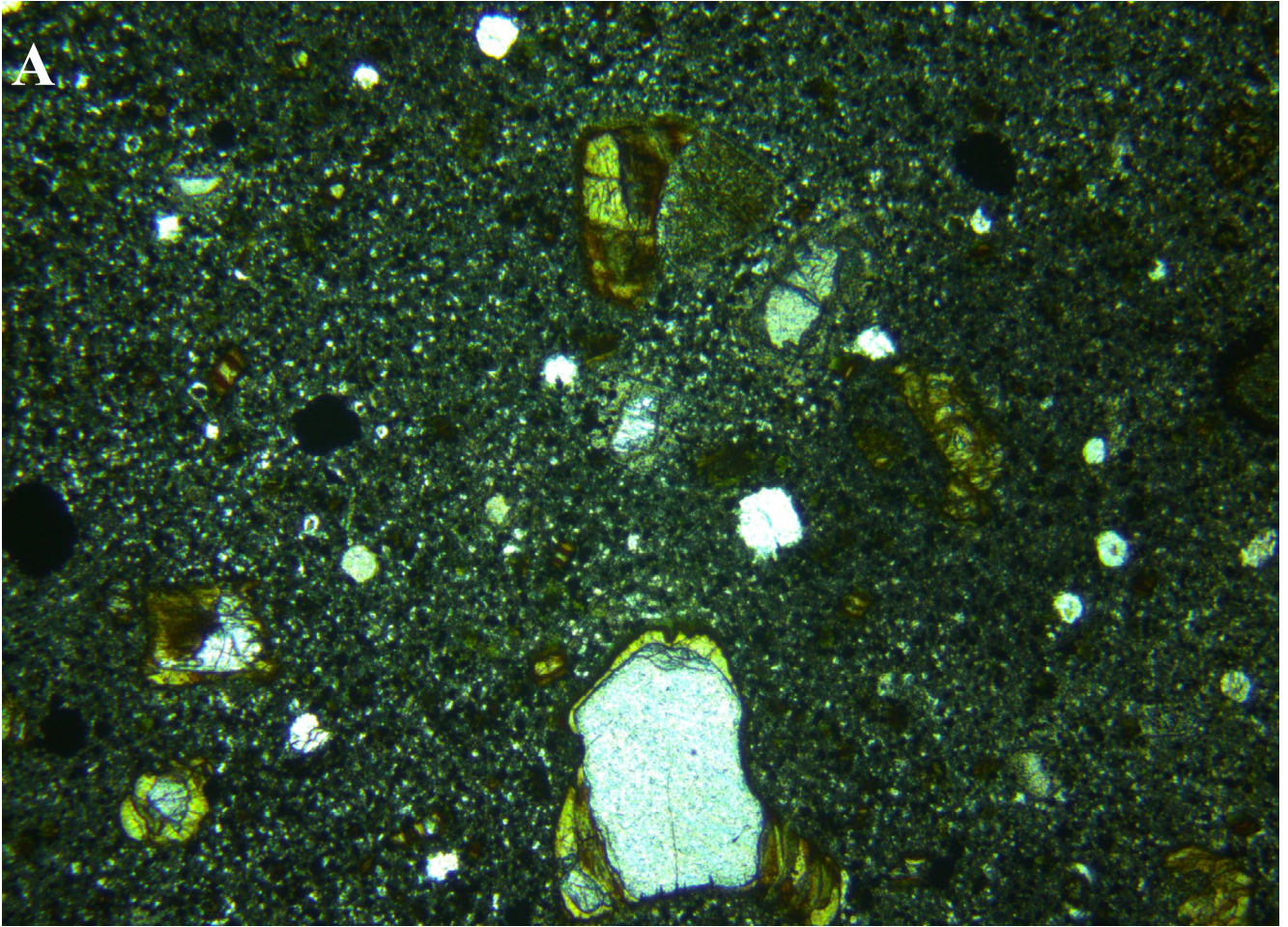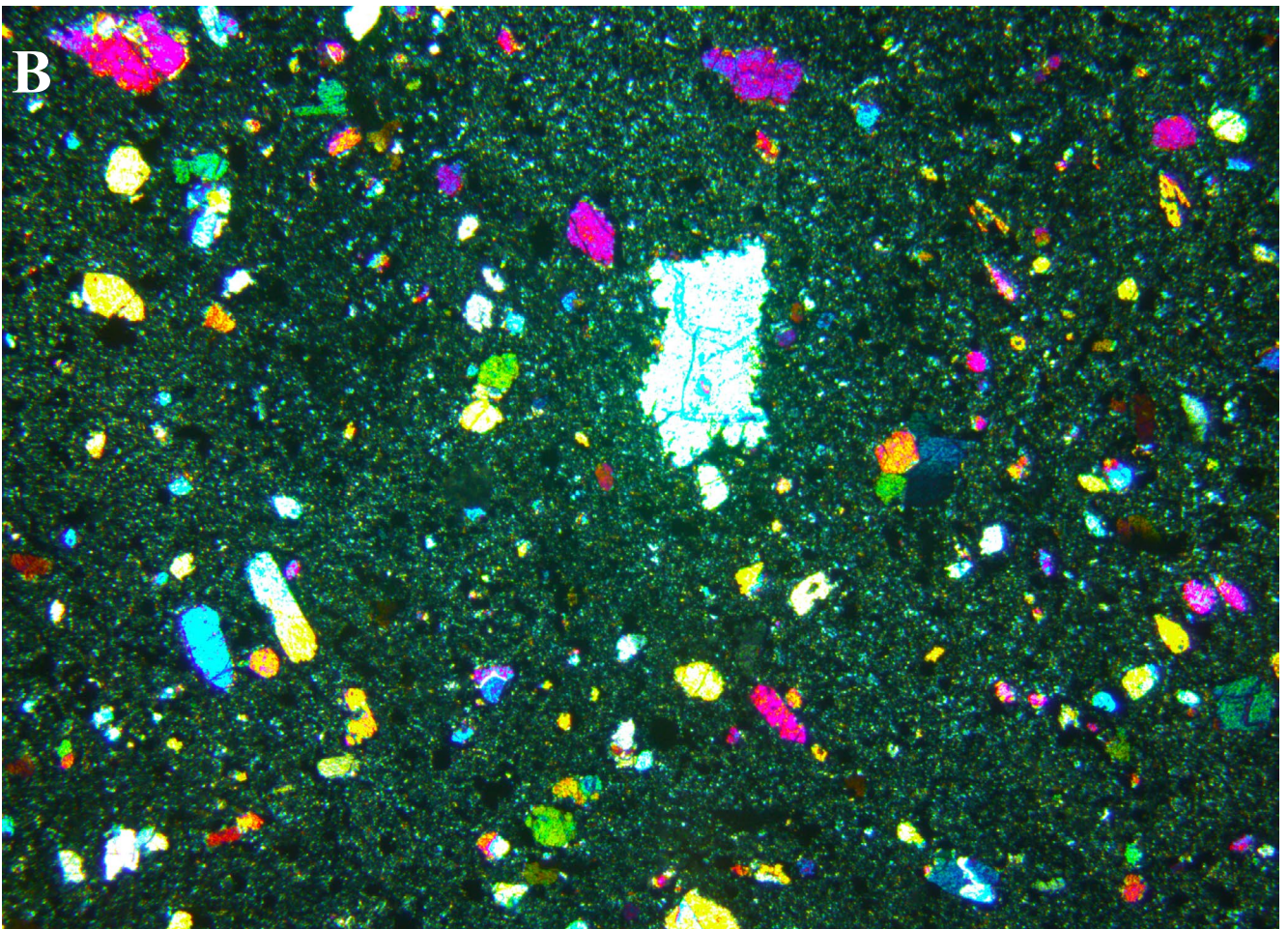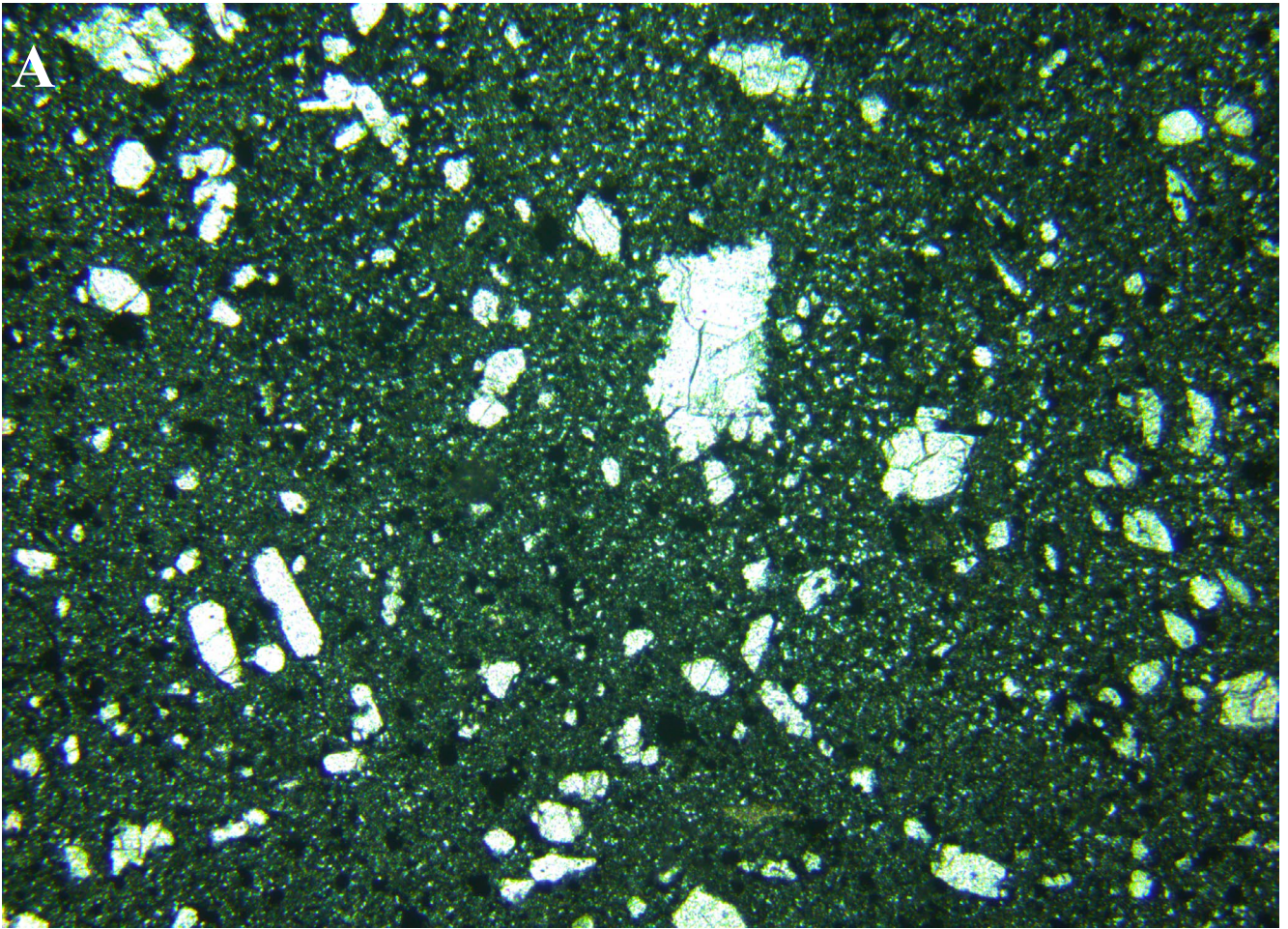
Figure 14. Photomicrograph of sample TJ3591, transitional olivine basalt, Rabalga Track, far NW Tasmania. Partly altered olivine microphenocrysts in an inter-granular groundmass; amygdale with zeolite at centre right. Field of view~4.6 x 3.4 mm. (a) plane polarised light (b) crossed nicols.
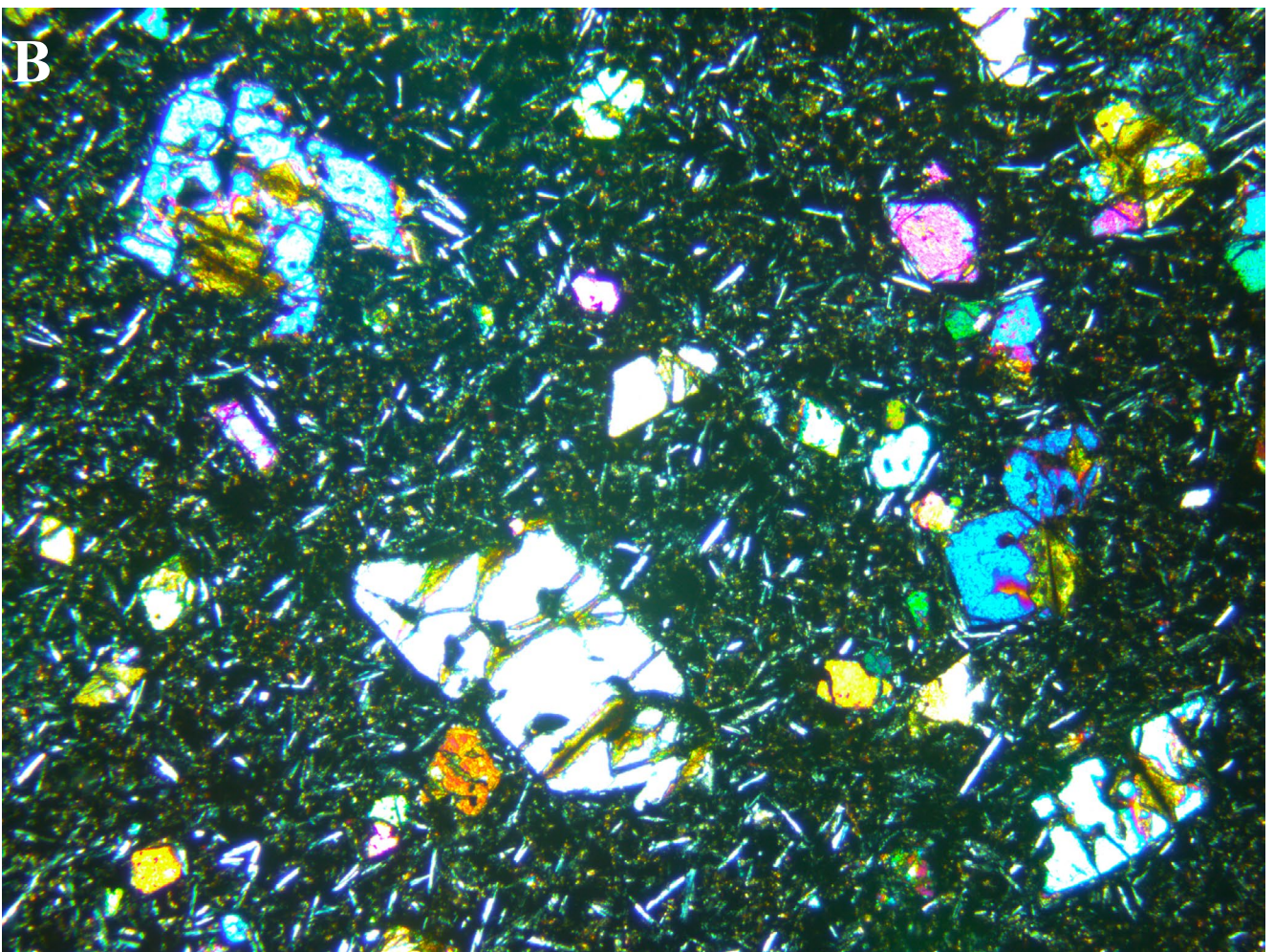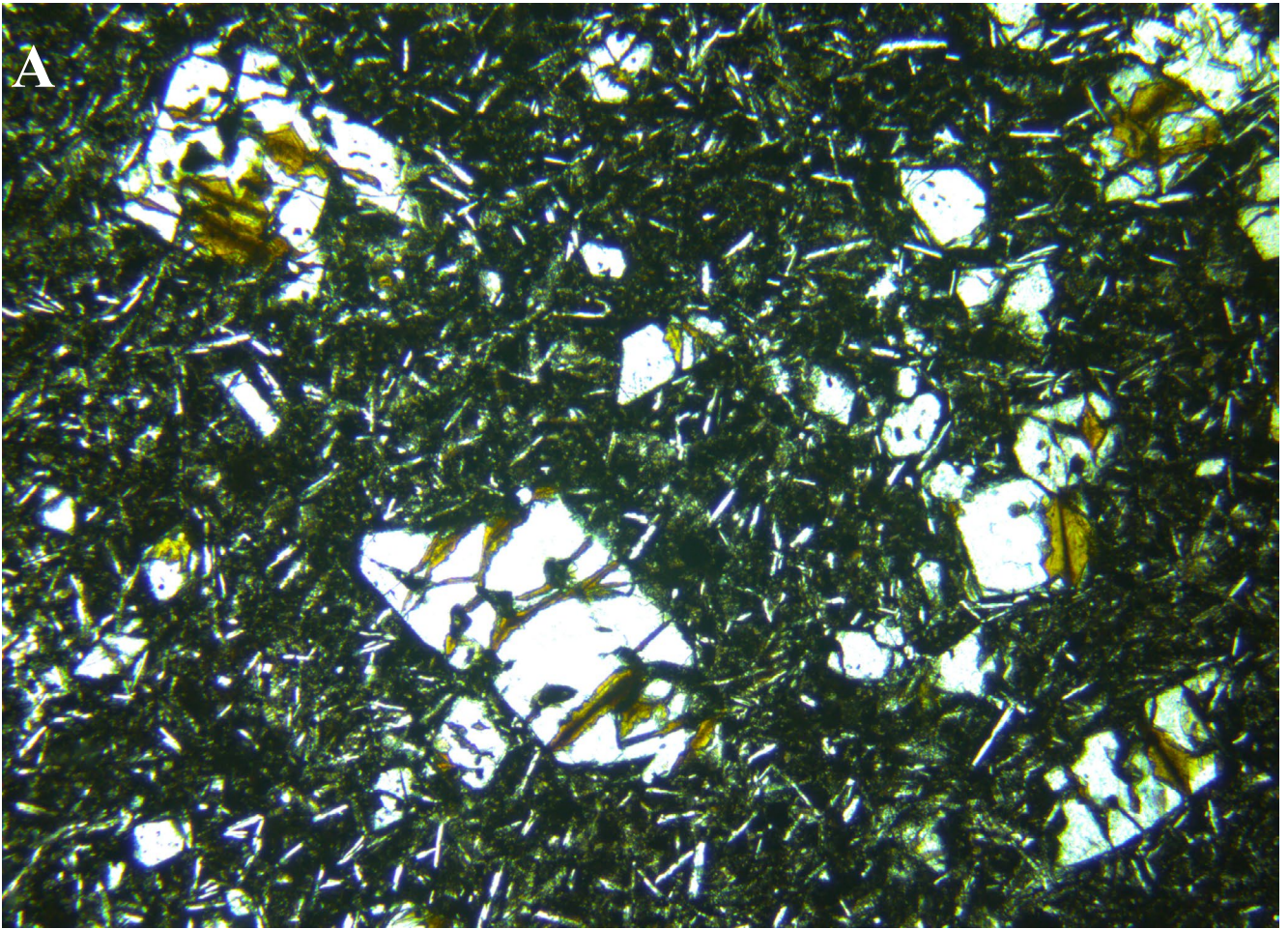
Figure 15. Photomicrograph of sample KJ634, basanite, Eastons Creek, far NW Tasmania. Partly altered olivine microphenocrysts in an intersertal groundmass. Field of view~4.6 x 3.4 mm. (a) plane polarised light (b) crossed nicols.
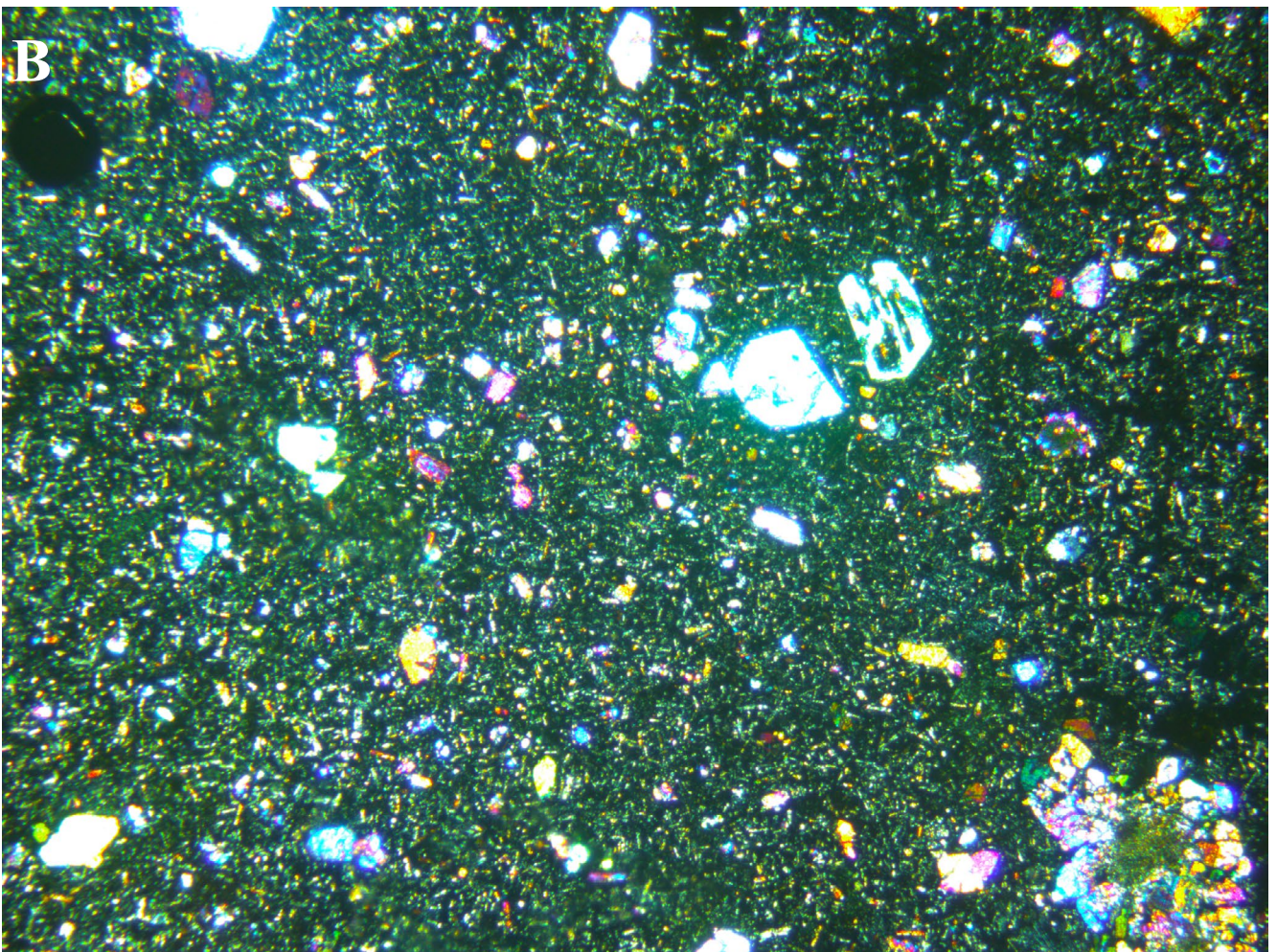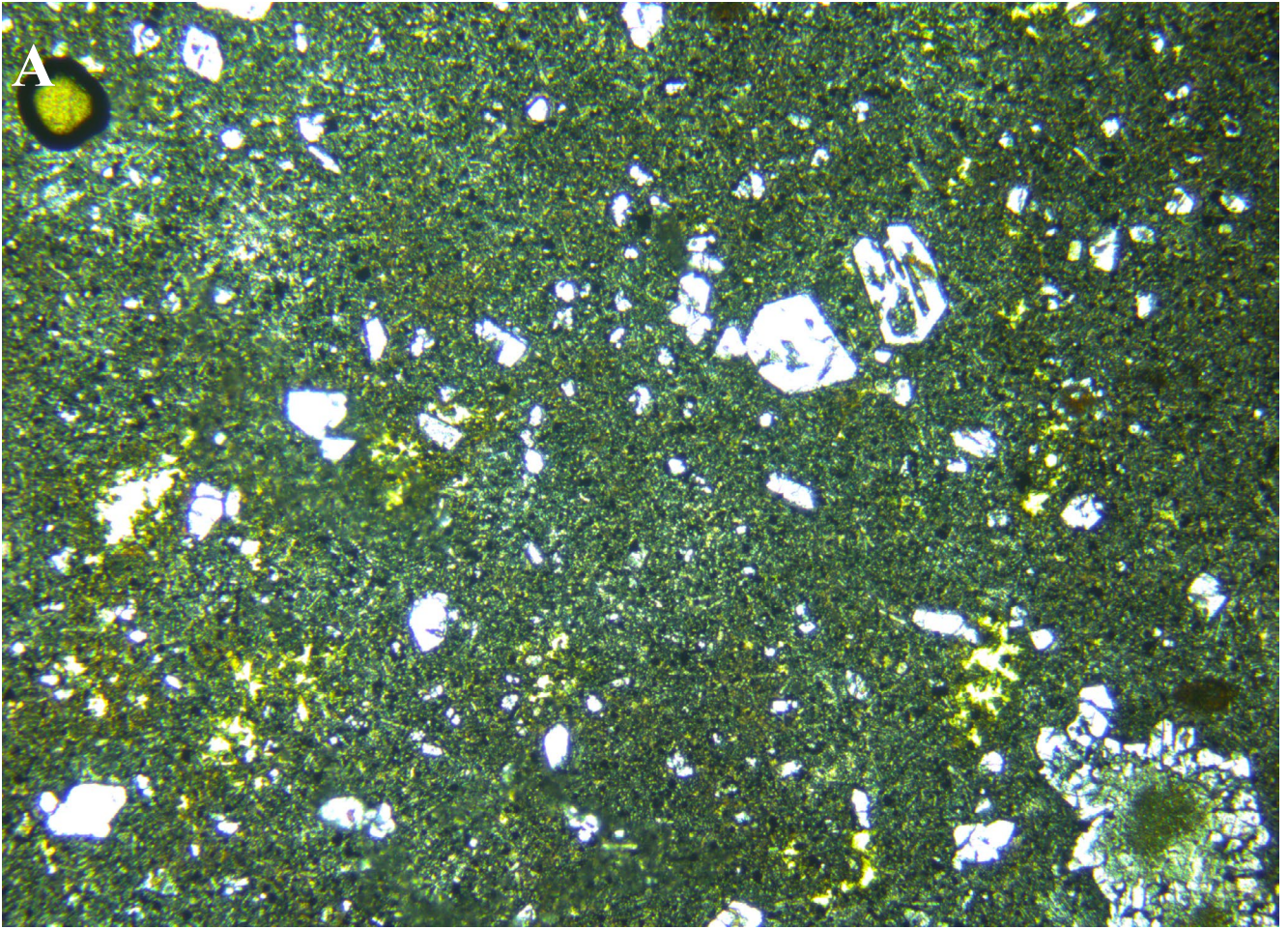
Figure 16. Photomicrograph of sample TJ3228, nepheline hawaiite, Neasey Plains, far NW Tasmania. Olivine microphenocrysts, reacted lherzolite xenolith (lower right) and spinel xenocrysts (upper left) in a very fine-grained feldspathoidal groundmass. Field of view~4.6 x 3.4 mm. (a) plane polarised light (b) crossed nicols.
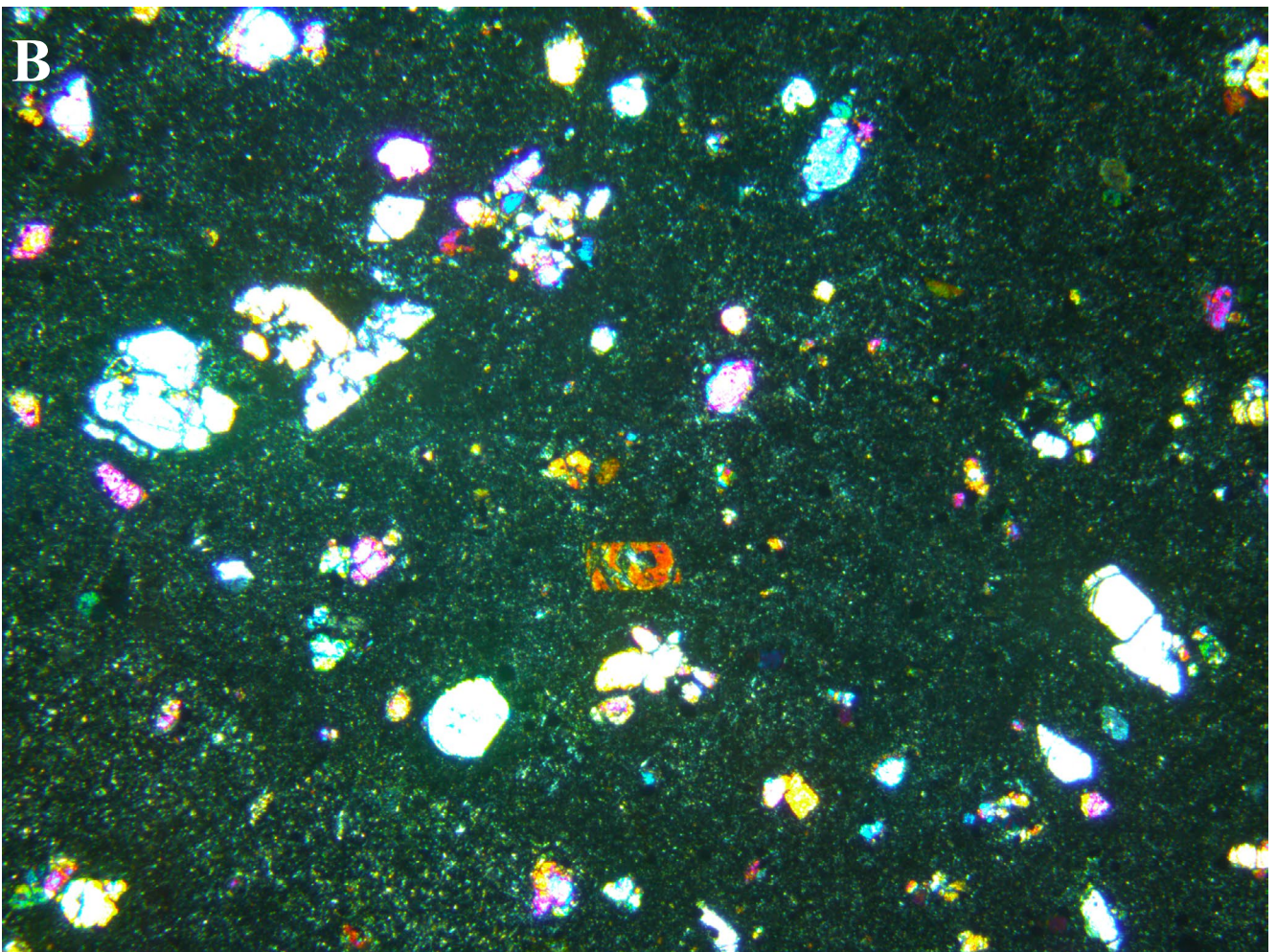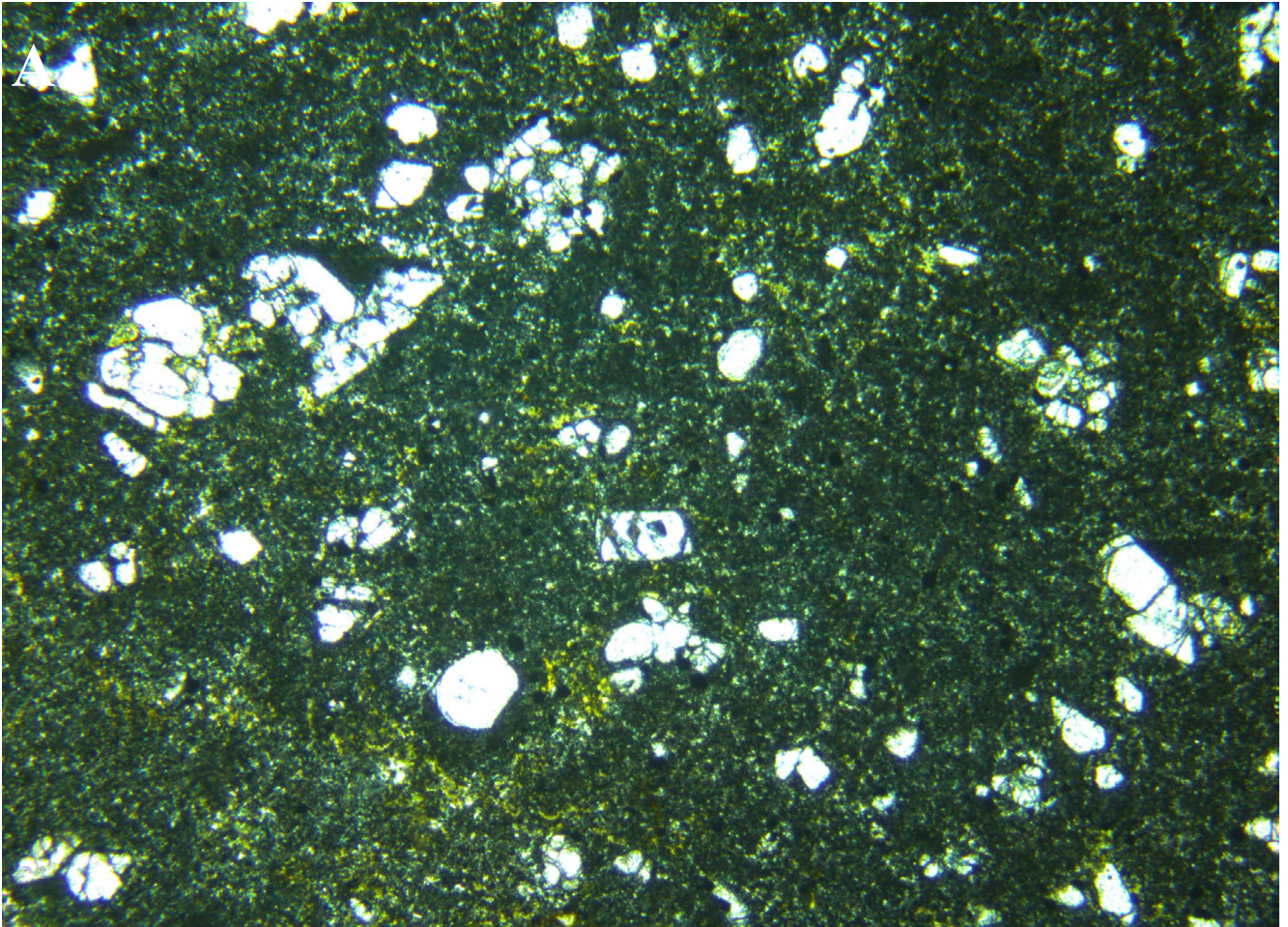
Figure 17. Photomicrograph of sample CVH, nepheline hawaiite, Coastview Hill, NW Tasmania. Olivine microphenocrysts in a turbid very fine-grained groundmass. Field of view~4.6 x 3.4 mm. (a) plane polarised light (b) crossed nicols.

Figure 18. Photomicrograph of sample SRN, nepheline hawaiite, South Riana, NW Tasmania. Embayed and partly altered xenocrysts, mainly olivine, in a very fine-grained feldspathoidal groundmass, Field of view~4.6 x 3.4 mm. (a) plane polarised light (b) crossed nicols.
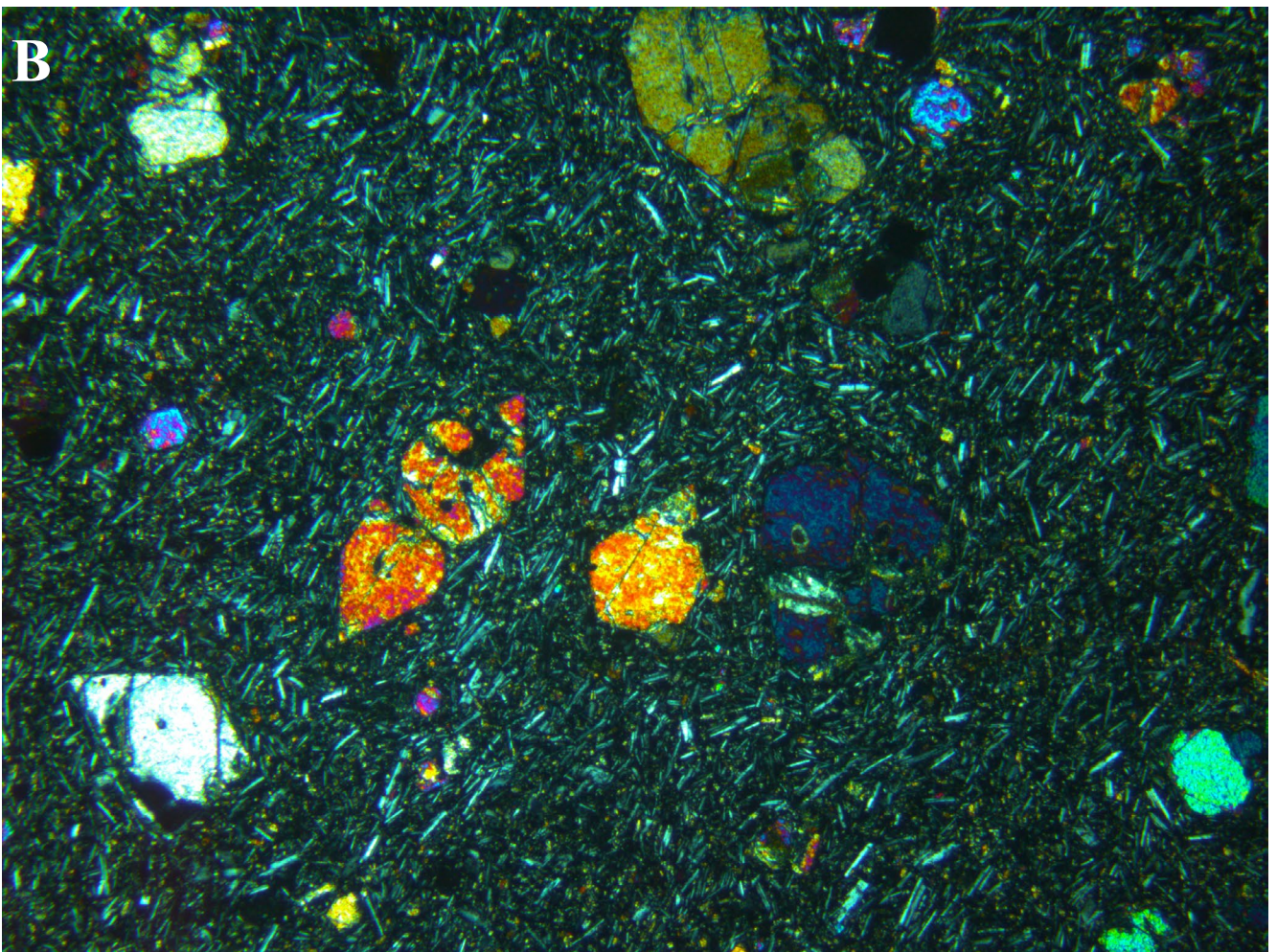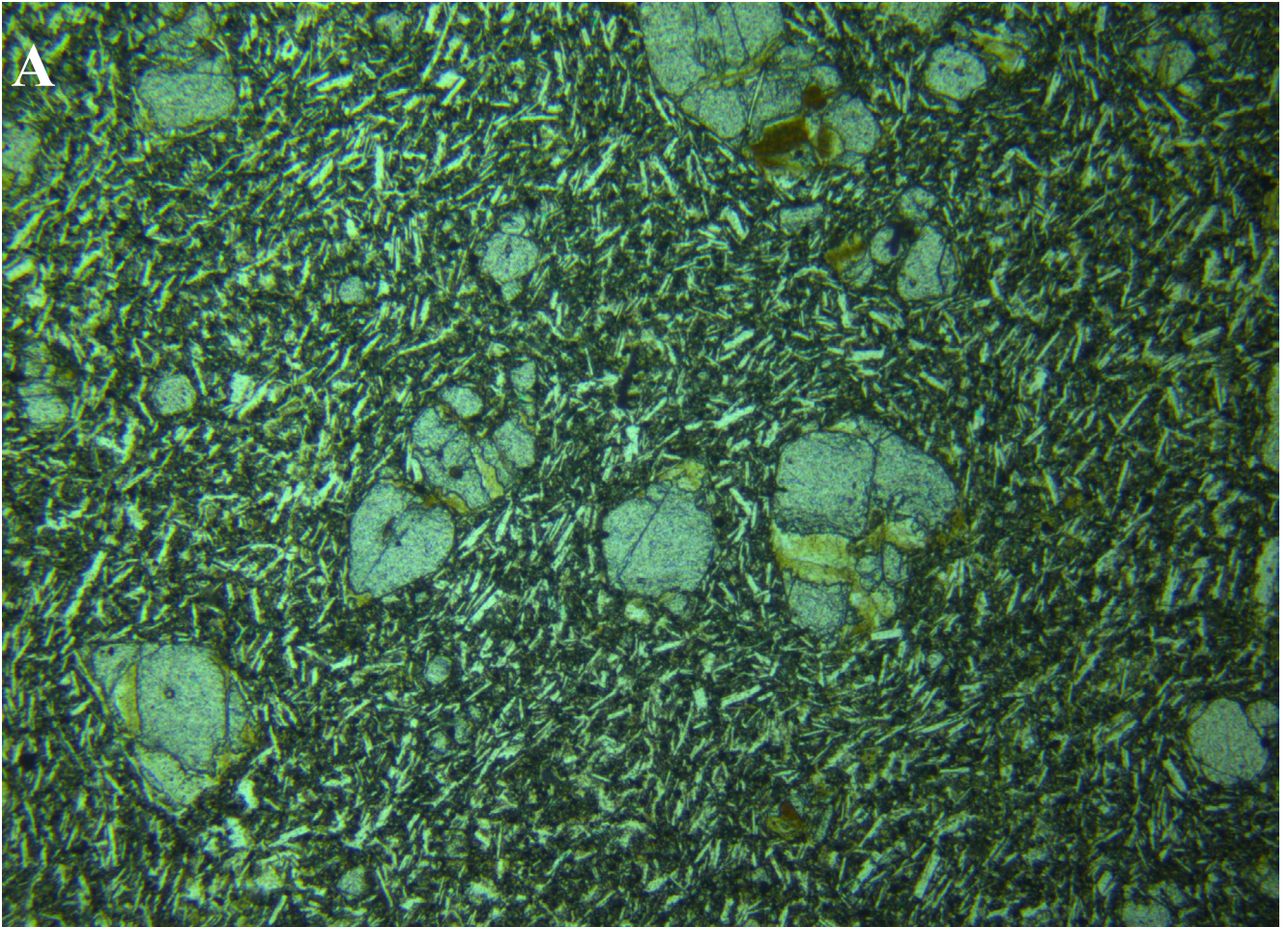
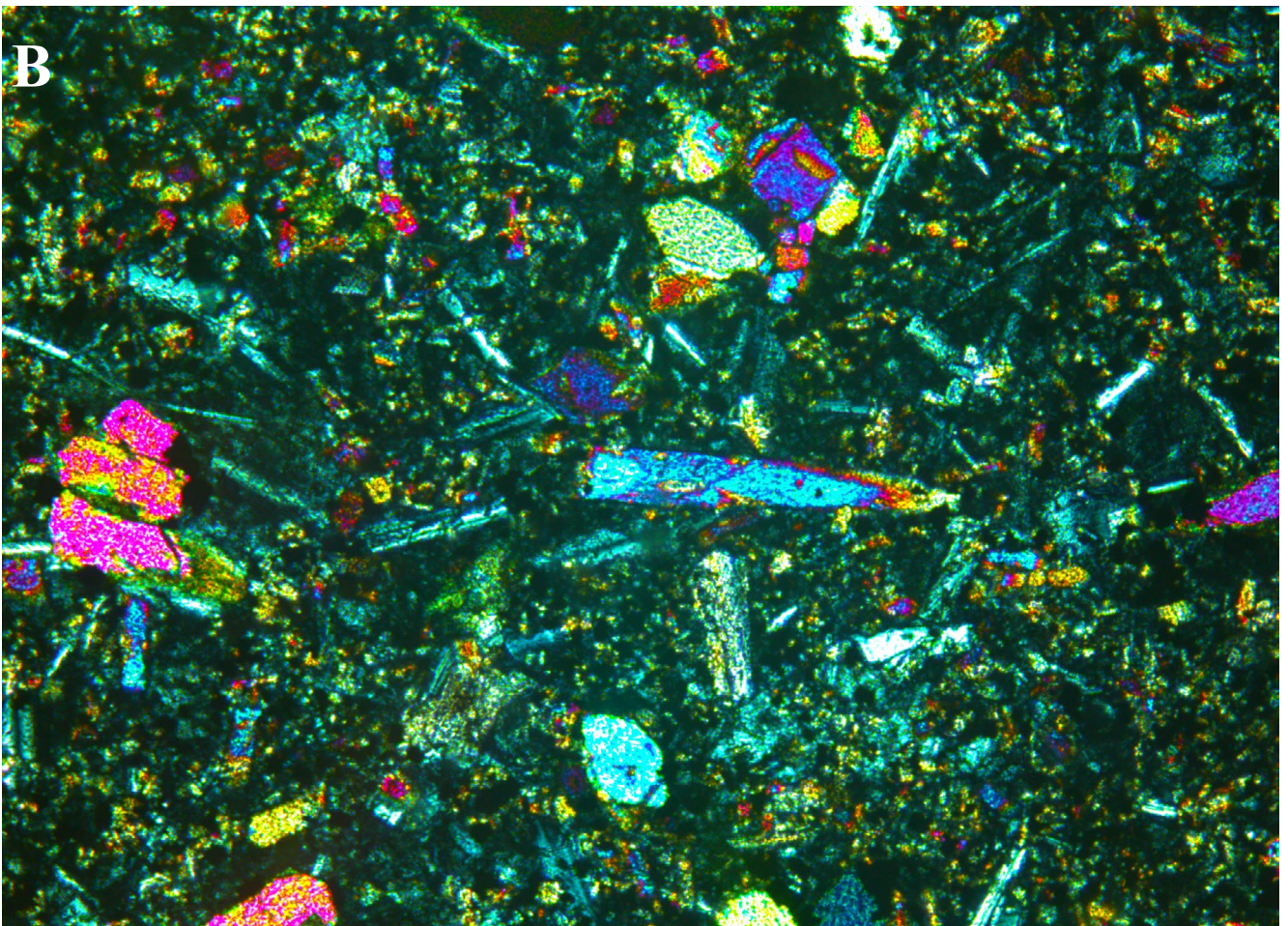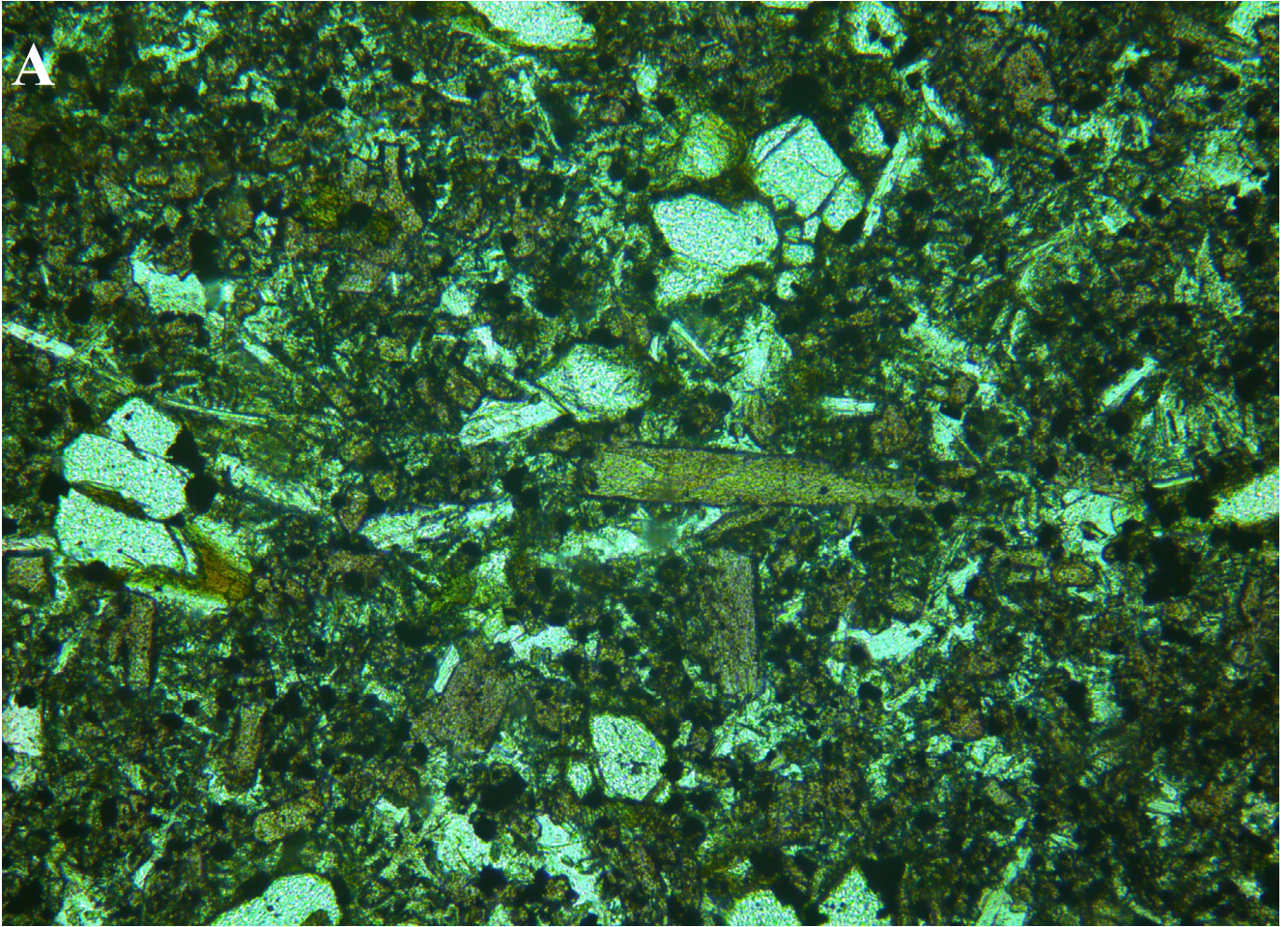Figure 19. Photomicrograph of sample LLC, alkali olivine basalt, Lillicos Beach, NW Tasmania. Slightly altered olivine phenocrysts in a fluidal intergranular groundmass. Field of view~4.6 x 3.4 mm. (a) plane polarised light (b) crossed nicols.

Figure 20. Photomicrograph of sample AJ99, olivine nephelinite, Olivers Hill, NE Tasmania. Embayed olivine xenocrysts (e.g. centre) and euhedral olivine micro-phenocrysts in a very fine-grained feldspathoidal groundmass. Field of view~4.6 x 3.4 mm. (a) plane polarised light (b) crossed nicols.
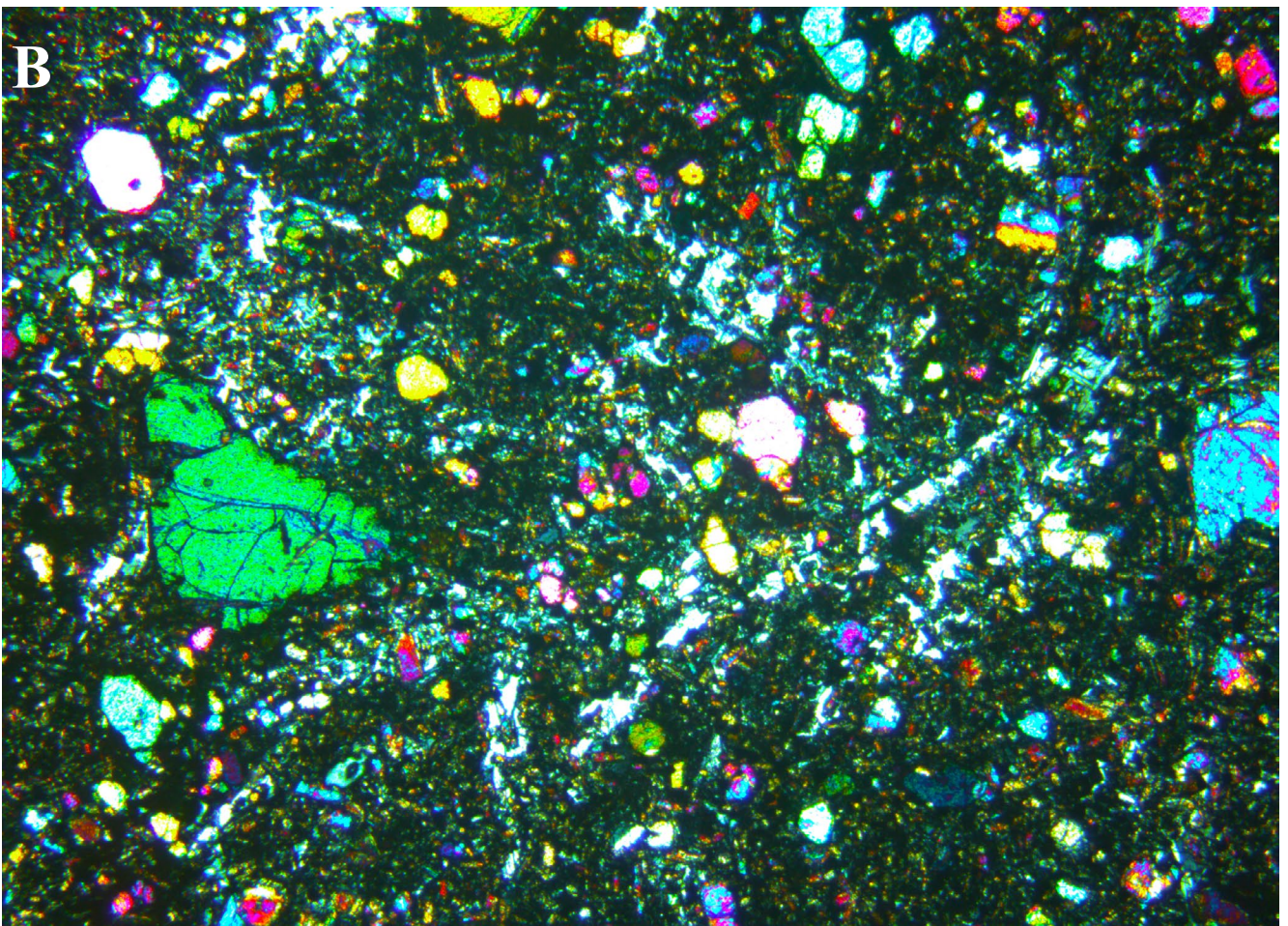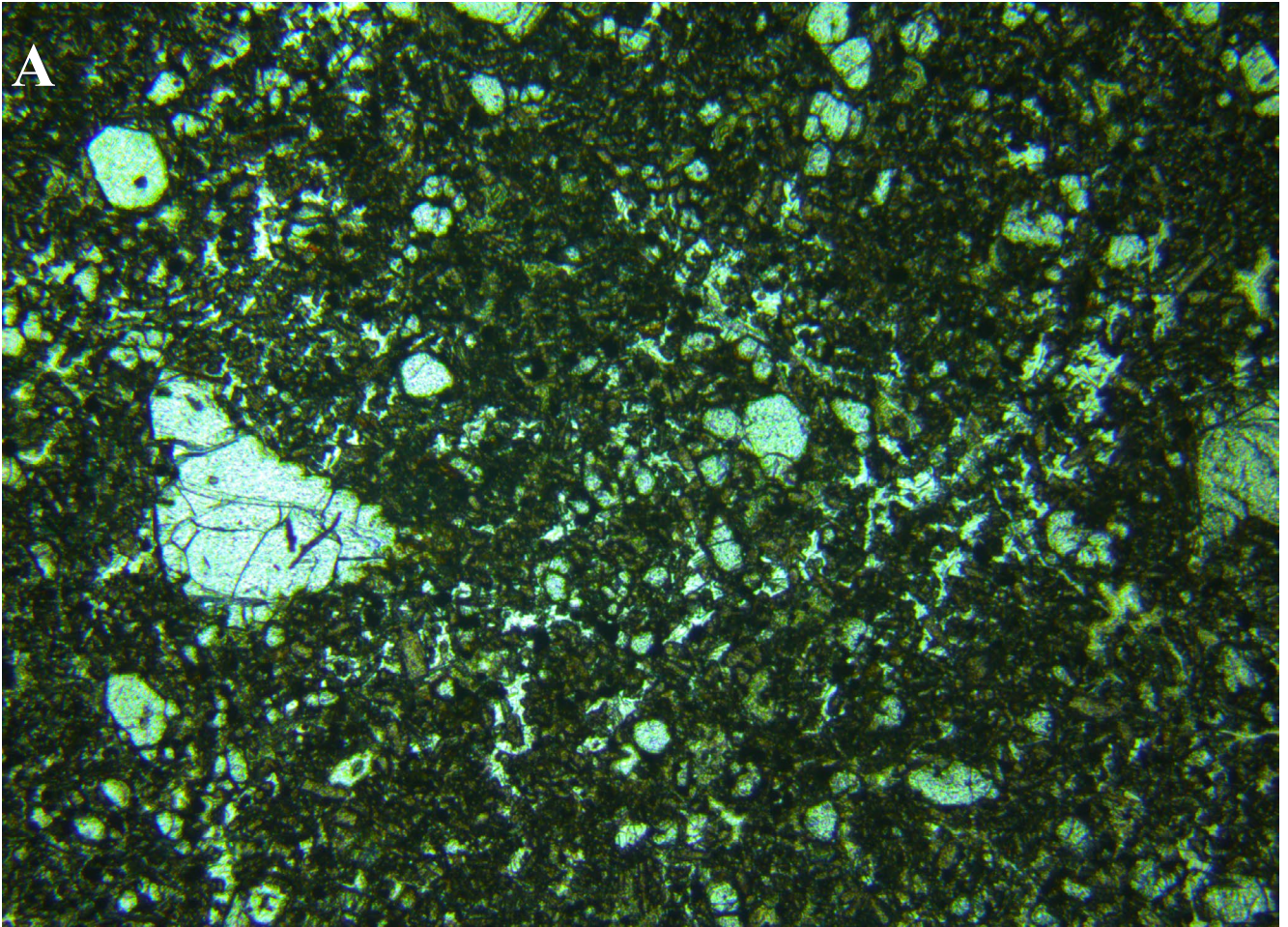
Figure 21. Photomicrograph of sample AJ1424, basanite, northern hill via Sweets Creek, NE Tasmania. Olivine phenocrysts and poikilitic plagioclase platelets (e.g. lower centre) in a fine-grained groundmass. Field of view ~4.6 x 3.4 mm. (a) plane polarised light (b) crossed nicols.
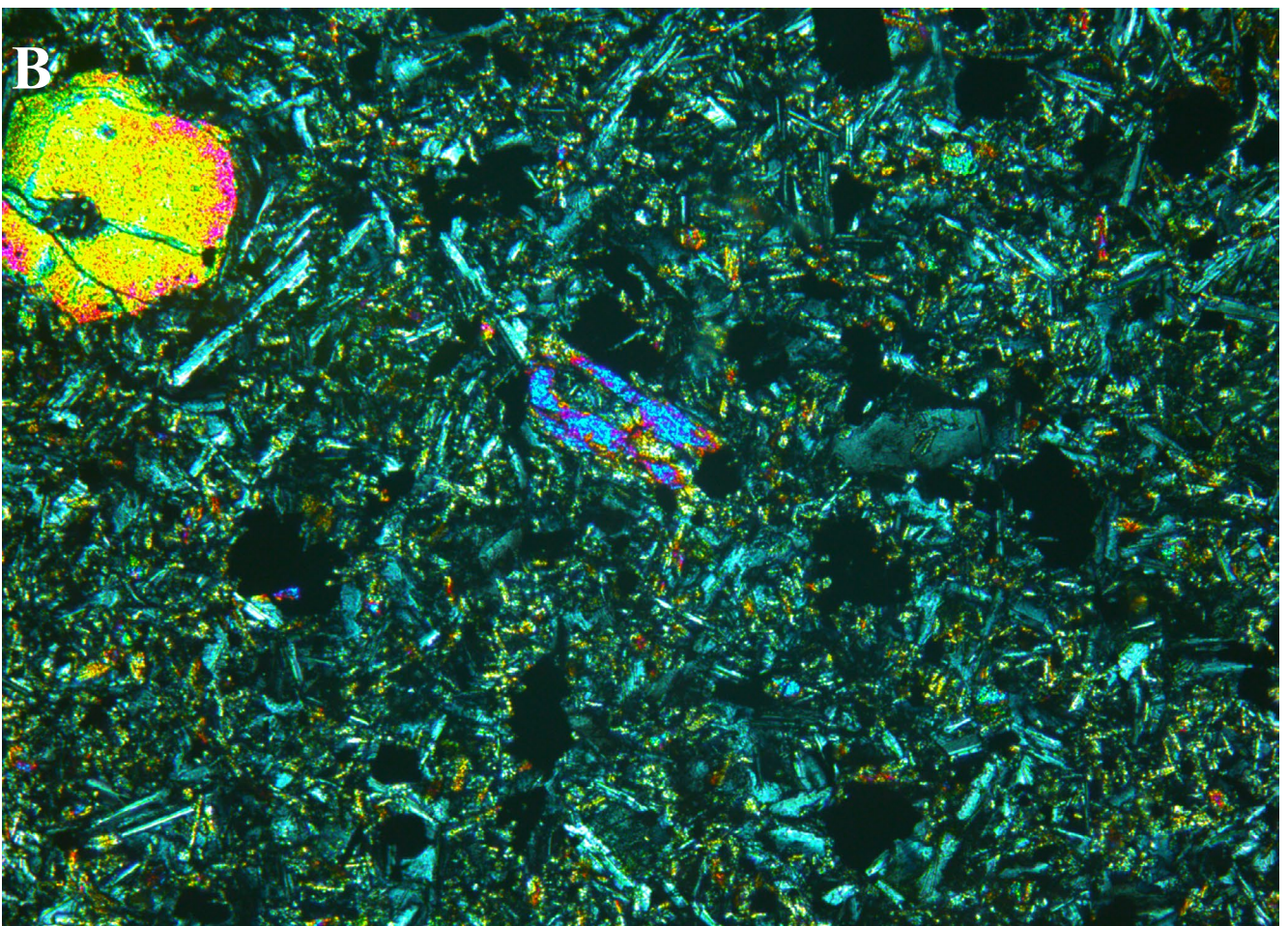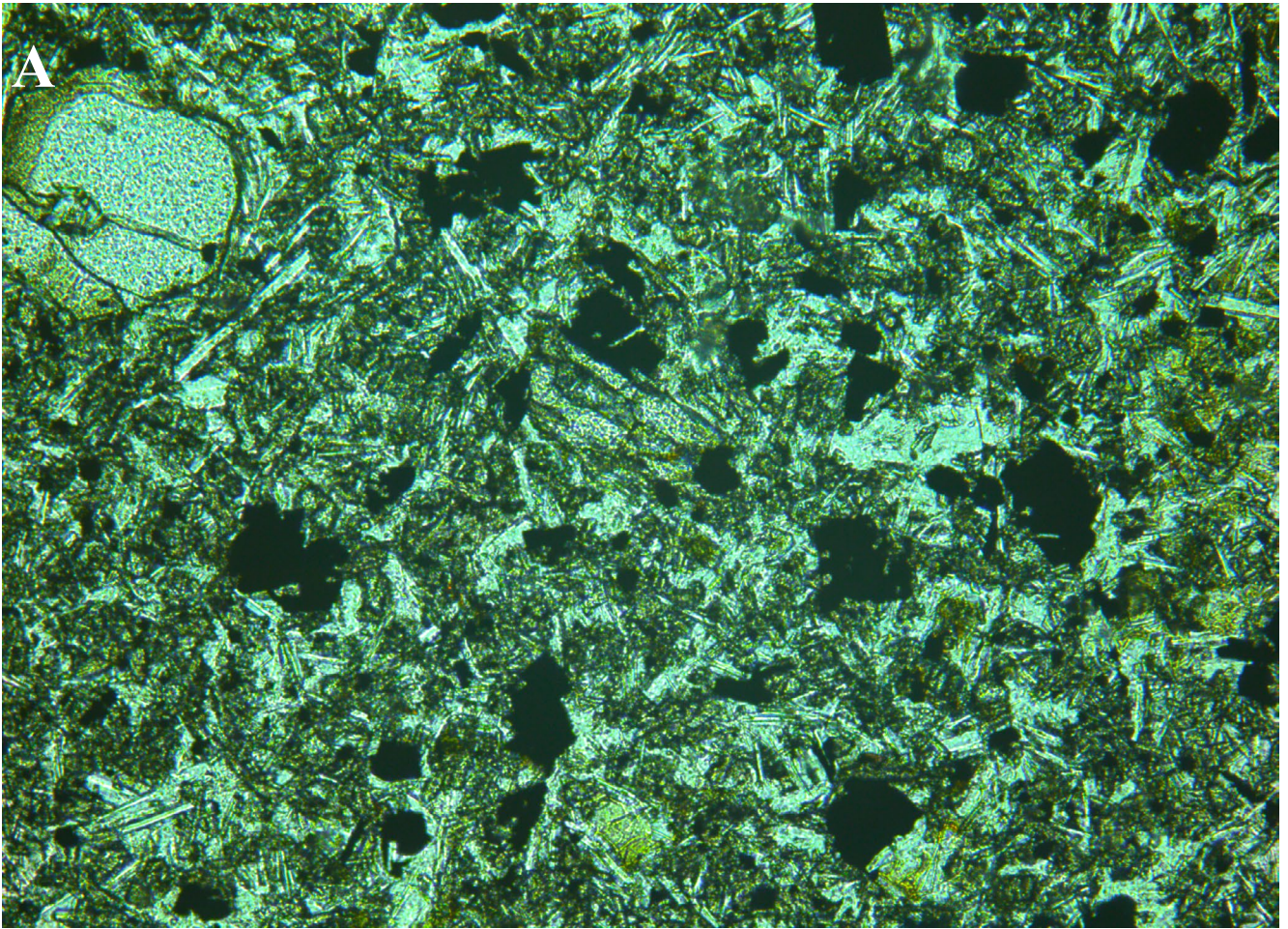
Figure 22. Photomicrograph of sample AJ1425, hawaiite, southern hill via Sweets Creek, NE Tasmania. Olivine microphenocryst (upper left) and augite granule (centre) in an intergranular groundmass. Field of view ~1.9 x 1.4 mm. (a) plane polarised light (b) crossed nicols.
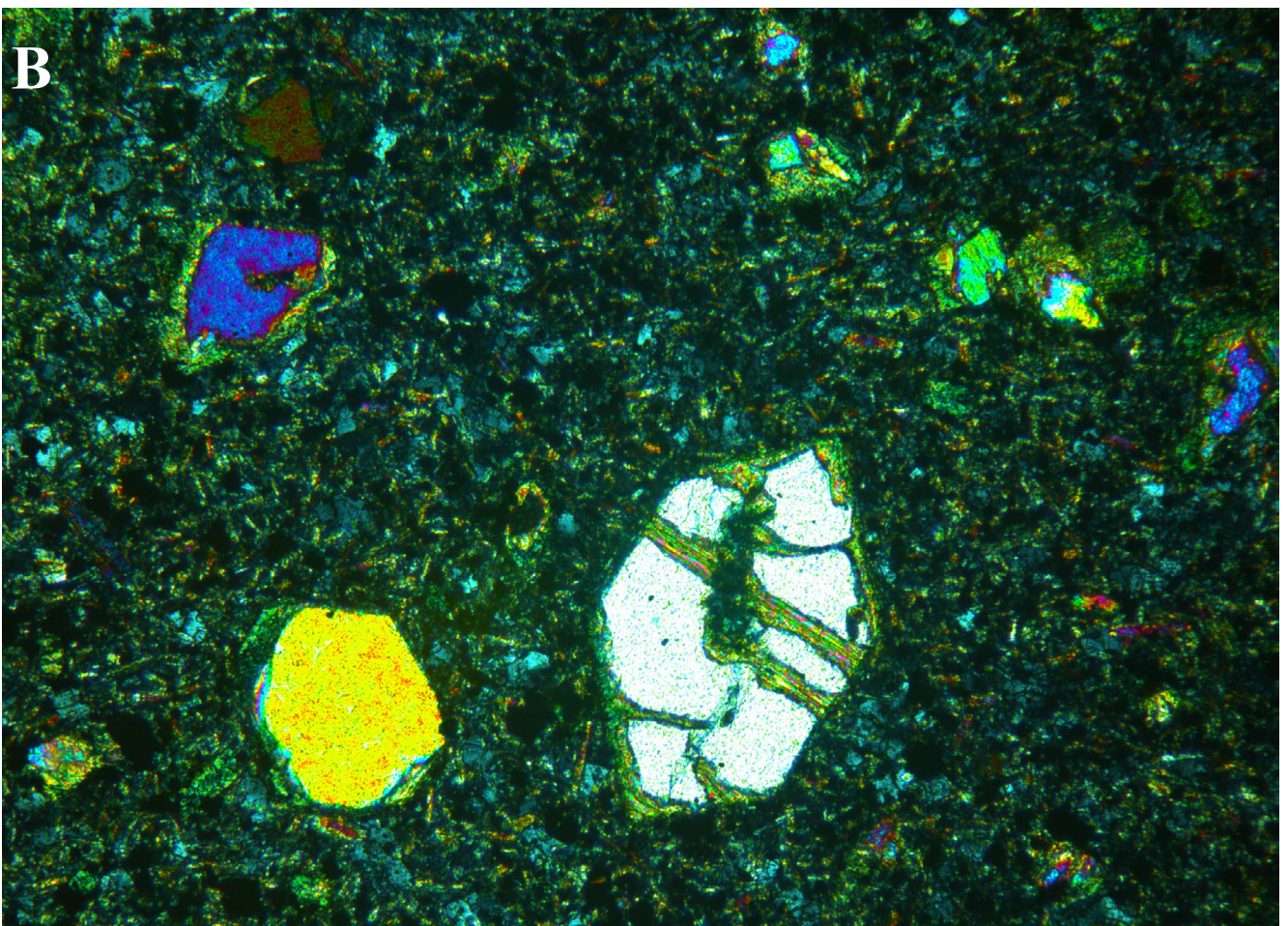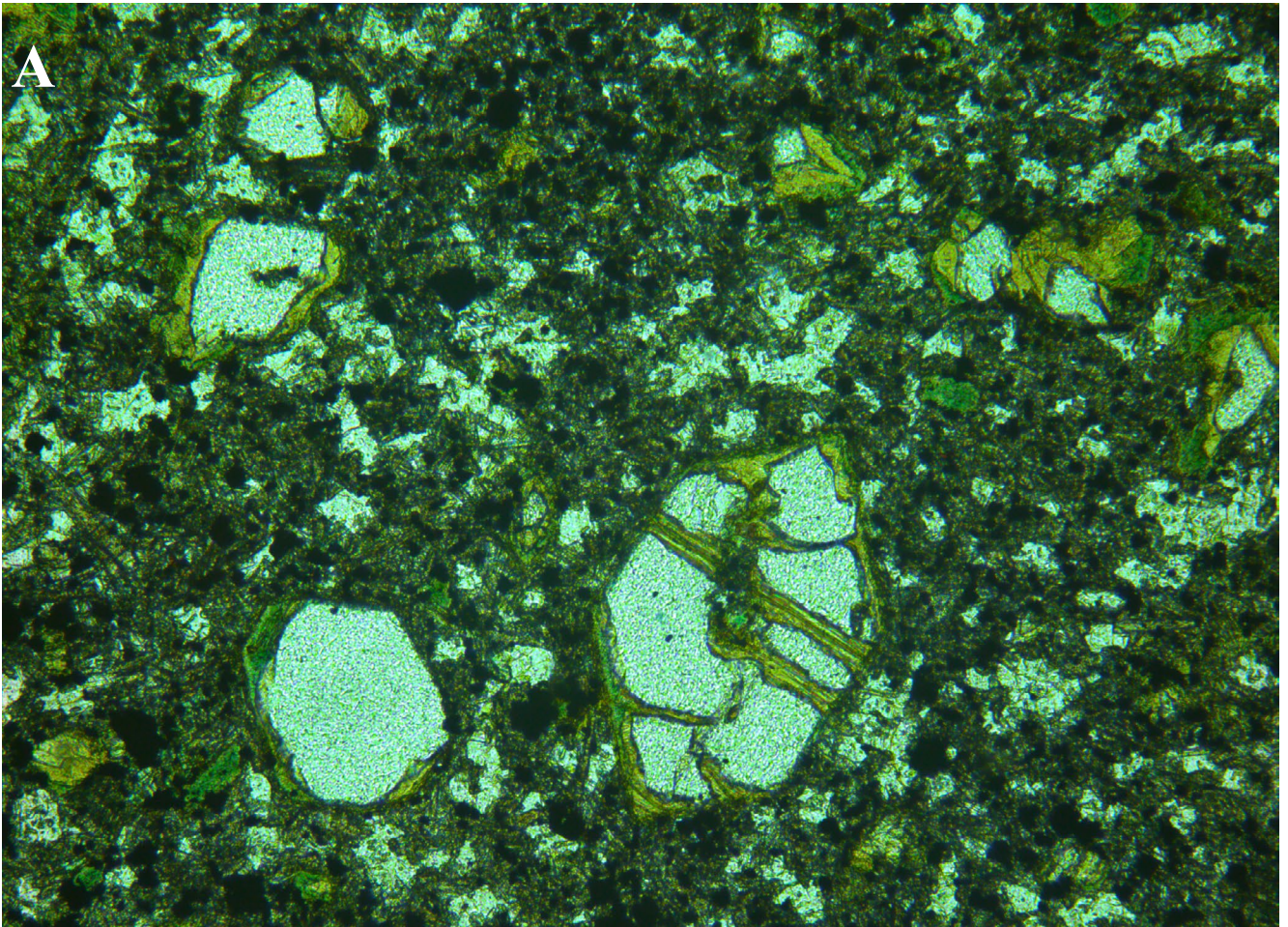
Figure 23. Photomicrograph of sample AJ1426, olivine nephelinite, Upper Esk, NE Tasmania. Partly altered olivine microphenocrysts in a very fine-grained feldspathoidal groundmass. Field of view ~1.9 x 1.4 mm. (a) plane polarised light (b) crossed nicols.

Figure 24. Photomicrograph of sample PP20.5, olivine nephelinite, Beauty Flat, NE Tasmania. Fine-grained groundmass showing titaniferous augite grains (pink to yellow), olivine microphenocrysts and small plagioclase laths. Field of view ~1.9 x 1.4 mm. (a) plane polarised light (b) crossed nicols.
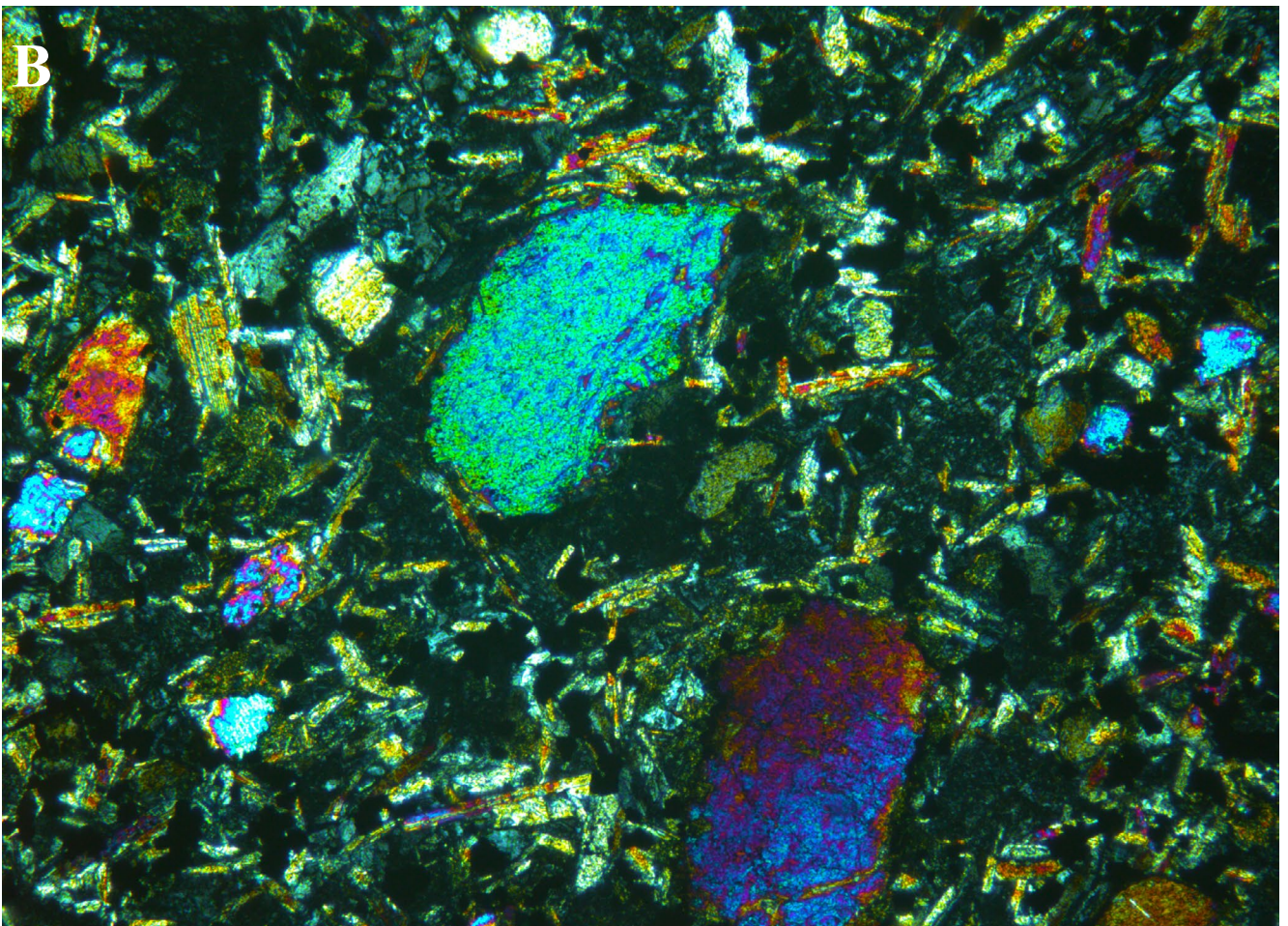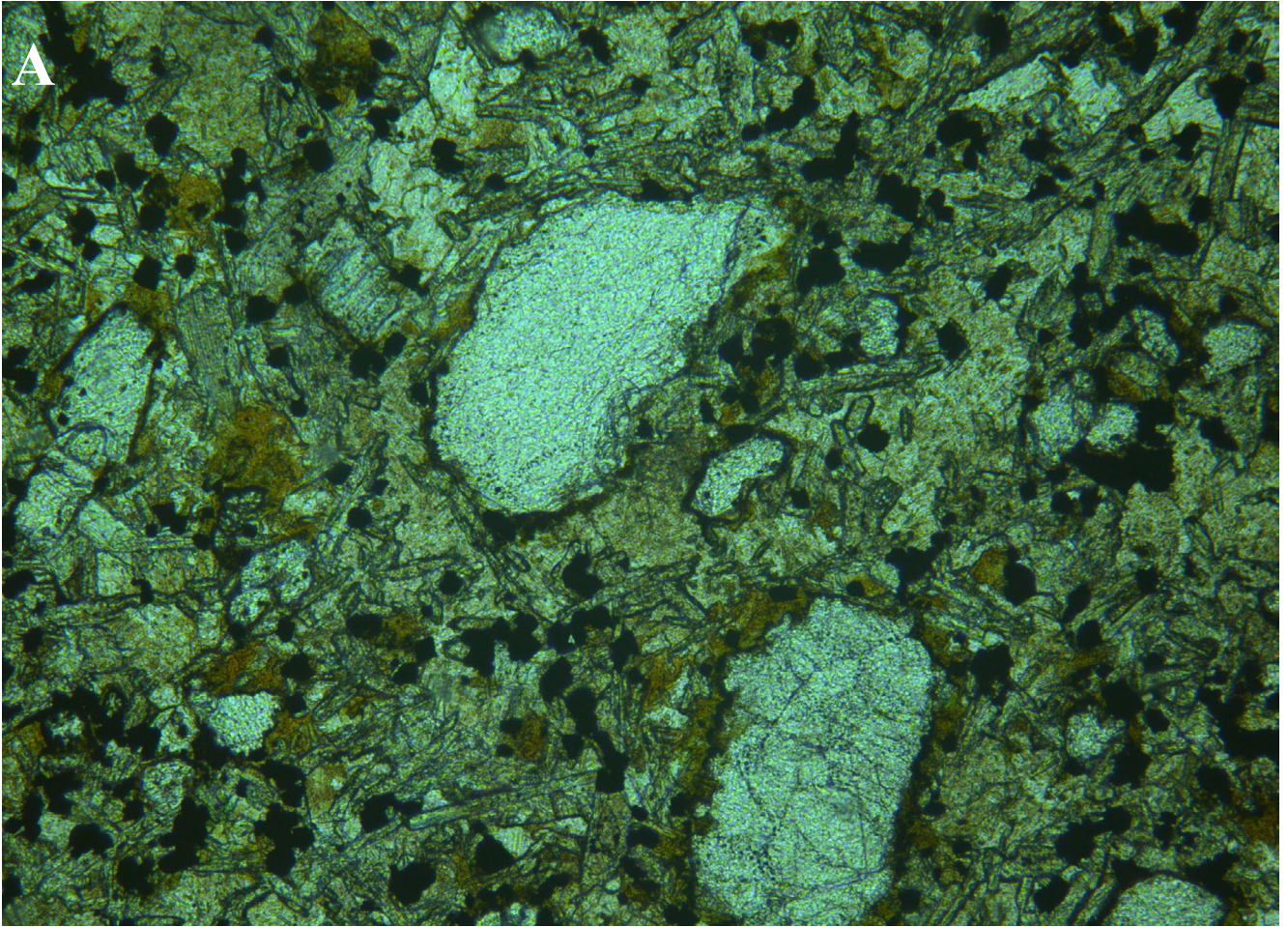
Figure 25. Photomicrograph of sample WSc, olivine nephelinite, West Scottsdale, NE Tasmania. Small olivine microphenocrysts in a fine-grained groundmass of mainly platy titaniferous augite, magnetite and nepheline. Field of view ~1.9 x 1.4 mm. (a) plane polarised light (b) crossed nicols.
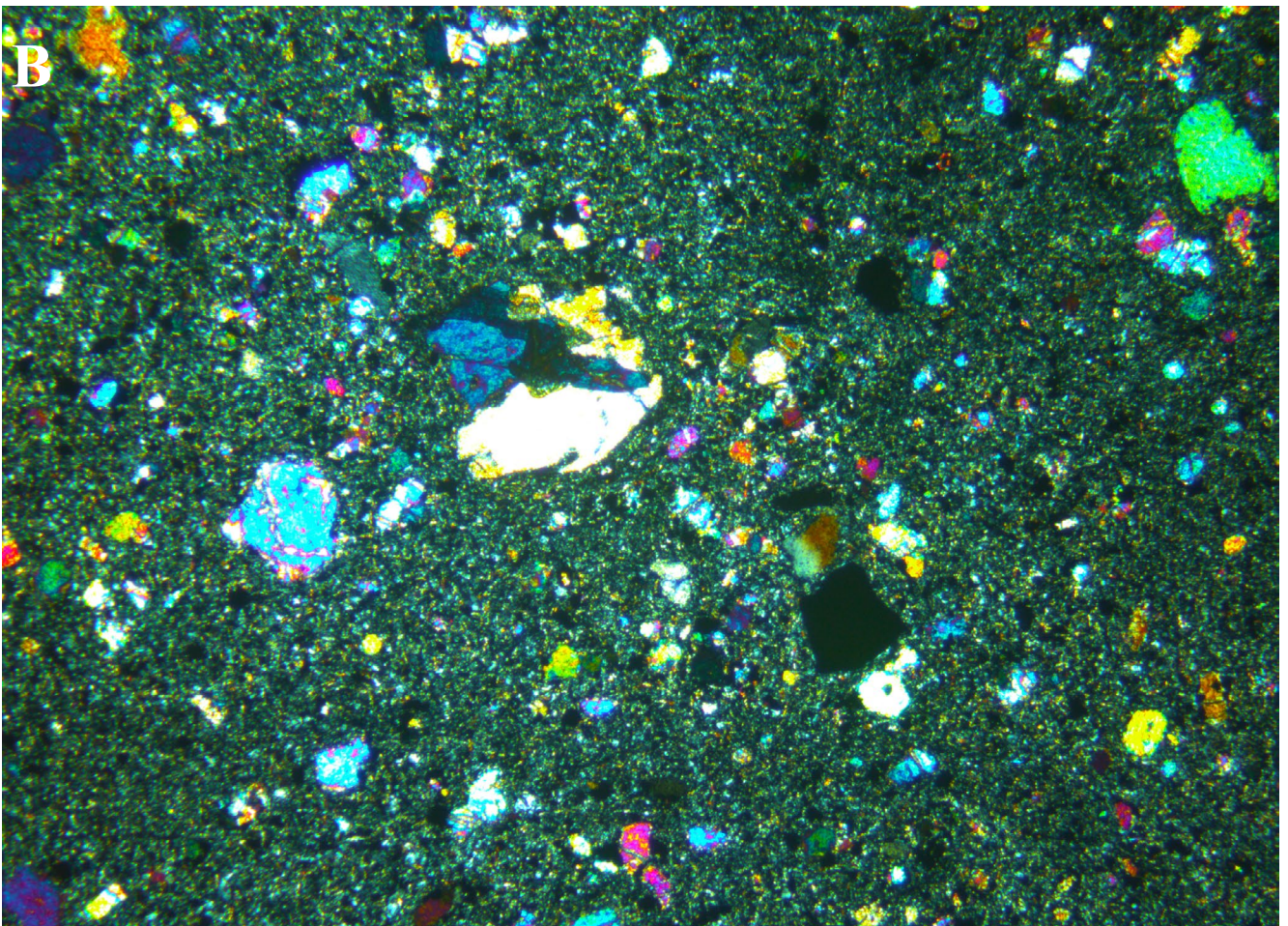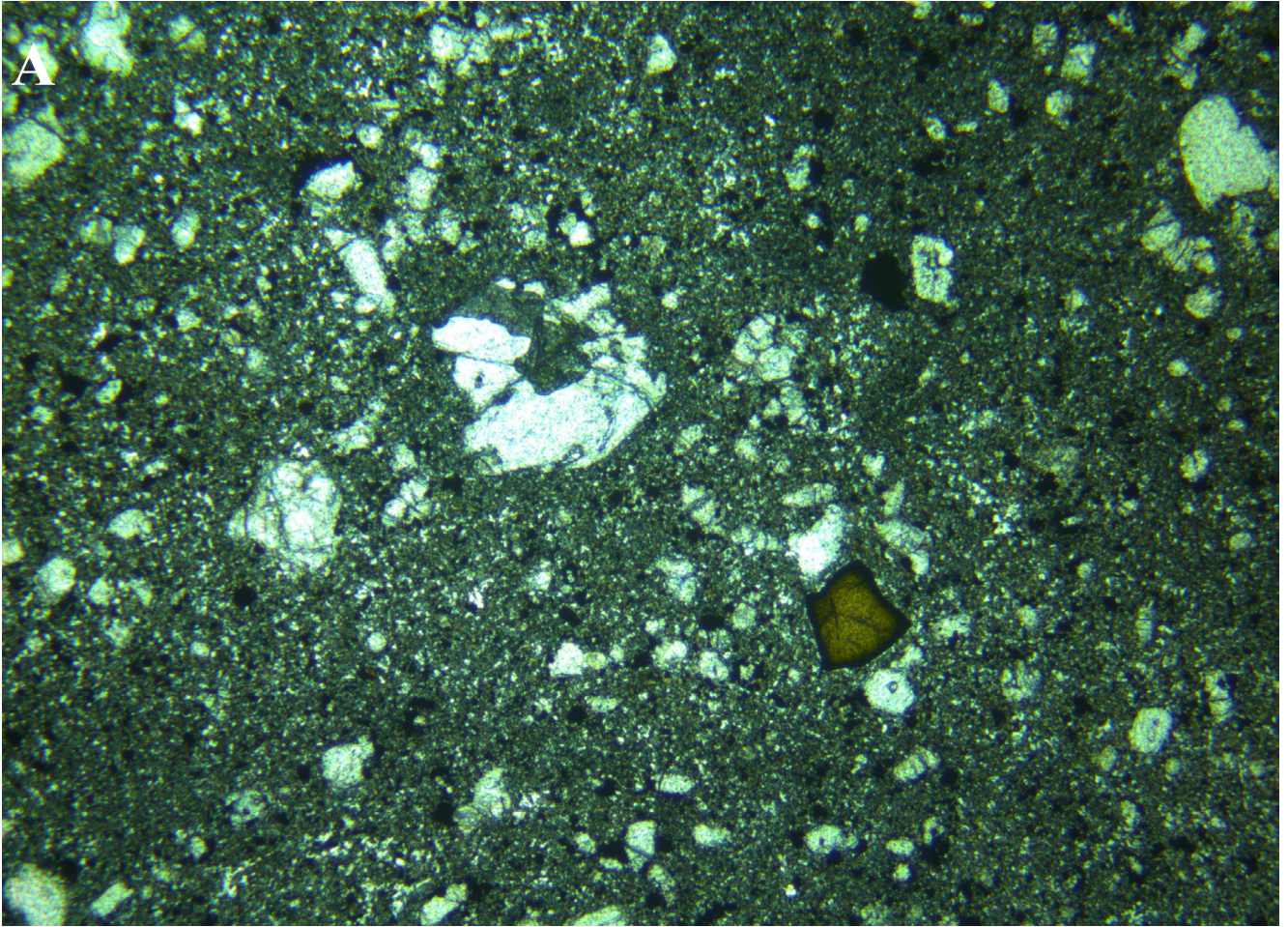
Figure 26. Photomicrograph of sample SDL, olivine nephelinite, The Sideling, NE Tasmania. Olivine and brown spinel xenocrysts grading into a very fine-grained feldspathoidal groundmass. Field of view ~4.6 x 3.4 mm. (a) plane polarised light (b) crossed nicols.
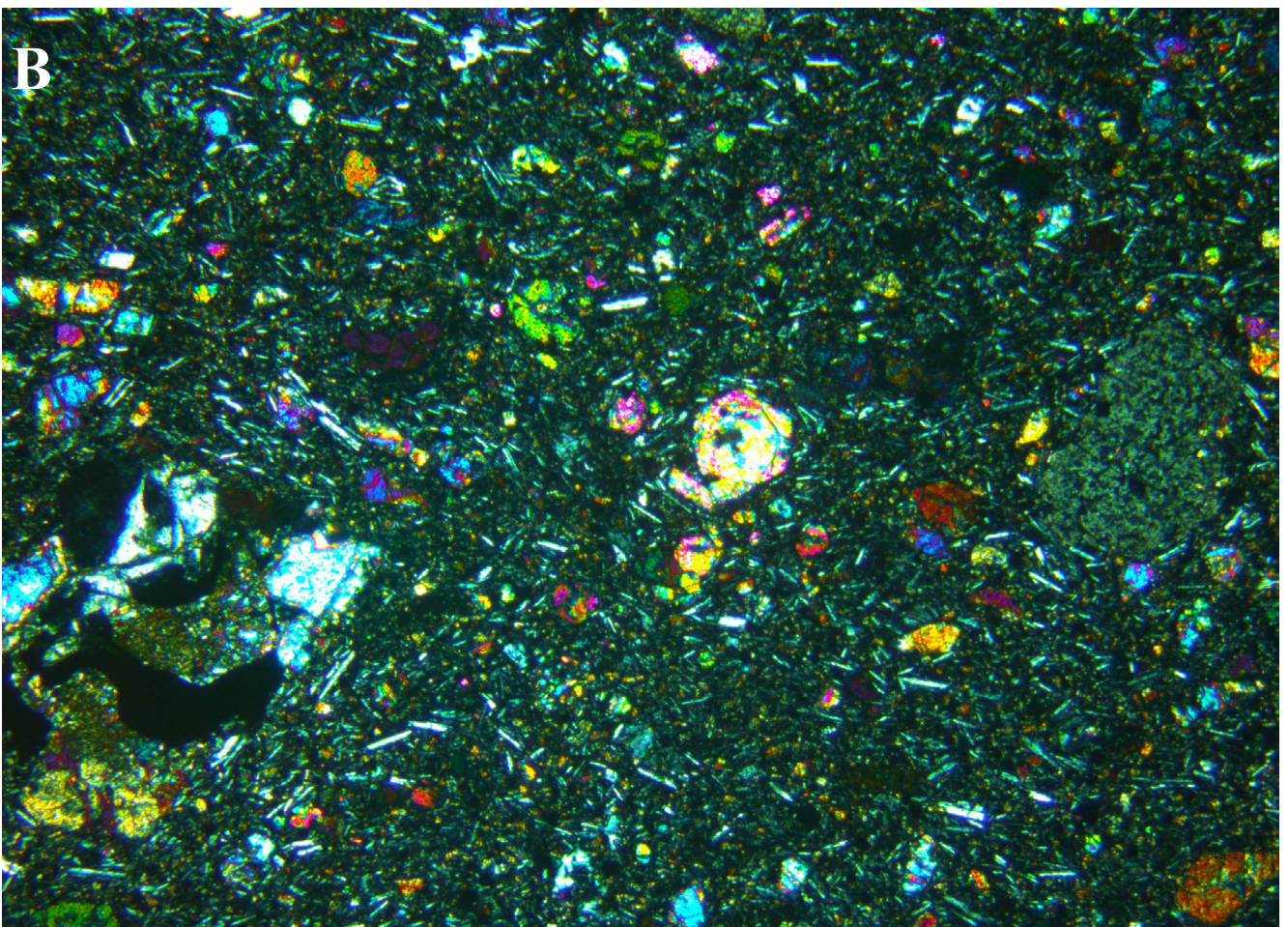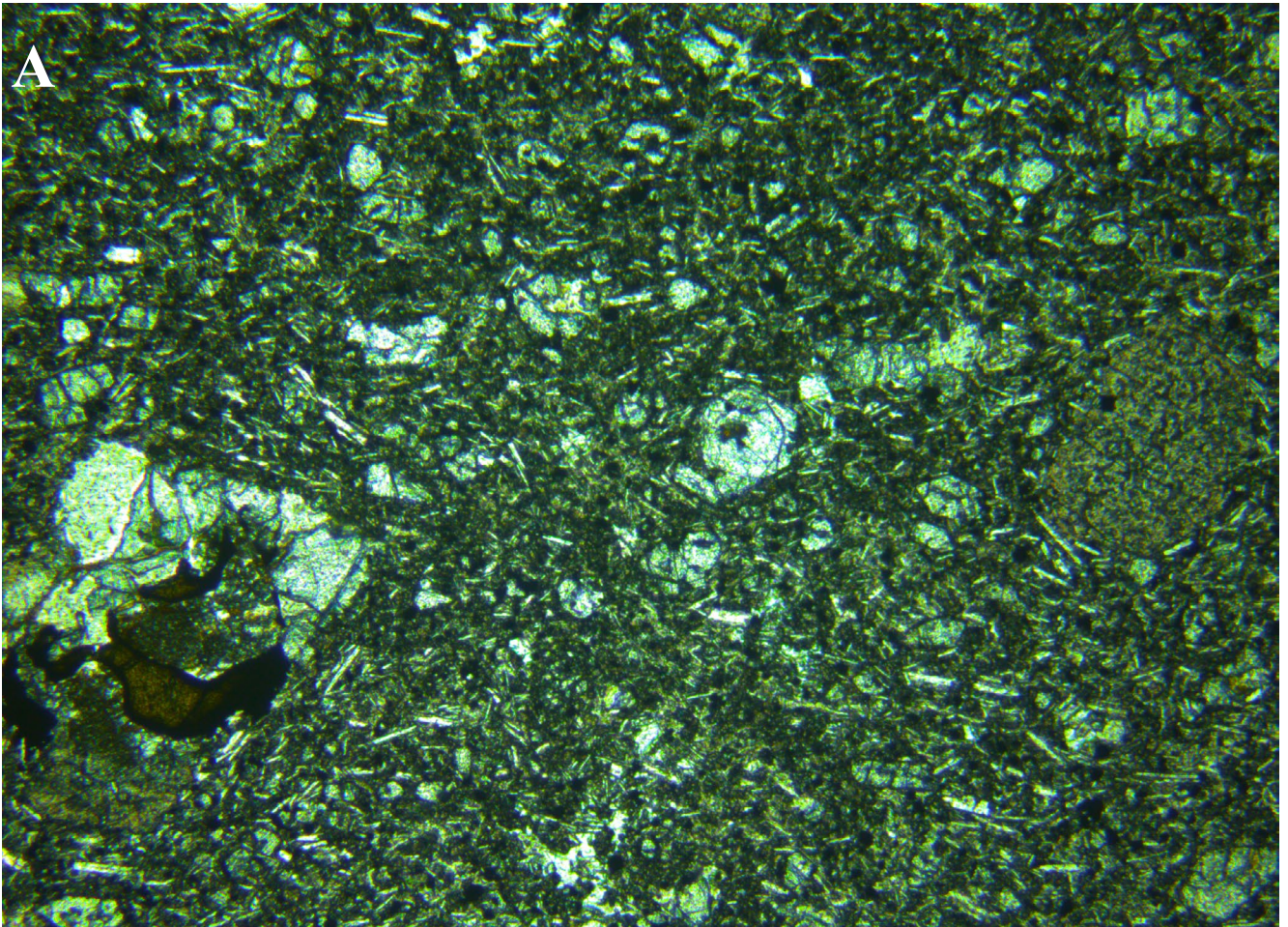
Figure 27. Photomicrograph of sample BLS, basanite, Blessington, NE Tasmania. Lherzolite xenolith with brown spinel (lower left), titaniferous augite phenocrysts (right) and olivine microphenocrysts in a weakly fluidal groundmass with aligned plagioclase laths. Field of view ~4.6 x 3.4 mm. (a) plane polarised light (b) crossed nicols.
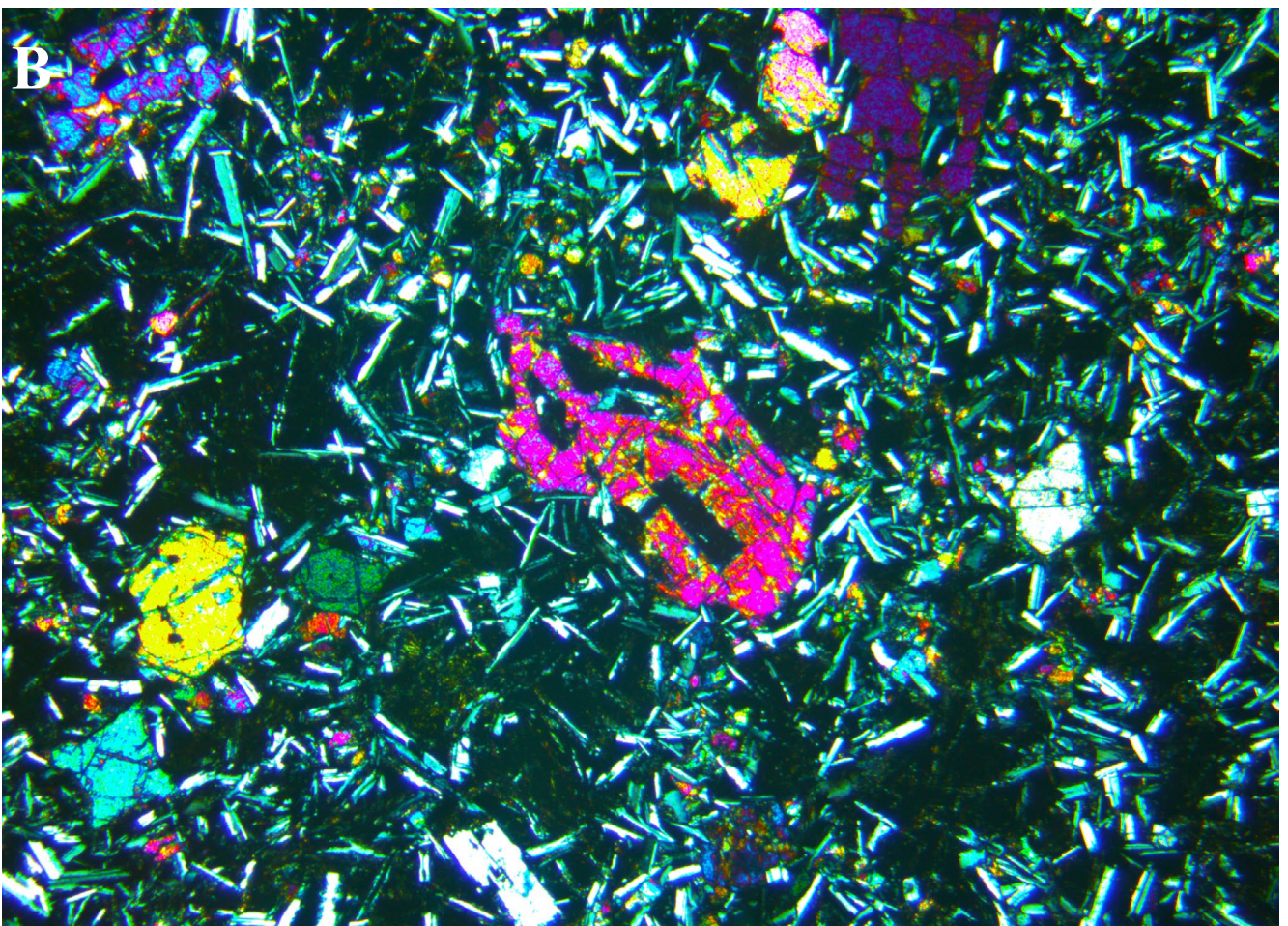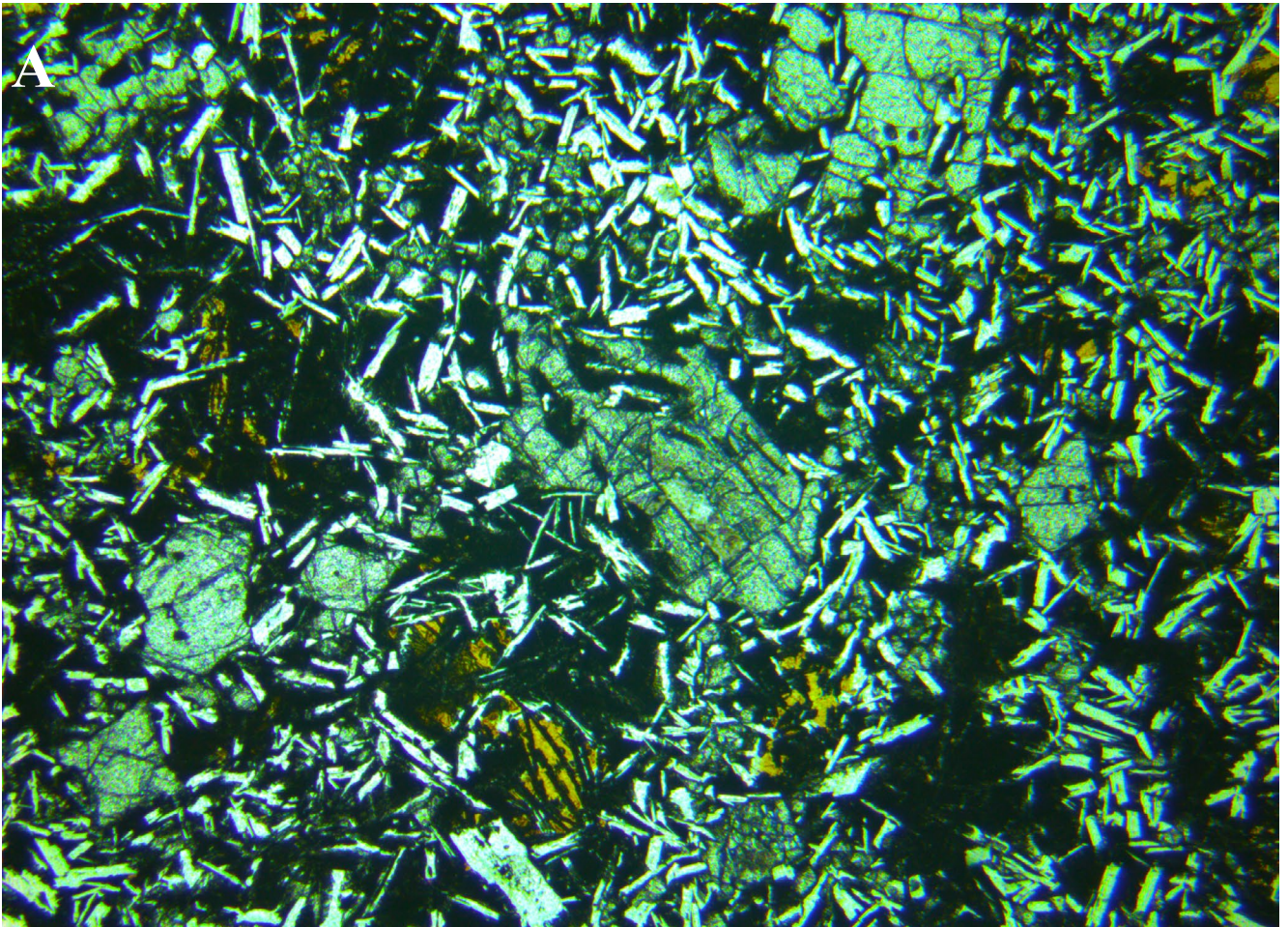
Figure 28. Photomicrograph of sample SB9, olivine tholeiite, "Eastbourne", midlands, Tasmania. Embayed to skeletal olivine phenocrysts (e.g. centre) and plagioclase laths in a dark turbid mesostasis of "black glass" with minor brown alteration. Field of view ~4.6 x 3.4 mm. (a) plane polarised light (b) crossed nicols.
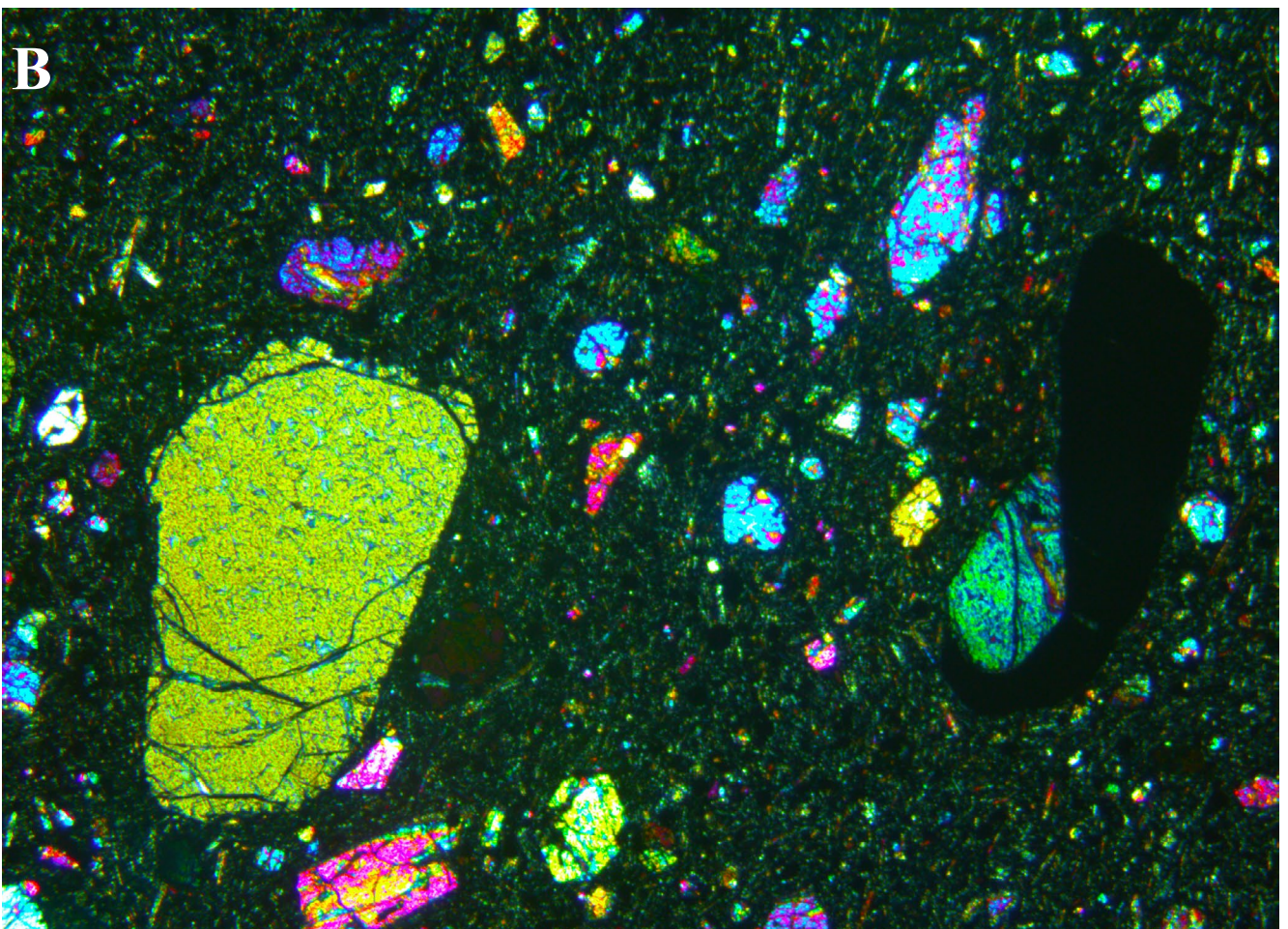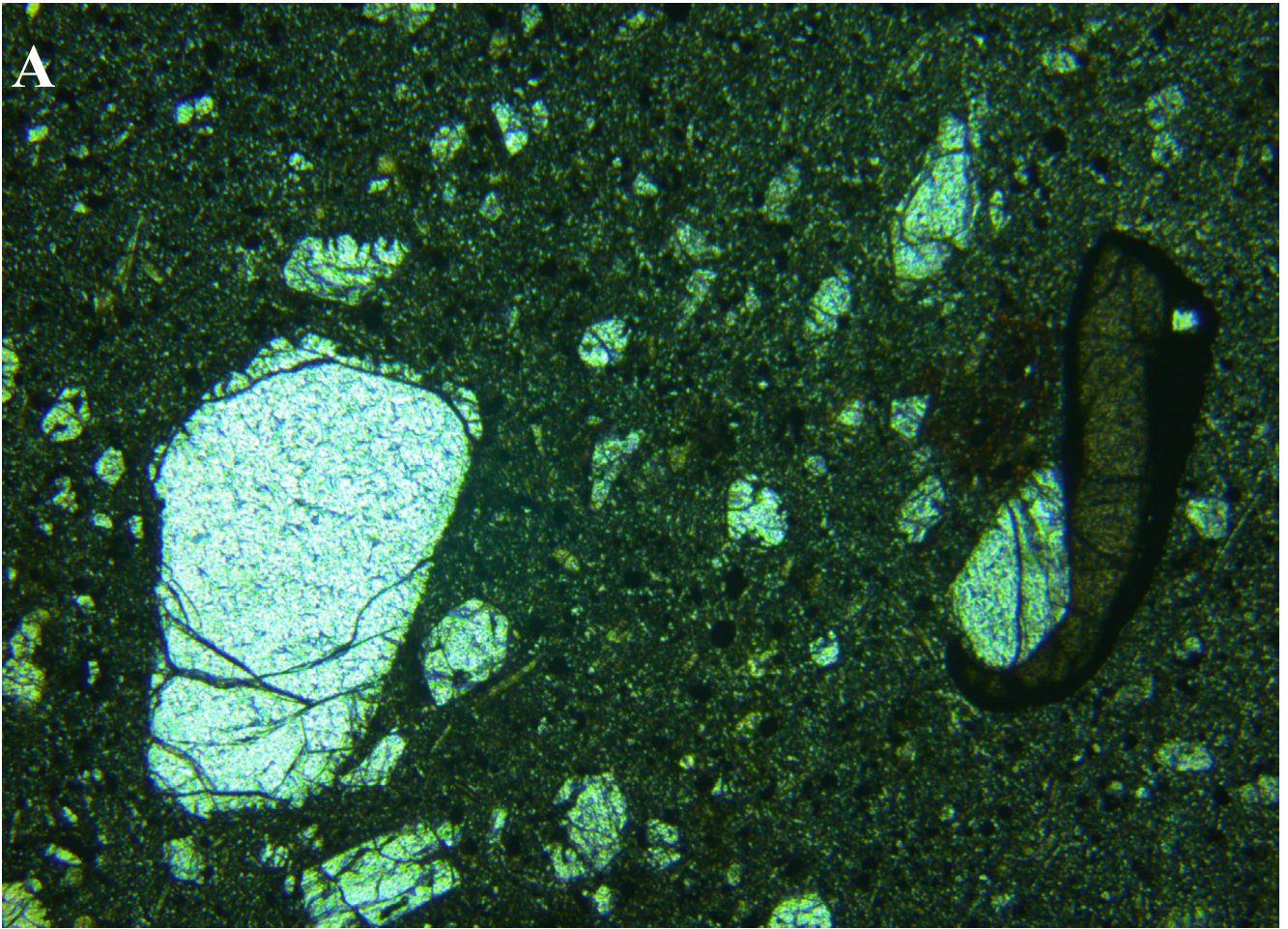
Figure 29. Photomicrograph of sample SB11, nepheline hawaiite, Llewellyn, midlands, Tasmania. Disaggregated lherzolite debris including olivine xenocryst (left), spinel-olivine xenocryst (right) and smaller olivine xenocrysts in a very fine-grained groundmass. Field of view ~4.6 x 3.4 mm. (a) plane polarised light (b) crossed nicols.
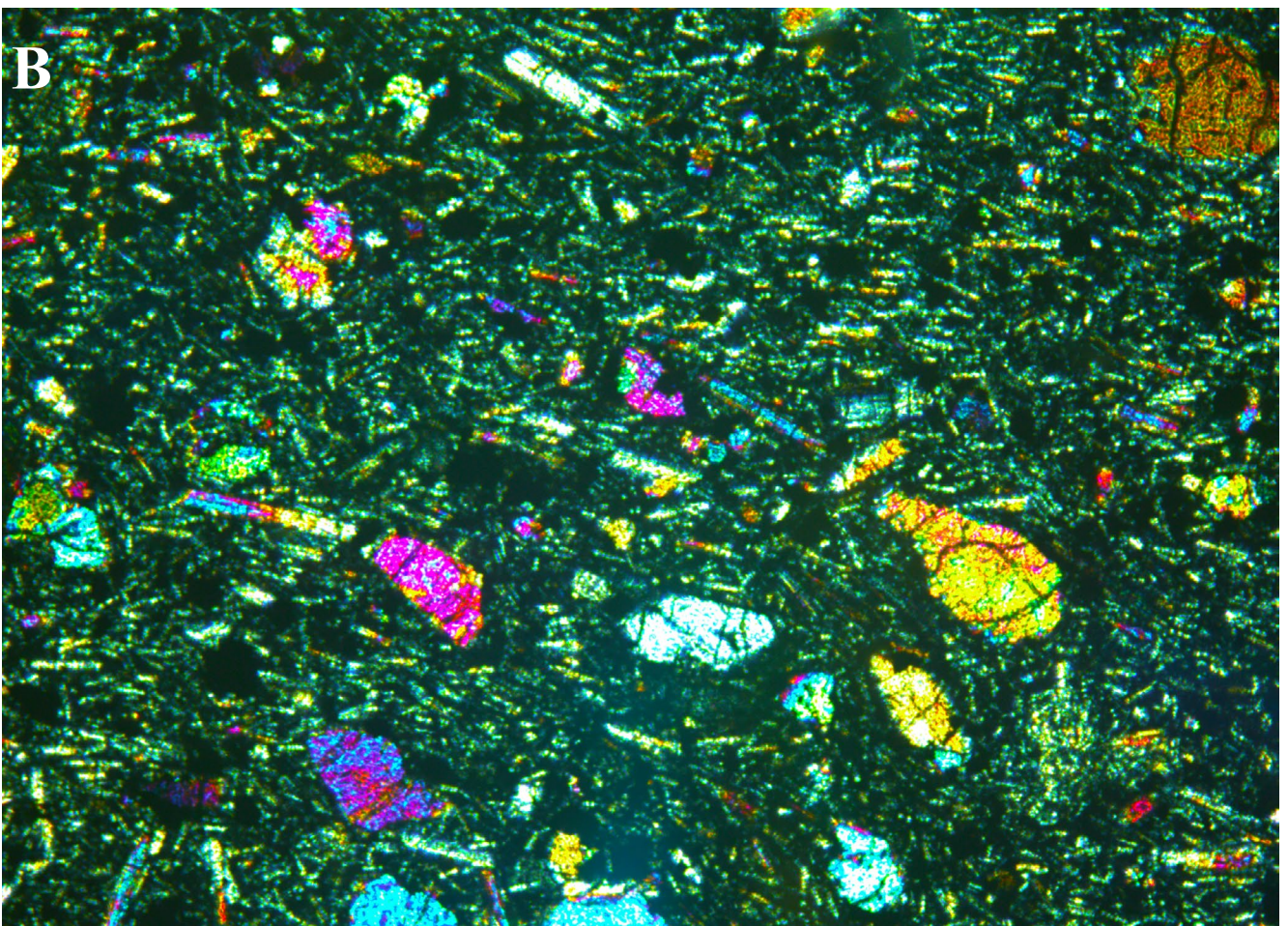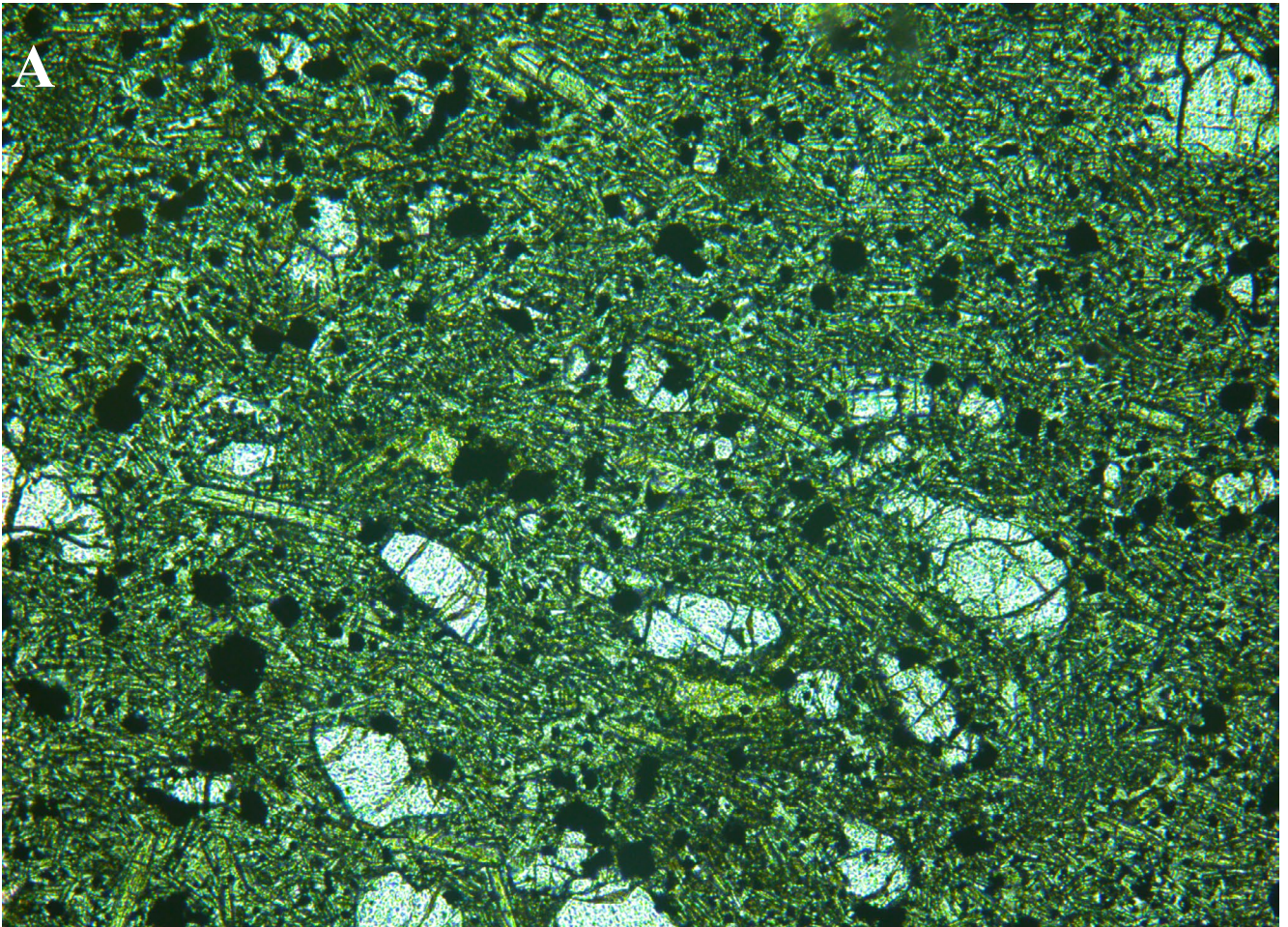
Figure 30. Photomicrograph of sample SB11, nepheline hawaiite, Llewellyn, midlands, Tasmania. Enlargement of groundmass showing olivine microphenocrysts, aligned clinopyroxene prisms and magnetite grains. Field of view ~1.9 x 1.4 mm. (a) plane polarised light (b) crossed nicols.
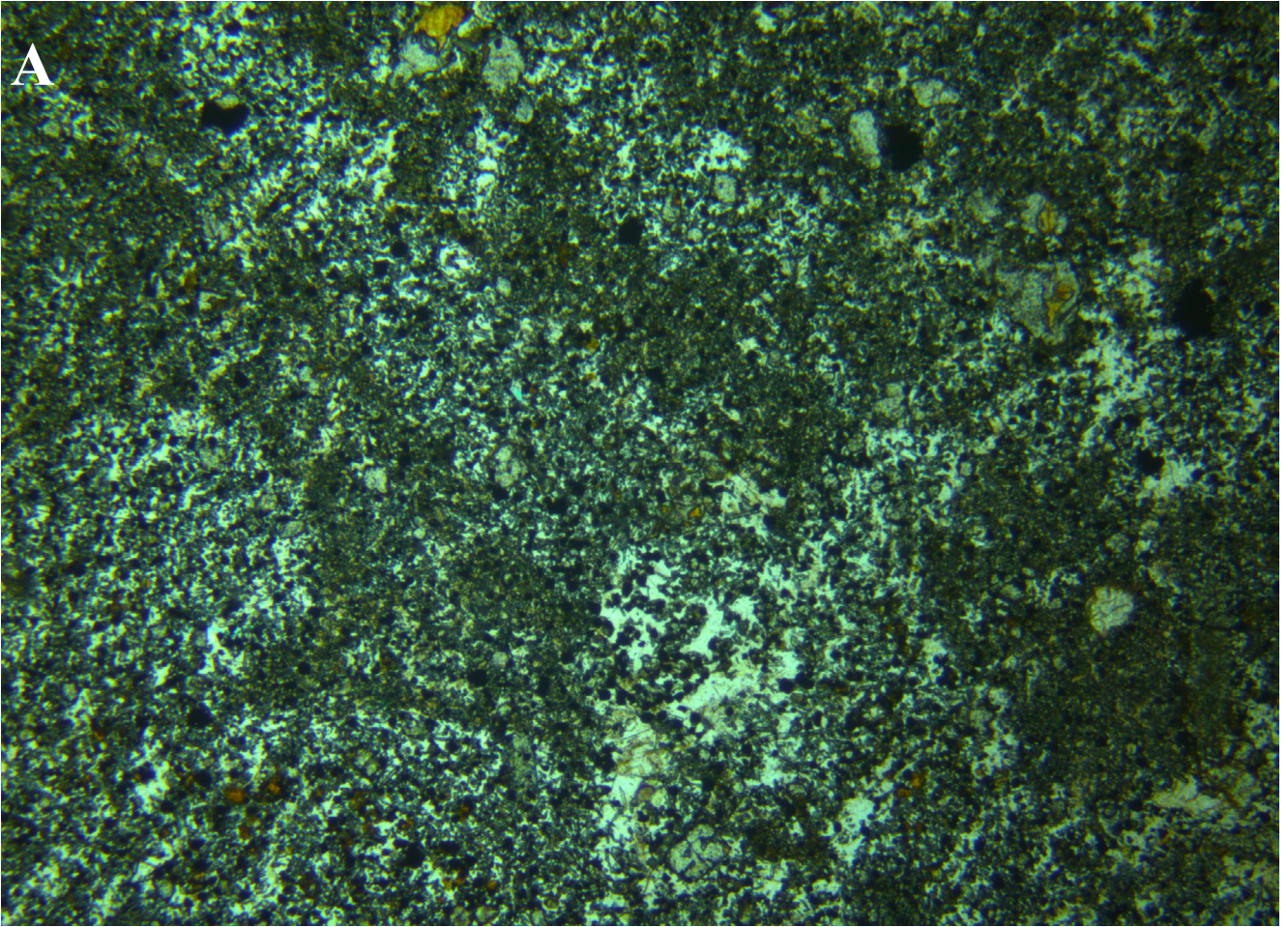
Figure 31. Photomicrograph of sample LSB24, nepheline hawaiite, Burburys Sugarloaf, midlands, Tasmania. Poikilitic platelets of anorthoclase with abundant inclusions in a fine-grained feldspathoidal groundmass. Field of view ~4.6 x 3.4 mm. (a) plane polarised light (b) crossed nicols.

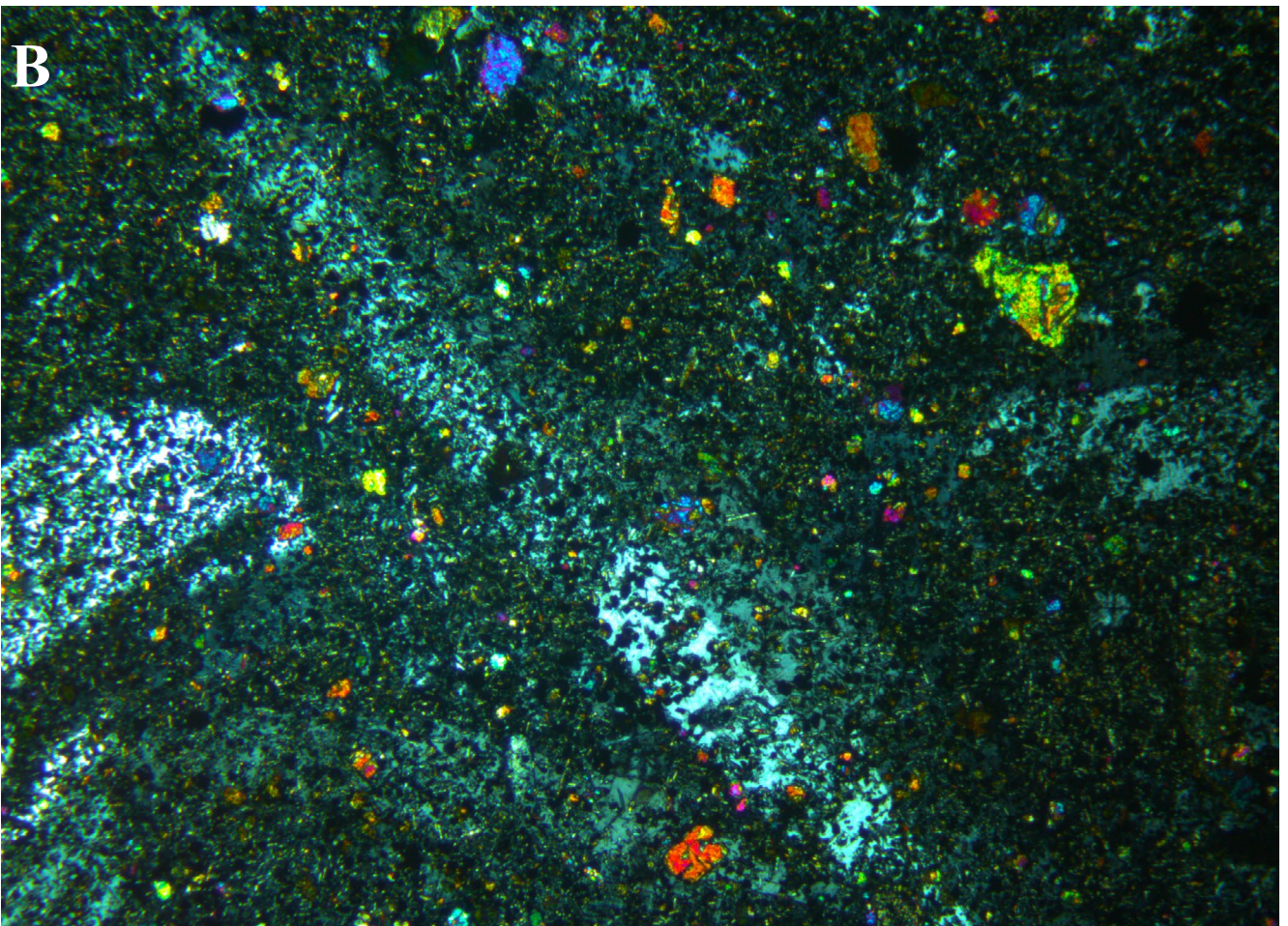Figure 32. Photomicrograph of sample LSB24, nepheline hawaiite, Burburys Sugarloaf, midlands, Tasmania. Lherzolite xenolith with reaction rim (right), poikilitic anorthoclase platelets and a fine-grained groundmass; amygdale filled with (?) analcite (left). Field of view ~4.6 x 3.4 mm. (a) plane polarised light (b) crossed nicols.
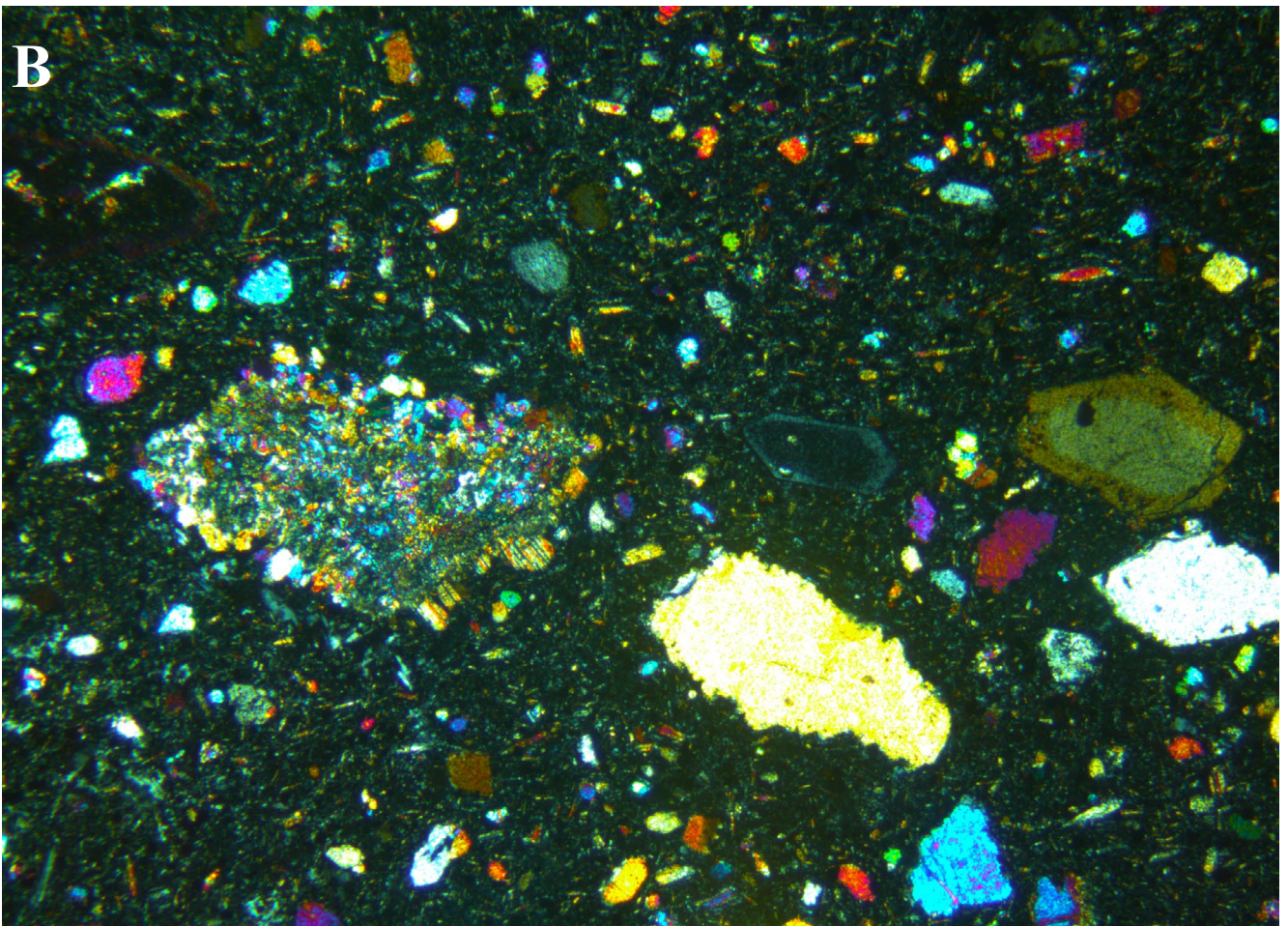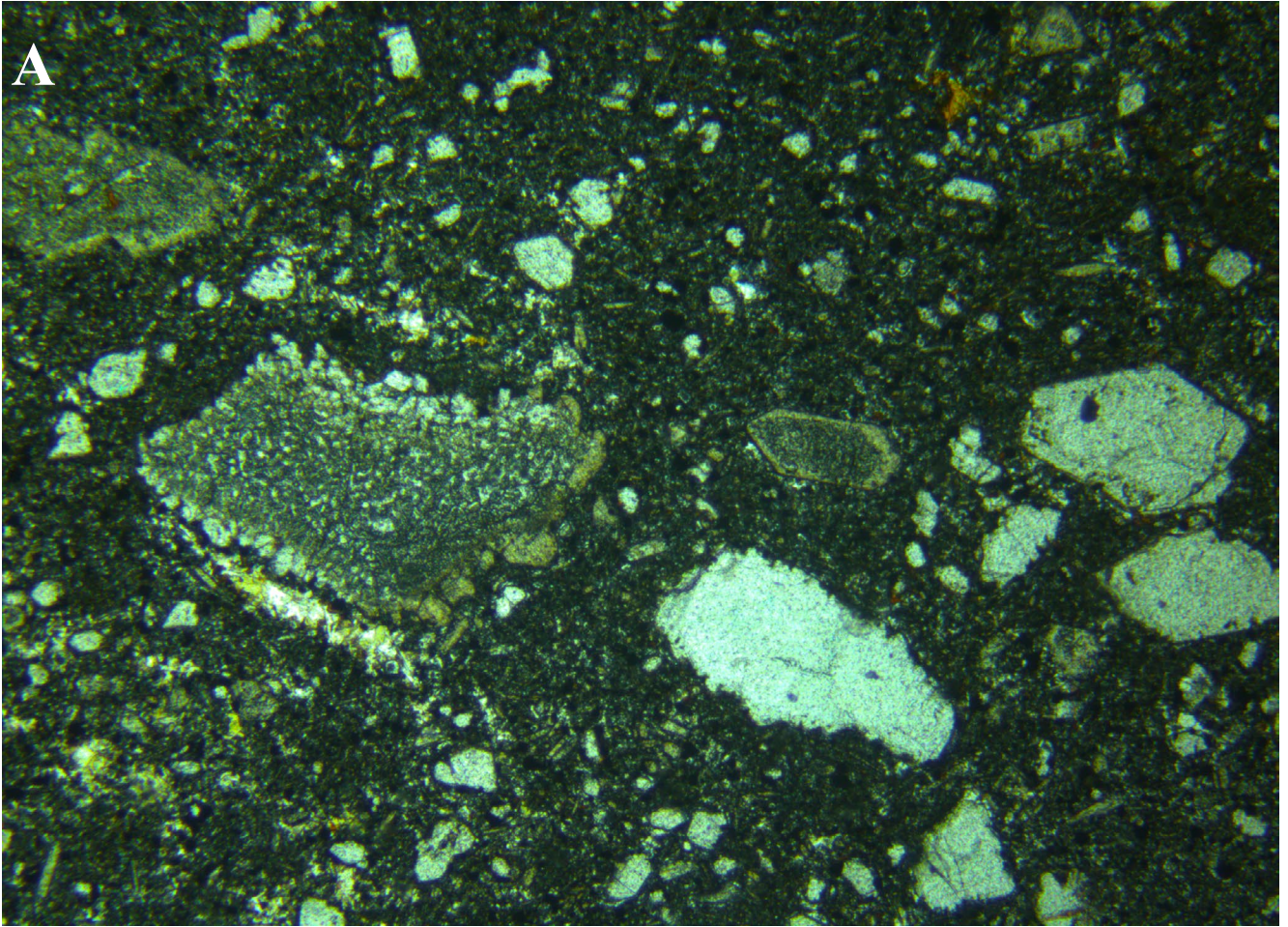
Figure 33. Photomicrograph of sample LCr, olivine nephelinite, west Lake Crescent, central Tasmania. Reacted lherzolite xenolith (left), anhedral olivine xenocryst (lower right), Ti-augite microphenocrysts (e.g. centre right) and olivine microphenocrysts (right) in a very fine-grained feldspathoidal groundmass. Field of view ~4.6 x 3.4 mm. (a) plane polarised light (b) crossed nicols.

Figure 34. Photomicrograph of sample LCr, olivine nephelinite, west Lake Crescent, central Tasmania. Olivine xenocrysts with reaction coronas (right); opaque xenocryst of reacted spinel (left), olivine and Ti-augite microphenocrysts in a fine-grained feldspathoidal groundmass. Field of view ~4.6 x 3.4 mm. (a) plane polarised light (b) crossed nicols.
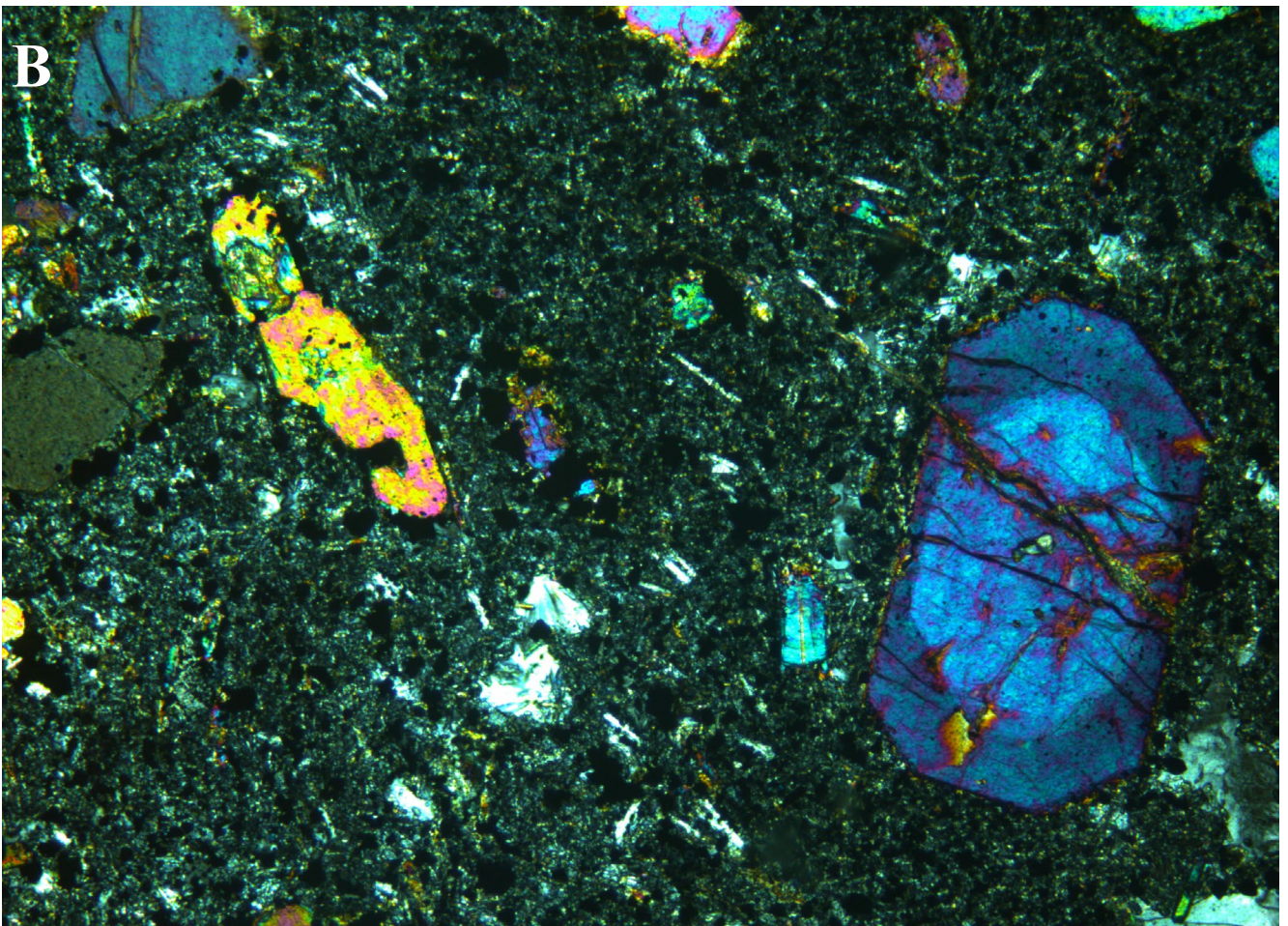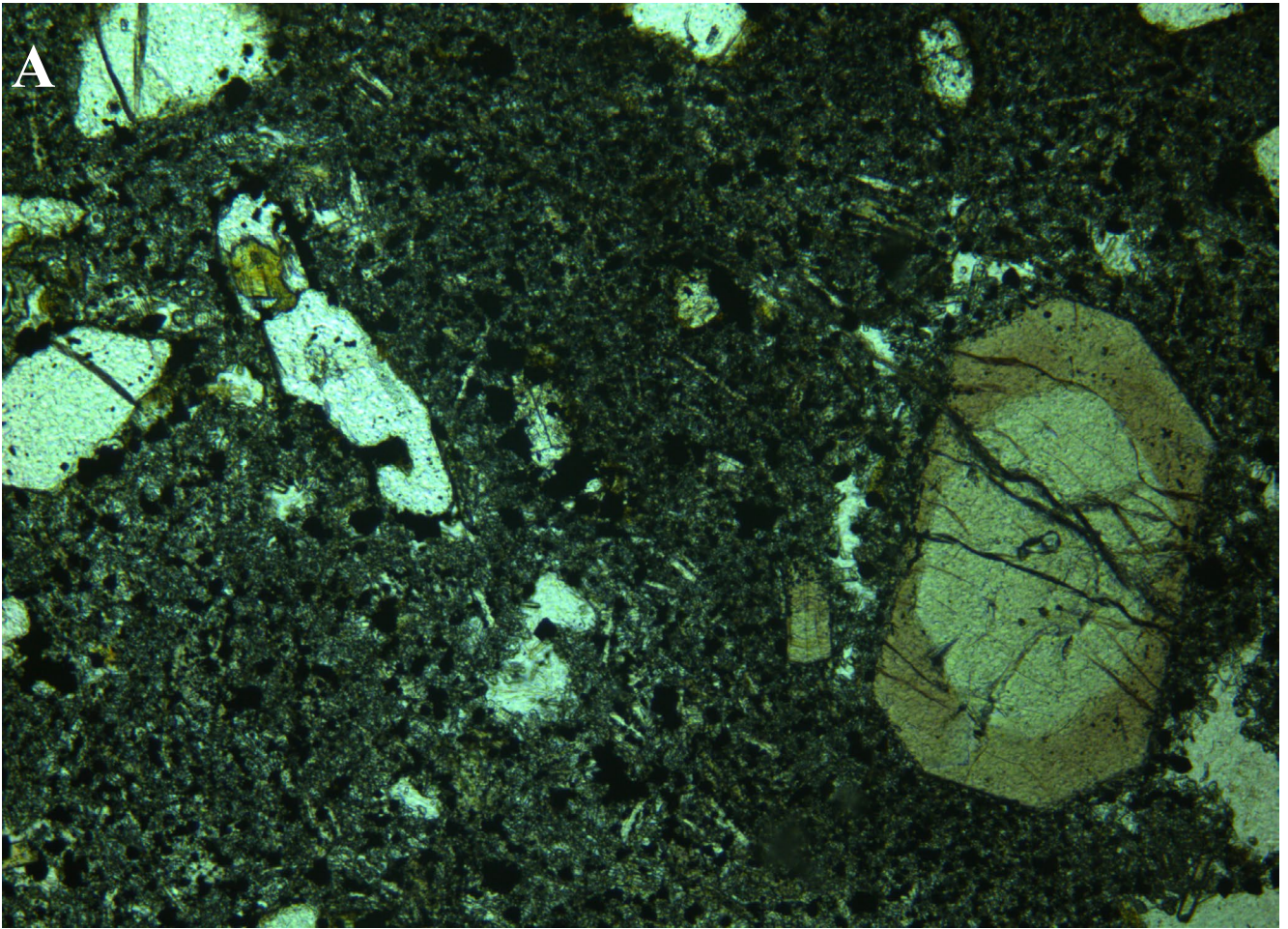
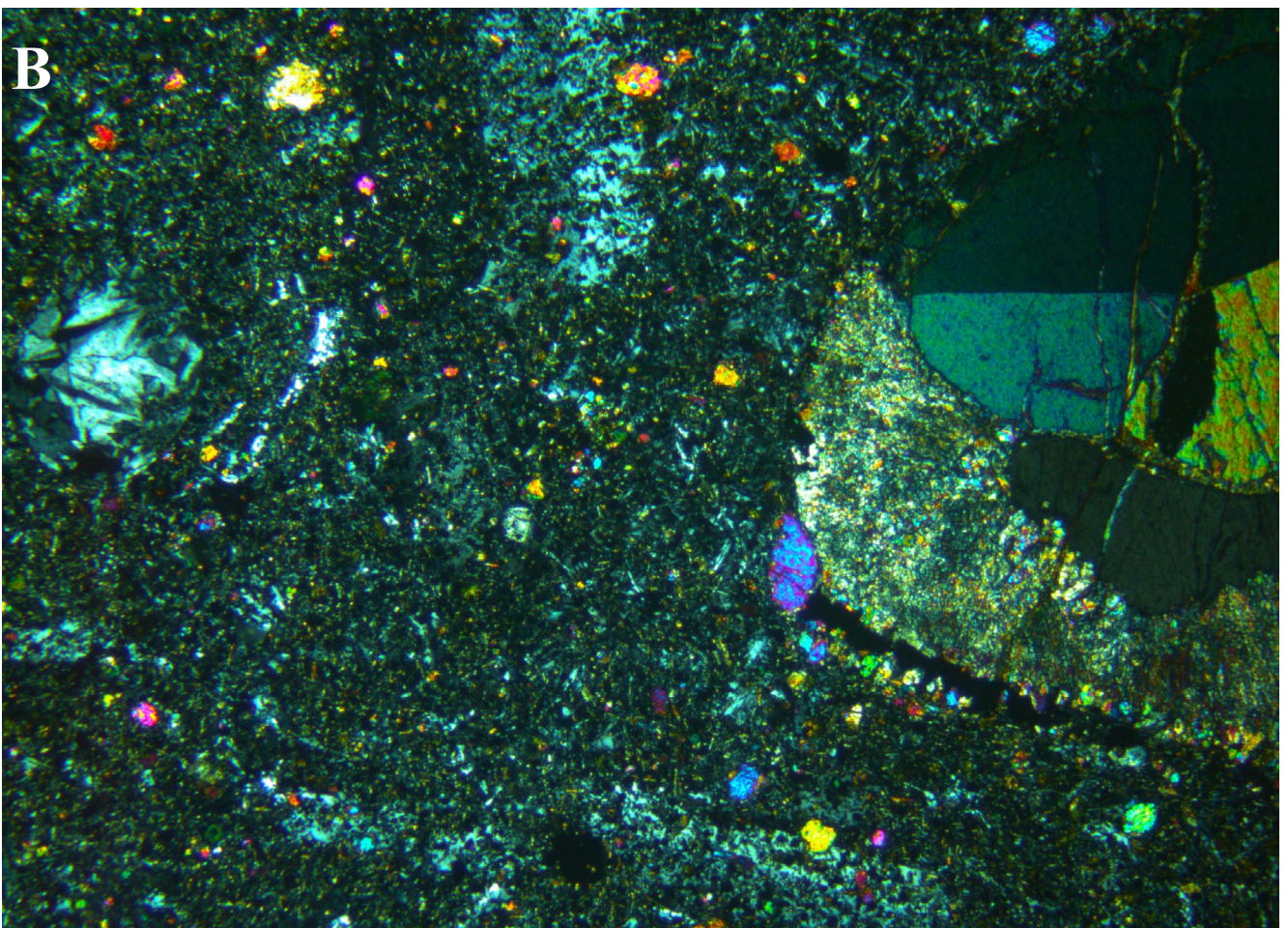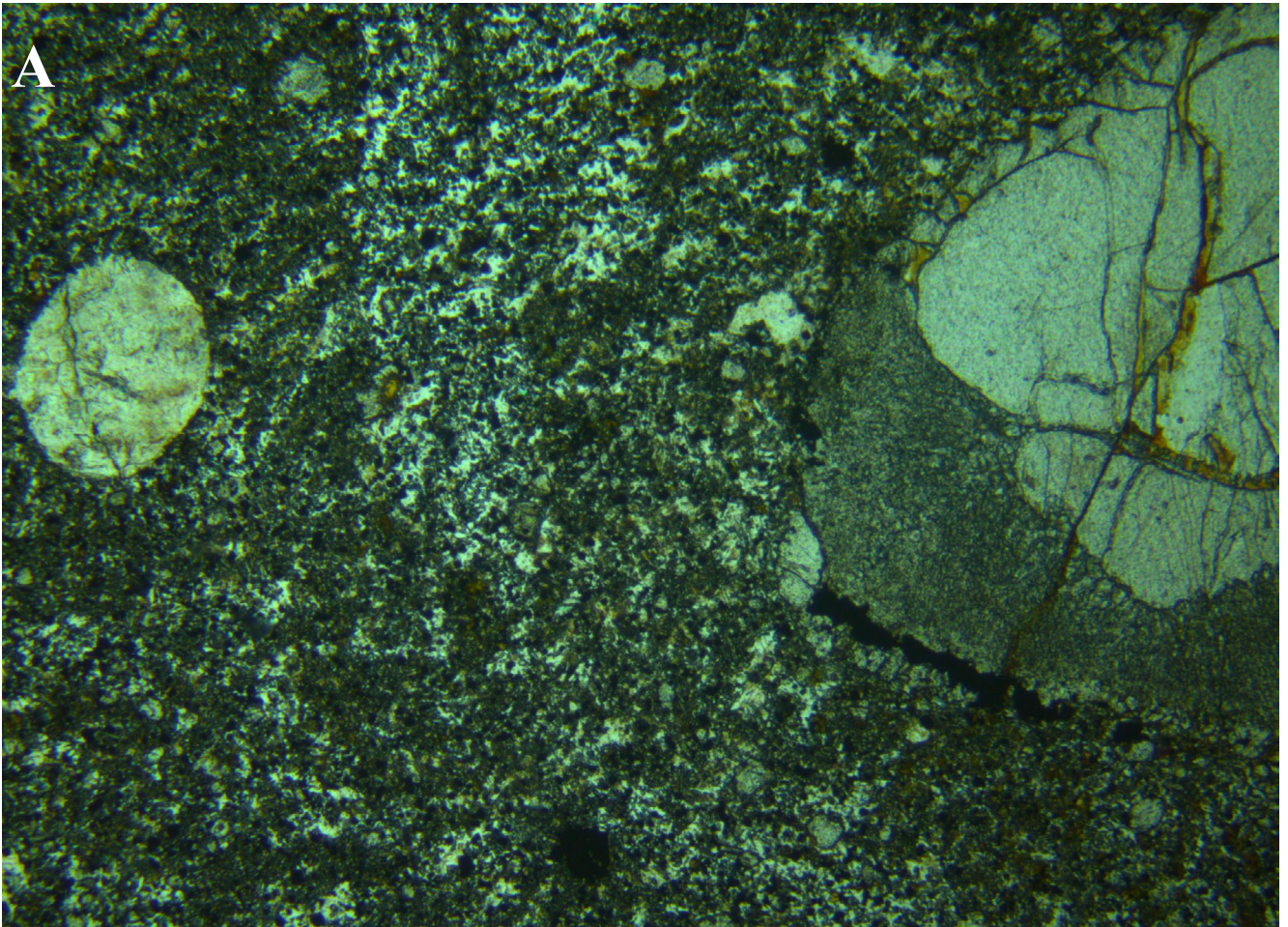Figure 35. Photomicrograph of sample ATr, olivine melilitite, Alma Tier, central Tasmania. Euhedral Ti-augite microphenocryst (right), and olivine microphenocrysts in a very fine-grained groundmass with aligned melilite laths. Field of view ~1.9 x 1.4 mm. (a) plane polarised light (b) crossed nicols.
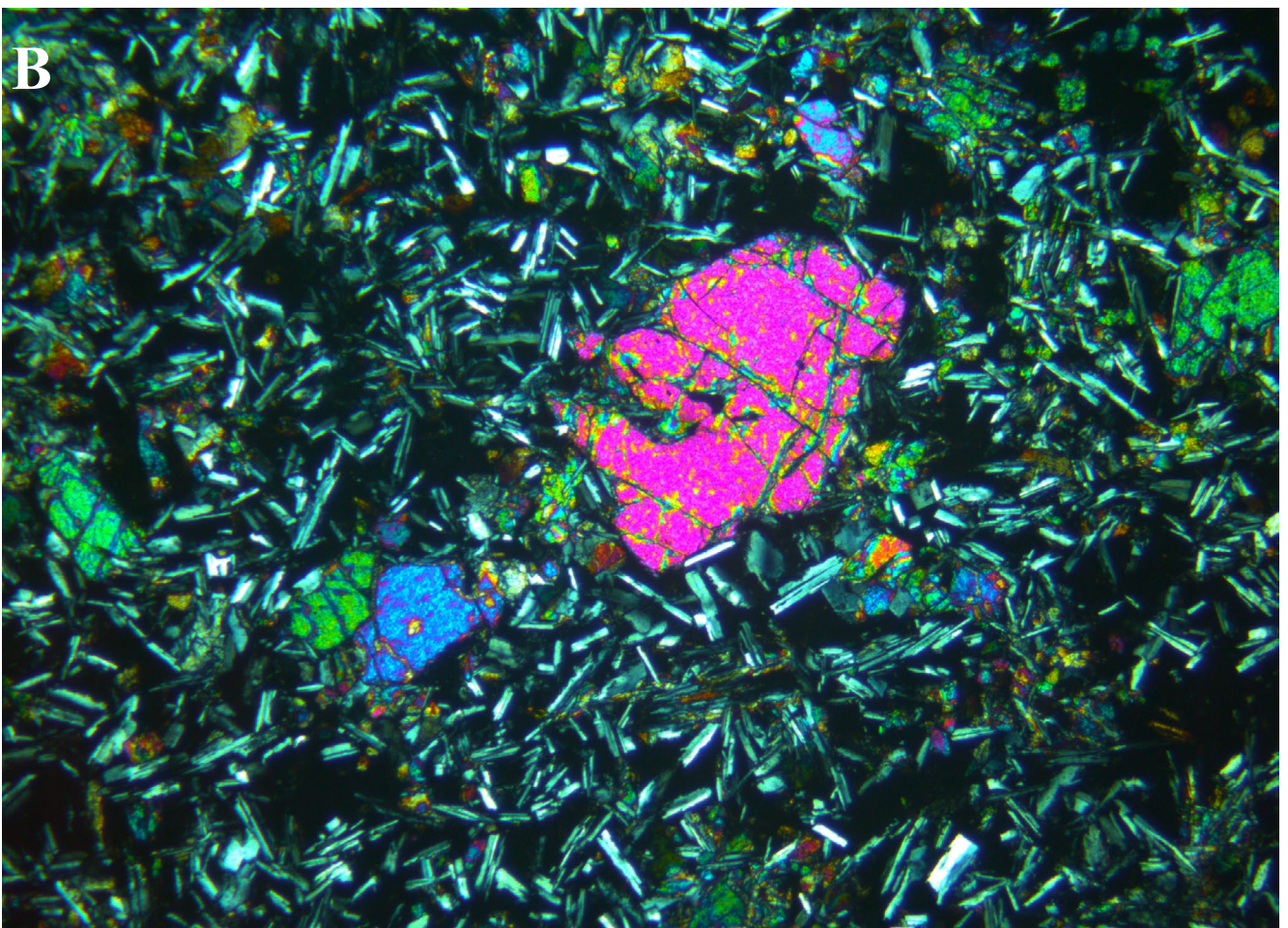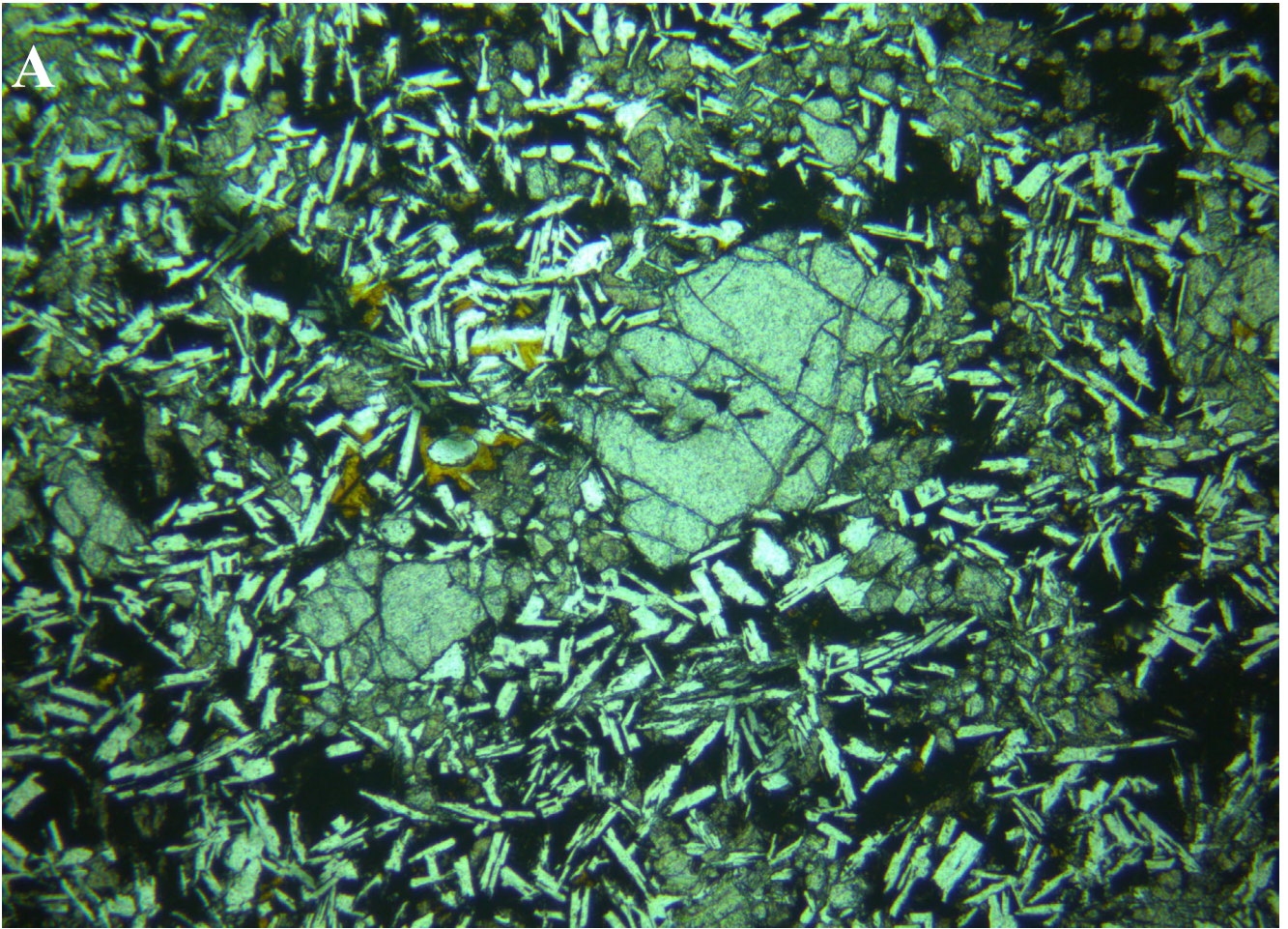
Figure 36. Photomicrograph of sample BRJ1, quartz tholeiite, Brighton, S Tasmania. Slightly embayed olivine phenocrysts in a dominantly intergranular/intersertal groundmass of augite granules, plagioclase laths and a partly altered mesostasis of "black glass." Field of view ~4.6 x 3.4 mm. (a) plane polarised light (b) crossed nicols.
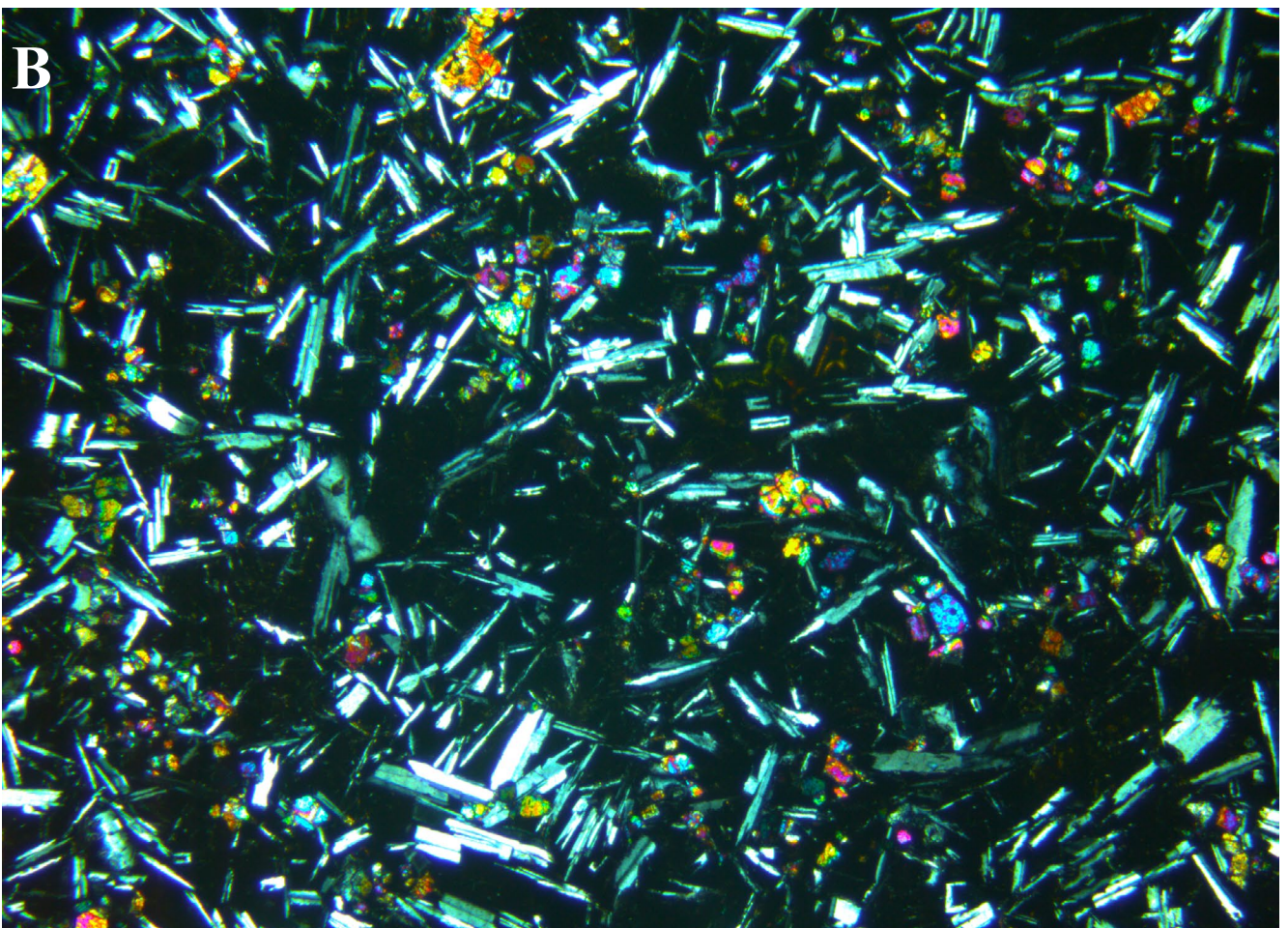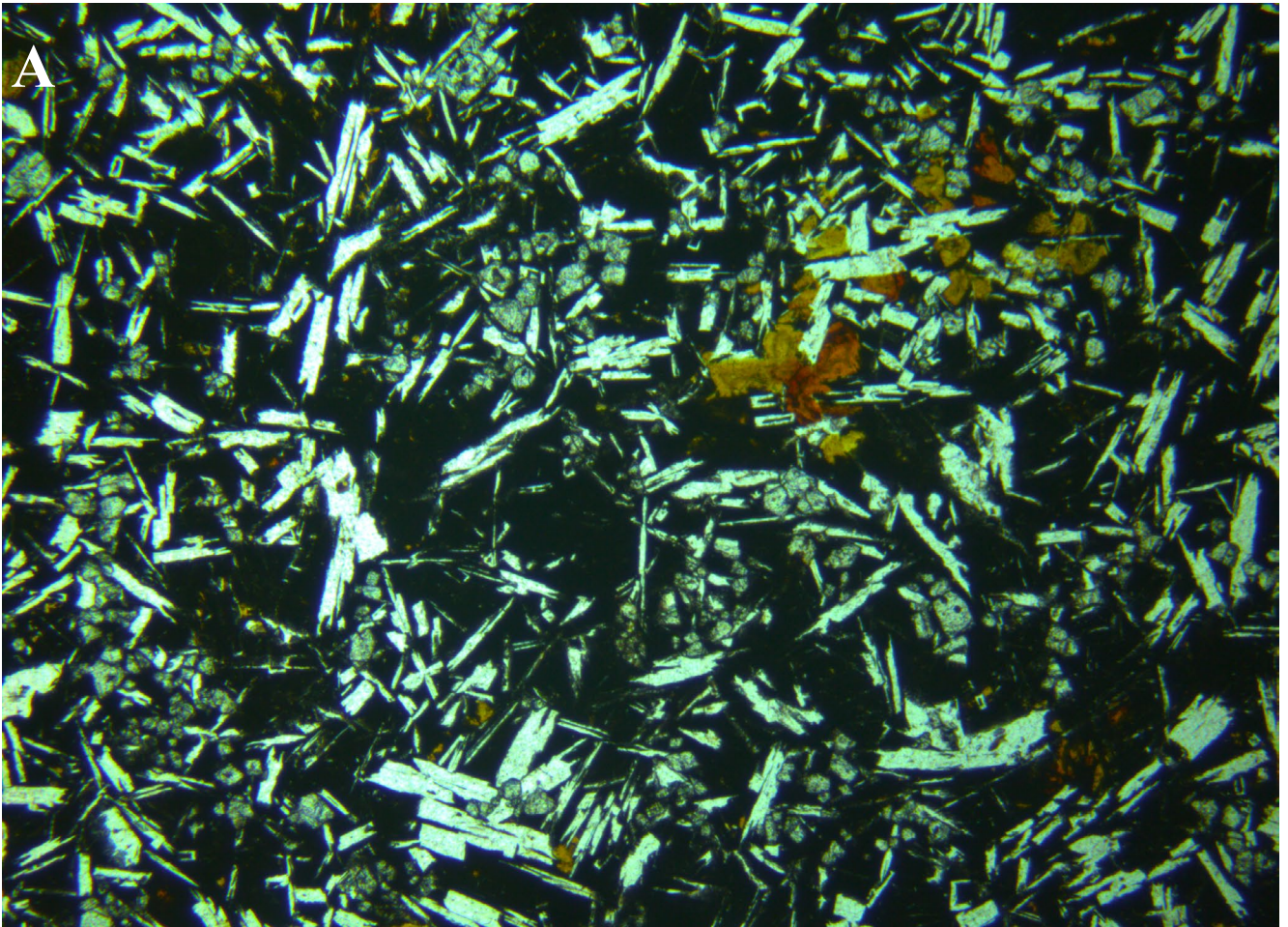
Figure 37. Photomicrograph of sample HBJ23, quartz tholeiite, Claremont, S Tasmania. Intersertal texture with plagioclase laths, small partly altered olivine granules and abundant "black glass." Field of view ~4.6 x 3.4 mm. (a) plane polarised light (b) crossed nicols.
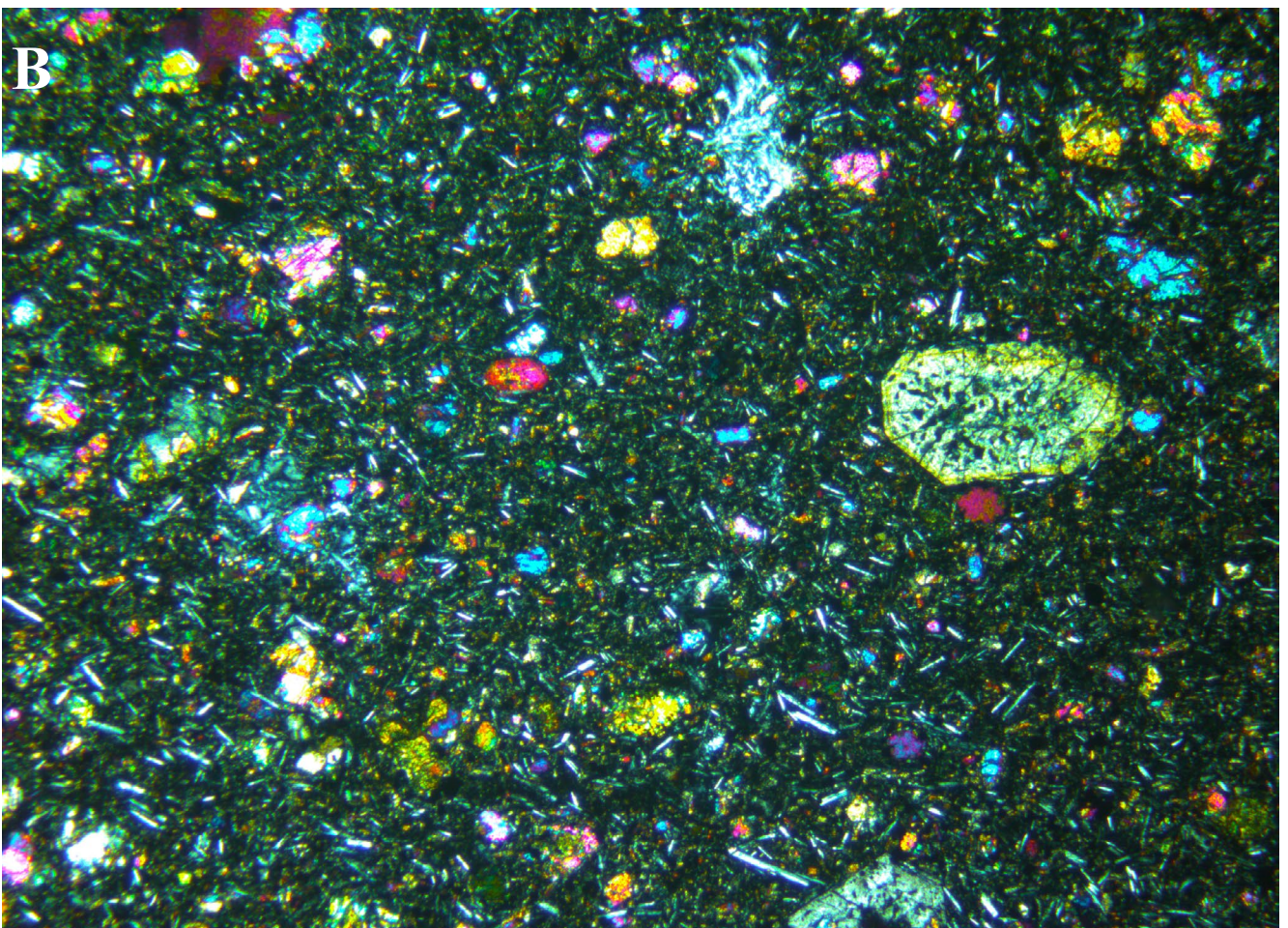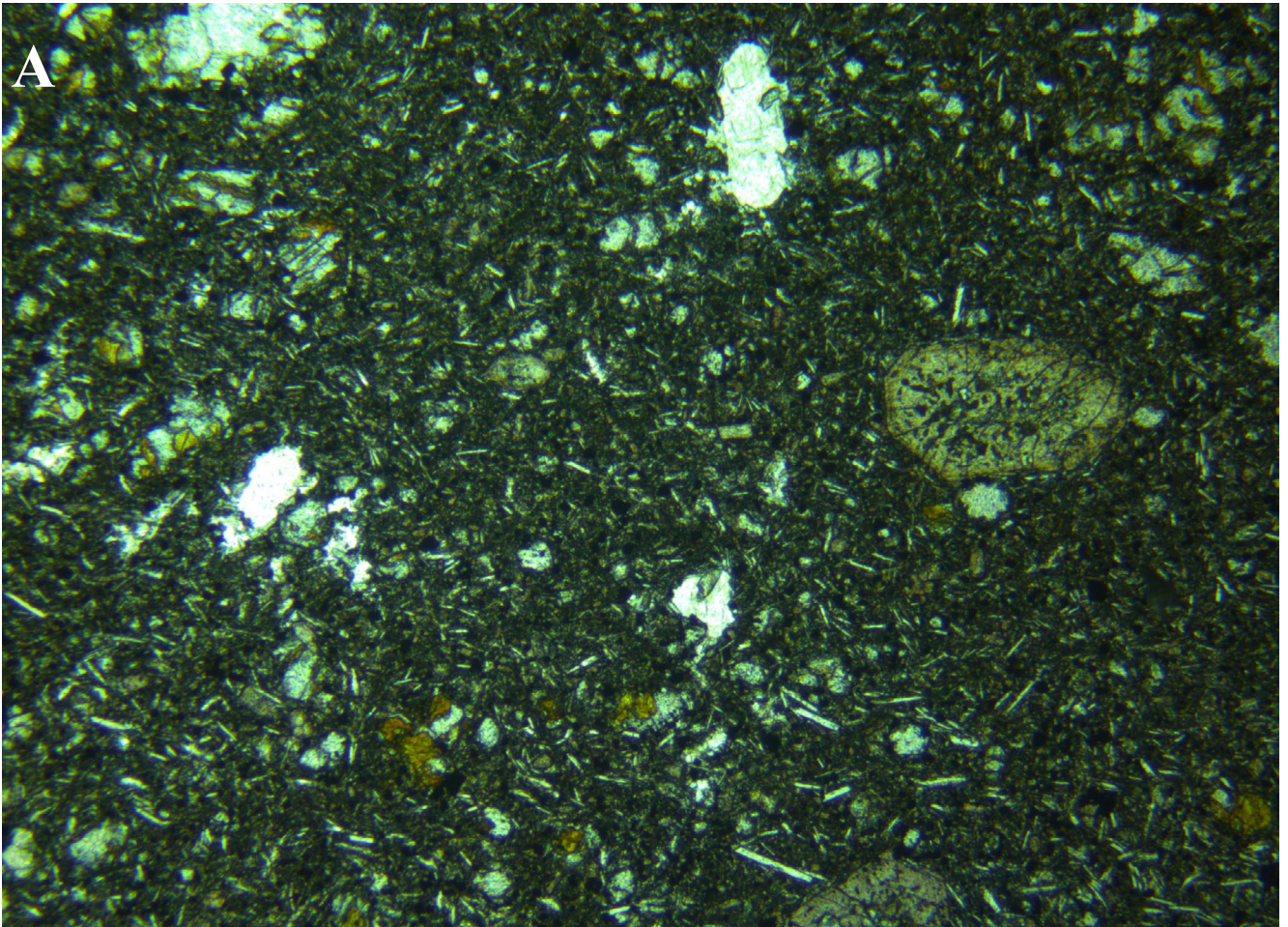
Figure 38. Photomicrograph of sample GFN, basanite, Glenfern, S Tasmania. Microphenocrysts of euhedral Ti-augite (pink-yellow) and olivine (e.g. upper left), with small aligned plagioclase laths in a fine-grained intergranular groundmass. Field of view ~4.6 x 3.4 mm. (a) plane polarised light (b) crossed nicols.
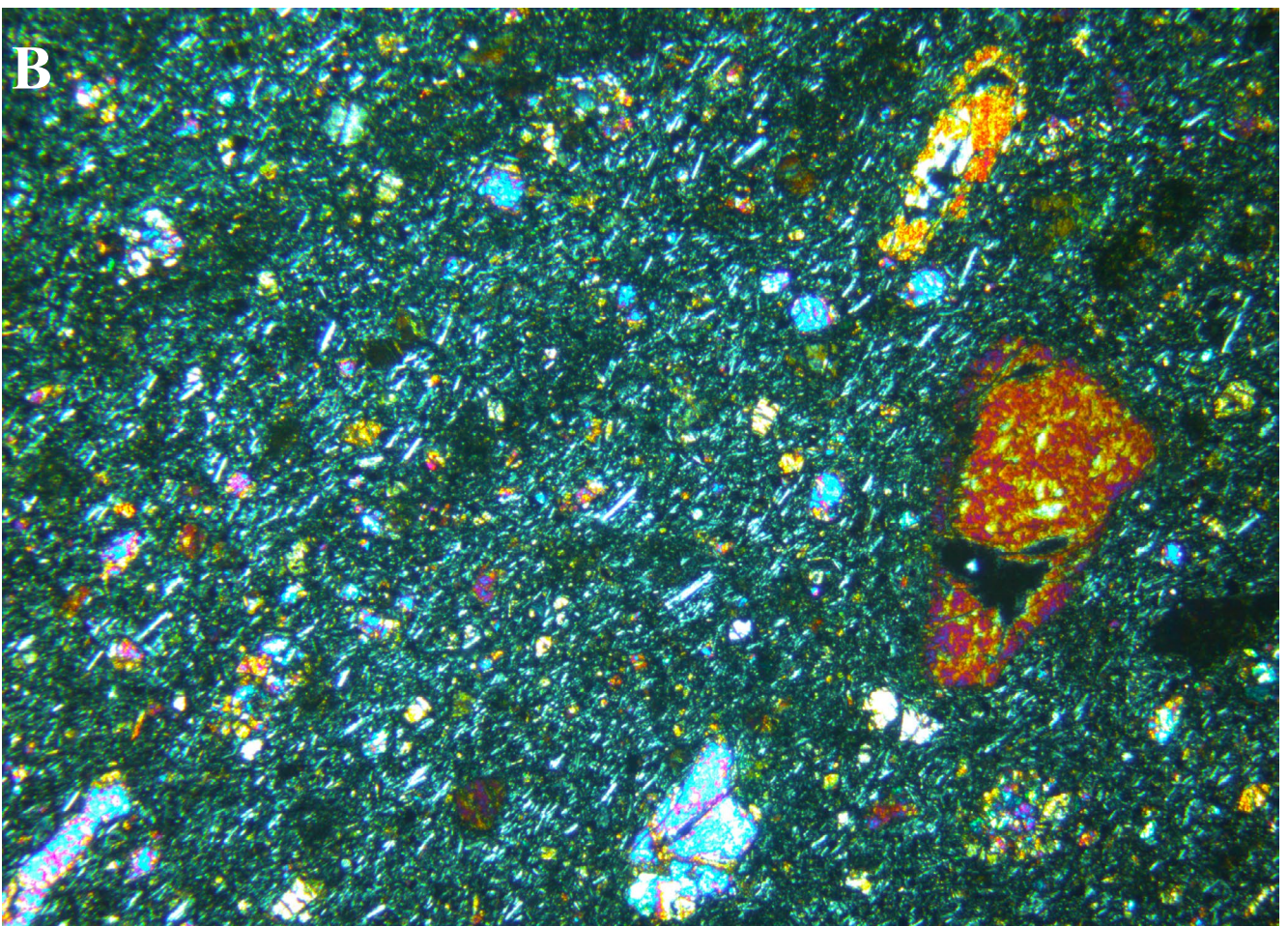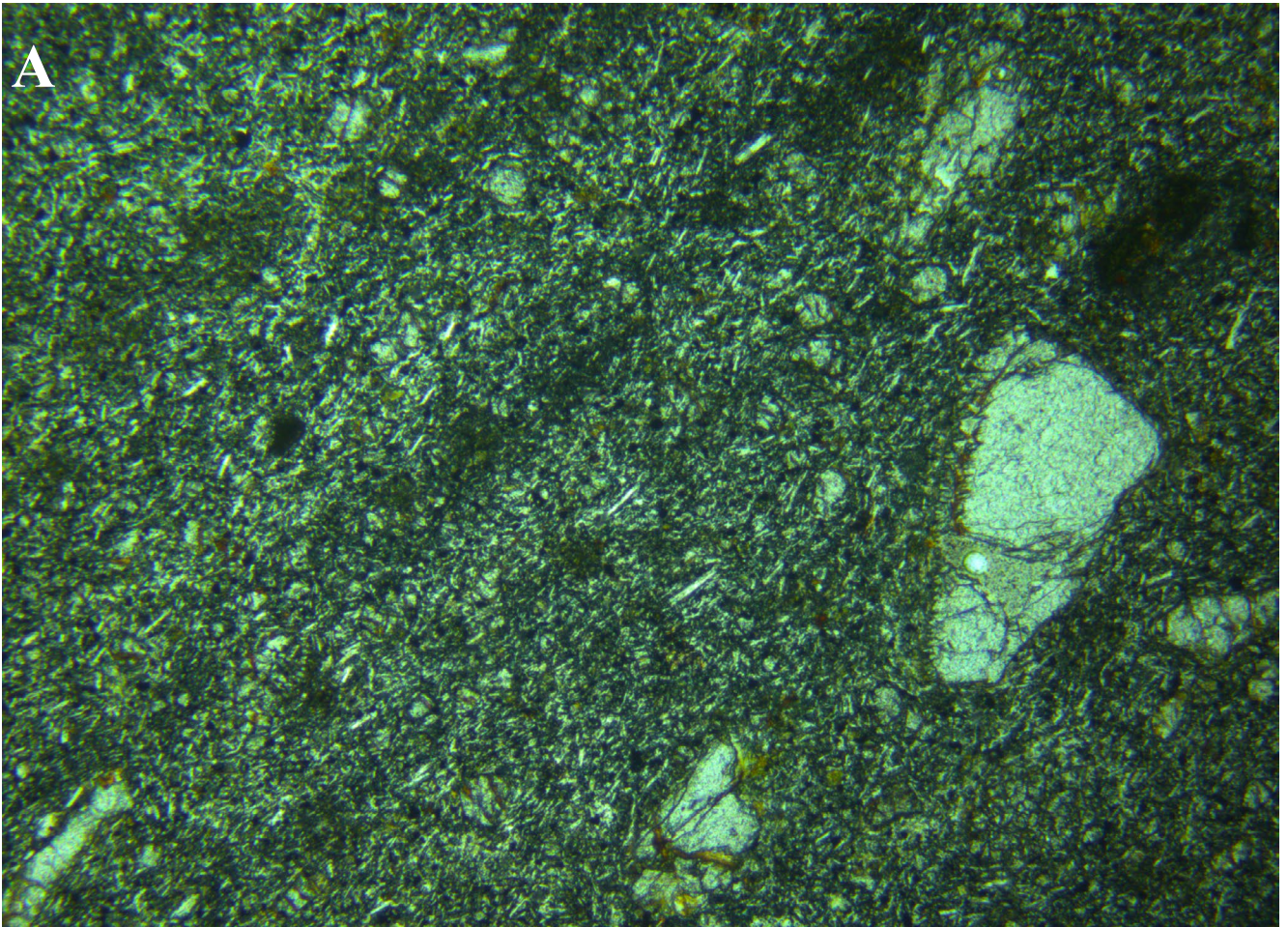
Figure 39. Photomicrograph of sample HBJ6, hawaiite, Pickett Hill, S Tasmania. Olivine xenocrysts in a fine-grained fluidal groundmass. Field of view ~4.6 x 3.4 mm. (a) plane polarised light (b) crossed nicols.

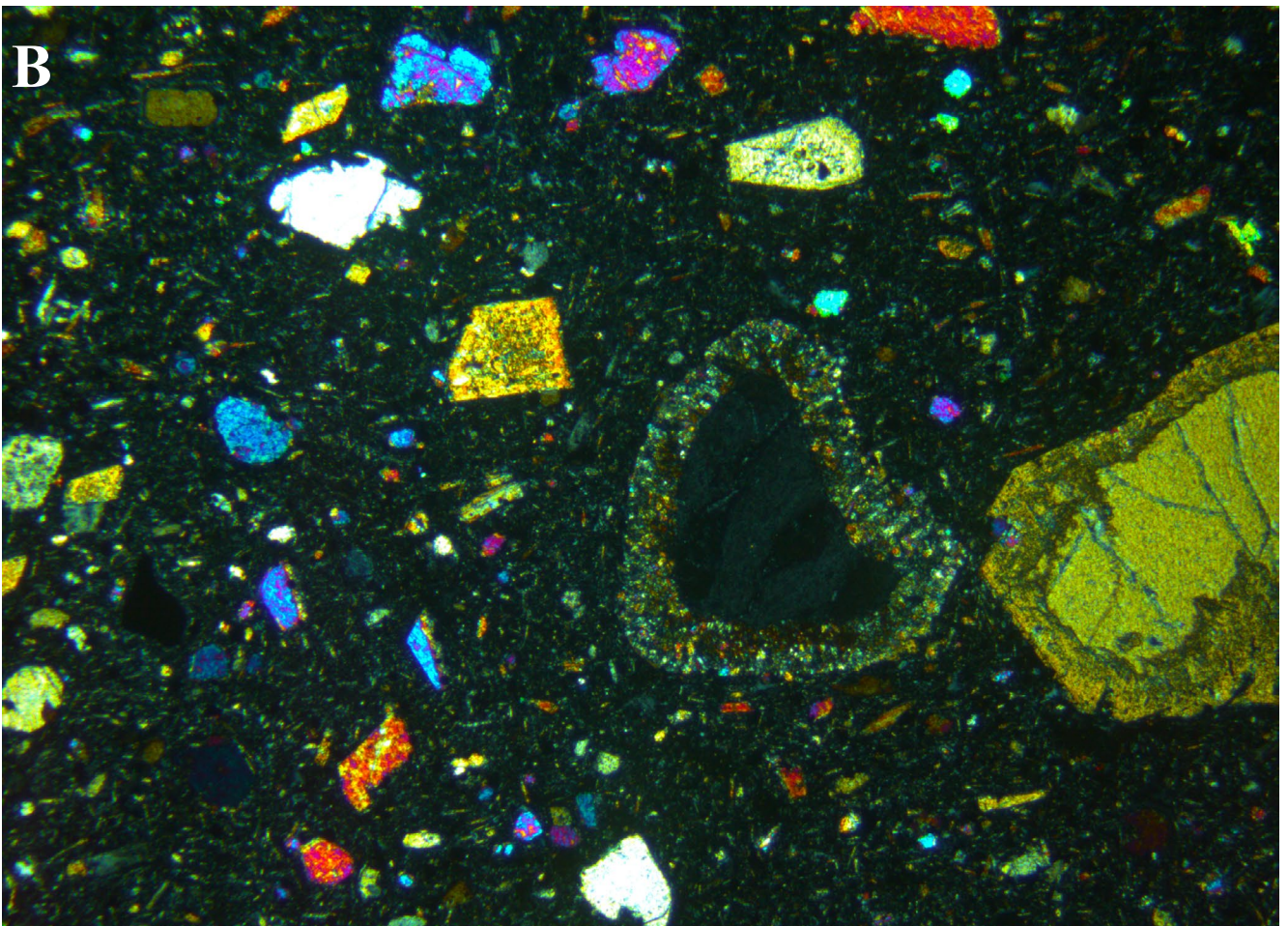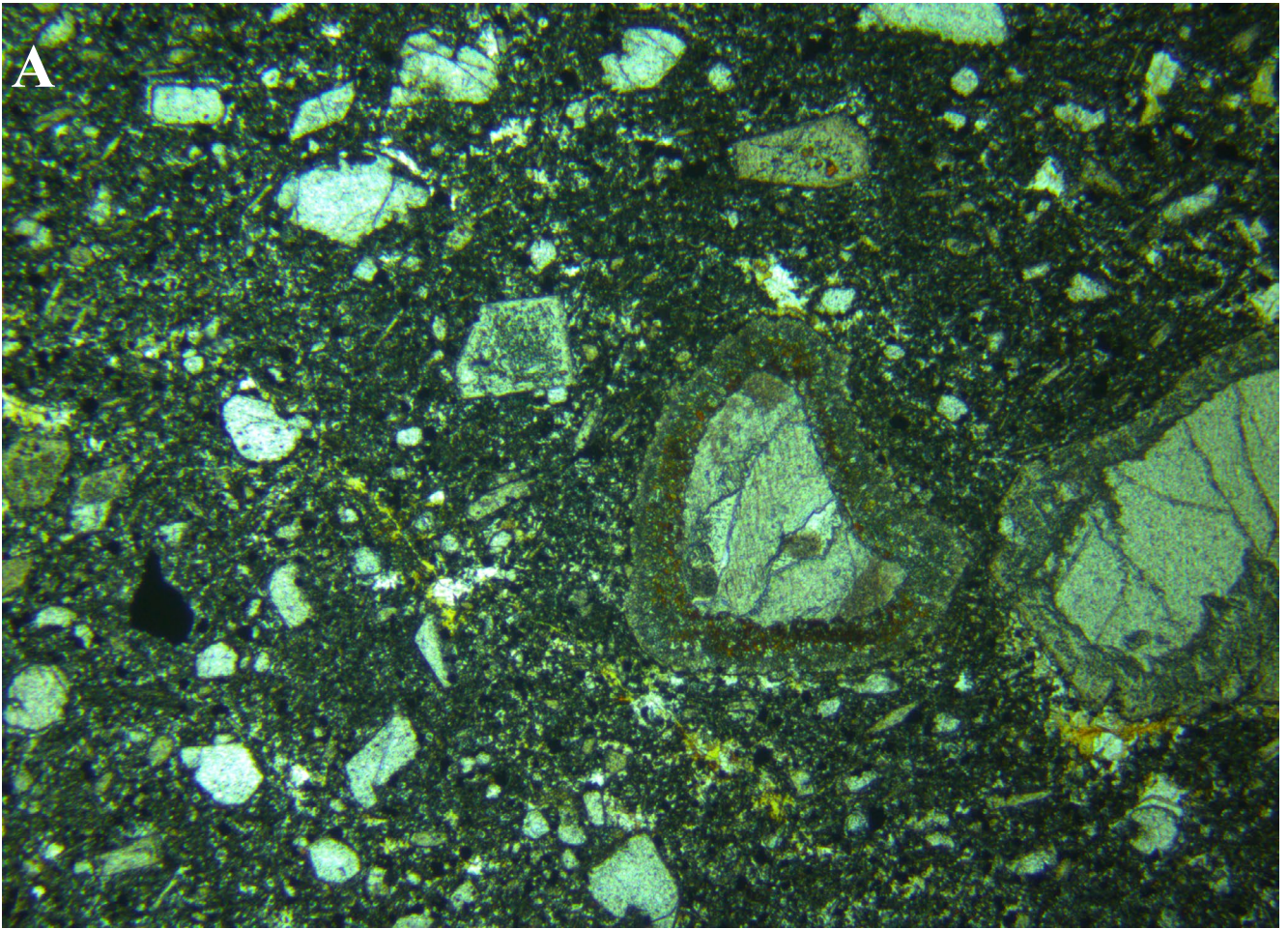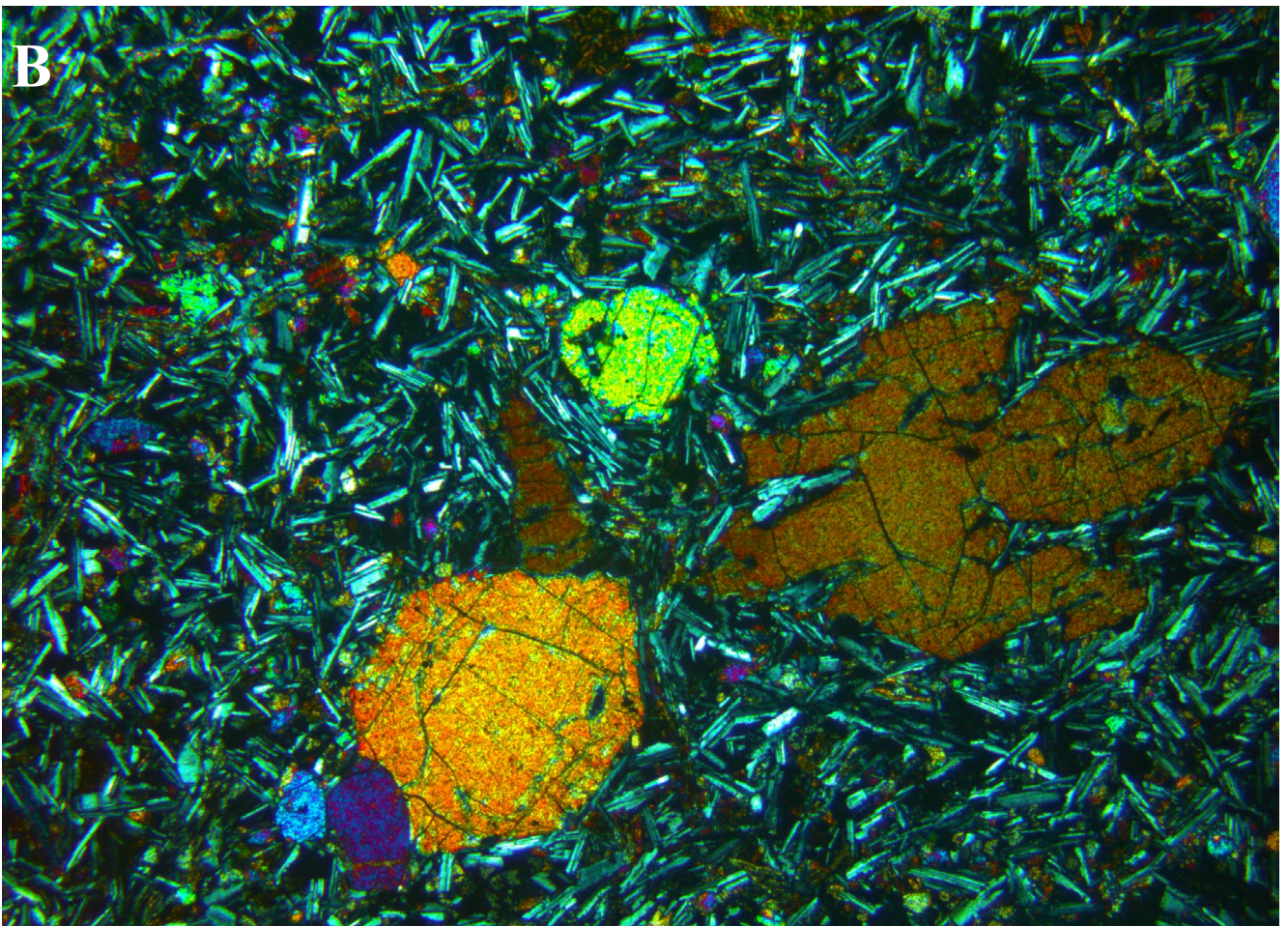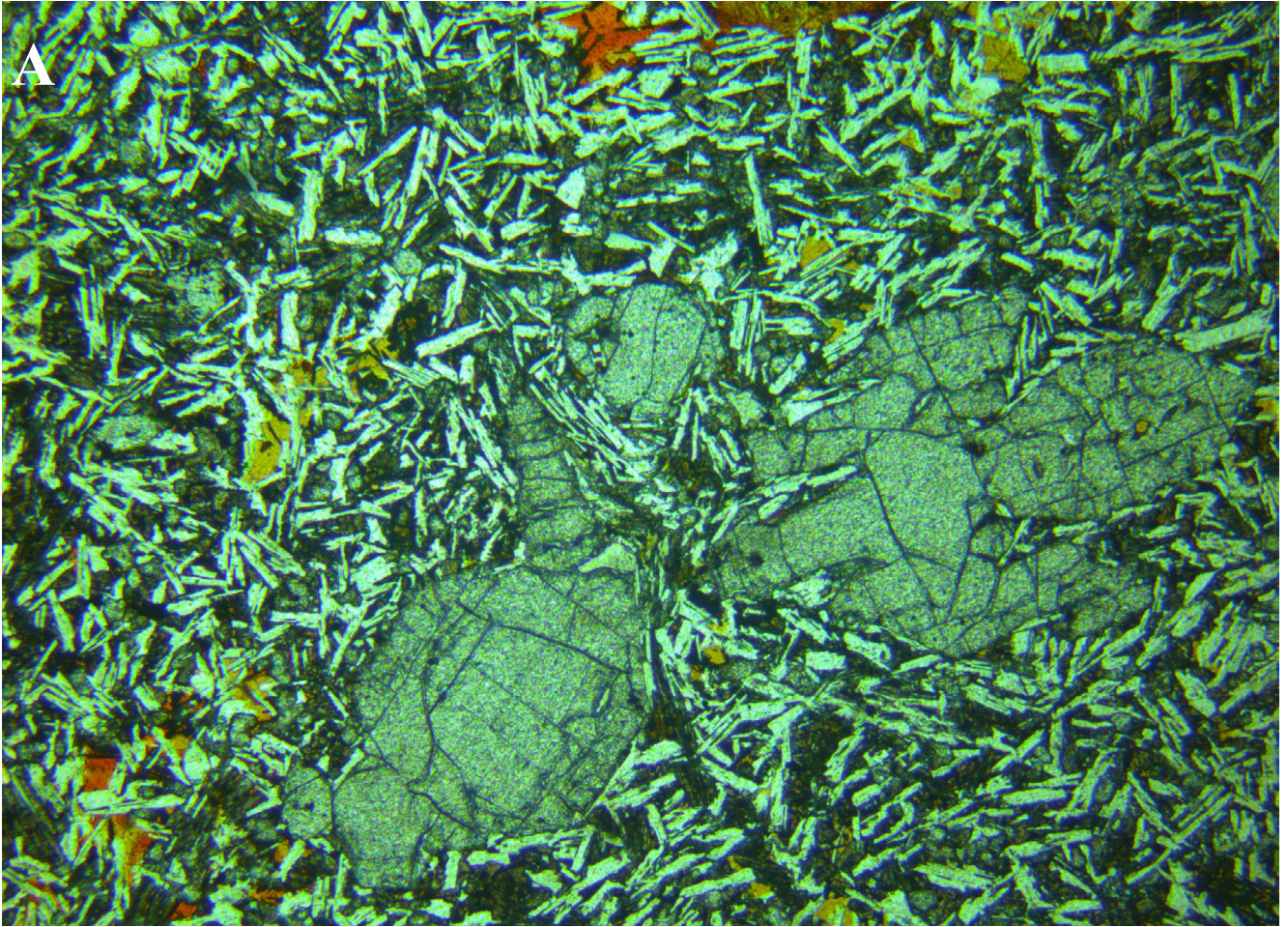Figure 40. Photomicrograph of sample SBA21, olivine tholeiite, Marion Bay, SE Tasmania. Embayed olivine phenocrysts in an intergranular groundmass with minor alteration. Field of view ~4.6 x 3.4 mm. (a) plane polarised light (b) crossed nicols.

APPENDIX 3

Laboratory Report LJN2023-031

XRD Analysis

MINERAL RESOURCES TASMANIA
LABORATORY REPORT
LJN2023-031

XRD ANALYSIS

An unpublished Mineral
Resources Tasmania
Report for:

J. L. Everard MRT

By: T Coyte

Date: 22 January 2024

Mineral Resources Tasmania
Department of State Growth

INTRODUCTION

Twelve samples were submitted for analysis by J Everard from Mineral Resources Tasmania (MRT) on the 7th of April 2023. The details are shown below in Table 1.

Table 1. Sample Details

Reg#	Field No.	Location	Sample Description	Easting	Northing	Datum
R005353	TJ3228	Knoll, Neasey Plains	Nepheline hawaiite	357220	5441980	GDA94 - MGA Zone 55
R010192	CVH	Coastview Hill, via Hampshire	Olivine nephelinite	398910	5432780	GDA94 - MGA Zone 55
R010187	SRN	South Riana plug	Basanite	415690	5431180	GDA94 - MGA Zone 55
R010218	ATr	Alma Tier	Olivine melilitite	504140	5332900	GDA94 - MGA Zone 55
R010205	LCr	W side of Lake Crescent	Olivine nephelinite	511380	5330210	GDA94 - MGA Zone 55
G402497	GFN	Glenfern	Basanite	498010	5257240	GDA94 - MGA Zone 55
R010202	SDL	The Sideling	Olivine nephelinite	533810	5430980	GDA94 - MGA Zone 55
R010201	WSc	West Scottsdale	Olivine nephelinite	540710	5440980	GDA94 - MGA Zone 55
R004332	AJ99	Olivers Hill	Olivine nephelinite	562632	5427613	GDA94 - MGA Zone 55
R004366	AJ1424	Sweets Creek (North)	Basanite	559530	5418160	GDA94 - MGA Zone 55
R004368	AJ1426	Upper Esk	Olivine nephelinite	560920	5413380	GDA94 - MGA Zone 55
R027027	PP20.5	Pebble Plain DDH/20.5m, Beauty Flat	Olivine nephelinite	582760	5403860	GDA94 - MGA Zone 55

XRD ANALYSIS

Method: Minerology by XRD

Date: 23/6/2023

Analyst: L Unwin

Sample Preparation:

The samples were prepared, examined, and analysed in the MRT laboratories, Mornington, Tasmania. They were run on a Rigaku Miniflex 600 X-Ray Diffractometer system: a 600W generator 150mm goniometer with a Cu tube; 40kV/15mA, sample spinner and a Scintillation counter (SC) with Be window, a graphite counter monochromator and a Kß Ni- filter. The analysis was performed using the following conditions: +3° to 63° 2Theta scanning and measuring range, with a scanning speed of 0.5 °/min with a resolution of 0.02° by step. The mineral identification software used for sample analysis is PDXL2 using the ICCD database.

Quartz, if present, is used as an internal standard; and if not present, it is often added to the sample for a supplementary scan.

Table 2. XRD Instrument parameters

Measurement conditions			
X-Ray:	40 kV , 15 mA	Scan speed / Duration time:	0.5000 deg/min
Goniometer:	MiniFlex600	Step width:	0.0200 deg
Attachment:	ASC-6	Scan axis:	Theta/2-Theta
Filter:	None	Scan range:	3.0000 - 63.0000 deg
CBO selection slit:	-	Incident slit:	1.250deg
Diffracted beam mono.:	Bent	Length limiting slit:	10.0mm
Detector:	SC-70	Receiving slit #1:	1.250deg
Scan mode:	Continuous	Receiving slit #2:	0.3mm

Table 3. Summary of XRD results

Mineral	Formula	R004368	R010202	R010218	R010201	R010205
Clinopyroxene	Variable	*	*	*	*	*
Plagioclase	$(Na,Ca)(Al,Si)_4O_8$	*	*	*	*	*
Magnetite	$Fe^{2+}Fe^{3+}_2O_4$	*	*	*	*	*
Nepheline	$Na_3K(Al_4Si_4O_{16})$	*	*	*	*	*
Analcime	$NaAl(Si_2O_6) \cdot (H_2O)$	*				*
Olivine	$Mg_2(SiO_4)$	*	*	*	*	*
Fluorapatite	$Ca_5(PO_4)_3F$	*	*	*	*	*
Smectite	Variable				*	
Philipsite	Variable	*				
Chlorite	$(Fe,Mg,Al)_6(Si,Al)_4O_{10}(OH)_8$	*		*	*	
Anorthoclase	$Na,K)AlSi_3O_8$				*	
Mica	$KAl_2(AlSi_3O_{10})(OH)_2$					*
Mesolite	$Na_2Ca_2Al_6Si_9O_{30} \cdot 8(H_2O)$			*	*	
Amphibole	Variable					*
Melilite	$Ca_2(Al,Mg,Fe)((Al,Si,B)SiO_7)$			*		

Table 3 cont. Summary of XRD results

Mineral	Formula	R005353	R004366	R010187	R004332	R010192
Clinopyroxene	Variable	*	*	*	*	*
Plagioclase	$(Na,Ca)(Al,Si)_4O_8$		*	*		*
Magnetite	$Fe^{2+}Fe^{3+}_2O_4$	*	*	*	*	*
Nepheline	$Na_3K(Al_4Si_4O_{16})$	*	*	*	*	*
Analcime	$NaAl(Si_2O_6) \cdot (H_2O)$		*	*	*	*
Olivine	$Mg_2(SiO_4)$	*	*	*	*	*
Fluorapatite	$Ca_5(PO_4)_3F$	*	*	*	*	*
Smectite	Variable	*	*	*		
Chlorite	$(Fe,Mg,Al)_6(Si,Al)_4O_{10}(OH)_8$		*	*		*
Anorthoclase	$Na,K)AlSi_3O_8$		*	*		
Mica	$KAl_2(AlSi_3O_{10})(OH)_2$		*			
Chabazite	$(Ca,K_2,Na_2)_2[Al_2Si_4O_{12}]_2 \cdot 12H_2O$		*			
Stilbite	$NaCa_4[Al_9Si_{27}O_{72}] \cdot nH_2O$	*				
Serpentine	$Mg_3Si_2O_5(OH)_4$			*		
Spinel Group	Variable			*		

Table 3 cont. Summary of XRD results

Mineral	Formula	R027027	G407297
Clinopyroxene	Variable	*	*
Plagioclase	$(Na,Ca)(Al,Si)_4O_8$	*	*
Magnetite	$Fe^{2+}Fe^{3+}_2O_4$	*	*
Nepheline	$Na_3K(Al_4Si_4O_{16})$	*	*
Olivine	$Mg_2(SiO_4)$	*	*
Fluorapatite	$Ca_5(PO_4)_3F$	*	*
Smectite	Variable	*	
Chlorite	$(Fe,Mg,Al)_6(Si,Al)_4O_{10}(OH)_8$	*	
Anorthoclase	$Na,K)AlSi_3O_8$	*	*
Mica	$KAl_2(AlSi_3O_{10})(OH)_2$	*	
Chabazite	$(Ca,K_2,Na_2)_2[Al_2Si_4O_{12}]_2 \cdot 12H_2O$	*	
Zeolite	Variable		*

XRD Results-R004368

General Information

Measurement date:	10/3/2023	Interpretative date:	13/6/2023
Job Number/Client:	LJN2023-031	XRD	Rigaku Miniflex 600
Registration Number:	R004368	Analyst:	LUnwin
Quantitative Method:	Mineralogy Only	Process Medium:	Wholerock
Sample Holder:	Standard	Speed (deg/min):	0.5
Comment:	Shifted -0.1, 550°C heat treatment, HCl leach		

Analysis Results

Phase name	Formula
Clinopyroxene*	Variable
Analcime	$NaAl(Si_2O_6) \cdot (H_2O)$
Nepheline	$Na_3K(Al_4Si_4O_{16})$
Plagioclase*	$(Na,Ca)(Al,Si)_4O_8$
Magnetite	$Fe^{2+}Fe^{3+}_2O_4$
Olivine*	$Mg_2(SiO_4)$
Fluorapatite	$Ca_5(PO_4)_3F$
Chlorite*	$(Fe,Mg,Al)_6(Si,Al)_4O_{10}(OH)_8$
Philipsite	Variable

Notes
Peak overlap may interfere with identifications and quantitative calculations.
Amorphous minerals and minerals present in trace amounts may not be detected.
Clinopyroxene* probably Augite
Plagioclase*   probably Albite
Olivine*   possibly Forsterite
Chlorite*   probably Chamosite 7.1Å removed by HCl leach and 550°C heat treatment

Phase Data Pattern
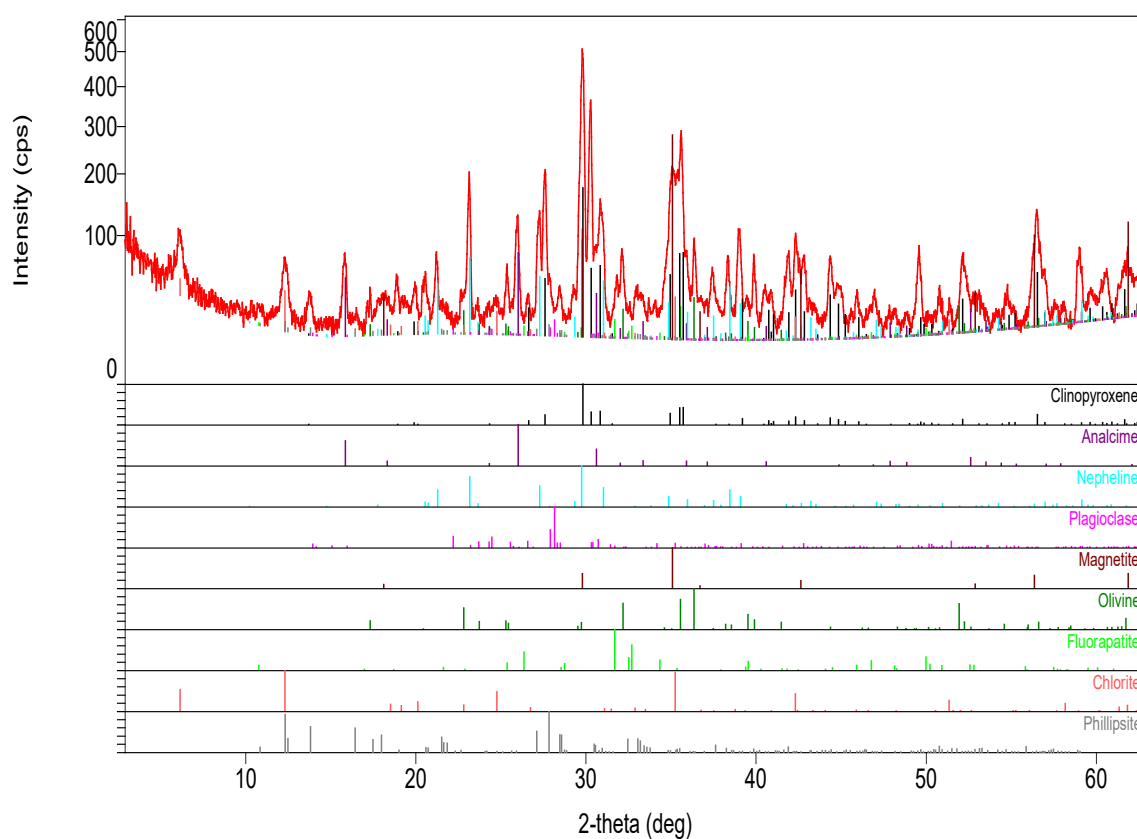
Phase Data Pattern: Blue- HCl leach, Red – raw data
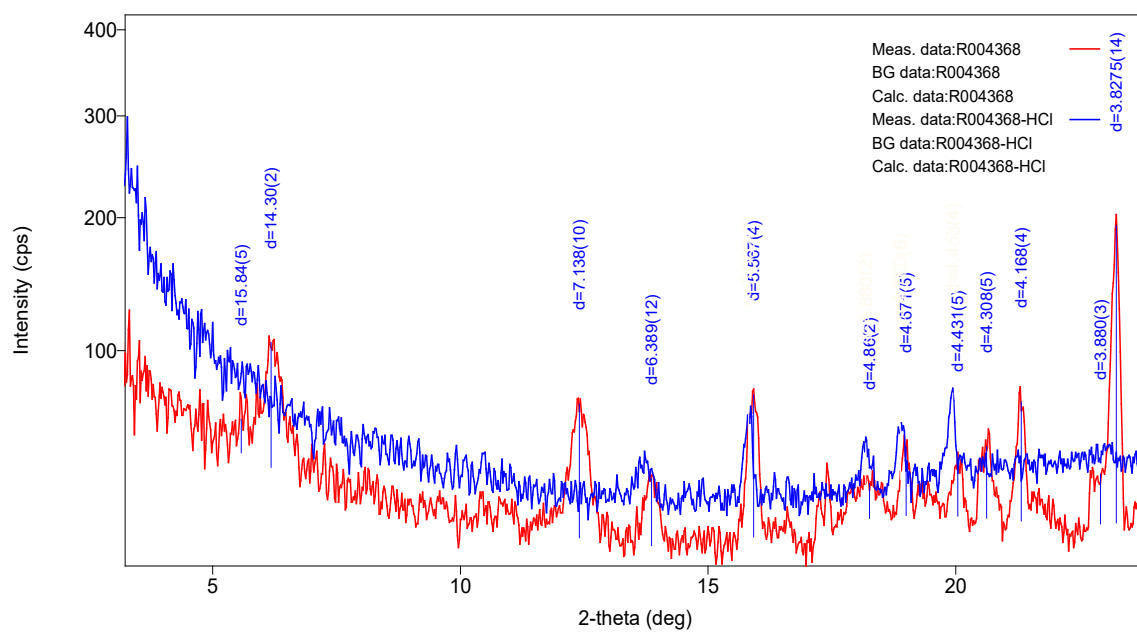
Phase Data Pattern: Blue- 550°C, Red – raw data
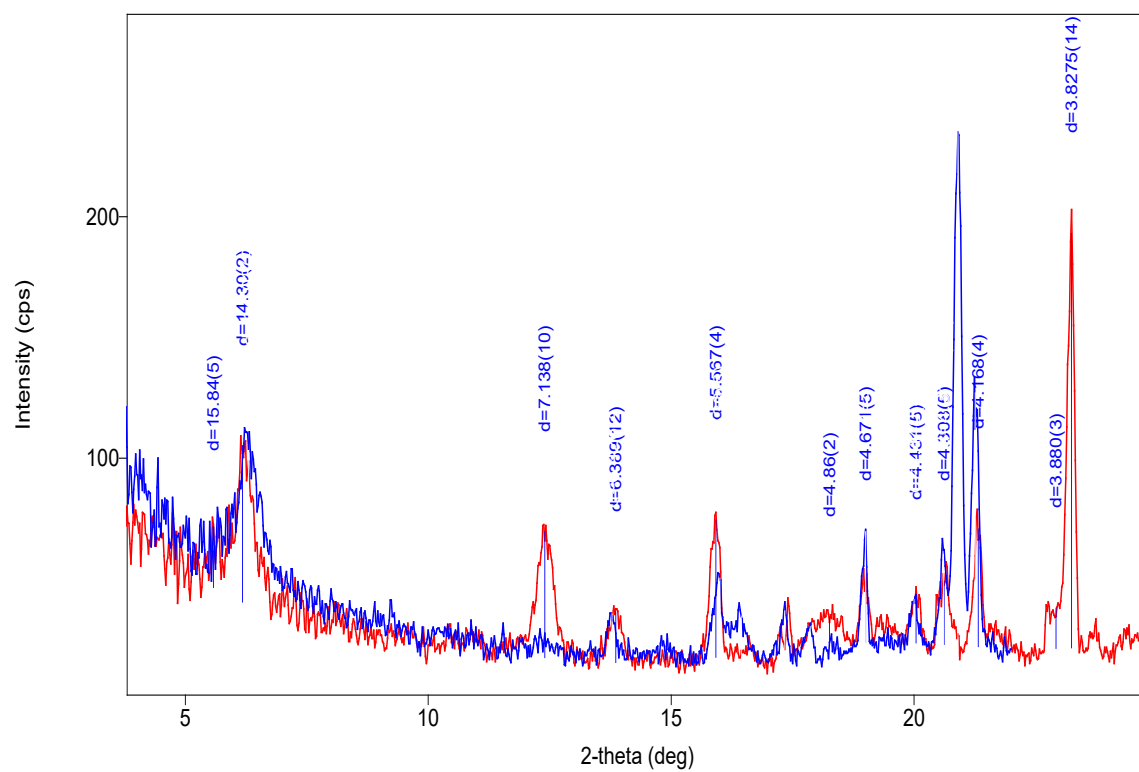
XRD Results-R010202

General Information

Measurement date:	10/3/2023	**Interpretative date:**	21/4/2023
Job Number/Client:	LJN2023-031	**XRD**	Rigaku Miniflex 600
Registration Number:	R010202	**Analyst:**	LUnwin
Quantitative Method:	Mineralogy Only	**Process Medium:**	Wholerock
Sample Holder:	Standard	**Speed (deg/min):**	0.5
Comment:	Shifted -0.1, HCl leach		

Analysis Results

Phase name	Formula
Clinopyroxene*	Variable
Nepheline*	$Na_3K(Al_4Si_4O_{16})$
Plagioclase*	$(Na,Ca)(Al,Si)_4O_8$
Magnetite	$Fe^{2+}Fe^{3+}_2O_4$
Olivine*	$Mg_2(SiO_4)$
Fluorapatite	$Ca_5(PO_4)_3F$

Notes

Peak overlap may interfere with identifications and quantitative calculations.
Amorphous minerals and minerals present in trace amounts may not be detected.
Clinopyroxene* probably Augite
Olivine*   possibly Forsterite
Nepheline*   removed by HCl leach
Plagioclase*   probably Albite
K-feldspar   not detected by XRD but miniscule 3.8Å peak remaining after HCl leach

Phase Data Pattern

*DB pattern is displayed.
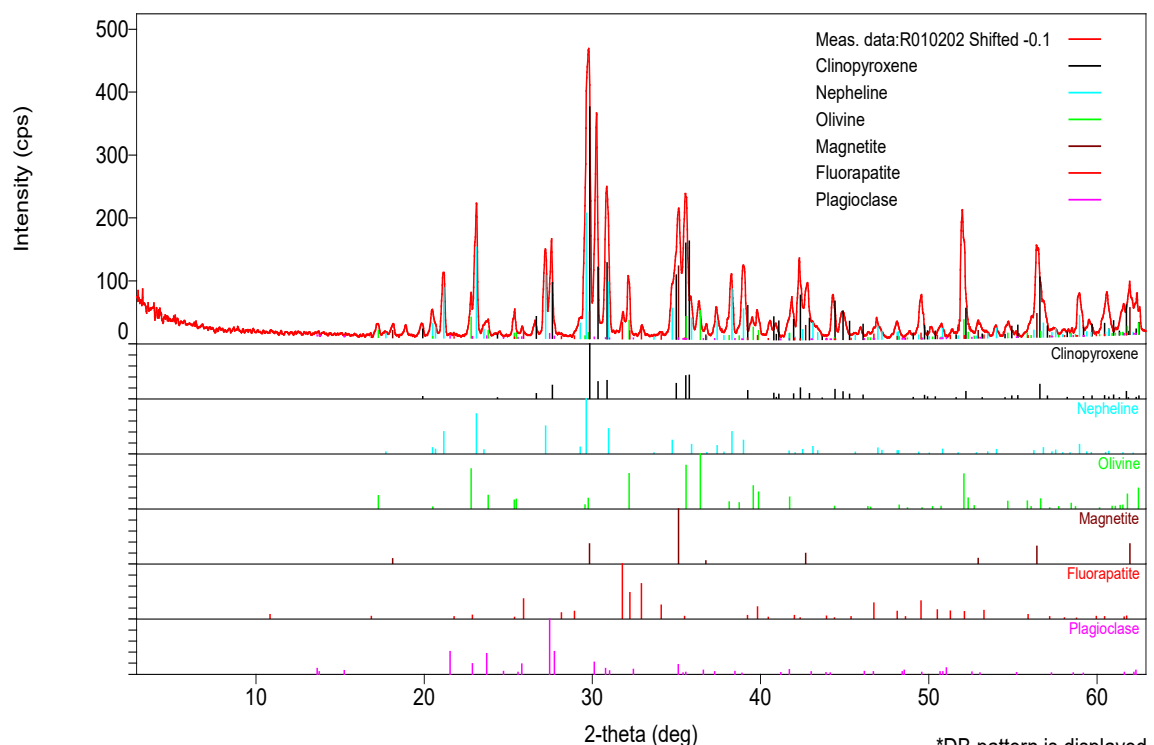
Phase Data Pattern: Blue –HCl leach, Red – raw data
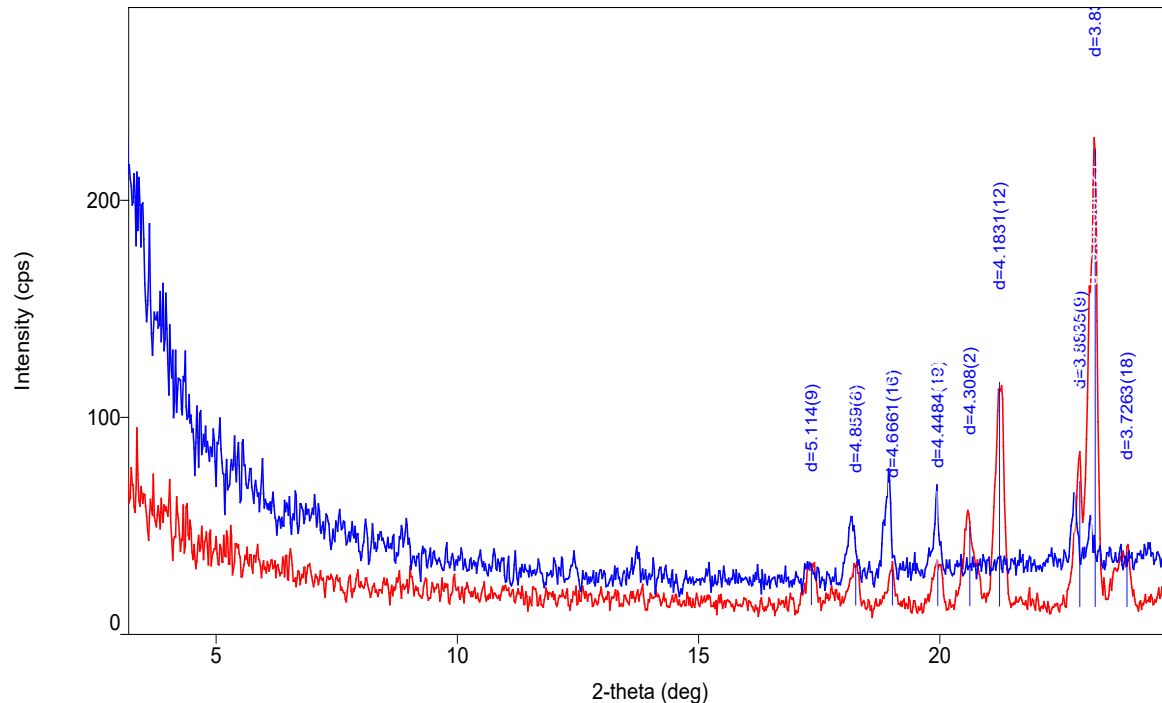
XRD Results-R010218

General Information

Measurement date:	10/3/2023	**Interpretative date:**	16/5/2023
Job Number/Client:	LJN2023-031	**XRD**	Rigaku Miniflex 600
Registration Number:	R010218	**Analyst:**	LUnwin
Quantitative Method:	Mineralogy Only	**Process Medium:**	Wholerock
Sample Holder:	Standard	**Speed (deg/min):**	0.5
Comment:	Shifted -0.07, HCl leach, 105°C and 550°C heat treatments		

Analysis Results

Phase name	Formula
Clinopyroxene*	Variable
Nepheline	$Na_3K(Al_4Si_4O_{16})$
Plagioclase*	$(Na,Ca)(Al,Si)_4O_8$
Magnetite	$Fe^{2+}Fe^{3+}_2O_4$
Olivine*	$(Mg_2(SiO_4)$
Fluorapatite	$Ca_5(PO_4)_3(Cl/F/OH)$
Chlorite*	$(Fe,Mg,Al)_6(Si,Al)_4O_{10}(OH)_8$
Melilite	$Ca_2(Al,Mg,Fe)((Al,Si,B)SiO_7)$
Mesolite*	$Na_2Ca_2Al_6Si_9O_{30} \cdot 8(H_2O)$

Notes
Peak overlap may interfere with identifications and quantitative calculations.
Amorphous minerals and minerals present in trace amounts may not be detected.
Clinopyroxene* probably Augite
Plagioclase* probably Albite
Olivine* possibly Forsterite
Nepheline* removed by HCl leach
Mesolite* removed by HCl leach
Chlorite* possibly Chamosite, removed by HCl leach
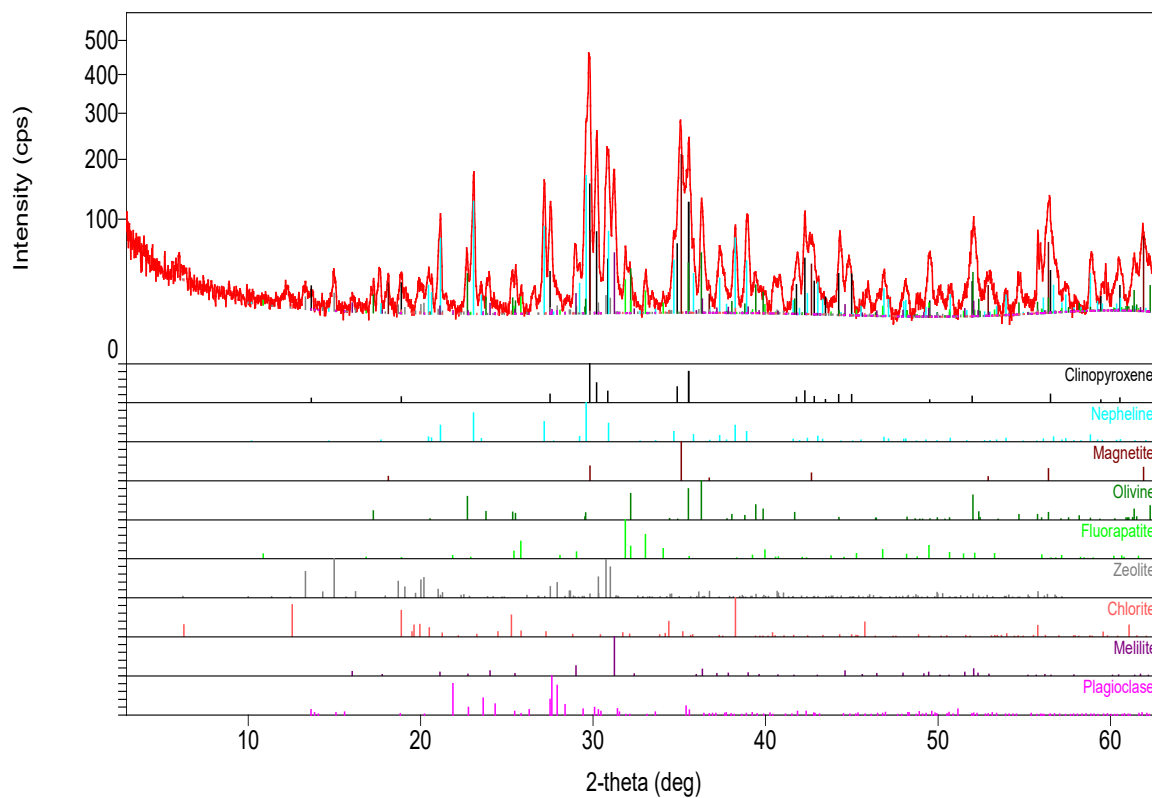
Phase Data Pattern

Phase Data Pattern: Blue- 550°C, Red – raw data
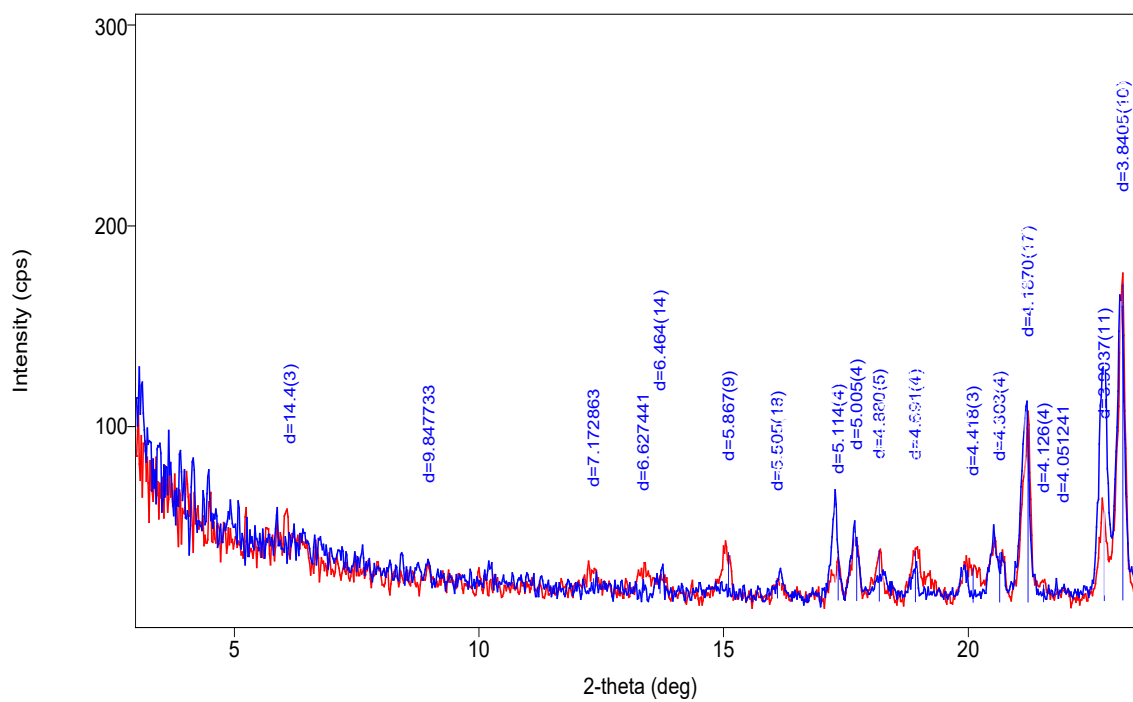
Phase Data Pattern Blue – 105°C treatment, Red - raw data
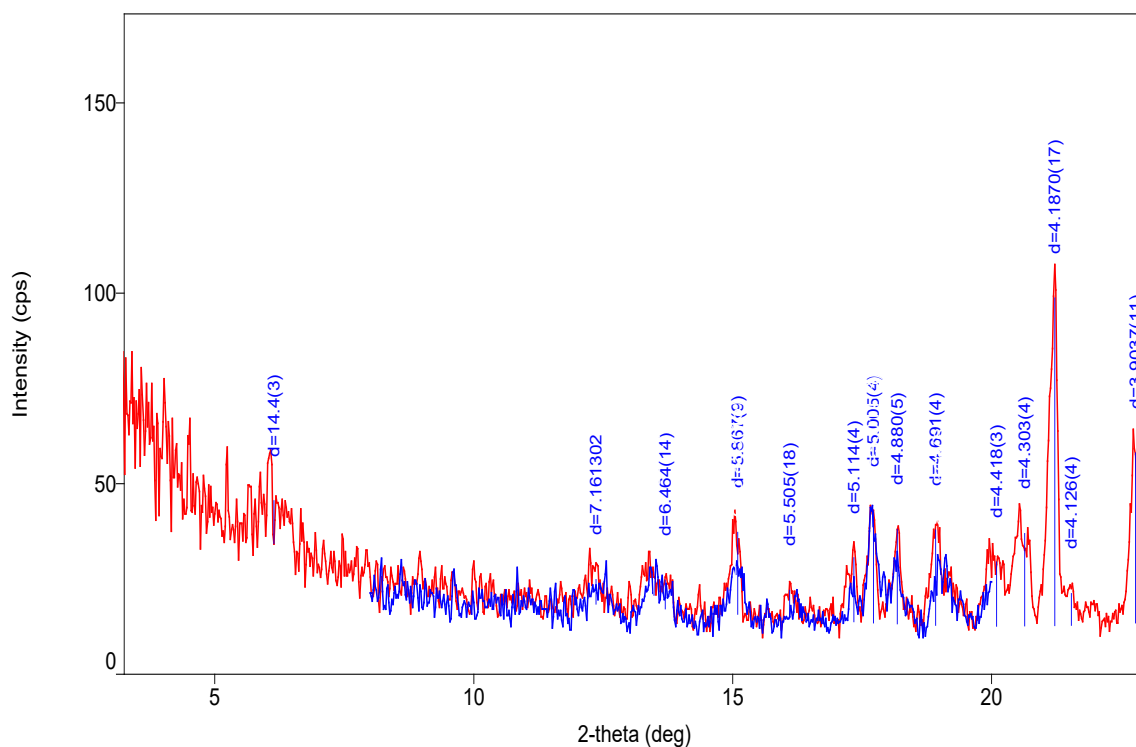
Phase Data Pattern Blue – HCl leach, Red - raw data
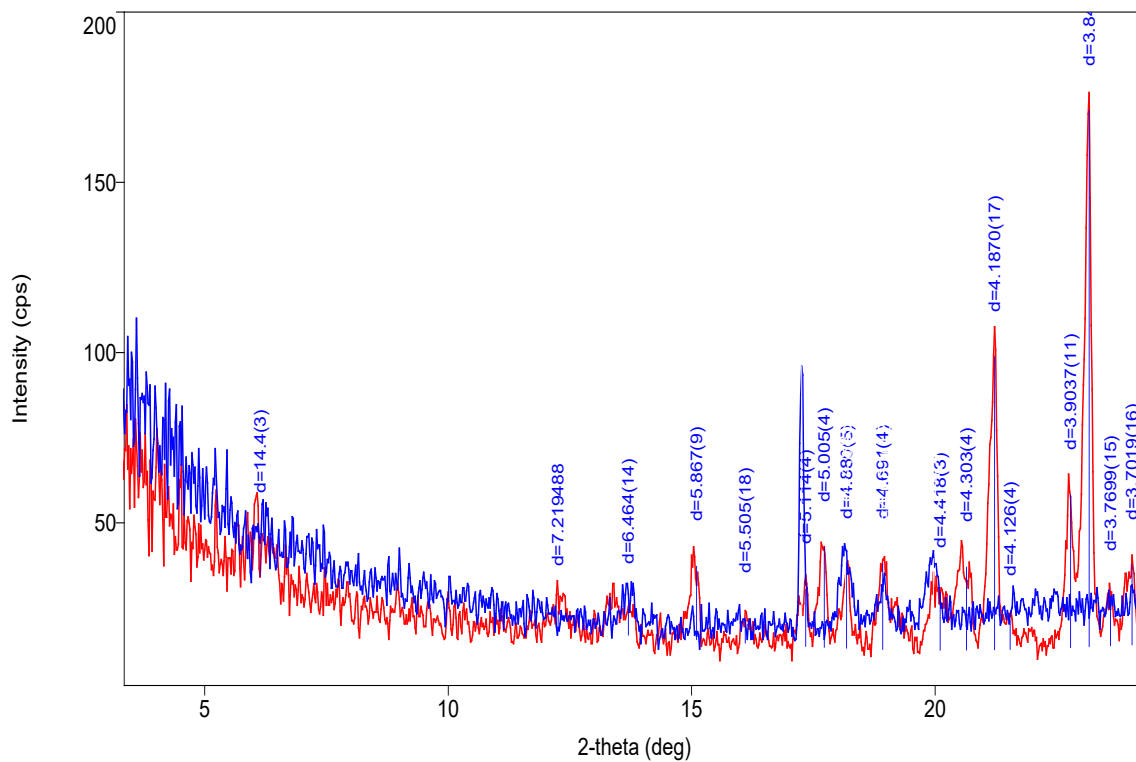
XRD Results-R010201

General Information

Measurement date:	17/3/2023	**Interpretative date:**	16/5/2023
Job Number/Client:	LJN2023-031	**XRD**	Rigaku Miniflex 600
Registration Number:	R010201	**Analyst:**	LUnwin
Quantitative Method:	Mineralogy Only	**Process Medium:**	Wholerock
Sample Holder:	Standard	**Speed (deg/min):**	0.5
Comment:	Shifted -0.01, HCl leach, 500°C heat treatment		

Analysis Results

Phase name	Formula
Clinopyroxene*	Variable
Mesolite*	$Na_2Ca_2Al_6Si_9O_{30} \cdot 8(H_2O)$
Nepheline	$Na_3K(Al_4Si_4O_{16})$
Chlorite*	$(Fe,Mg,Al)_6(Si,Al)_4O_{10}(OH)_8$
Plagioclase*	$(Na,Ca)(Al,Si)_4O_8$
Magnetite	$Fe^{2+}Fe^{3+}_2O_4$
Olivine*	$Mg_2(SiO_4)$
Anorthoclase	$(Na,K)AlSi_3O_8$
Smectite*	Variable
Fluorapatite	$Ca_5(PO_4)_3F$

Notes
Peak overlap may interfere with identifications and quantitative calculations.
Amorphous minerals and minerals present in trace amounts may not be detected.
Clinopyroxene* probably Diopside
Olivine*   possibly Forsterite
Mesolite*   removed by HCl leach and 500°C heat treatment
Anorthoclase   3.8Å not removed by HCl leach
Nepheline*   removed by HCl leach
Chlorite*   possibly Chamosite, removed by HCl leach and 500°C treatments
Smectite*   reduced by HCl leach

Phase Data Pattern
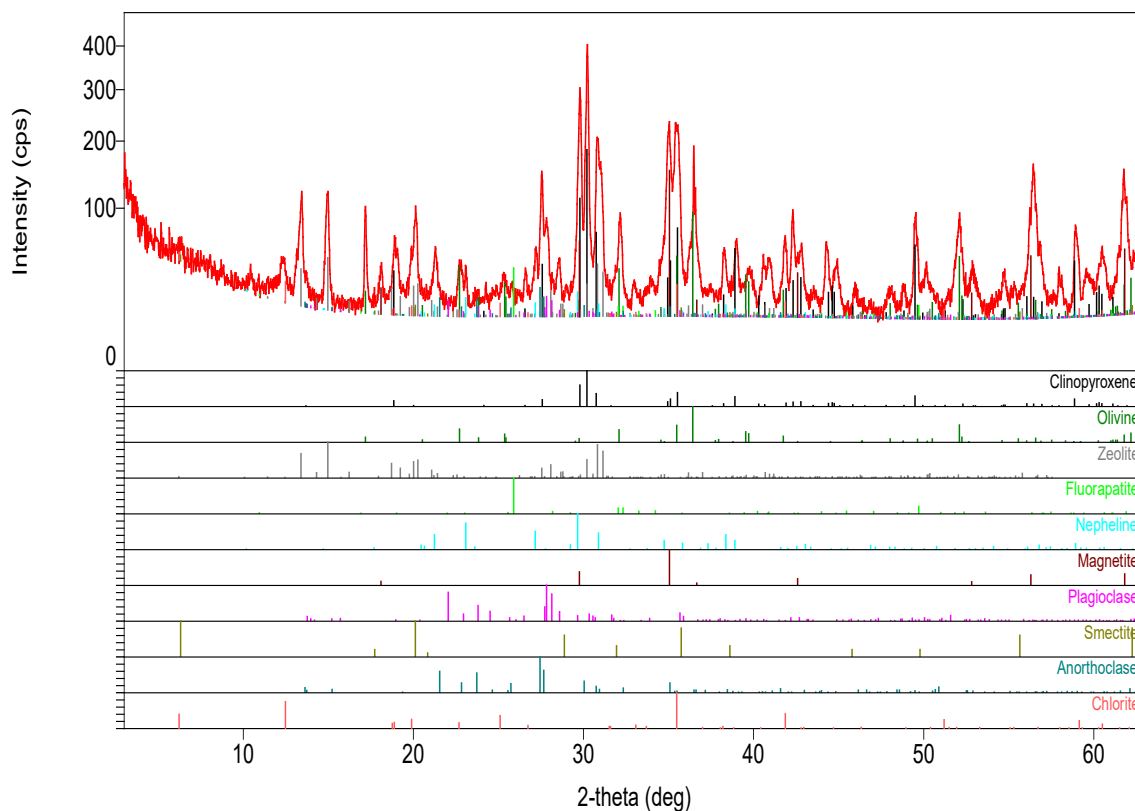
Phase Data Pattern: Blue –500°C, Red – raw data
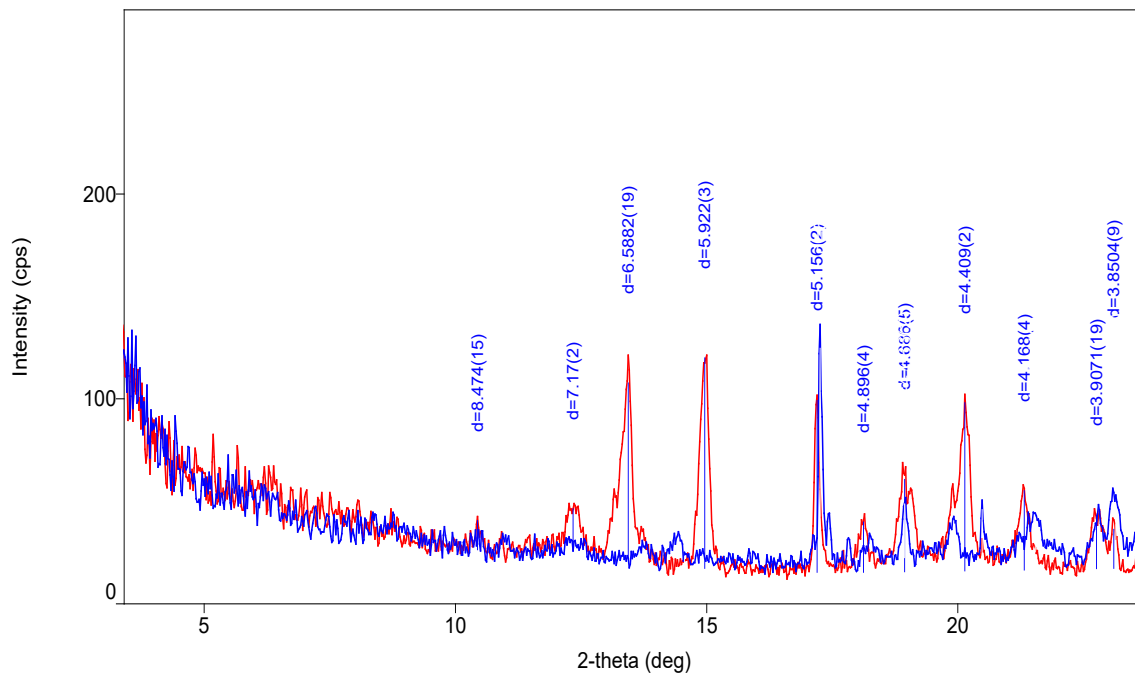
Phase Data Pattern: Blue –HCl leach, (qtz added), Red – raw data
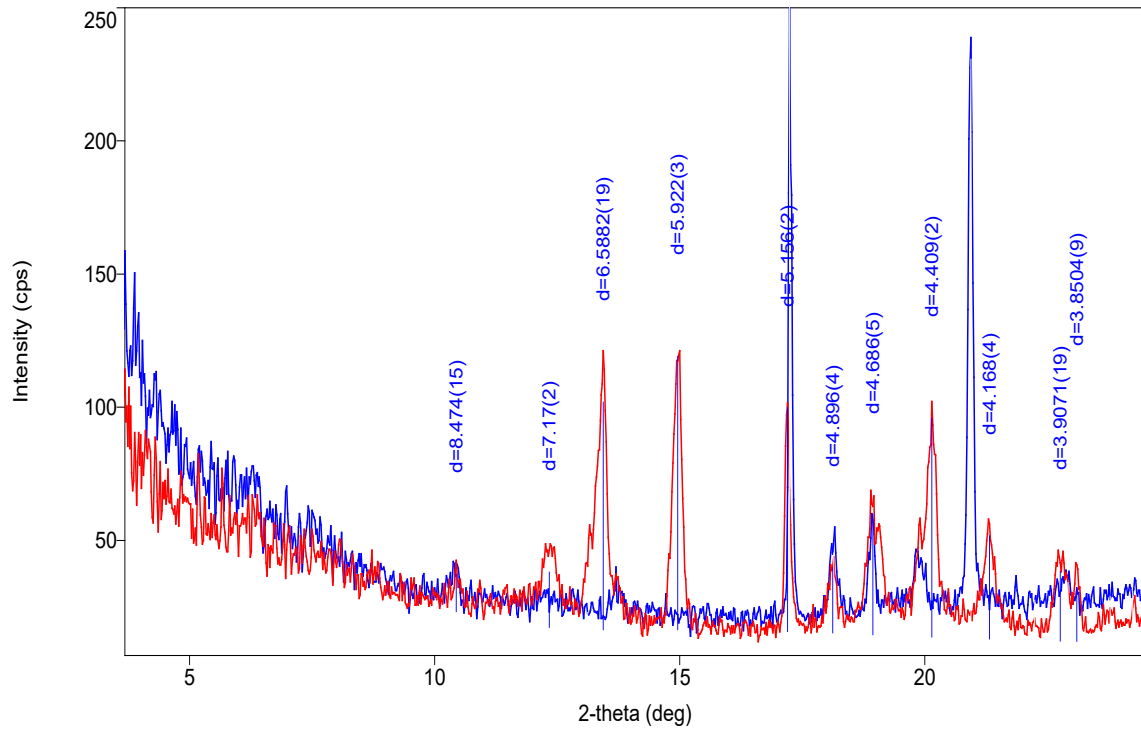
XRD Results-R010205

General Information

Measurement date:	17/3/2023	**Interpretative date:**	18/4//2023
Job Number/Client:	LJN2023-031	**XRD**	Rigaku Miniflex 600
Registration Number:	R010205	**Analyst:**	LUnwin
Quantitative Method:	Mineralogy Only	**Process Medium:**	Wholerock
Sample Holder:	Standard	**Speed (deg/min):**	0.5
Comment:	Shifted -0.01, 105°C heat treatment		

Analysis Results

Phase name	Formula
Clinopyroxene*	$(Ca,Na)(Mg,Fe,Al)Si_2O_6$
Analcime	$NaAl(Si_2O_6) \cdot (H_2O)$
Nepheline	$Na_3K(Al_4Si_4O_{16})$
Plagioclase*	$NaAlSi_3O_8$
Magnetite	$Fe^{2+}Fe^{3+}_2O_4$
Olivine*	$Mg_2(SiO_4)$
Amphibole*	Variable
Mica*	$KAl_2(AlSi_3O_{10})(OH)_2$
Fluorapatite	$Ca_5(PO_4)_3(Cl/F/OH)$

Notes
Peak overlap may interfere with identifications and quantitative calculations.
Amorphous minerals and minerals present in trace amounts may not be detected.
Clinopyroxene* probably Augite
Olivine*   possibly Forsterite
Amphibole*   possibly Hastingsite
Mica*   10Å peak unaffected by 105°C heat treatment

Phase Data Pattern
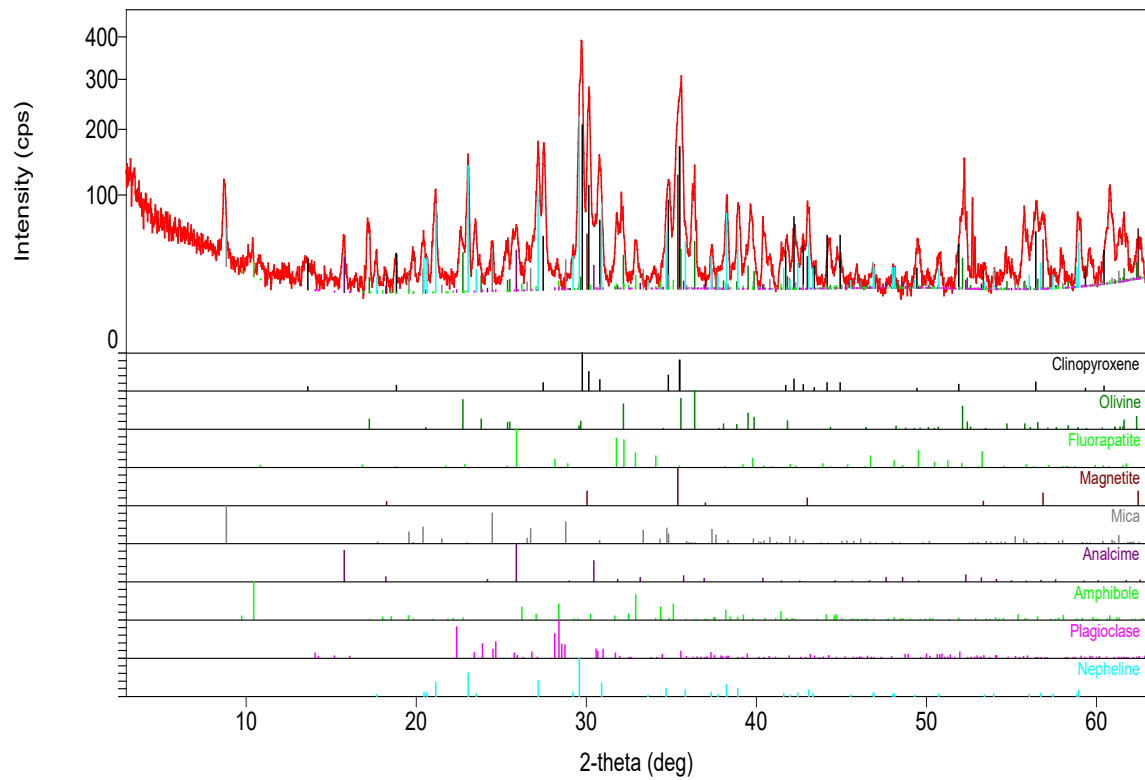
Phase Data Pattern: Blue – heated to 105°C, Red – raw data
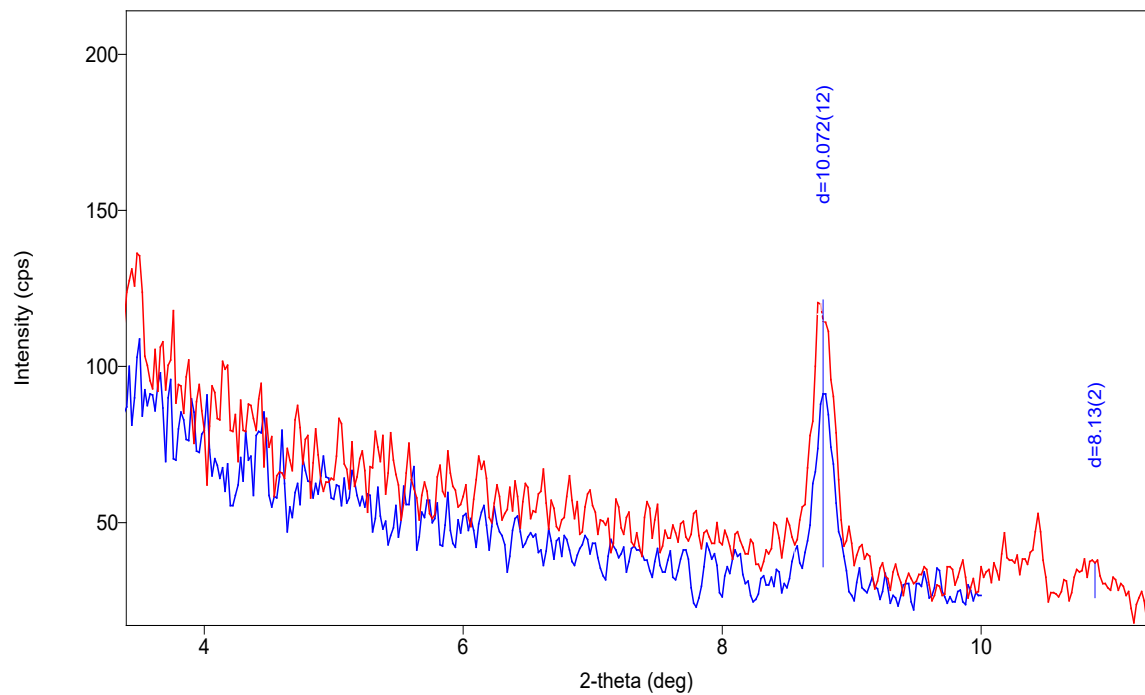
XRD Results-R005353

General Information

Measurement date:	21/3/2023	**Interpretative date:**	18/4/2023
Job Number/Client:	LJN2023-031	**XRD**	Rigaku Miniflex 600
Registration Number:	R005353	**Analyst:**	LUnwin
Quantitative Method:	Mineralogy Only	**Process Medium:**	Wholerock
Sample Holder:	Standard	**Speed (deg/min):**	0.5
Comment:	Shifted 0.01, HCl leach treatment		

Analysis Results

Phase name	Formula
Clinopyroxene*	Variable
Nepheline*	$Na_3K(Al_4Si_4O_{16})$
Magnetite	$Fe^{2+}Fe^{3+}_2O_4$
Olivine*	$Mg_2(SiO_4)$
Stilbite*	$NaCa_4[Al_9Si_{27}O_{72}] \cdot nH_2O$
Smectite*	Variable
Fluorapatite	$Ca_5(PO_4)_3F$

Notes
Peak overlap may interfere with identifications and quantitative calculations.
Amorphous minerals and minerals present in trace amounts may not be detected.
Smectite*   probably Mixed-Layer
Clinopyroxene* probably Augite
Olivine*   possibly Forsterite
Stilbite*   removed by HCl leach
Nepheline*   removed by HCl leach
Smectite*   removed by HCl leach
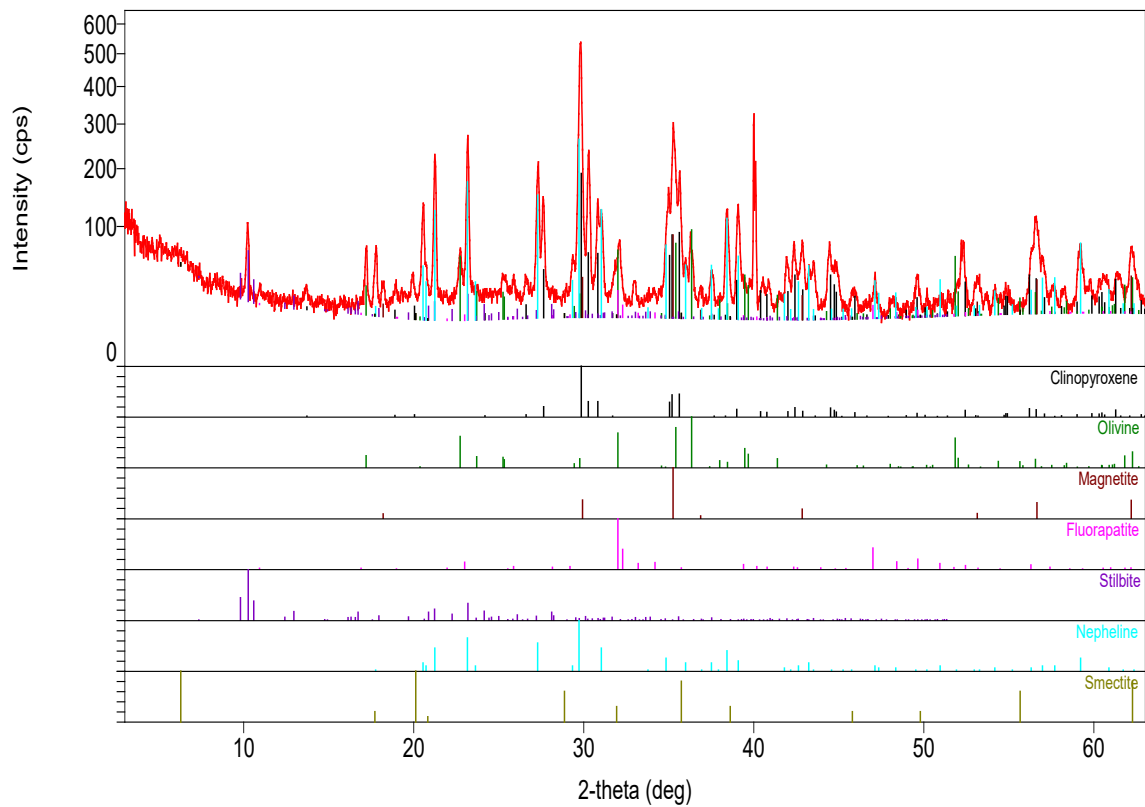
Phase Data Pattern

Phase Data Pattern: Blue – HCl leach, Red – raw data
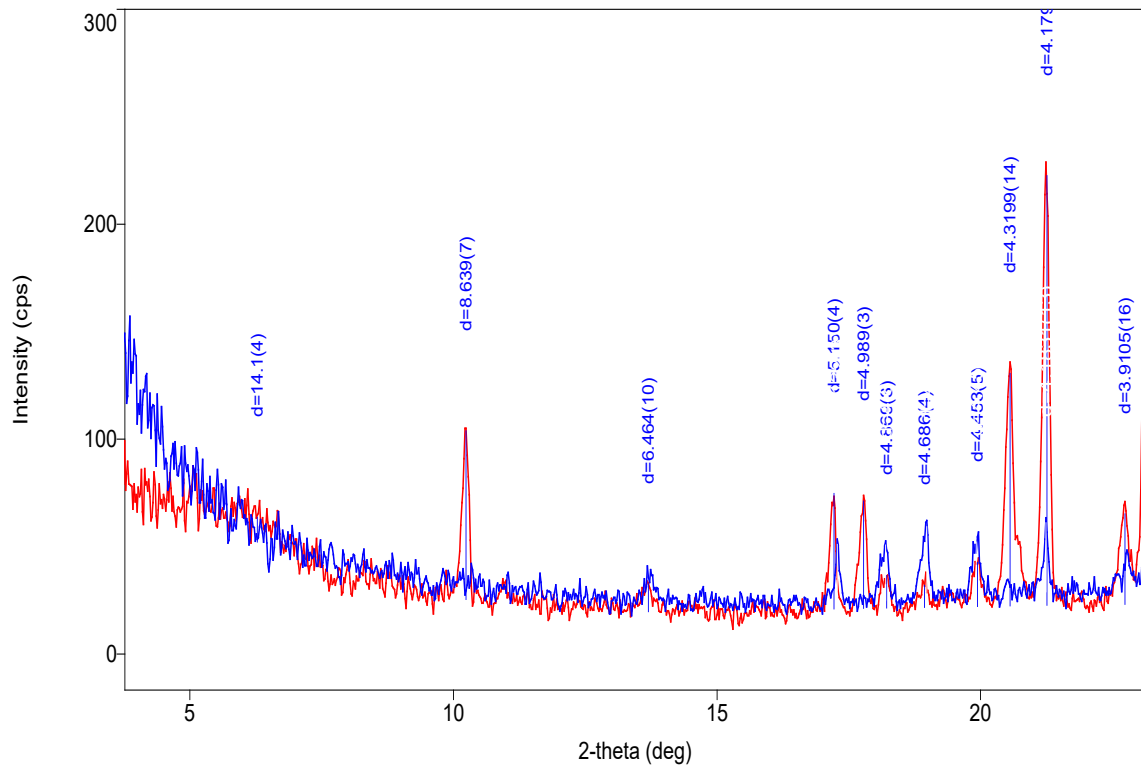
XRD Results-R004366

General Information

Measurement date:	21/3/2023	Interpretative date:	18/4/2023
Job Number/Client:	LJN2023-031	XRD	Rigaku Miniflex 600
Registration Number:	R004366	Analyst:	LUnwin
Quantitative Method:	Mineralogy Only	Process Medium:	Wholerock
Sample Holder:	Standard	Speed (deg/min):	0.5
Comment:	Shifted -0.09, HCl leach and 550°C heat treatments, checked for magnetic properties		

Analysis Results.

Phase name	Formula
Clinopyroxene*	Variable
Chabazite*	$(Ca,K_2,Na_2)_2[Al_2Si_4O_{12}]_2 \cdot 12H_2O$
Analcime	$NaAl(Si_2O_6) \cdot (H_2O)$
Nepheline*	$Na_3K(Al_4Si_4O_{16})$
Plagioclase	$(Na,Ca)(Al,Si)_4O_8$
Magnetite	$Fe^{2+}Fe^{3+}_2O_4$
Chlorite*	$(Fe,Mg,Al)_6(Si,Al)_4O_{10}(OH)_8$
Olivine*	$Mg_2(SiO_4)$
Smectite*	Various
Mica	$KAl_2(AlSi_3O_{10})(OH)_2$
Anorthoclase*	$(Na,K)AlSi_3O_8$
Fluorapatite	$Ca_5(PO_4)_3F$

Notes

Peak overlap may interfere with identifications and quantitative calculations.
Amorphous minerals and minerals present in trace amounts may not be detected.
Clinopyroxene*   probably Augite
Olivine*   possibly Forsterite
Chabazite*   removed by HCl leach
Anorthoclase*   3.8Å not removed HCl leach
Chlorite*   possibly Chamosite, removed by HCl leach
Nepheline*   removed by HCl leach
Smectite*   possibly Tri-octahedral, 15Å shifted to the right by 550°C treatment, removed by HCl leach

Phase Data Pattern

Phase Data Pattern: Blue – HCl leach, Red – raw data
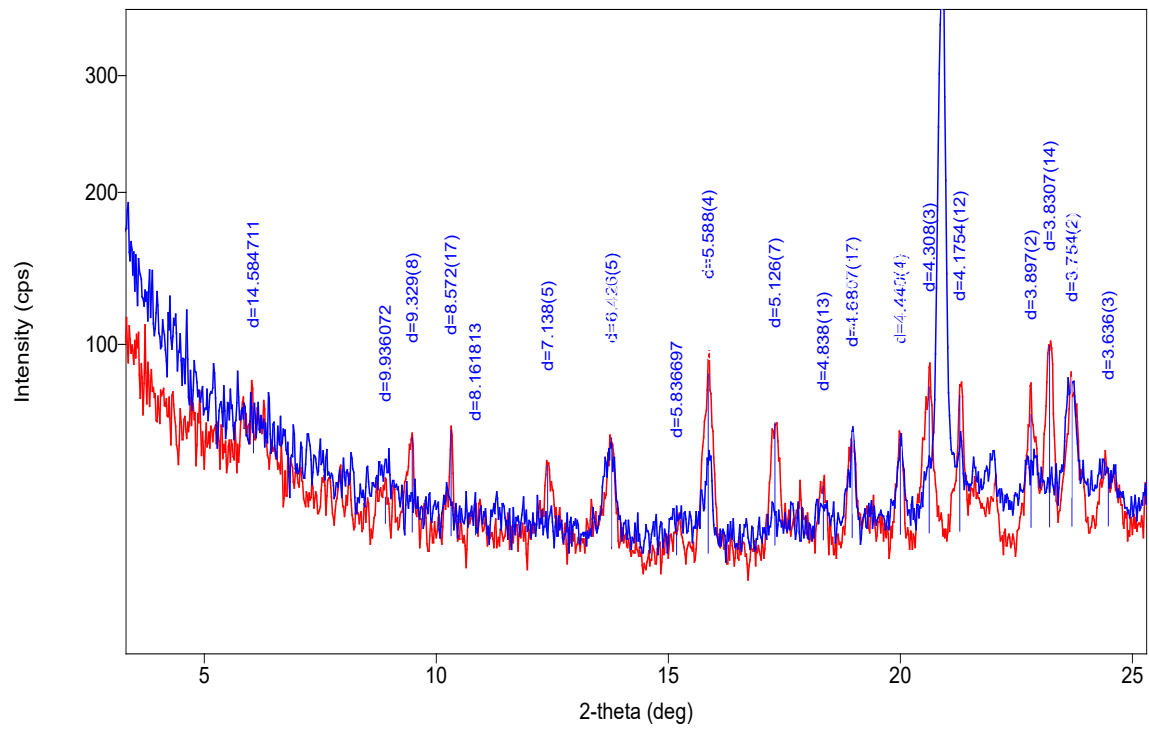
Phase Data Pattern: Blue – 550°C, Red – raw data
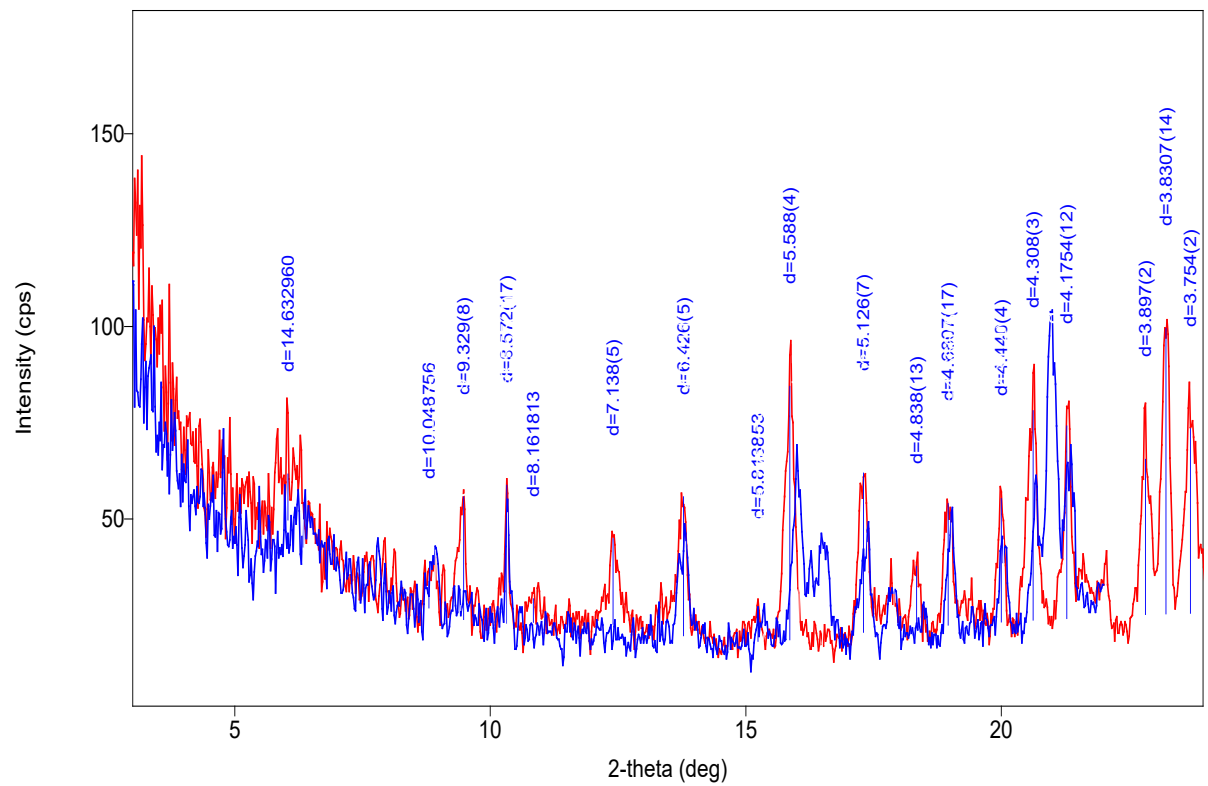
XRD Results-R010187

General Information

Measurement date:	22/3/2023	**Interpretative date:**	23/4/2023
Job Number/Client:	LJN2023-031	**XRD**	Rigaku Miniflex 600
Registration Number:	R010187	**Analyst:**	LUnwin
Quantitative Method:	Mineralogy Only	**Process Medium:**	Wholerock
Sample Holder:	Standard	**Speed (deg/min):**	0.5
Comment:	Shifted -0.01, HCl leach, 580°C and 400°C heat treatments, Glycolation		

Analysis Results

Phase name	Formula
Clinopyroxene*	Variable
Analcime	$NaAl(Si_2O_6) \cdot (H_2O)$
Nepheline	$Na_3K(Al_4Si_4O_{16})$
Plagioclase	$(Na,Ca)(Al,Si)_4O_8$
Magnetite	$Fe^{2+}Fe^{3+}_2O_4$
Olivine*	$Mg_2(SiO_4)$
Fluorapatite	$Ca_5(PO_4)_3F$
Spinel Group	Variable
Anorthoclase*	$(Na,K)AlSi_3O_8$
Serpentine*	$Mg_3Si_2O_5(OH)_4$
Smectite*	Various
Chlorite*	$(Fe,Mg,Al)_6(Si,Al)_4O_{10}(OH)_8$

Notes

Peak overlap may interfere with identifications and quantitative calculations.

Amorphous minerals and minerals present in trace amounts may not be detected.

Clinopyroxene*   probably Augite

Olivine*   possibly Forsterite

Anorthoclase   3.8Å not removed HCl leach

Nepheline*   removed by HCl leach

Smectite*   possibly Beidellite, 14Å unaffected by HCl leach, 400°C and 580°C treatments should collapse to 10Å but shifted slightly to the right with no collapse indicating high Al content

Chlorite*   possibly Chlorite/Serpentine Mix, removed by HCl leach, 7.1Å intensified at 400°C and destroyed at 580°C (Chlorite component) with the 14A peak shifting slightly down

Serpentine*   7A peak is still mostly present @ 580°C, removed by HCl leach
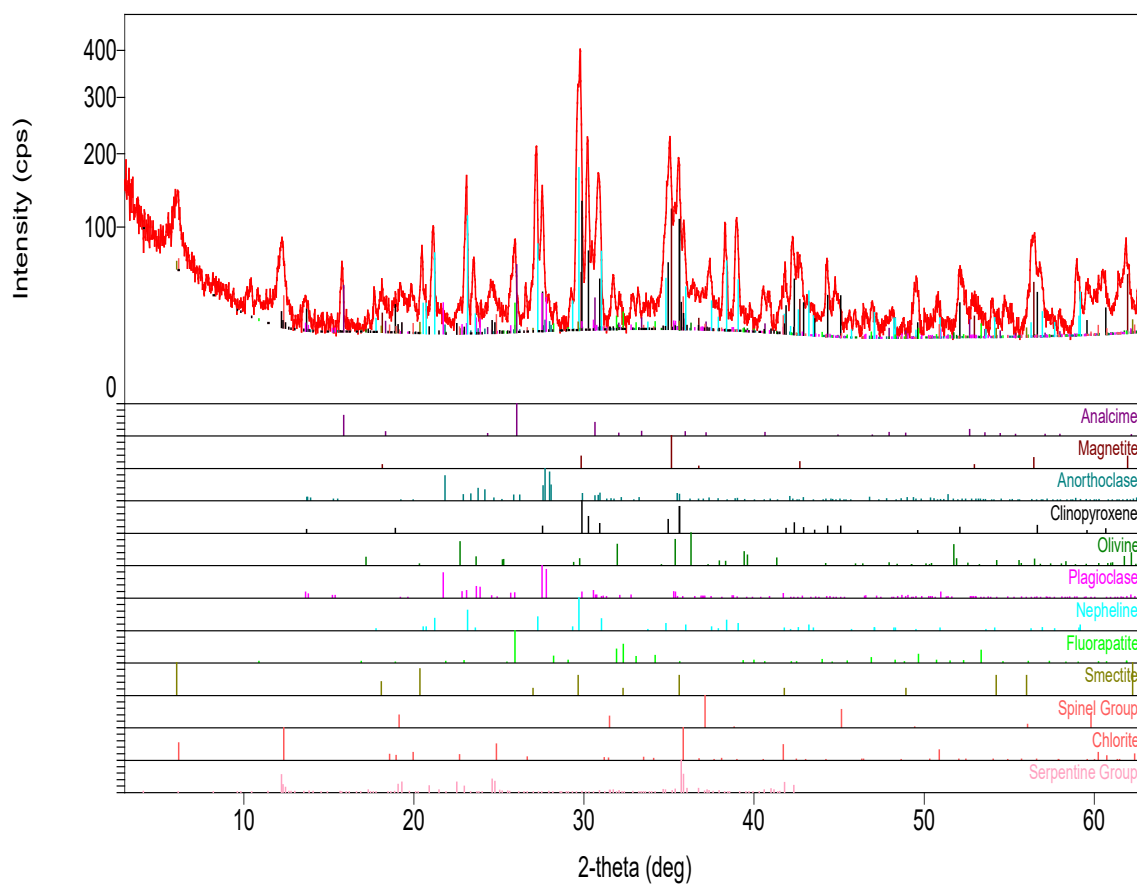
Phase Data Pattern

Phase Data Pattern: Blue – heated to 400°C Red – Raw data
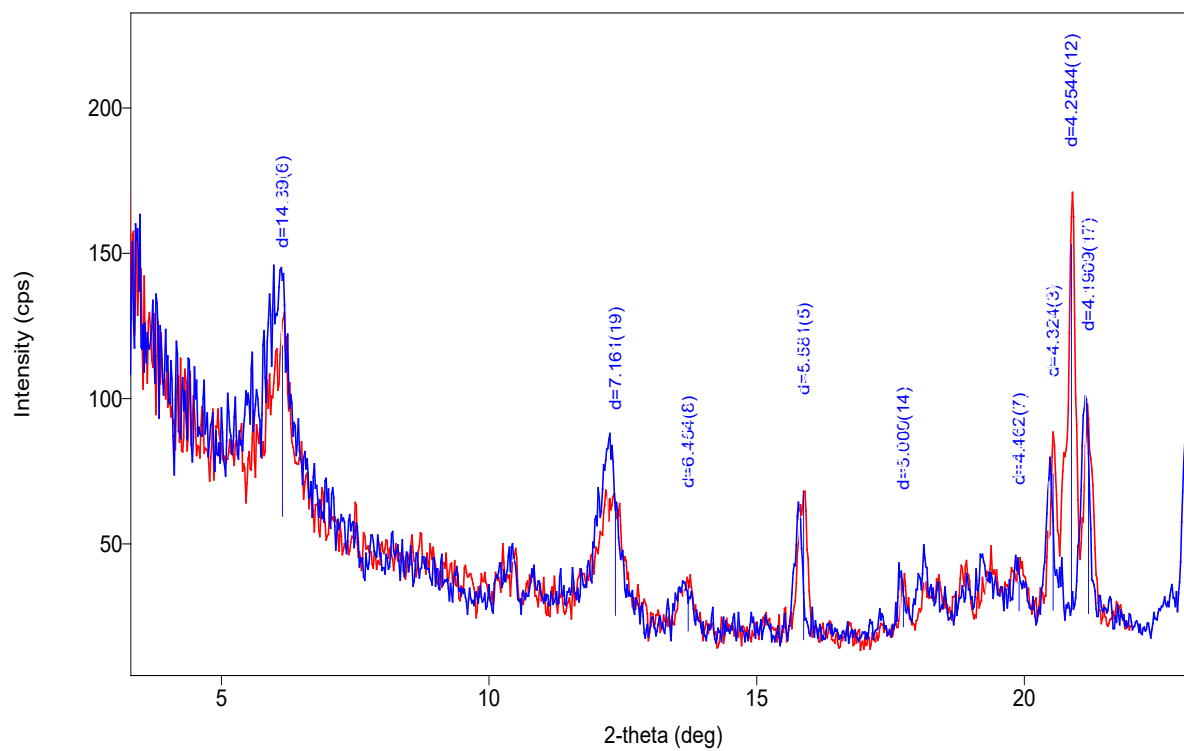
Phase Data Pattern: Blue – heated to 580°C Red – Raw data
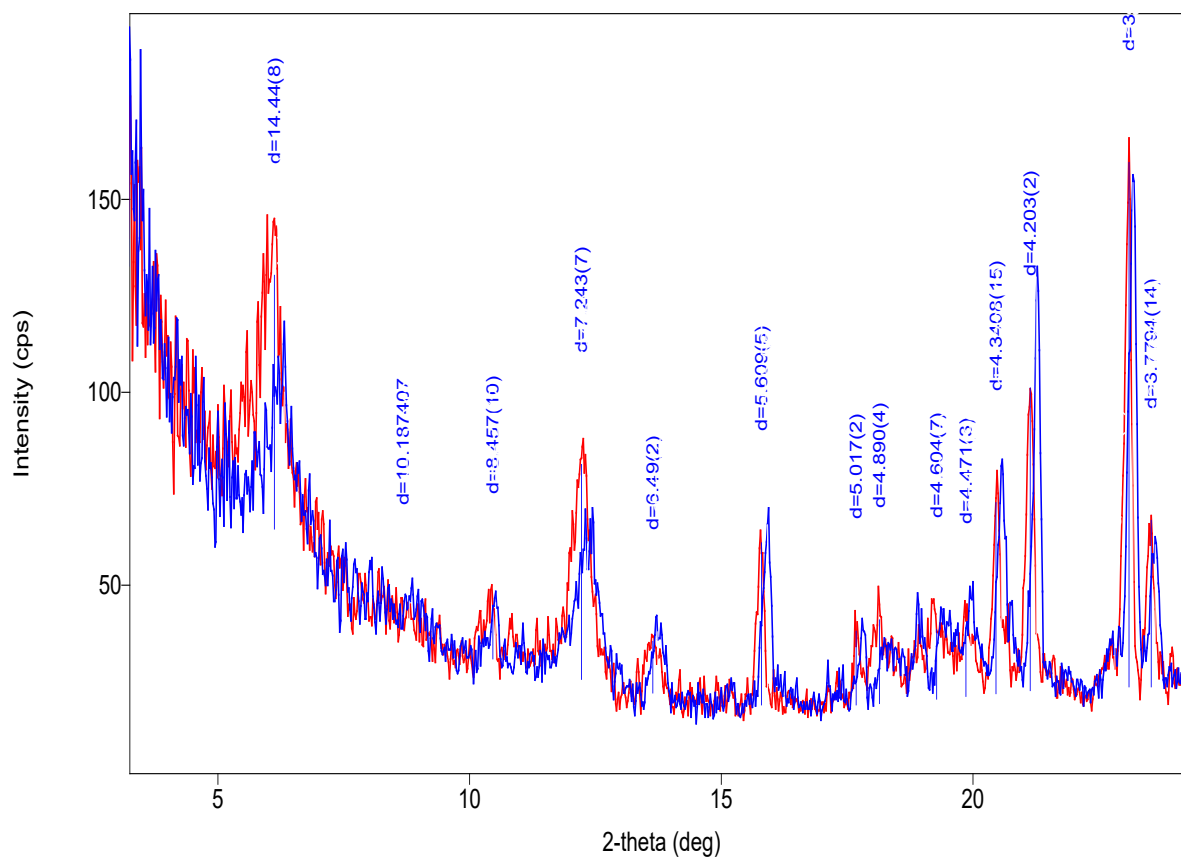
Phase Data Pattern: Blue – HCl leach, Red – Raw data
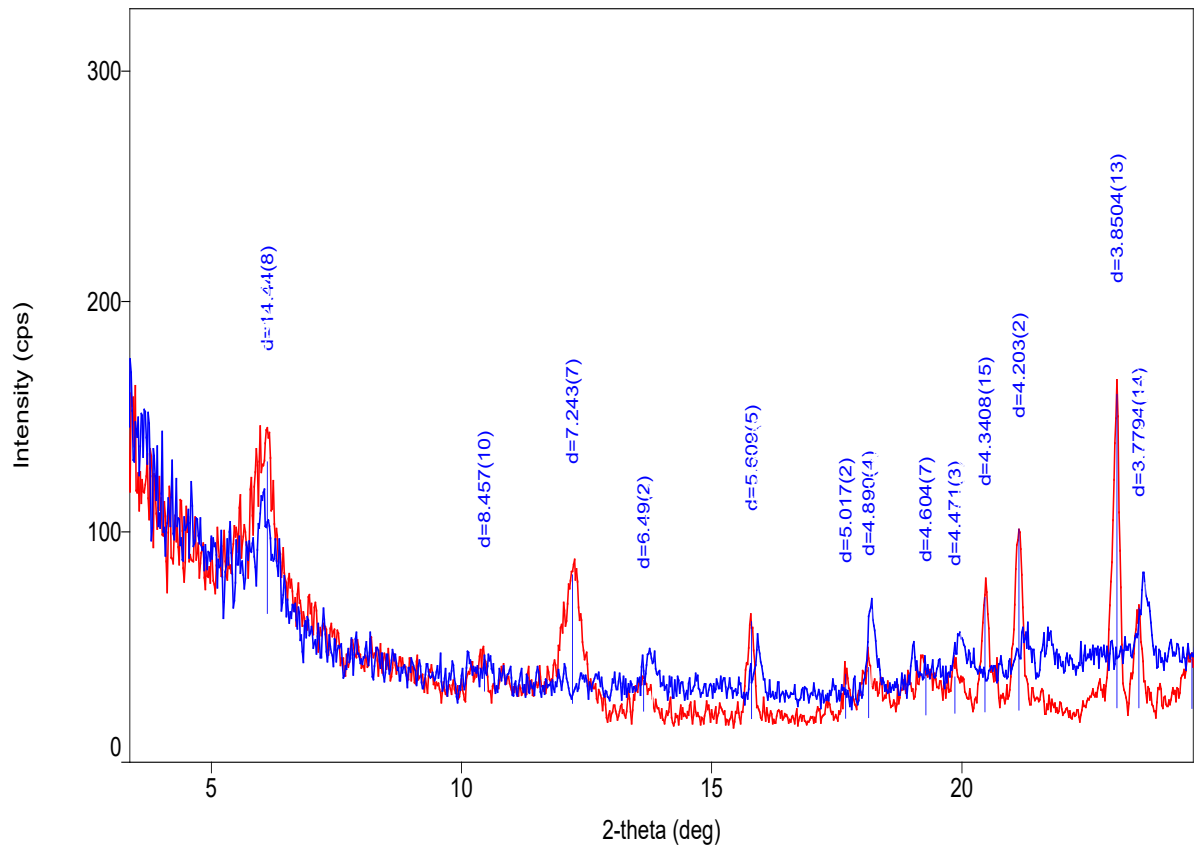
Phase Data Pattern: Blue – Glycolation, Red – Raw data
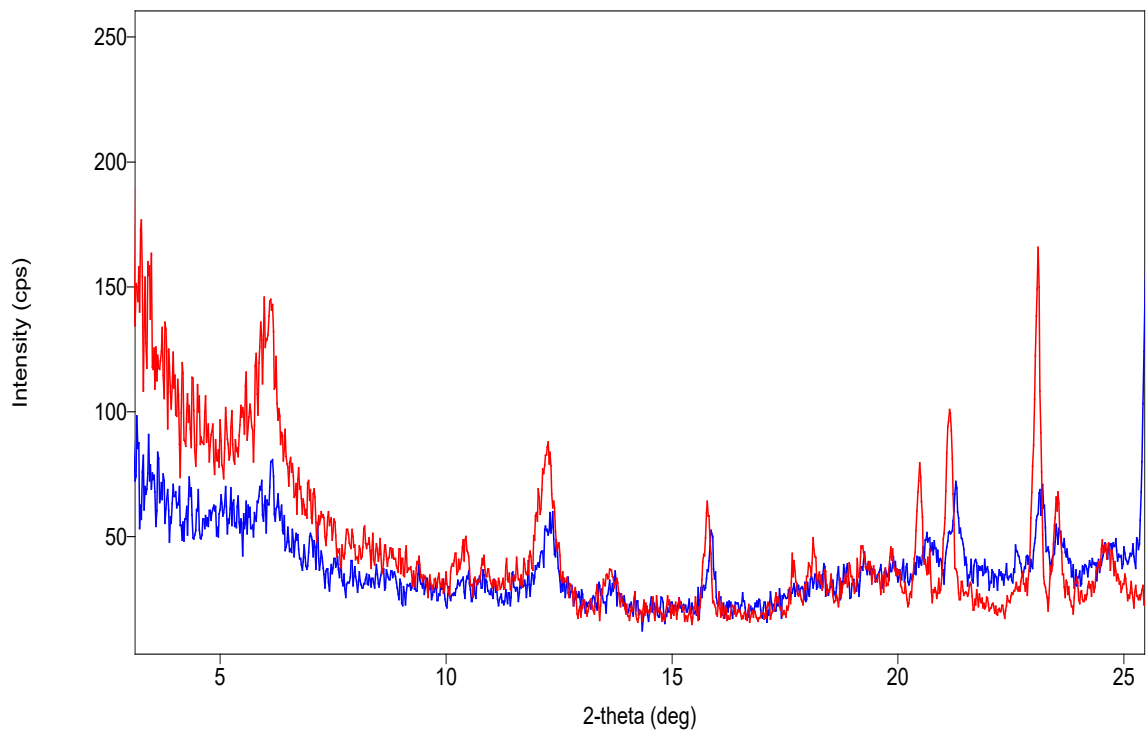
XRD Results-R004332

General Information

Measurement date:	22/3/2023	**Interpretative date:**	21/4/2023
Job Number/Client:	LJN2023-031	**XRD**	Rigaku Miniflex 600
Registration Number:	R004332	**Analyst:**	LUnwin
Quantitative Method:	Mineralogy Only	**Process Medium:**	Wholerock
Sample Holder:	Standard	**Speed (deg/min):**	0.5
Comment:	HCl leach treatment with quartz added for calibration		

Analysis Results

Phase name	Formula
Clinopyroxene*	Variable
Nepheline*	$Na_3K(Al_4Si_4O_{16})$
Magnetite	$Fe^{2+}Fe^{3+}_2O_4$
Olivine*	$Mg_2(SiO_4)$
Analcime	$NaAl(Si_2O_6)\cdot(H_2O)$
Fluorapatite	$Ca_5(PO_4)_3F$

Notes
Peak overlap may interfere with identifications and quantitative calculations.
Amorphous minerals and minerals present in trace amounts may not be detected.
Clinopyroxene* probably Augite
Olivine*   possibly Forsterite
Nepheline*   removed by HCl leach
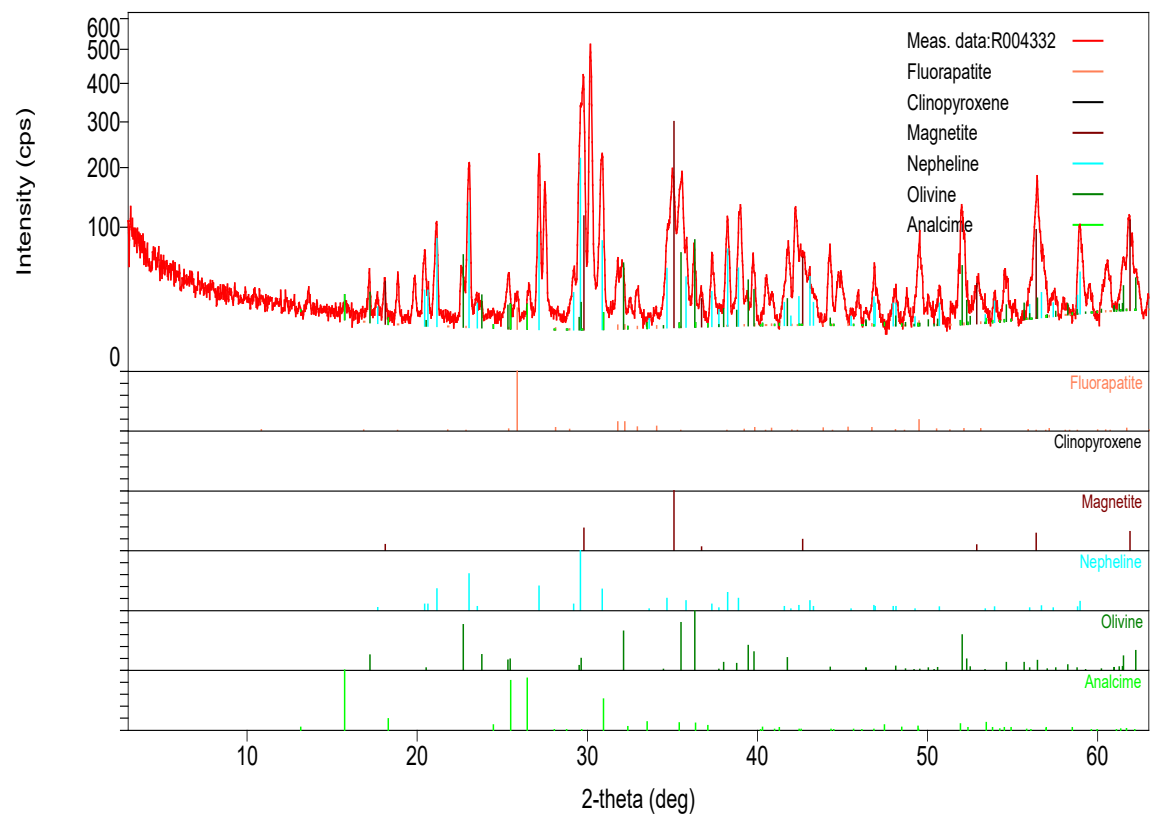
Phase Data Pattern

Phase Data Pattern: Blue – HCl leach (qtz added), Red – raw data
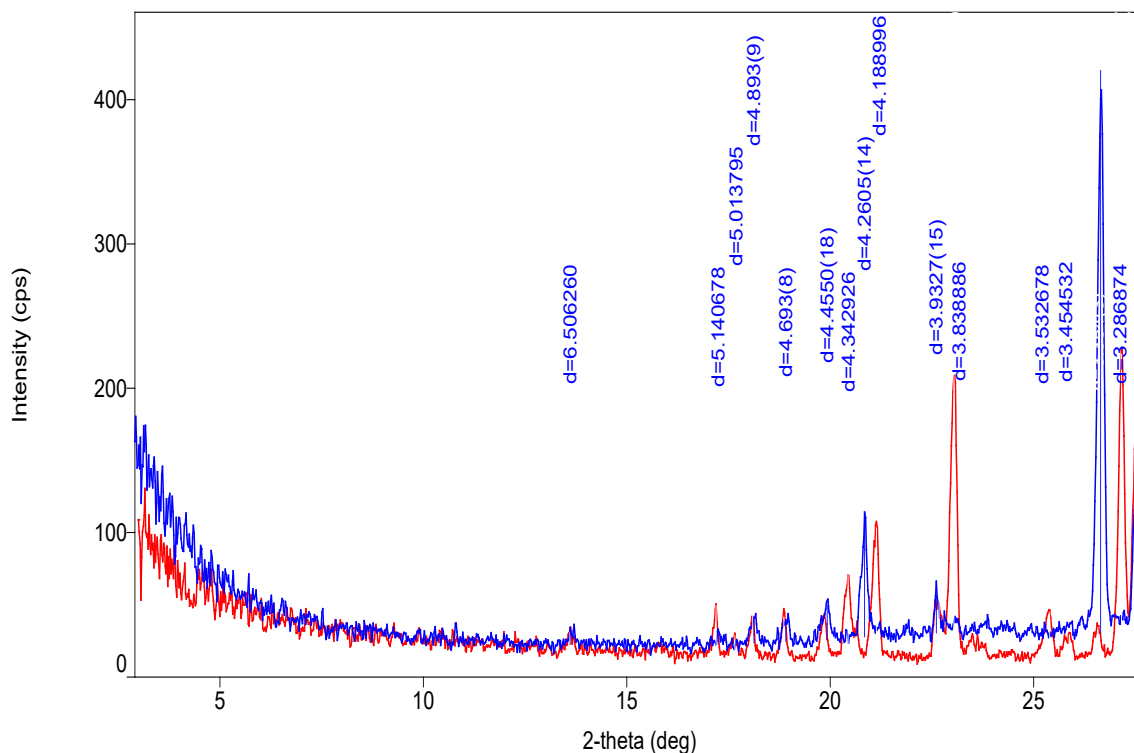
XRD Results-R010192

General Information

Measurement date:	22/3/2023	Interpretative date:	13/6/2023
Job Number/Client:	LJN2023-031	XRD	Rigaku Miniflex 600
Registration Number:	R010192	Analyst:	LUnwin
Quantitative Method:	Mineralogy Only	Process Medium:	Wholerock
Sample Holder:	Standard	Speed (deg/min):	0.5
Comment:	HCl leach, 580°C and 400°C heat treatments		

Analysis Results

Phase name	Formula
Clinopyroxene*	Variable
Analcime	$NaAl(Si_2O_6) \cdot (H_2O)$
Chlorite*	$(Fe,Mg,Al)_6(Si,Al)_4O_{10}(OH)_8$
Nepheline*	$Na_3K(Al_4Si_4O_{16})$
Plagioclase*	$(Na,Ca)(Al,Si)_4O_8$
Magnetite	$Fe^{2+}Fe^{3+}_2O_4$
Olivine*	$Mg_2(SiO_4)$

Fluorapatite	$Ca_5(PO_4)_3F$

Notes

Peak overlap may interfere with identifications and quantitative calculations.

Amorphous minerals and minerals present in trace amounts may not be detected.

Clinopyroxene* probably Augite

Olivine*   possibly Forsterite

Chlorite*   possibly Chamosite 7.1Å removed by HCl leach

Nepheline*   removed by HCl leach

Plagioclase*   possibly Albite

Phase Data Pattern
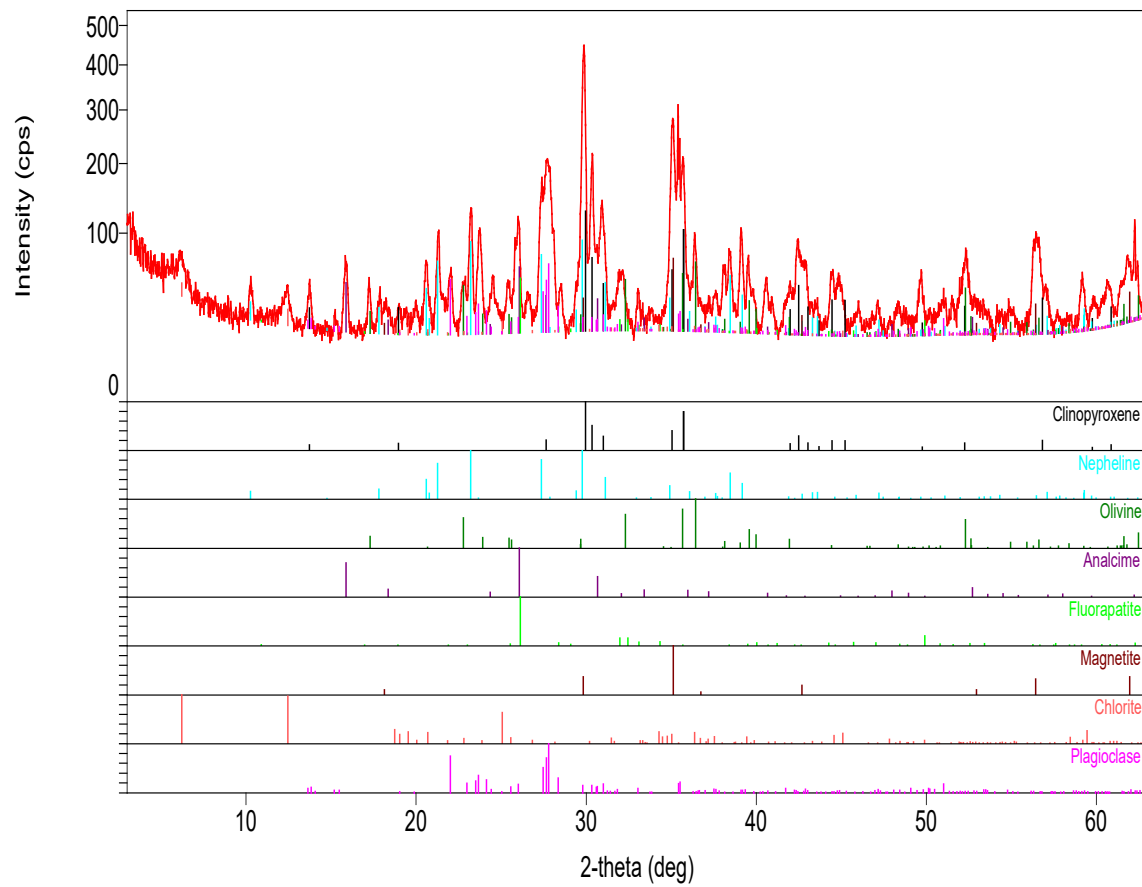
Phase Data Pattern: Blue – 400°C, Red – raw data
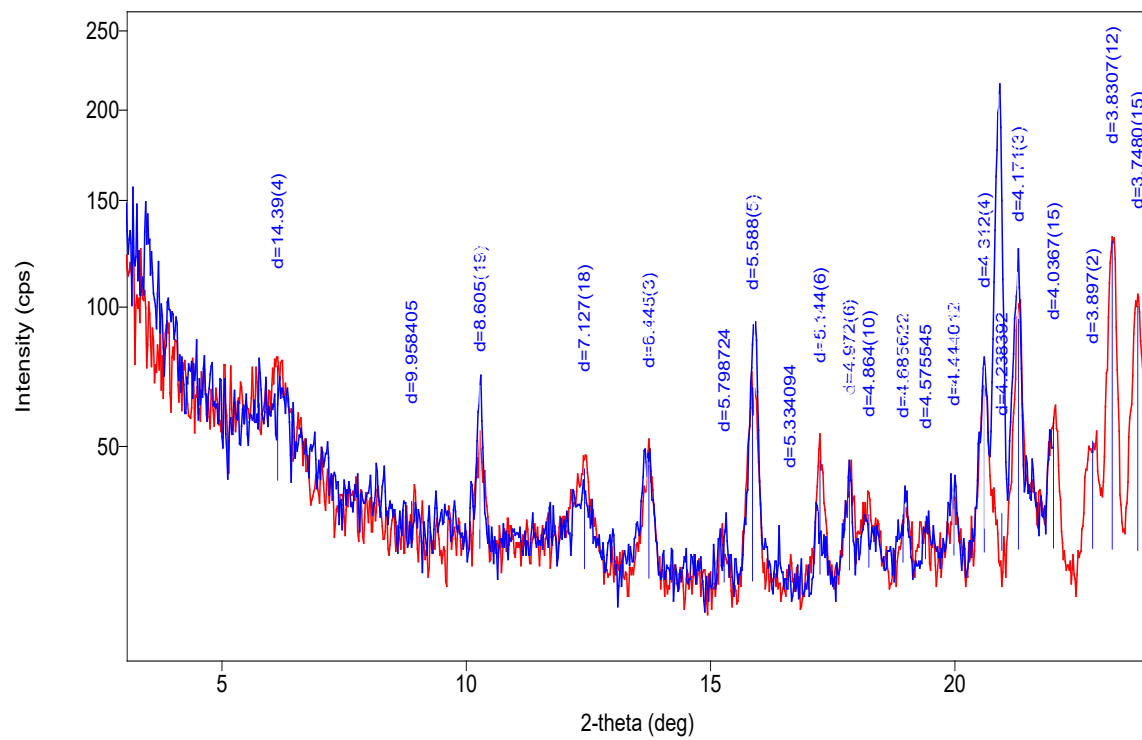
Phase Data Pattern: Blue – HCl, Red – raw data
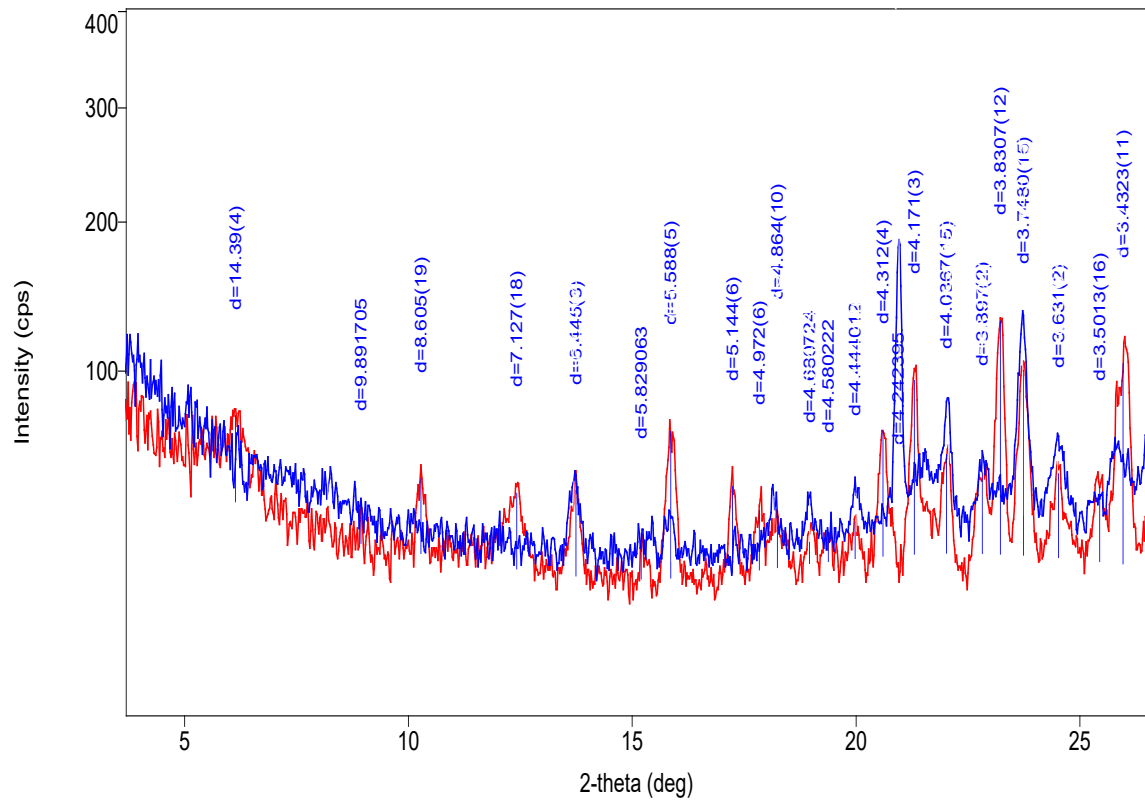
Phase Data Pattern: Blue – 580°C, Red – raw data
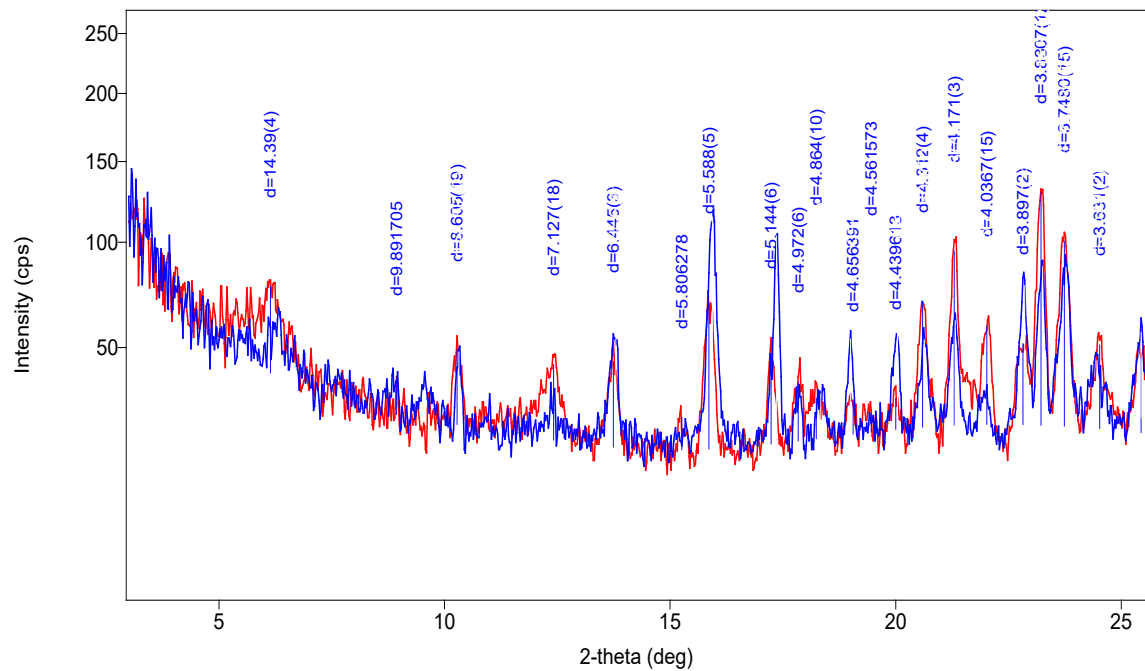
XRD Results-R027027

General Information

Measurement date:	22/3/2023	**Interpretative date:**	28/4/2023
Job Number/Client:	LJN2023-031	**XRD**	Rigaku Miniflex 600
Registration Number:	R027027	**Analyst:**	LUnwin
Quantitative Method:	Mineralogy Only	**Process Medium:**	Wholerock
Sample Holder:	Standard	**Speed (deg/min):**	0.5
Comment:	Shifted -0.07, HCl leach treatment		

Analysis Results

Phase name	Formula
Clinopyroxene*	Variable
Nepheline	$Na_3K(Al_4Si_4O_{16})$
Plagioclase*	$(Na,Ca)(Al,Si)_4O_8$
Magnetite	$Fe^{2+}Fe^{3+}_2O_4$
Olivine*	$Mg_2(SiO_4)$
Chlorite*	$(Fe,Mg,Al)_6(Si,Al)_4O_{10}(OH)_8$
Chabazite*	$(Ca,K_2,Na_2)_2[Al_2Si_4O_{12}]_2 \cdot 12H_2O$
Smectite*	Variable
Mica	$KAl_2(AlSi_3O_{10})(OH)_2$
Anorthoclase*	$(Na,K)AlSi_3O_8$
Fluorapatite	$Ca_5(PO_4)_3F$

Notes

Peak overlap may interfere with identifications and quantitative calculations.
Amorphous minerals and minerals present in trace amounts may not be detected.
Clinopyroxene* probably Diopside
Olivine*   possibly Forsterite
Anorthoclase*   3.8Å not removed by HCl leach
Chabazite *   removed by HCl leach
Nepheline*   removed by HCl leach
Smectite*   possibly Beidellite, after HCl leach 14Å is reduced slightly and a shift to 9Å
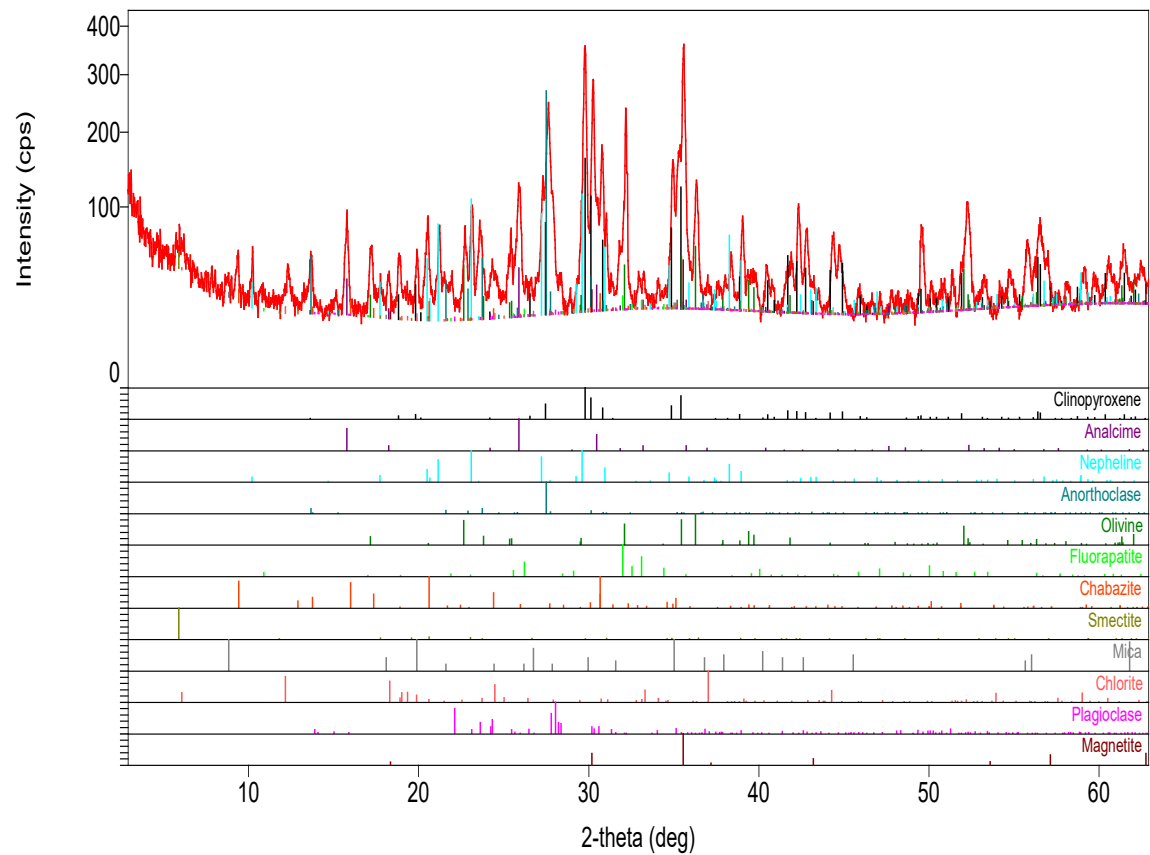Chlorite*   possibly Chamosite, removed by HCl leach
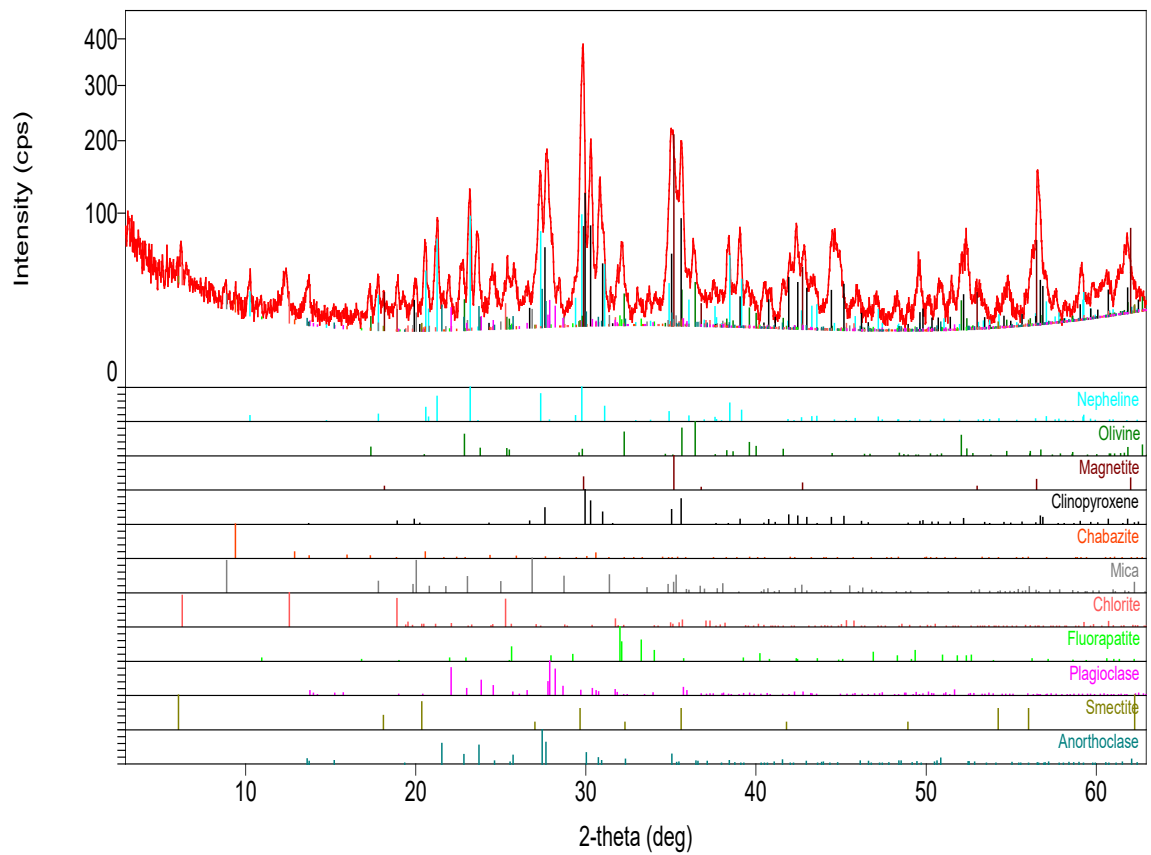
Phase Data Pattern

Phase Data Pattern: Blue – HCl leach, Red - Raw data
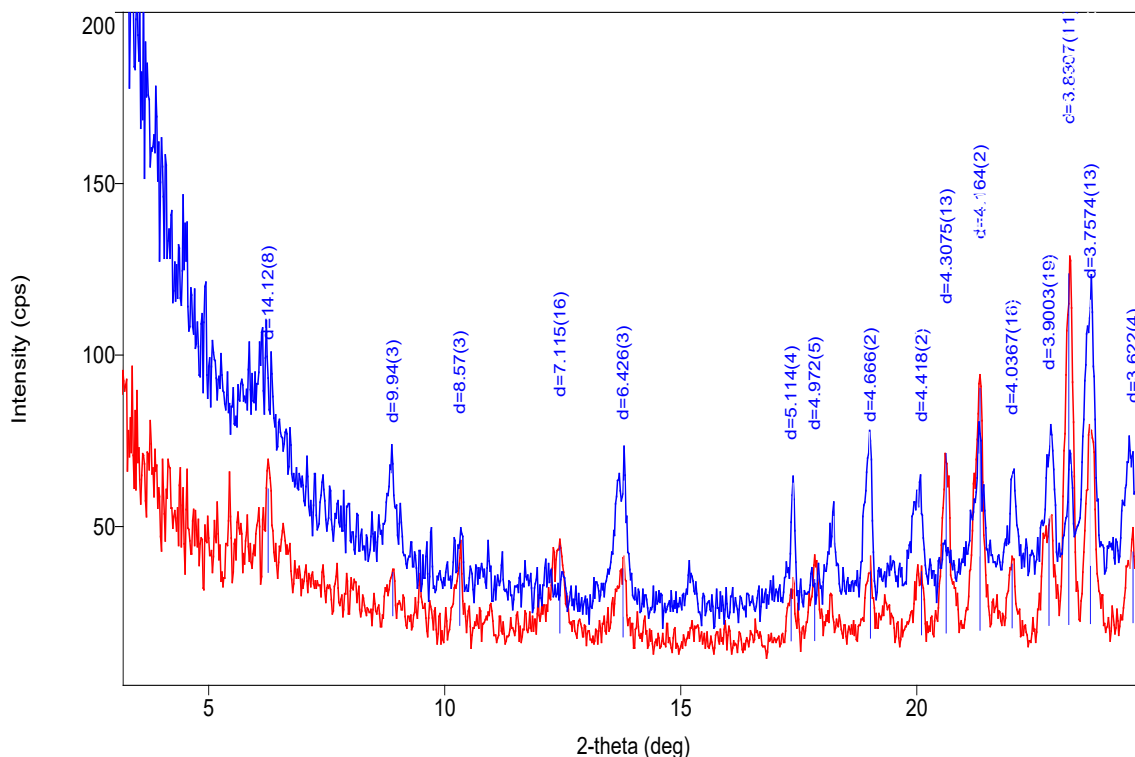
XRD Results-G402497

General Information

Measurement date:	20/4/2023	**Interpretative date:**	16/5/2023
Job Number/Client:	LJN2023-031	**XRD**	Rigaku Miniflex 600
Registration Number:	G402497	**Analyst:**	LUnwin
Quantitative Method:	Mineralogy Only	**Process Medium:**	Wholerock
Sample Holder:	Standard	**Speed (deg/min):**	0.5
Comment:	Shifted -0.01, HCl leach, 580°C and 500°C heat treatments		

Analysis Results

Phase name	Formula
Clinopyroxene*	Variable
Nepheline	$Na_3K(Al_4Si_4O_{16})$
Plagioclase*	$(Na,Ca)(Al,Si)_4O_8$
Anorthoclase*	$(Na,K)AlSi_3O_8$
Magnetite	$Fe^{2+}Fe^{3+}_2O_4$
Zeolite	Variable
Fluorapatite	$Ca_5(PO_4)_3F$

Olivine*	$Mg_2(SiO_4)$

Notes

Peak overlap may interfere with identifications and quantitative calculations.

Amorphous minerals and minerals present in trace amounts may not be detected.

Clinopyroxene* probably Augite

Plagioclase*   probably Albite

Olivine*   possibly Forsterite

Illite   possibly present but unresolved by XRD

Phase Data Pattern
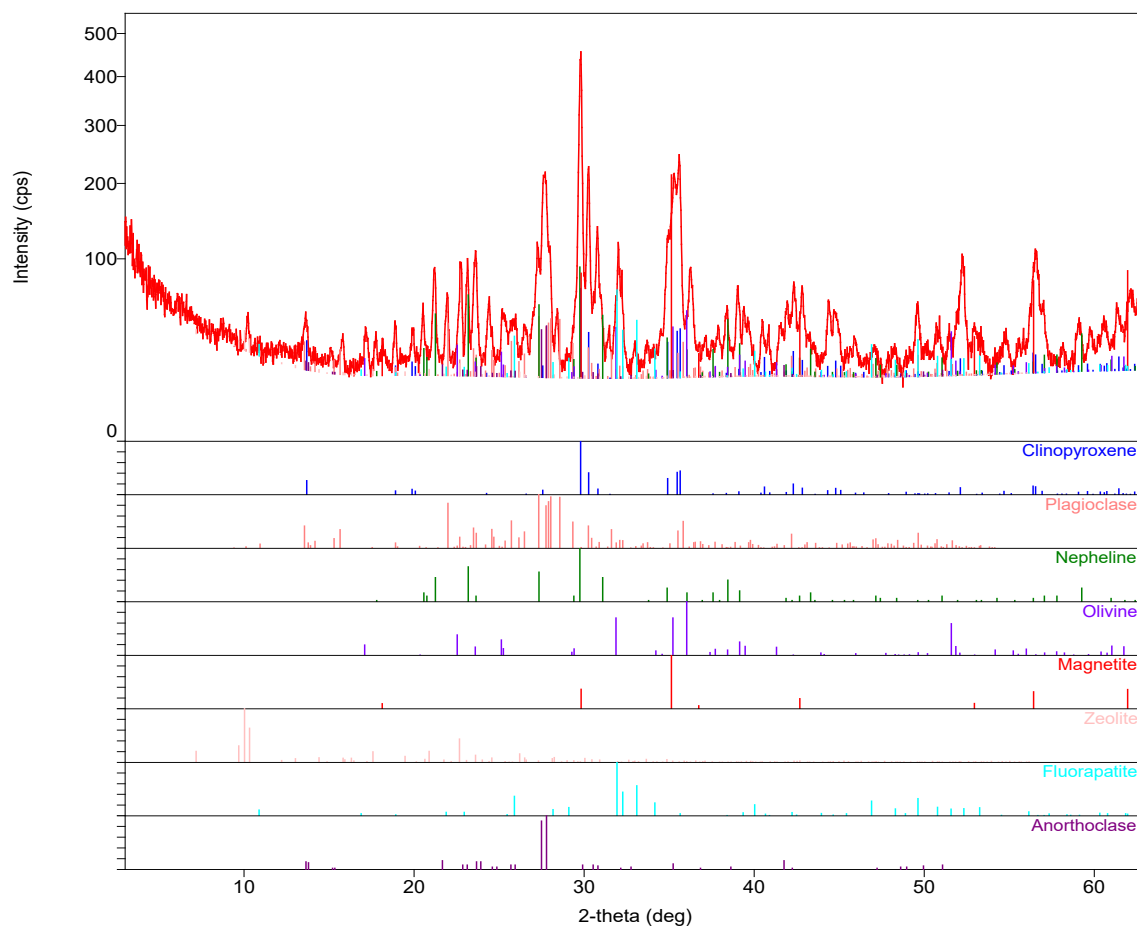
Phase Data Pattern: Blue – HCl leach, Red - Raw data
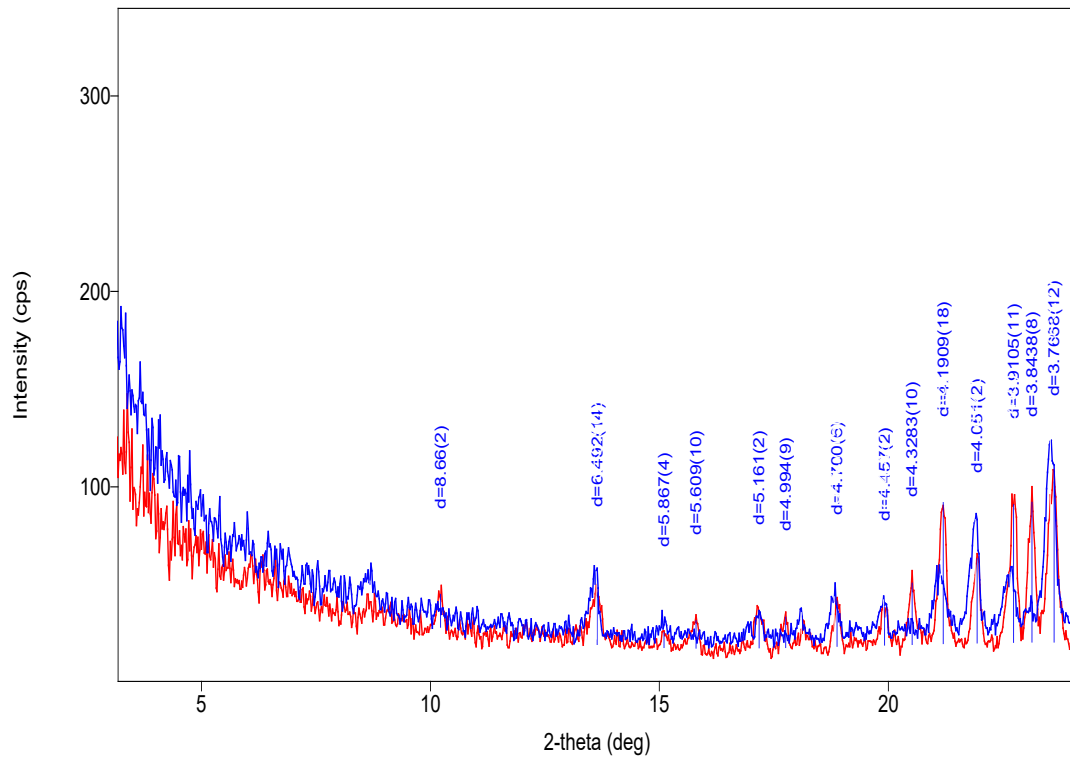
Phase Data Pattern: Blue – 580°C, Red – raw data
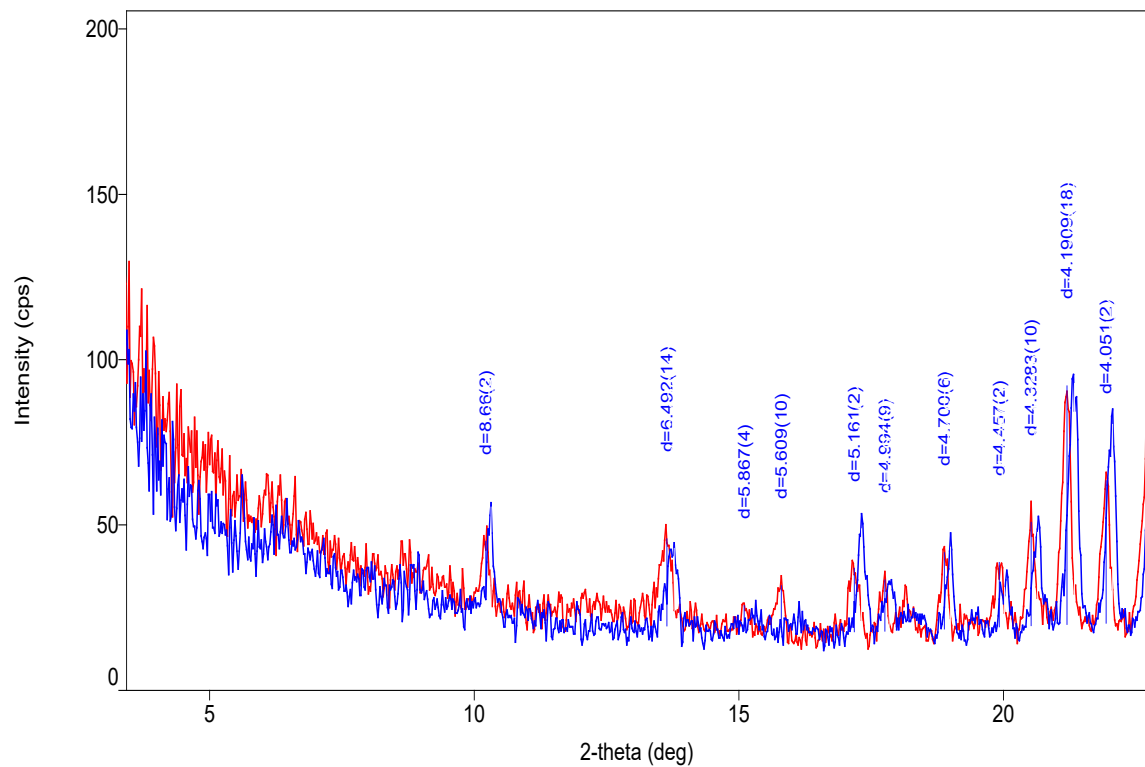
Phase Data Pattern: Blue – 500°C, Red – raw data
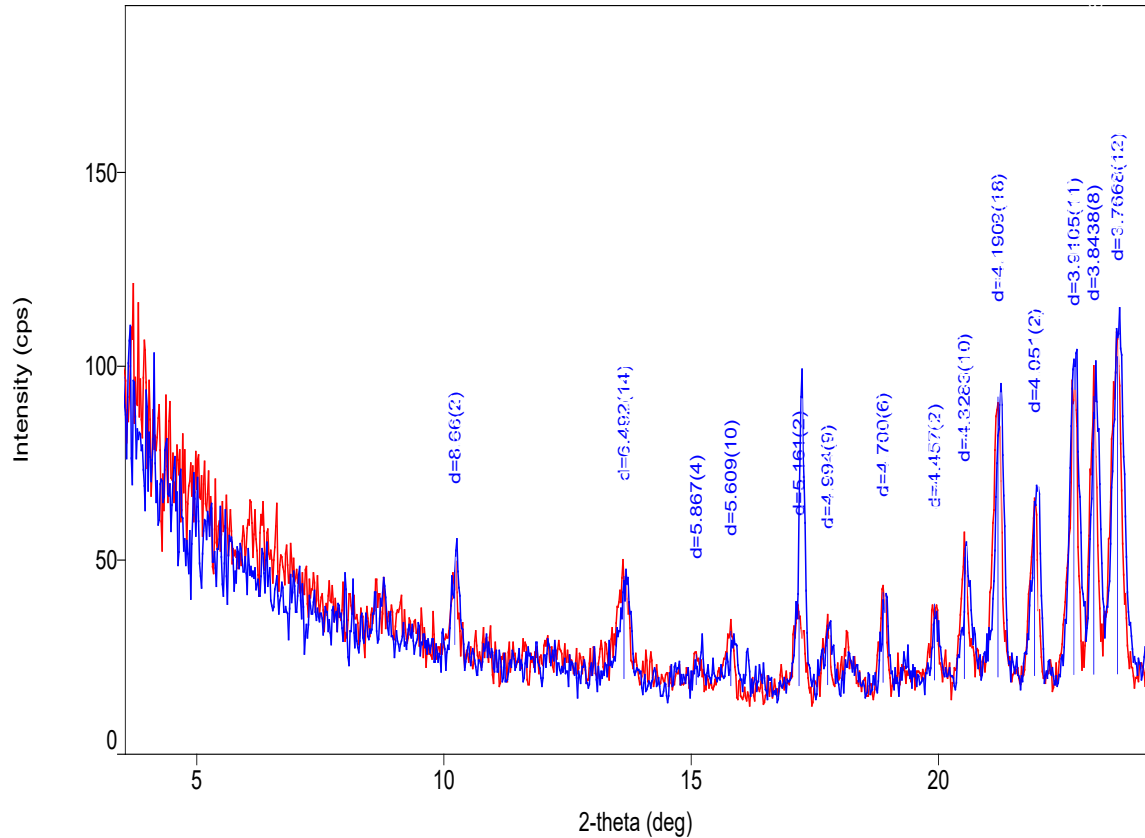
T.Coyte

Senior Technical Officer

DISCLAIMERS

While every care has been taken in the preparation of this report, no warranty is given as to the correctness of the information and no liability is accepted for any statement or opinion or for any error or omission. No reader should act or fail to act on the basis of any material contained herein. Readers should consult professional advisers. As a result the Crown in Right of the State of Tasmania and its employees, contractors and agents expressly disclaim all and any liability (including

Appendix_C_XRD_results_LJN2023-031 JLE Laboratory Report (002)

all liability from or attributable to any negligent or wrongful act or omission) to any persons whatsoever in respect of anything done or omitted to be done by any such person in reliance whether in whole or in part upon any of the material in this report. The MRT laboratories are not NATA registered but work to similar standards. This and other data collected in MRT laboratories may enter the MRT databases but every attempt will be made to ensure it remains closed file and not be available externally, unless at your request.

LABORATORY DETAILS

Mineral Resources Tasmania (MRT) operates a laboratory facility at its offices at Mornington, Tasmania. In the interests of full disclosure, these laboratories do not have NATA accreditation. However, all tests are performed according to relevant Australian Standards cited in the report and subject to internal peer review processes. The analytical facilities at MRT are periodically compared against other similar laboratories in other jurisdictions with favourable results.

APPENDIX 4

Results of ^{40}Ar/^{39}Ar incremental heating experiments

APPENDIX D

Results of ^{40}Ar/^{39}Ar incremental heating experiments

TJ3602 (R005376)	Whole rock			hawaiite			Wedge Plains Link Road				
T (°C)	cumulative ^{39}Ar$_K$	increment ^{39}Ar$_K$	Atmos. %	36Ar/39Ar	37Ar/39Ar	38Ar/39Ar	40Ar/39Ar	40Ar/36Ar	Age (Ma)		1σ
450	0.003	0.003	61.58	1.4335E-01	2.1292E-01	1.2912E-01	6.8788E+01	4.7987E+02	145.9	±	28.1
500	0.006	0.003	83.30	4.2440E-01	1.6000E-01	2.1296E-01	1.5056E+02	3.5476E+02	139.0	±	29.9
600	0.012	0.006	78.93	1.7036E-01	1.3135E-01	1.0558E-01	6.3791E+01	3.7444E+02	75.6	±	5.9
650	0.016	0.004	91.08	3.6773E-01	1.1393E-01	1.3859E-01	1.1932E+02	3.2448E+02	60.2	±	22.0
700	0.023	0.007	72.64	7.6786E-02	1.4489E-01	8.8546E-02	3.1246E+01	4.0693E+02	48.4	±	12.1
750	0.030	0.007	56.00	4.5708E-02	1.4903E-01	6.9583E-02	2.4126E+01	5.2783E+02	60.0	±	17.3
840	0.036	0.006	43.62	3.2054E-02	1.8491E-01	8.0083E-02	2.1709E+01	6.7727E+02	69.0	±	16.9
900	0.049	0.013	69.85	3.7625E-02	1.5709E-01	6.8835E-02	1.5928E+01	4.2332E+02	27.4	±	6.1
960	0.089	0.040	6.73	1.4001E-03	9.7041E-02	1.7518E-02	6.0630E+00	4.3303E+03	32.1	±	3.1
1020	0.164	0.075	38.13	9.7557E-03	1.2300E-01	1.9662E-02	7.5647E+00	7.7542E+02	26.6	±	2.3
1100	0.337	0.173	5.60	1.0242E-03	7.5165E-02	1.5948E-02	5.3263E+00	5.2007E+03	28.5	±	0.6
1200	0.975	0.638	8.23	1.4064E-03	5.5502E-02	1.5696E-02	5.0222E+00	3.5708E+03	26.2	±	0.3
1400	0.991	0.016	51.89	2.0817E-02	1.3170E-01	4.3172E-02	1.1863E+01	5.6986E+02	32.4	±	4.9
1600	1.000	0.009	14.99	6.8752E-03	1.5688E-01	5.8250E-02	1.3498E+01	1.9633E+03	64.7	±	5.6

Sample mass = 600 mg
J-value = 0.00318766 ± 0.00000317
Integrated age = 29.1 ± 0.4 Ma
Plateau age = 27.0 ± 0.3 Ma (900-1400°C)

TJ3591 (R005365)	Whole rock			transitional olivine basalt	Rabalga Track						
T (°C)	cum. ^{39}Ar$_K$	increment	Atmos. %	36Ar/39Ar	37Ar/39Ar	38Ar/39Ar	40Ar/39Ar	40Ar/36Ar	Age (Ma)		1σ
400	0.001	0.001	16.62	4.2587E-02	4.1046E-02	3.3699E-01	7.5687E+01	1.7772E+03	330.5	±	90.6
450	0.006	0.005	64.48	5.2200E-01	2.1781E-01	4.3953E-01	2.3920E+02	4.5824E+02	432.3	±	20.0
500	0.012	0.006	72.35	2.2240E-01	1.7861E-01	2.6377E-01	9.0833E+01	4.0843E+02	138.9	±	13.7
600	0.018	0.006	72.69	1.8442E-01	2.6758E-01	2.8068E-01	7.4963E+01	4.0648E+02	114.0	±	12.7
650	0.028	0.010	58.68	5.4745E-02	2.0236E-01	1.6119E-01	2.7568E+01	5.0357E+02	64.3	±	10.0
700	0.061	0.033	87.32	4.6013E-02	2.0712E-01	1.1864E-01	1.5581E+01	3.3862E+02	11.3	±	3.0
800	0.095	0.034	20.38	7.5534E-03	1.2848E-01	4.9804E-02	1.0930E+01	1.4470E+03	49.2	±	2.3
900	0.108	0.013	83.11	1.0246E-01	1.9731E-01	1.6740E-01	3.6440E+01	3.5563E+02	35.0	±	6.3
1000	0.624	0.516	12.52	2.8633E-03	4.2789E-02	2.1107E-02	6.7565E+00	2.3597E+03	33.5	±	0.3
1060	0.702	0.078	29.20	8.6353E-03	8.3360E-02	2.7623E-02	8.7452E+00	1.0127E+03	35.1	±	1.1
1120	0.955	0.253	13.68	3.3529E-03	4.8458E-02	1.7699E-02	7.2421E+00	2.1600E+03	35.5	±	0.5
1200	0.963	0.008	21.94	9.9682E-03	2.2283E-01	1.3238E-01	1.3375E+01	1.3418E+03	58.9	±	7.6
1400	0.976	0.013	29.25	1.3617E-02	2.2684E-01	9.3720E-02	1.3723E+01	1.0078E+03	54.9	±	9.5
1600	1.000	0.024	13.11	5.5116E-03	1.7073E-01	7.5711E-02	1.2351E+01	2.2410E+03	60.6	±	3.6

Sample mass = 600 mg
J-value = 0.00318766 ± 0.00000317
Integrated date = 39.0 ± 0.4 Ma
Plateau age = 34.3 ± 0.3 Ma (900-1120°C)

KJ634 (R005410)	Whole rock			basanite			Eastons Creek, lower flow				
T (°C)	cum. ^{39}Ar$_K$	increment	Atmos. %	36Ar/39Ar	37Ar/39Ar	38Ar/39Ar	40Ar/39Ar	40Ar/36Ar	Age (Ma)		1σ
400	0.006	0.006	99.14	1.9197E-01	1.7225E-01	1.0057E-01	5.7233E+01	2.9814E+02	2.8	±	4.2
500	0.020	0.014	78.66	6.1335E-02	2.8194E-01	8.1754E-02	2.3041E+01	3.7566E+02	28.0	±	2.4
600	0.053	0.033	18.49	5.5160E-03	1.0452E-01	7.7631E-02	8.8014E+00	1.5956E+03	40.7	±	0.9
680	0.097	0.044	21.40	4.1816E-03	3.3068E-02	3.5963E-02	5.7890E+00	1.3844E+03	25.8	±	0.6
760	0.340	0.243	9.56	1.6917E-03	2.7944E-02	2.3050E-02	5.2346E+00	3.0943E+03	26.9	±	0.3
850	0.491	0.151	10.65	1.8244E-03	4.9075E-02	2.0757E-02	5.0556E+00	2.7711E+03	25.6	±	0.5
950	0.663	0.172	10.64	1.7429E-03	9.6202E-02	2.0745E-02	4.7997E+00	2.7539E+03	24.4	±	0.3
1020	0.777	0.114	8.95	1.3728E-03	7.9225E-02	2.1907E-02	4.4902E+00	3.2709E+03	23.2	±	0.3
1100	0.807	0.030	8.26	1.2963E-03	1.0593E-01	2.7304E-02	4.5650E+00	3.5216E+03	23.8	±	1.0
1200	0.891	0.084	10.99	1.9488E-03	4.4373E-01	2.2327E-02	4.9645E+00	2.5475E+03	25.1	±	0.4
1300	0.920	0.029	21.71	4.4542E-03	1.3376E+00	3.6549E-02	5.6293E+00	1.2638E+03	25.1	±	0.9
1400	0.947	0.027	32.49	7.3806E-03	1.5146E+00	3.6956E-02	6.3888E+00	8.6562E+02	24.5	±	1.6
1600	1.000	0.053	57.05	2.2104E-02	1.6788E+00	3.3734E-02	1.1256E+01	5.0923E+02	27.6	±	0.4

Sample mass = 600 mg
J-value = 0.00318766 ± 0.00000317
Integrated age = 25.8 ± 0.1 Ma
Plateau age = 25.4 ± 0.2 Ma (680-1600°C)

TJ3228 (R005353)   Whole rock   nepheline hawaiite   Knoll, Neasey Plains

T (°C)	cum. $^{39}Ar_K$	increment	Atmos. %	36Ar/39Ar	37Ar/39Ar	38Ar/39Ar	40Ar/39Ar	40Ar/36Ar	Age (Ma)		1σ
450	0.010	0.010	95.58	1.1731E-01	3.7538E-02	1.8236E-01	3.6292E+01	3.0936E+02	9.2	±	4.0
500	0.028	0.018	44.22	1.6026E-02	2.1109E-02	1.6677E-01	1.0733E+01	6.6968E+02	34.0	±	1.5
600	0.071	0.043	55.05	1.4286E-02	2.3522E-02	1.4137E-01	7.6935E+00	5.3852E+02	19.7	±	1.3
650	0.142	0.071	32.77	6.5932E-03	1.7520E-02	1.2387E-01	5.9689E+00	9.0531E+02	22.8	±	0.5
700	0.197	0.055	51.44	1.3059E-02	2.3414E-02	5.3167E-02	7.5270E+00	5.7639E+02	20.8	±	0.9
750	0.306	0.109	16.18	2.6287E-03	1.3781E-02	1.0435E-01	4.8217E+00	1.8343E+03	23.0	±	0.2
840	0.390	0.084	25.66	4.4089E-03	1.2728E-02	1.1072E-01	5.1015E+00	1.1571E+03	21.6	±	0.4
900	0.512	0.122	13.87	2.0869E-03	1.2617E-02	9.7372E-02	4.4650E+00	2.1396E+03	21.8	±	0.3
960	0.558	0.046	7.97	1.1443E-03	2.3731E-02	4.2530E-02	4.2461E+00	3.7106E+03	22.2	±	1.1
1020	0.672	0.114	11.25	1.6092E-03	1.2847E-02	9.0025E-02	4.2452E+00	2.6381E+03	21.4	±	0.2
1100	0.779	0.107	13.48	1.9117E-03	1.5231E-02	8.2214E-02	4.2087E+00	2.2015E+03	20.7	±	0.3
1200	0.848	0.069	10.02	1.3588E-03	1.8118E-02	6.6776E-02	4.0223E+00	2.9602E+03	20.5	±	0.7
1400	0.911	0.063	12.60	1.7214E-03	2.2540E-02	5.3223E-02	4.0497E+00	2.3525E+03	20.1	±	0.6
1600	1.000	0.089	28.24	4.7982E-03	3.7105E-02	4.8595E-02	5.0379E+00	1.0500E+03	20.6	±	0.5

Sample mass = 600 mg
J-value = 0.00318766 ± 0.00000317
Integrated age = 21.5 ± 0.2 Ma
Plateau age = 21.4 ± 0.2 Ma (600-1600°C)

CVH (R010192)   Whole rock   basanite   Coastview Hill, via Hampshire

T (°C)	cum. $^{39}Ar_K$	increment	Atmos. %	36Ar/39Ar	37Ar/39Ar	38Ar/39Ar	40Ar/39Ar	40Ar/36Ar	Age (Ma)		1σ
400	0.004	0.004	46.06	5.1833E-02	6.9872E-01	1.4852E-01	3.3169E+01	6.3991E+02	100.0	±	8.8
450	0.014	0.010	81.11	8.5407E-02	3.8677E-01	9.9185E-02	3.1105E+01	3.6420E+02	33.4	±	4.2
500	0.018	0.004	58.28	2.9362E-02	2.4096E-01	9.3687E-02	1.4884E+01	5.0692E+02	35.3	±	4.9
600	0.059	0.041	63.87	2.2378E-02	2.3384E-01	5.3478E-02	1.0354E+01	4.6270E+02	21.3	±	1.4
650	0.112	0.053	28.43	5.6893E-03	1.2896E-01	4.1309E-02	5.9069E+00	1.0383E+03	24.0	±	0.9
700	0.162	0.050	2.84	4.3008E-04	9.8628E-02	2.2454E-02	4.2383E+00	9.8547E+03	23.4	±	0.9
750	0.308	0.146	13.83	2.0938E-03	9.0056E-02	1.8766E-02	4.4529E+00	2.1267E+03	21.8	±	0.3
840	0.499	0.191	8.82	1.2421E-03	8.3075E-02	1.8425E-02	4.1149E+00	3.3128E+03	21.3	±	0.3
900	0.560	0.061	1.30	1.8657E-04	1.0418E-01	2.3168E-02	3.6483E+00	1.9555E+04	20.4	±	0.8
960	0.641	0.081	3.89	5.5929E-04	1.2256E-01	2.8625E-02	4.0325E+00	7.2100E+03	22.0	±	0.7
1020	0.687	0.046	8.44	1.1756E-03	1.3941E-01	4.4922E-02	4.0190E+00	3.4186E+03	20.9	±	1.1
1100	0.725	0.038	2.43	4.1459E-04	2.6224E-01	5.8028E-02	4.2534E+00	1.0259E+04	23.6	±	0.6
1200	0.844	0.119	0.01	9.8184E-05	7.0247E-01	4.7146E-02	3.6420E+00	3.7094E+04	20.7	±	0.5
1300	0.892	0.048	4.98	9.5758E-04	1.2737E+00	5.9735E-02	3.7808E+00	3.9482E+03	20.4	±	1.1
1400	0.952	0.060	0.01	9.9476E-05	1.3990E+00	6.7816E-02	3.4848E+00	3.5032E+04	19.8	±	0.8
1600	1.000	0.048	13.58	2.4185E-03	1.5090E+00	7.6310E-02	4.4529E+00	1.8411E+03	21.9	±	1.0

Sample mass = 600 mg
J-value = 0.00318766 ± 0.00000317
Integrated age = 22.0 ± 0.2 Ma
Plateau age = 21.5 ± 0.2 Ma (600-1600°C)

SRN (R010187)   Whole rock   basanite   South Riana plug

T (°C)	cum. $^{39}Ar_K$	increment	Atmos. %	36Ar/39Ar	37Ar/39Ar	38Ar/39Ar	40Ar/39Ar	40Ar/36Ar	Age (Ma)		1σ
400	0.006	0.006	92.38	4.3434E-02	1.8677E-01	1.3030E-01	1.3905E+01	3.2015E+02	6.1	±	7.4
450	0.023	0.017	61.88	7.7548E-02	2.3502E-01	1.4159E-01	3.7030E+01	4.7752E+02	79.4	±	4.5
500	0.031	0.008	48.08	8.0015E-02	1.9200E-01	1.7400E-01	4.9176E+01	6.1458E+02	141.1	±	6.3
600	0.044	0.013	61.43	1.0583E-01	1.4494E-01	1.6887E-01	5.0915E+01	4.8108E+02	109.5	±	4.0
650	0.067	0.023	77.63	8.2071E-02	1.2869E-01	1.3470E-01	3.1239E+01	3.8064E+02	39.6	±	4.0
700	0.093	0.026	63.04	3.9609E-02	6.7231E-02	8.8892E-02	1.8587E+01	4.6925E+02	39.0	±	3.4
750	0.139	0.046	62.73	3.4516E-02	7.4835E-02	8.9340E-02	1.6278E+01	4.7160E+02	34.5	±	1.6
840	0.183	0.044	73.15	3.5029E-02	4.9266E-02	7.4699E-02	1.4174E+01	4.0463E+02	21.7	±	1.9
900	0.237	0.054	68.04	2.6180E-02	3.4456E-02	6.1422E-02	1.1394E+01	4.3521E+02	20.8	±	1.3
960	0.310	0.073	64.90	2.1819E-02	2.2844E-02	4.6590E-02	9.9605E+00	4.5650E+02	19.9	±	1.6
1020	0.420	0.110	50.63	1.3764E-02	2.0320E-02	3.5864E-02	8.0585E+00	5.8546E+02	22.7	±	0.5
1100	0.647	0.227	50.67	1.3394E-02	1.5943E-02	2.9520E-02	7.8366E+00	5.8510E+02	22.0	±	0.2
1200	0.918	0.271	27.27	4.9956E-03	3.5395E-02	2.6312E-02	5.4312E+00	1.0872E+03	22.5	±	0.5
1400	0.944	0.026	60.71	4.5284E-02	8.4802E-02	1.0819E-01	2.2059E+01	4.8711E+02	49.1	±	3.1
1600	1.000	0.056	41.14	1.7298E-02	5.2011E-02	7.2801E-02	1.2442E+01	7.1925E+02	41.5	±	1.3

Sample mass = 600 mg
J-value = 0.00318766 ± 0.00000317
Integrated date = 28.2 ± 0.3 Ma
Plateau age = 22.0 ± 0.3 Ma (840-1200°C)

LLC (R010186) Whole rock alkali olivine basalt Lillicos Beach, lower flow

T (°C)	cum. $^{39}Ar_K$	increment	Atmos. %	36Ar/39Ar	37Ar/39Ar	38Ar/39Ar	40Ar/39Ar	40Ar/36Ar	Age (Ma)		1σ
400	0.008	0.008	95.30	1.7346E-01	2.5186E-01	1.9290E-01	5.3792E+01	3.1011E+02	14.5	±	5.1
500	0.016	0.008	84.34	9.3105E-02	1.6650E-01	1.7083E-01	3.2633E+01	3.5050E+02	29.1	±	4.2
600	0.036	0.020	49.84	3.5833E-02	1.3948E-01	1.4002E-01	2.1253E+01	5.9311E+02	60.2	±	1.7
680	0.069	0.033	55.05	2.7845E-02	1.0055E-01	1.2385E-01	1.4962E+01	5.3731E+02	38.2	±	1.3
760	0.158	0.089	40.88	1.4918E-02	6.5082E-02	6.3302E-02	1.0813E+01	7.2487E+02	36.3	±	0.5
850	0.300	0.142	34.20	1.1523E-02	4.6788E-02	6.6671E-02	9.9748E+00	8.6561E+02	37.2	±	0.4
950	0.444	0.144	23.41	6.8087E-03	6.3793E-02	6.2442E-02	8.5995E+00	1.2630E+03	37.4	±	0.4
1020	0.562	0.118	15.16	4.1059E-03	8.7861E-02	4.0662E-02	7.9847E+00	1.9447E+03	38.4	±	0.2
1100	0.674	0.112	6.32	1.5866E-03	1.1338E-01	2.7921E-02	7.3048E+00	4.6039E+03	38.8	±	0.4
1200	0.749	0.075	9.31	2.3382E-03	2.2667E-01	3.3433E-02	7.2611E+00	3.1054E+03	37.3	±	0.4
1300	0.890	0.141	3.12	9.2184E-04	7.9836E-01	2.7116E-02	6.8270E+00	7.4058E+03	37.5	±	0.3
1400	0.945	0.055	6.17	1.6400E-03	1.0092E+00	3.6748E-02	6.6417E+00	4.0498E+03	35.4	±	0.4
1600	1.000	0.055	25.13	9.2151E-03	1.2406E+00	3.6600E-02	1.0490E+01	1.1383E+03	44.5	±	0.5

Sample mass = 600 mg
J-value = 0.00318766 ± 0.00000317
Integrated age = 38.1 ± 0.2 Ma
Plateau age = 37.5 ± 0.2 Ma (680-1400°C)

AJ99 (R004332) Whole rock olivine nephelinite Olivers Hill, via Ringarooma

T (°C)	cum. $^{39}Ar_K$	increment	Atmos. %	36Ar/39Ar	37Ar/39Ar	38Ar/39Ar	40Ar/39Ar	40Ar/36Ar	Age (Ma)		1σ
400	0.007	0.007	91.12	8.9643E-02	3.0127E-01	1.4447E-01	2.9074E+01	3.2434E+02	14.8	±	2.5
450	0.013	0.006	55.19	2.7534E-02	1.3791E-01	1.0940E-01	1.4751E+01	5.3575E+02	37.5	±	3.8
500	0.024	0.011	93.60	2.7542E-02	8.8542E-02	9.8450E-02	8.7162E+00	3.1646E+02	3.2	±	2.3
600	0.066	0.042	23.80	3.0697E-03	4.5649E-02	7.4012E-02	3.8242E+00	1.2458E+03	16.6	±	0.6
650	0.111	0.045	39.61	6.5168E-03	4.7397E-02	1.1680E-01	4.8809E+00	7.4897E+02	16.8	±	0.8
700	0.180	0.069	18.09	2.2450E-03	3.1335E-02	9.5694E-02	3.6812E+00	1.6397E+03	17.1	±	0.3
750	0.259	0.079	35.03	5.9147E-03	4.1271E-02	1.2029E-01	5.0081E+00	8.4671E+02	18.5	±	0.5
840	0.424	0.165	25.16	3.4700E-03	1.6265E-02	2.8943E-02	4.0990E+00	1.1813E+03	17.4	±	0.2
900	0.598	0.174	19.25	2.3696E-03	1.4865E-02	2.0935E-02	3.6590E+00	1.5441E+03	16.8	±	0.2
960	0.728	0.130	24.94	3.2640E-03	2.5944E-02	2.4227E-02	3.8875E+00	1.1910E+03	16.6	±	0.5
1020	0.826	0.098	17.45	2.3036E-03	6.4577E-02	2.4466E-02	3.9010E+00	1.6935E+03	18.3	±	0.4
1100	0.879	0.053	19.45	2.8585E-03	2.4268E-01	3.4772E-02	4.2775E+00	1.4964E+03	19.6	±	1.0
1200	0.940	0.061	55.62	1.3204E-02	3.4033E+00	8.7844E-02	6.5827E+00	4.9853E+02	16.7	±	0.6
1400	0.989	0.049	75.09	3.6439E-02	7.2024E+00	9.4912E-02	1.3644E+01	3.7443E+02	19.5	±	1.9
1600	1.000	0.011	75.40	2.0949E-01	4.9553E+00	1.5709E-01	8.1633E+01	3.8967E+02	112.2	±	3.1

Sample mass = 600 mg
I-value = 0.00318766 ± 0.00000317
Integrated age = 18.5 ± 0.2 Ma
Plateau age = 17.5 ± 0.2 (600-1400°C)

AJ1424 (R004366) Whole rock basanite northern hill, via Sweets Creek, upper Esk

T (°C)	cum. $^{39}Ar_K$	increment	Atmos. %	36Ar/39Ar	37Ar/39Ar	38Ar/39Ar	40Ar/39Ar	40Ar/36Ar	Age (Ma)		1σ
400	0.010	0.010	32.49	9.0121E-02	3.2127E+00	1.4223E-01	8.1240E+01	9.0145E+02	291.1	±	5.0
450	0.020	0.010	53.75	1.2588E-01	2.1565E+00	1.3077E-01	6.8921E+01	5.4750E+02	174.7	±	5.2
500	0.037	0.017	88.87	7.7825E-02	2.6431E+00	1.3720E-01	2.5682E+01	3.2999E+02	16.4	±	2.5
600	0.078	0.041	63.01	1.8945E-02	1.2753E+00	1.3289E-01	8.7608E+00	4.6244E+02	18.5	±	1.6
650	0.116	0.038	36.20	6.5165E-03	4.8567E-01	7.2054E-02	5.2458E+00	8.0501E+02	19.0	±	1.3
700	0.227	0.111	9.56	1.2634E-03	3.5414E-01	5.5353E-02	3.6523E+00	2.8909E+03	18.8	±	0.7
750	0.397	0.170	13.91	1.6241E-03	2.1776E-01	3.3704E-02	3.3601E+00	2.0689E+03	16.4	±	0.5
840	0.626	0.229	6.93	8.2749E-04	2.1148E-01	1.9398E-02	3.3240E+00	4.0169E+03	17.6	±	0.2
900	0.799	0.173	3.21	4.3772E-04	3.7900E-01	2.3351E-02	3.1684E+00	7.2385E+03	17.4	±	0.3
960	0.803	0.004	79.90	3.8832E-02	5.8173E+00	2.5408E-01	1.3841E+01	3.5643E+02	16.0	±	0.5
1020	0.810	0.007	84.36	5.4614E-02	6.2363E+00	1.8839E-01	1.8600E+01	3.4057E+02	16.7	±	0.4
1100	0.831	0.021	15.02	1.7598E-03	9.9413E-01	9.4466E-02	2.9904E+00	1.6993E+03	14.4	±	0.4
1200	0.882	0.051	4.48	2.7542E-03	8.5270E+00	1.0151E-01	3.8465E+00	1.3966E+03	21.0	±	1.3
1300	0.981	0.099	3.51	7.1921E-03	2.6347E+01	1.4014E-01	4.0139E+00	5.5810E+02	22.4	±	0.8
1400	0.989	0.008	39.35	1.7109E-02	3.9428E+01	2.4412E-01	5.3261E+00	3.1129E+02	18.9	±	3.7
1600	1.000	0.011	5.64	2.0215E-02	5.6968E+01	2.3133E-01	2.9797E+01	1.4740E+03	160.4	±	2.8

Sample mass = 600 mg
J-value = 0.00318766 ± 0.00000317
Integrated age = 25.4 ± 0.2 Ma
Plateau age = 17.5 ± 0.2 Ma (500-1020°C)

AJ1425 (R004367)   Whole rock   **hawaiite**   **southern hill, via Sweets Creek, upper Esk**

T (°C)	cum. $^{39}Ar_K$	increment	Atmos. %	36Ar/39Ar	37Ar/39Ar	38Ar/39Ar	40Ar/39Ar	40Ar/36Ar	Age (Ma)		1σ
400	0.003	0.003	66.78	1.9166E-01	2.3109E+00	2.7429E-01	8.4564E+01	4.4123E+02	154.9	±	10.5
450	0.011	0.008	94.25	1.7085E-01	3.3249E+00	2.0702E-01	5.3326E+01	3.1213E+02	17.6	±	4.5
500	0.013	0.002	50.52	4.3670E-02	1.2463E+00	2.6069E-01	2.5382E+01	5.8123E+02	70.8	±	8.8
600	0.021	0.008	93.87	7.0393E-02	1.4715E+00	1.3492E-01	2.2069E+01	3.1352E+02	7.8	±	3.1
650	0.037	0.016	54.41	2.0576E-02	1.0823E+00	7.1036E-02	1.1053E+01	5.3719E+02	28.7	±	2.6
700	0.076	0.039	35.85	7.0714E-03	8.5880E-01	3.3958E-02	5.6759E+00	8.0266E+02	20.7	±	1.3
750	0.146	0.070	33.98	5.4558E-03	6.2499E-01	2.5965E-02	4.6341E+00	8.4938E+02	17.4	±	0.3
840	0.321	0.175	15.34	1.9247E-03	5.4244E-01	1.7852E-02	3.4689E+00	1.8023E+03	16.7	±	0.3
900	0.473	0.152	9.78	1.2219E-03	6.6506E-01	1.7508E-02	3.2083E+00	2.6256E+03	16.4	±	0.2
960	0.587	0.114	8.51	1.1283E-03	8.5517E-01	1.8791E-02	3.1888E+00	2.8262E+03	16.6	±	0.2
1020	0.731	0.144	27.53	3.6809E-03	8.4370E-01	2.3676E-02	3.7481E+00	1.0183E+03	15.4	±	0.3
1100	0.762	0.031	19.25	2.4042E-03	9.5088E-01	3.3619E-02	3.3468E+00	1.3920E+03	15.4	±	1.2
1200	0.816	0.054	23.88	3.6648E-03	3.2639E+00	2.9146E-02	3.5332E+00	9.6410E+02	15.3	±	0.8
1300	0.869	0.053	16.22	4.4571E-03	1.0066E+01	3.5527E-02	3.4715E+00	7.7887E+02	16.6	±	0.9
1400	0.921	0.052	38.15	7.3355E-03	1.1598E+01	3.9770E-02	3.4192E+00	4.6612E+02	12.1	±	0.6
1600	1.000	0.079	9.83	4.4730E-03	1.0961E+01	3.6314E-02	5.0684E+00	1.1331E+03	26.1	±	0.5

Sample mass = 600 mg
J-value = 0.00318766 ± 0.00000317
Integrated date = 17.7 ± 0.2 Ma
Plateau age = 16.3 ± 0.2 Ma (750-1300°C)

AJ1426 (R004368)   Whole rock   **olivine nephelinite**   **Upper Esk**

T (°C)	cum. $^{39}Ar_K$	increment	Atmos. %	36Ar/39Ar	37Ar/39Ar	38Ar/39Ar	40Ar/39Ar	40Ar/36Ar	Age (Ma)		1σ
450	0.002	0.002	0.02	9.6909E-05	1.6866E+00	3.2190E-01	4.5680E+01	4.7137E+05	245.4	±	33.5
500	0.022	0.020	95.24	1.9548E-01	1.6496E+00	1.0202E-01	6.0547E+01	3.0973E+02	16.5	±	4.0
600	0.076	0.054	90.58	1.1087E-01	1.5681E+00	6.6038E-02	3.6063E+01	3.2528E+02	19.4	±	1.7
650	0.143	0.067	86.53	6.1521E-02	9.8899E-01	4.3729E-02	2.0951E+01	3.4055E+02	16.1	±	1.3
700	0.230	0.087	81.69	4.1787E-02	5.3101E-01	3.2958E-02	1.5095E+01	3.6124E+02	15.8	±	1.1
750	0.410	0.180	73.88	2.9646E-02	6.0413E-01	4.2620E-02	1.1825E+01	3.9886E+02	17.6	±	0.7
840	0.517	0.107	57.26	1.4783E-02	1.1075E-01	2.7995E-02	7.6426E+00	5.1699E+02	18.6	±	0.9
900	0.619	0.102	56.19	1.1775E-02	1.3680E-01	2.9554E-02	6.2018E+00	5.2669E+02	15.5	±	0.8
960	0.716	0.097	53.37	1.0360E-02	2.4176E-01	3.9781E-02	5.7303E+00	5.5311E+02	15.2	±	0.6
1020	0.780	0.064	41.43	7.1264E-03	6.7951E-01	7.7714E-02	4.9874E+00	6.9985E+02	16.6	±	1.5
1100	0.836	0.056	34.14	5.7294E-03	3.3831E+00	1.5822E-01	4.2404E+00	7.4011E+02	15.9	±	1.0
1200	0.891	0.055	61.12	1.6148E-02	2.9940E+01	3.5447E-01	4.1436E+00	2.5660E+02	9.4	±	1.1
1300	0.934	0.043	75.80	2.7873E-02	4.9878E+01	3.9473E-01	5.9353E+00	2.1294E+02	8.5	±	1.5
1400	0.965	0.031	18.86	2.0962E-02	6.5699E+01	3.8288E-01	6.6197E+00	3.1579E+02	31.8	±	2.5
1600	1.000	0.035	81.28	5.3337E-02	4.1503E+01	2.8596E-01	1.5570E+01	2.9191E+02	17.1	±	2.5

Sample mass = 600 mg
I-value = 0.00318766 ± 0.00000317
Integrated age = 17.1 ± 0.3 Ma
Plateau age = 16.8 ± 0.4 Ma (500-1100°C)

PP20.5 (R027027)   Whole rock   **olivine nephelinite**   **Pebble Plain DDH/20.5m, via Beauty Flat**

T (°C)	cum. $^{39}Ar_K$	increment	Atmos. %	36Ar/39Ar	37Ar/39Ar	38Ar/39Ar	40Ar/39Ar	40Ar/36Ar	Age (Ma)		1σ
400	0.001	0.001	90.27	5.2963E-01	3.3722E-01	1.7141E-01	1.7336E+02	3.2733E+02	94.4	±	94.5
500	0.019	0.018	88.06	1.0582E-01	3.1565E-01	8.7380E-02	3.5512E+01	3.3558E+02	24.2	±	2.0
600	0.042	0.023	67.42	3.9401E-02	1.6485E-01	8.6047E-02	1.7279E+01	4.3856E+02	32.0	±	1.9
680	0.068	0.026	35.49	1.2998E-02	7.5892E-02	6.9926E-02	1.0834E+01	8.3352E+02	39.6	±	1.6
760	0.196	0.128	21.91	6.8491E-03	5.1027E-02	5.7035E-02	9.2446E+00	1.3497E+03	40.9	±	0.3
850	0.285	0.089	9.19	2.5737E-03	5.2040E-02	4.2977E-02	8.2783E+00	3.2165E+03	42.6	±	0.6
950	0.516	0.231	11.41	3.1961E-03	5.2040E-02	5.0982E-02	8.2700E+00	2.5875E+03	41.5	±	0.4
1020	0.629	0.113	12.12	3.2505E-03	6.0623E-02	4.4315E-02	7.9150E+00	2.4350E+03	39.4	±	0.4
1100	0.679	0.050	3.07	7.9338E-04	7.2494E-02	3.0975E-02	7.4788E+00	9.4266E+03	41.1	±	0.5
1200	0.838	0.159	8.31	2.2651E-03	2.3426E-01	2.8058E-02	7.8648E+00	3.4722E+03	40.9	±	0.2
1300	0.863	0.025	9.60	2.7693E-03	1.5447E+00	4.8047E-02	7.3351E+00	2.6488E+03	37.6	±	1.5
1400	0.963	0.100	23.07	6.4543E-03	1.5352E+00	4.9516E-02	7.7935E+00	1.2075E+03	34.1	±	0.3
1600	1.000	0.037	26.75	9.3436E-03	1.8419E+00	5.4946E-02	9.8287E+00	1.0519E+03	40.9	±	1.2

Sample mass = 600 mg
J-value = 0.00318766 ± 0.00000317
Integrated age = 39.7 ± 0.2 Ma
Plateau age = 41.0 ± 0.2 Ma (680-1200°C)

WSc (R010201) Whole rock olivine nephelinite Sledge Track, West Scottsdale

T (°C)	cum. ^{39}Ar$_K$	increment	Atmos. %	36Ar/39Ar	37Ar/39Ar	38Ar/39Ar	40Ar/39Ar	40Ar/36Ar	Age (Ma)		1σ
500	0.012	0.012	93.86	2.8302E-01	5.5495E-02	1.2220E-01	8.9122E+01	3.1489E+02	31.2	±	13.3
600	0.029	0.017	77.58	3.7677E-01	6.7699E-02	1.7972E-01	1.4352E+02	3.8093E+02	176.1	±	3.9
680	0.048	0.019	80.74	1.7408E-01	6.3008E-02	1.0583E-01	6.3728E+01	3.6610E+02	69.2	±	7.4
760	0.072	0.024	78.83	8.8419E-02	5.7435E-02	7.2066E-02	3.3165E+01	3.7509E+02	39.9	±	9.3
850	0.103	0.031	38.85	2.8373E-02	5.6649E-02	4.8408E-02	2.1598E+01	7.6120E+02	74.3	±	8.0
950	0.145	0.042	33.17	1.7694E-02	5.8654E-02	4.2523E-02	1.5777E+01	8.9166E+02	59.5	±	3.1
1020	0.217	0.072	27.93	8.3989E-03	3.6198E-02	2.6503E-02	8.9038E+00	1.0601E+03	36.4	±	2.5
1100	0.342	0.125	18.46	4.8297E-03	3.7377E-02	2.1936E-02	7.7448E+00	1.6036E+03	35.8	±	0.8
1200	0.790	0.448	15.66	3.7264E-03	5.5804E-02	1.8320E-02	7.0326E+00	1.8873E+03	33.7	±	0.3
1300	0.869	0.079	50.92	2.0251E-02	5.8981E-02	4.1506E-02	1.1772E+01	5.8130E+02	32.8	±	1.9
1400	0.933	0.064	58.05	1.6634E-02	4.1489E-02	2.8991E-02	8.4897E+00	5.1038E+02	20.3	±	3.1
1600	1.000	0.067	63.73	1.5931E-02	4.9097E-02	2.7019E-02	7.4087E+00	4.6505E+02	15.3	±	2.4

Sample mass = 600 mg
J-value = 0.00318766 ± 0.00000317
Integrated age = 37.6 ± 0.6 Ma
Plateau age = 34.2 ± 0.4 Ma (1020-1300°C)

SDL (R010201) Whole rock olivine nephelinite The Sideling (Knockup), via Weelaty

T (°C)	cum. ^{39}Ar$_K$	increment	Atmos. %	36Ar/39Ar	37Ar/39Ar	38Ar/39Ar	40Ar/39Ar	40Ar/36Ar	Age (Ma)		1σ
450	0.007	0.007	71.49	1.3793E-01	6.3957E-01	2.0333E-01	5.6972E+01	4.1300E+02	91.0	±	19.2
500	0.015	0.008	82.42	1.3793E-01	6.3957E-01	2.0333E-01	4.9420E+01	3.5800E+02	49.3	±	19.5
600	0.033	0.018	3.97	1.0947E-03	3.1132E-01	1.7015E-01	7.5745E+00	6.9200E+03	41.2	±	5.7
650	0.039	0.006	93.85	2.7206E-01	9.6296E-01	2.2699E-01	8.5605E+01	3.1500E+02	30.0	±	29.4
700	0.062	0.023	55.75	1.2902E-02	2.7752E-01	1.5133E-01	6.8290E+00	5.2900E+02	17.2	±	7.1
800	0.095	0.033	31.92	5.8938E-03	1.3474E-01	1.4919E-01	5.4518E+00	9.2500E+02	21.1	±	6.0
900	0.115	0.020	31.96	8.3618E-03	8.4235E-02	1.3919E-01	7.7381E+00	9.2500E+02	29.9	±	6.3
960	0.162	0.047	2.86	5.9862E-04	5.5966E-02	1.4317E-01	6.0503E+00	1.0107E+04	33.3	±	1.3
1020	0.195	0.033	1.54	2.6524E-04	5.4200E-02	1.3824E-01	4.8388E+00	1.8243E+04	27.0	±	2.7
1100	0.204	0.009	17.14	3.2520E-03	2.2318E-01	1.5777E-01	5.5372E+00	1.7027E+03	26.1	±	0.5
1200	0.397	0.193	37.09	9.9449E-03	3.2599E-01	1.0631E-01	7.8856E+00	7.9294E+02	28.2	±	1.2
1400	0.613	0.216	61.12	2.8627E-02	3.6206E-01	9.7976E-02	1.3824E+01	4.8289E+02	30.6	±	0.9
1600	1.000	0.387	56.72	2.2673E-02	1.7488E-01	7.9539E-02	1.1817E+01	5.2120E+02	29.1	±	0.6

Sample mass = 600 mg
J-value = 0.00318766 ± 0.00000317
Integrated age = 29.7 ± 0.6 Ma
Plateau age = 29.4 ± 0.5 Ma (900-1600°C)

BLS (R010204) Whole rock basanite Blessington plug

T (°C)	cum. ^{39}Ar$_K$	increment	Atmos. %	36Ar/39Ar	37Ar/39Ar	38Ar/39Ar	40Ar/39Ar	40Ar/36Ar	Age (Ma)		1σ
400	0.006	0.006	13.24	1.1926E-02	9.2460E-02	7.9958E-02	2.6575E+01	2.2284E+03	127.8	±	10.6
500	0.044	0.038	9.72	3.7156E-03	1.0469E-01	8.9561E-02	1.1237E+01	3.0243E+03	57.3	±	2.5
600	0.048	0.004	59.24	4.8839E-02	7.4316E-02	8.6242E-02	2.4379E+01	4.9917E+02	56.2	±	18.2
700	0.065	0.017	41.05	1.9139E-02	9.3974E-02	7.6717E-02	1.3787E+01	7.2038E+02	46.0	±	3.8
850	0.085	0.020	9.76	2.3101E-03	1.1336E-01	1.3193E-01	6.9339E+00	3.0015E+03	35.5	±	3.6
950	0.104	0.019	21.61	5.9313E-03	1.0906E-01	9.1143E-02	8.1010E+00	1.3658E+03	36.0	±	3.6
1020	0.606	0.502	3.92	9.0585E-04	5.2951E-02	1.6974E-02	6.7436E+00	7.4445E+03	36.7	±	0.1
1100	0.634	0.028	11.92	3.0235E-03	7.7313E-02	5.3972E-02	7.4702E+00	2.4707E+03	37.3	±	2.3
1200	0.706	0.072	15.04	3.9877E-03	5.1405E-02	2.9017E-02	7.8363E+00	1.9651E+03	37.7	±	0.9
1400	0.978	0.272	6.77	1.6141E-03	4.1767E-02	1.7103E-02	7.0246E+00	4.3520E+03	37.1	±	0.2
1600	1.000	0.022	22.73	6.0591E-03	6.9033E-02	4.2301E-02	7.8813E+00	1.3007E+03	34.6	±	1.9

Sample mass = 600 mg
J-value = 0.00318766 ± 0.00000317
Integrated age = 38.5 ± 0.2 Ma
Plateau age = 36.8 ± 0.2 Ma (850-1600°C)

SB9 (R005506) Whole rock olivine tholeiite "Eastbourne", via Avoca

T (°C)	cum. ^{39}Ar$_K$	increment	Atmos. %	36Ar/39Ar	37Ar/39Ar	38Ar/39Ar	40Ar/39Ar	40Ar/36Ar	Age (Ma)		1σ
500	0.030	0.030	85.14	1.2230E-01	3.3893E-01	1.0429E-01	4.2443E+01	3.4705E+02	35.9	±	2.5
600	0.060	0.030	63.08	3.4306E-02	6.8456E-02	8.8955E-02	1.6090E+01	4.6903E+02	33.8	±	1.6
680	0.222	0.162	24.70	6.1554E-03	6.6077E-02	7.1738E-02	7.3726E+00	1.1977E+03	31.5	±	0.4
760	0.442	0.220	6.49	1.2747E-03	9.5584E-02	6.6722E-02	5.7178E+00	4.4856E+03	30.3	±	1.4
850	0.640	0.198	10.24	1.9916E-03	2.7991E-01	6.7221E-02	5.5664E+00	2.7949E+03	28.4	±	2.0
950	0.826	0.186	14.38	2.8735E-03	5.7804E-01	7.2070E-02	5.6296E+00	1.9592E+03	27.4	±	0.5
1020	0.902	0.076	9.33	1.9234E-03	8.3483E-01	8.4285E-02	5.4425E+00	2.8296E+03	28.0	±	0.5
1100	0.933	0.031	87.10	1.2463E-01	3.3190E-01	1.0589E-01	4.2279E+01	3.3925E+02	31.1	±	2.5
1200	0.963	0.030	88.05	1.2647E-01	3.3893E-01	1.0429E-01	4.2443E+01	3.3559E+02	28.9	±	2.5
1300	0.968	0.005	62.51	3.0833E-02	3.8684E+00	1.0105E-01	1.4137E+01	4.5849E+02	30.2	±	6.3
1400	0.985	0.017	42.79	9.2285E-03	4.4306E+00	8.7917E-02	5.6213E+00	6.0912E+02	18.4	±	2.3
1600	1.000	0.015	37.80	2.0812E-02	8.2958E+00	8.0273E-02	1.4644E+01	7.0365E+02	51.8	±	5.8

Sample mass = 600mg
J-value = 0.00318766 ± 0.00000317
Integrated age = 29.8 ± 0.5 Ma
Plateau age = 29.6 ± 0.6 Ma (500-1300°C)

SB11 (R005508)   Whole rock   nepheline hawaiite   Llewellyn, via Conara

T (°C)	cum. $^{39}Ar_K$	increment	Atmos. %	36Ar/39Ar	37Ar/39Ar	38Ar/39Ar	40Ar/39Ar	40Ar/36Ar	Age (Ma)		1σ
400	0.029	0.029	52.03	2.9251E-02	4.9625E-02	3.2699E-01	1.6634E+01	5.6867E+02	45.2	±	0.9
450	0.106	0.077	26.78	6.7744E-03	2.4653E-02	2.9530E-01	7.4969E+00	1.1067E+03	31.2	±	0.4
500	0.210	0.104	13.81	2.9691E-03	2.1069E-02	2.7682E-01	6.3681E+00	2.1448E+03	31.2	±	0.4
600	0.511	0.301	4.71	9.1016E-04	1.1957E-02	2.5462E-01	5.7143E+00	6.2784E+03	30.9	±	0.2
650	0.792	0.281	6.36	1.1999E-03	1.2807E-02	2.3625E-01	5.5831E+00	4.6529E+03	29.7	±	0.2
700	0.879	0.087	8.02	1.5079E-03	1.0410E-02	2.1164E-01	5.5713E+00	3.6948E+03	29.1	±	0.2
750	0.923	0.044	18.60	4.0102E-03	2.0703E-02	1.8061E-01	6.3892E+00	1.5932E+03	29.5	±	0.9
840	0.937	0.014	31.22	7.9103E-03	4.4070E-02	1.5062E-01	7.5047E+00	9.4872E+02	29.3	±	2.2
900	0.946	0.009	50.41	1.8026E-02	1.0000E-01	2.1146E-01	1.0579E+01	5.8688E+02	29.8	±	1.8
960	0.959	0.013	57.01	2.4618E-02	2.1013E-01	3.2130E-01	1.2759E+01	5.1828E+02	31.2	±	4.2
1020	0.965	0.006	85.69	7.6281E-02	5.2181E-01	5.5382E-01	2.6288E+01	3.4462E+02	21.5	±	4.8
1100	0.981	0.016	9.55	8.8507E-03	6.6944E-01	3.8885E-01	2.6880E+01	3.0371E+03	134.6	±	2.2
1200	0.990	0.009	8.88	2.6703E-02	1.2991E+01	2.4423E+00	7.7781E+01	2.9129E+03	370.2	±	3.1
1400	0.996	0.006	87.48	6.3324E-01	9.7583E+00	1.2556E+00	2.1307E+02	3.3648E+02	148.0	±	4.9
1600	1.000	0.004	77.11	1.0472E+00	3.3737E+00	7.4071E-01	4.0097E+02	3.8291E+02	463.8	±	9.5

Sample mass = 600 mg
J-value = 0.00318766 ± 0.00000317
Integrated age = 38.5 ± 0.1 Ma
Plateau age = 30.3 ± 0.2 Ma (450-960°C)

LSB24 (R004501)   Whole rock   nepheline hawaiite   Burburys Sugarloaf, via Ross

T (°C)	cum. $^{39}Ar_K$	increment	Atmos. %	36Ar/39Ar	37Ar/39Ar	38Ar/39Ar	40Ar/39Ar	40Ar/36Ar	Age (Ma)		1σ
400	0.001	0.001	86.52	8.6616E-02	4.2758E-01	1.5264E-01	2.9574E+01	3.4144E+02	22.8	±	10.0
450	0.013	0.012	69.61	5.3920E-02	3.4743E-01	1.1127E-01	2.2879E+01	4.2432E+02	39.5	±	3.9
500	0.022	0.009	61.43	2.2398E-02	1.9132E-01	1.4814E-01	1.0778E+01	4.8121E+02	23.7	±	2.6
600	0.031	0.009	23.70	8.8380E-03	1.8578E-01	1.3973E-01	1.0988E+01	1.2432E+03	47.5	±	2.4
650	0.050	0.019	26.95	6.8430E-03	8.7472E-02	1.6159E-01	7.5066E+00	1.0970E+03	31.1	±	1.1
700	0.087	0.037	21.34	4.1922E-03	3.0570E-02	1.3248E-01	5.8209E+00	1.3885E+03	26.0	±	0.7
750	0.178	0.091	9.18	1.6748E-03	1.4779E-02	7.6016E-02	5.4040E+00	3.2266E+03	27.9	±	0.4
840	0.369	0.191	5.07	8.8697E-04	1.0479E-02	4.6198E-02	5.1766E+00	5.8363E+03	27.9	±	0.2
900	0.482	0.113	5.62	9.7731E-04	1.0613E-02	2.9287E-02	5.1480E+00	5.2675E+03	27.6	±	0.3
960	0.559	0.077	8.19	1.4136E-03	1.5034E-02	2.5014E-02	5.1154E+00	3.6188E+03	26.7	±	0.5
1020	0.643	0.084	5.16	8.8588E-04	1.9057E-02	2.2494E-02	5.0695E+00	5.7226E+03	27.3	±	0.3
1100	0.752	0.109	6.67	1.1430E-03	3.1755E-02	2.0443E-02	5.0517E+00	4.4196E+03	26.8	±	0.2
1200	0.911	0.159	6.28	1.1296E-03	1.7590E-01	1.9007E-02	5.1261E+00	4.5381E+03	27.3	±	0.3
1400	0.988	0.077	28.47	6.7567E-03	1.3604E+00	5.4343E-02	6.6806E+00	9.8874E+02	27.2	±	0.2
1600	1.000	0.012	20.59	6.7223E-03	1.3446E+00	7.1942E-02	9.1803E+00	1.3656E+03	41.3	±	2.1

Sample mass = 600 mg
J-value = 0.00318766 ± 0.00000317
Integrated age = 27.8 ± 0.1 Ma
Plateau age = 27.3 ± 0.1 Ma (700-1400°C)

LCr (R010205)   Whole rock   olivine nephelinite   Western side of Lake Crescent

T (°C)	cum. $^{39}Ar_K$	increment	Atmos. %	36Ar/39Ar	37Ar/39Ar	38Ar/39Ar	40Ar/39Ar	40Ar/36Ar	Age (Ma)		1σ
500	0.025	0.025	84.57	4.0903E-02	2.9128E-01	9.6135E-02	1.4295E+01	3.4948E+02	12.6	±	2.1
600	0.031	0.006	14.52	3.0958E-03	9.4620E-02	2.3909E-01	6.2763E+00	2.0274E+03	30.5	±	9.5
680	0.061	0.030	29.86	7.1354E-03	6.1681E-02	3.1972E-01	7.0725E+00	9.9119E+02	28.2	±	1.0
760	0.149	0.088	5.30	1.0453E-03	1.9808E-02	2.6874E-01	5.8201E+00	5.5678E+03	31.3	±	0.5
850	0.385	0.236	6.02	1.1378E-03	1.0601E-02	9.8472E-02	5.5928E+00	4.9155E+03	29.8	±	0.1
950	0.582	0.197	5.65	1.0430E-03	1.3167E-02	4.5354E-02	5.4624E+00	5.2371E+03	29.2	±	0.3
1020	0.705	0.123	9.77	1.8232E-03	2.6760E-02	3.9796E-02	5.5204E+00	3.0279E+03	28.3	±	0.4
1100	0.825	0.120	9.15	1.7992E-03	6.5621E-02	3.8110E-02	5.7847E+00	3.2151E+03	29.8	±	0.6
1200	0.883	0.058	7.54	1.4594E-03	3.6443E-01	5.8009E-02	5.3803E+00	3.6866E+03	28.2	±	0.6
1300	0.950	0.067	13.29	2.9013E-03	1.4248E+00	9.2388E-02	5.6720E+00	1.9550E+03	27.9	±	0.4
1400	0.971	0.021	47.36	1.7112E-02	2.1150E+00	1.0737E-01	1.0368E+01	6.0589E+02	31.1	±	1.4
1600	1.000	0.029	57.10	4.4250E-02	1.8542E+00	1.0668E-01	2.2684E+01	5.1263E+02	55.1	±	1.1

Sample mass = 600 mg
J-value = 0.00318766 ± 0.00000317
Integrated age = 29.7 ± 0.2 Ma
Plateau age = 29.4 ± 0.2 Ma (600-1400°C)

ATr (R010218) — Whole rock — olivine melilitite — Alma Tier, via Interlaken

T (°C)	cum. $^{39}Ar_K$	increment	Atmos. %	36Ar/39Ar	37Ar/39Ar	38Ar/39Ar	40Ar/39Ar	40Ar/36Ar	Age (Ma)		1σ
450	0.009	0.009	91.59	1.5074E-01	2.7068E+00	7.3140E-02	4.8436E+01	3.2131E+02	23.3	±	3.6
500	0.026	0.017	73.79	8.4939E-02	2.1083E+00	7.9875E-02	3.3824E+01	3.9821E+02	50.3	±	3.6
600	0.059	0.033	84.50	9.2301E-02	1.8243E+00	6.2266E-02	3.2141E+01	3.4822E+02	28.4	±	1.6
650	0.101	0.042	54.58	2.7082E-02	8.3732E-01	3.8454E-02	1.4574E+01	5.3815E+02	37.6	±	1.1
700	0.161	0.060	36.53	1.2918E-02	5.9273E-01	2.9063E-02	1.0353E+01	8.0148E+02	37.3	±	0.7
750	0.249	0.088	33.29	1.0994E-02	4.4322E-01	2.3865E-02	9.6869E+00	8.8109E+02	36.7	±	0.3
840	0.441	0.192	19.84	5.5517E-03	3.0799E-01	1.8229E-02	8.1797E+00	1.4734E+03	37.2	±	0.3
900	0.603	0.162	21.65	6.1631E-03	3.8917E-01	1.8883E-02	8.3037E+00	1.3473E+03	36.9	±	0.4
960	0.684	0.081	30.79	9.6312E-03	9.6546E-01	2.3928E-02	9.0345E+00	9.3804E+02	35.5	±	0.4
1020	0.726	0.042	38.17	1.3609E-02	2.6277E+00	3.0754E-02	1.0046E+01	7.3816E+02	35.3	±	0.8
1100	0.759	0.033	37.05	1.3178E-02	4.2015E+00	3.1048E-02	9.6838E+00	7.3485E+02	34.7	±	1.2
1200	0.900	0.141	28.08	1.0795E-02	1.0373E+01	3.3295E-02	8.6036E+00	7.9701E+02	35.4	±	0.4
1300	0.967	0.067	28.31	1.4509E-02	2.3699E+01	5.2817E-02	8.8637E+00	6.1093E+02	36.6	±	0.7
1400	0.989	0.022	61.05	2.9738E-02	3.0097E+01	1.6937E-01	1.0707E+01	3.6004E+02	24.2	±	2.4
1600	1.000	0.011	87.06	1.0079E-01	2.1548E+01	1.4389E-01	3.2373E+01	3.2119E+02	24.2	±	3.3

Sample mass = 600 mg
I-value = 0.00318766 ± 0.00000317
Integrated age = 35.9 ± 0.2 Ma
Plateau age = 36.5 ± 0.2 Ma (650-1300°C)

BRJ1 (R010055) — Whole rock — quartz tholeiite — Crooked Billet Creek, Brighton

T (°C)	cum. $^{39}Ar_K$	increment	Atmos. %	36Ar/39Ar	37Ar/39Ar	38Ar/39Ar	40Ar/39Ar	40Ar/36Ar	Age (Ma)		1σ
450	0.056	0.056	66.70	3.1374E-02	9.2057E-01	8.5522E-02	1.3824E+01	4.4063E+02	26.2	±	1.5
500	0.070	0.014	33.65	8.5177E-03	2.3384E-01	7.5888E-02	7.4550E+00	8.7524E+02	28.1	±	2.6
600	0.178	0.108	20.59	4.1167E-03	2.4198E-01	6.1081E-02	5.8481E+00	1.4206E+03	26.4	±	0.9
650	0.419	0.241	15.09	2.9545E-03	3.7406E-01	6.0991E-02	5.6261E+00	1.9042E+03	27.1	±	0.4
700	0.660	0.241	18.66	3.6377E-03	3.7524E-01	6.0780E-02	5.6356E+00	1.5492E+03	26.0	±	0.4
750	0.781	0.121	13.84	2.8624E-03	1.3657E+00	5.5882E-02	5.3957E+00	1.8850E+03	26.4	±	0.8
840	0.904	0.123	10.40	2.0568E-03	6.7279E-01	5.8707E-02	5.3839E+00	2.6177E+03	27.4	±	0.8
900	0.922	0.018	58.57	1.1762E-02	8.8487E+00	6.2501E-02	4.8239E+00	4.1012E+02	11.5	±	3.2
960	0.941	0.019	59.41	1.1643E-02	8.7476E+00	6.5244E-02	4.7099E+00	4.0453E+02	11.0	±	3.2
1020	0.971	0.030	28.35	8.5528E-03	8.5542E+00	6.5083E-02	6.6697E+00	7.7983E+02	27.3	±	2.1
1100	0.984	0.013	74.53	1.9442E-02	5.5956E+00	1.0839E-01	7.1709E+00	3.6883E+02	10.5	±	6.3
1200	0.987	0.003	19.25	8.3249E-02	3.1005E+01	1.6456E-01	1.1566E+02	1.3894E+03	478.5	±	30.1
1300	0.990	0.003	46.40	7.1899E-02	6.7716E+01	9.9298E-02	3.4820E+01	4.8429E+02	108.8	±	40.2
1400	0.992	0.002	48.50	1.1512E-01	7.2014E+01	1.4332E-01	5.8969E+01	5.1226E+02	174.4	±	27.0
1600	1.000	0.008	10.62	9.7553E-02	1.1695E+02	7.9513E-02	1.8842E+02	1.9314E+03	826.2	±	8.2

Sample mass = 600 mg
I-value = 0.00318766 ± 0.00000317
Integrated age = 35.9 ± 0.3 Ma
Plateau age = 26.7 ± 0.3 Ma (450-840°C)

HBJ23 (R010093) — Whole rock — quartz tholeiite — Dragon Point, Claremont

T (°C)	cum. $^{39}Ar_K$	increment	Atmos. %	36Ar/39Ar	37Ar/39Ar	38Ar/39Ar	40Ar/39Ar	40Ar/36Ar	Age (Ma)		1σ
400	0.018	0.018	83.58	5.2992E-02	2.1074E-01	7.5379E-02	1.8744E+01	3.5371E+02	17.6	±	4.4
500	0.067	0.049	89.29	1.1882E-01	1.3041E-01	9.7849E-02	3.9340E+01	3.3109E+02	24.1	±	1.1
600	0.165	0.098	61.30	2.4491E-02	8.4132E-02	6.7467E-02	1.1824E+01	4.8279E+02	26.1	±	0.6
680	0.370	0.205	25.87	5.5200E-03	8.8275E-02	5.8834E-02	6.3061E+00	1.1424E+03	26.6	±	0.5
760	0.433	0.063	13.96	2.2778E-03	1.5625E-01	5.9905E-02	4.7643E+00	2.0916E+03	23.3	±	1.2
850	0.686	0.253	19.38	3.5945E-03	2.8736E-01	6.1070E-02	5.3954E+00	1.5010E+03	24.7	±	0.4
950	0.721	0.035	11.90	1.9710E-03	8.3463E-01	7.9788E-02	4.3937E+00	2.2292E+03	22.0	±	0.7
1020	0.866	0.145	22.24	4.5308E-03	8.9354E-01	7.8807E-02	5.7454E+00	1.2681E+03	25.4	±	0.7
1100	0.884	0.018	46.49	1.2727E-02	1.0893E+00	9.5410E-02	7.9413E+00	6.2400E+02	24.2	±	3.3
1200	0.933	0.049	60.32	2.0217E-02	1.5971E+00	7.6185E-02	9.7325E+00	4.8141E+02	22.0	±	1.6
1300	0.945	0.012	55.78	2.2077E-02	4.6052E+00	9.1068E-02	1.1100E+01	5.0280E+02	28.0	±	3.5
1400	0.952	0.007	47.49	1.7856E-02	2.0705E+00	1.0299E-01	1.0810E+01	6.0544E+02	32.3	±	9.6
1600	1.000	0.048	72.83	7.7927E-02	3.7789E+00	8.5937E-02	3.1254E+01	4.0106E+02	48.2	±	1.7

Sample mass = 600 mg
J-value = 0.00318766 ± 0.00000317
Integrated age = 26.1 ± 0.3 Ma
Plateau age = 25.1 ± 0.3 Ma (500-1400°C)

GFN (G402497) — **Whole rock** — **basanite** — **Glenfern**

	cum. $^{39}Ar_K$	increment	Atmos. %	36Ar/39Ar	37Ar/39Ar	38Ar/39Ar	40Ar/39Ar	40Ar/36Ar	Age (Ma)		1σ
400	0.002	0.002	71.62	4.3524E-01	7.1344E-02	2.6732E-01	1.7958E+02	4.1259E+02	271.5	±	13.7
500	0.005	0.003	78.84	3.6314E-01	5.9798E-02	2.1504E-01	1.3612E+02	3.7486E+02	158.4	±	7.4
600	0.033	0.028	90.91	2.4688E-01	8.6108E-02	1.4243E-01	8.0266E+01	3.2512E+02	41.5	±	2.2
680	0.064	0.031	83.38	1.6722E-01	6.6699E-02	1.1291E-01	5.9283E+01	3.5452E+02	55.8	±	1.8
760	0.195	0.131	66.54	5.6629E-02	4.9021E-02	6.1316E-02	2.5171E+01	4.4450E+02	47.7	±	6.0
850	0.393	0.198	56.15	3.4444E-02	5.2107E-02	3.8288E-02	1.8147E+01	5.2685E+02	45.1	±	1.1
950	0.485	0.092	67.75	5.5248E-02	9.0467E-02	5.3775E-02	2.4116E+01	4.3650E+02	44.1	±	0.6
1020	0.600	0.115	64.30	4.6222E-02	9.2294E-02	5.5060E-02	2.1259E+01	4.5993E+02	43.1	±	1.3
1100	0.704	0.104	64.88	5.0688E-02	1.1751E-01	6.8087E-02	2.3099E+01	4.5570E+02	46.0	±	1.4
1200	0.769	0.065	61.73	4.5914E-02	5.2677E-01	7.8963E-02	2.1940E+01	4.7785E+02	47.6	±	1.1
1300	0.893	0.124	70.38	6.5270E-02	8.8979E-01	7.4857E-02	2.7338E+01	4.1884E+02	46.0	±	0.4
1400	0.926	0.033	56.31	3.4335E-02	7.0295E-01	1.1771E-01	1.7951E+01	5.2283E+02	44.5	±	1.5
1600	1.000	0.074	69.65	1.7018E-01	1.0218E+00	1.0512E-01	7.2112E+01	4.2374E+02	121.7	±	3.1

Sample mass = 600mg
I-value = 0.00318766 ± 0.00000317
Integrated age = 52.3 ± 0.9 Ma
Plateau age = 45.5 ± 1.0 Ma (760-1400°C)

HBJ6 (R010076) — **Whole rock** — **hawaiite** — **Pickett Hill, via Kingston**

T (°C)	cum. $^{39}Ar_K$	increment	Atmos. %	36Ar/39Ar	37Ar/39Ar	38Ar/39Ar	40Ar/39Ar	40Ar/36Ar	Age (Ma)		1σ
400	0.003	0.003	46.55	7.2438E-02	1.4817E-01	2.1433E-01	4.5979E+01	6.3474E+02	136.0	±	5.5
500	0.013	0.010	63.83	8.2464E-02	2.0070E-01	1.7880E-01	3.8178E+01	4.6297E+02	77.7	±	3.2
600	0.023	0.010	36.39	2.3540E-02	1.2316E-01	1.9050E-01	1.9116E+01	8.1205E+02	68.5	±	3.7
680	0.031	0.008	6.13	2.2737E-03	8.2851E-02	1.8741E-01	1.0881E+01	4.7855E+03	57.7	±	4.2
760	0.069	0.038	34.87	1.8476E-02	7.3145E-02	1.9298E-01	1.5670E+01	8.4813E+02	57.7	±	1.7
850	0.136	0.067	26.99	8.5029E-03	4.1307E-02	1.1757E-01	9.3246E+00	1.0966E+03	38.6	±	0.4
950	0.280	0.144	28.99	7.6199E-03	4.2086E-02	7.5770E-02	7.7833E+00	1.0214E+03	31.4	±	0.5
1020	0.333	0.053	6.64	1.3315E-03	4.2985E-02	4.3693E-02	5.8991E+00	4.4303E+03	31.2	±	0.3
1100	0.503	0.170	18.72	3.9335E-03	4.5682E-02	3.4649E-02	6.2186E+00	1.5809E+03	28.7	±	0.2
1200	0.618	0.115	10.81	2.1176E-03	9.0137E-02	3.1941E-02	5.7498E+00	2.7152E+03	29.1	±	0.2
1300	0.746	0.128	6.53	1.2683E-03	2.8604E-01	2.7633E-02	5.4323E+00	4.2830E+03	28.8	±	0.3
1400	0.967	0.221	19.97	4.2994E-03	3.1358E-01	3.4965E-02	6.2703E+00	1.4584E+03	28.5	±	0.1
1600	1.000	0.033	67.07	8.3949E-02	3.4776E-01	6.5087E-02	3.6972E+01	4.4041E+02	68.6	±	0.6

Sample mass = 600 mg
J-value = 0.00318766 ± 0.00000032
Integrated age = 33.8 ± 0.1 Ma
Plateau age = 29.4 ± 0.2 Ma (950-1400°C)

SBA21 (R010159) — **Whole rock** — **olivine tholeiite** — **Marion Bay**

T (°C)	cum. $^{39}Ar_K$	increment	Atmos. %	36Ar/39Ar	37Ar/39Ar	38Ar/39Ar	40Ar/39Ar	40Ar/36Ar	Age (Ma)		1σ
400	0.023	0.023	10.38	2.0197E-02	1.7578E-01	3.1689E-01	5.7398E+01	2.8418E+03	273.8	±	7.8
450	0.044	0.021	11.08	1.6830E-02	9.3415E-02	3.0376E-01	4.4831E+01	2.6637E+03	215.7	±	4.7
500	0.051	0.007	10.14	9.9744E-03	1.0072E-01	2.8977E-01	2.9010E+01	2.9085E+03	143.9	±	19.6
600	0.099	0.048	63.16	9.3168E-02	1.3097E-01	2.6976E-01	4.3598E+01	4.6795E+02	90.0	±	3.0
700	0.158	0.059	25.60	1.7775E-02	2.5686E-01	1.5087E-01	2.0469E+01	1.1515E+03	85.4	±	2.5
750	0.207	0.049	48.31	4.6428E-02	1.4333E-01	1.9846E-01	2.8400E+01	6.1169E+02	82.4	±	3.1
800	0.440	0.233	25.22	1.2018E-02	2.6447E+00	7.3717E-02	1.3316E+01	1.1080E+03	56.3	±	0.8
850	0.511	0.071	47.04	2.8595E-02	3.4939E-01	1.3354E-01	1.7933E+01	6.2712E+02	53.7	±	3.5
900	0.593	0.082	60.95	4.5810E-02	2.0662E-01	1.7974E-01	2.2210E+01	4.8482E+02	49.1	±	1.9
960	0.641	0.048	81.33	1.1295E-01	9.5288E-02	2.4464E-01	4.1057E+01	3.6350E+02	43.5	±	2.6
1020	0.711	0.070	78.60	8.2300E-02	1.4766E-01	2.1598E-01	3.0936E+01	3.7589E+02	37.6	±	2.3
1100	0.760	0.049	70.65	4.0270E-02	5.4759E-01	9.2861E-02	1.6812E+01	4.1749E+02	28.1	±	2.4
1200	0.868	0.108	70.21	5.4139E-02	4.8686E+00	7.6242E-02	2.2291E+01	4.1174E+02	37.9	±	1.3
1400	0.939	0.071	51.76	2.7890E-02	8.1660E-01	7.3390E-02	1.5830E+01	5.6760E+02	43.3	±	2.0
1600	1.000	0.061	79.56	1.6419E-01	4.9181E+00	1.0826E-01	6.0545E+01	3.6874E+02	70.0	±	1.8

Sample mass = 600 mg
J-value = 0.00318766 ± 0.00000317
Integrated age = 64.2 ± 0.6 Ma

Note: J-values: Weighted mean of three fusions of irradiation standard LP-6 Biotite having a calibrated 40Ar/39Ar age of
128.4 ± 0.2 Ma, based on Fish Canyon Sanidine (28.02 ± 0.28Ma) (Baksi et al., 1996; Renne et al., 1998).